To the Graduate Council:

I am submitting herewith a dissertation written by Samir Abu Iqyas entitled "High-pressure crystallization of ethylene-octene copolymers." I have examined the final paper copy of this dissertation for form and content and recommend that it be accepted in partial fulfillment of the requirements for the degree of Doctor of Philosophy, with a major in Polymer Engineering.

Paul J. Phillips, Major Professor

We have read this dissertation
And recommend its acceptance:

Accepted for the Council:

Vice Provost and Dean of
Graduate Studies

Thesis
2002b
.H325

HIGH PRESSURE CRYSTALLIZATION OF ETHYLENE-OCTENE COPOLYMERS

A Dissertation
Presented for the
Doctor of Philosophy Degree
The University of Tennessee, Knoxville

Samir Abu Iqyas

August 2002

DEDICATION

I dedicate this dissertation to my parents

who always supported me through their prayers.

To my lovely wife Amal,

my joyful sons Bara and Mowath

for their patience and the beautiful moments.

ACKNOWLEDGMENT

Praise is to Allah, the cherisher, and sustainer of the worlds, for his guidance, help, and mercy. Without his grace, this work would not be possible.

I would like to express my sincere and deepest appreciation and gratitude to my advisor Professor Paul J. Phillips, for his support, helpful suggestions, and guidance throughout this research. Special thanks are extended to my dissertation committee members, Professors John R. Collier, Kevin M. Kit, and in particular Professor Roberto S. Benson for his help and valuable encouragements and suggestions.

I am also grateful to Dr. Marek Pyda for his helpful work on DSC, Dr. Claudia J. Rawn for her appreciable time and effort on the Philips High Temperature X-ray Diffraction. I extend my thanks to professors Charlie Brooks, David C. Joy, and Mr. Gregory Jones for their advice, time, and help on the SEM machine. My thanks to my colleagues in the group: John Wagner, Anita Dimeska, and Guan Xiaoping for the useful comments and help.

The financial support from the National Science Foundation (NSF) is highly acknowledged.

High regards to my parents, brothers, sisters, and lovely wife for their continued encouragement and support.

ABSTRACT

Polyethylenes generally crystallize in the orthorhombic form at atmospheric pressure, whereas the homopolymer is known to produce chain-extended crystals through the intervention of a hexagonal phase at pressures in excess of 3kbar. The crystallization of ethylene-octene copolymer with 4 hexyl branches per 1000 carbon atoms, at relatively low pressures, produced high melting points inconsistent with thin crystals. SEM studies demonstrate the presence of significant amounts of spherulites containing crystals ca. 100nm in thickness, consistent with the thermal behavior. Thick crystals suggest the formation of a phase that is capable of dissolving large number of hexyl groups during crystallization.

The phase diagrams of ethylene-octene copolymers have been constructed using polarized light intensity studies at elevated pressures. It has been established that the triple point is very sensitive to comonomer (hexyl branch) content and moves rapidly to low pressures as comonomer content is increased. It is believed that the triple point in the systems discussed here is between the melt, monoclinic and orthorhombic phases.

On dropping pressure to atmospheric, the metastable (monoclinic) phase decays to orthorhombic phase, necessitating the expulsion of excess hexyl groups to an amorphous phase. The process is akin to a eutectoid transformation and results in conversion of the thick monoclinic crystals to thin orthorhombic crystals, which are detected by SAXS and show the expected low melting points at atmospheric pressure.

The influences of crystallization temperature and of hexyl branch content on the band spacing have been elucidated for ethylene-octene copolymers, generating valuable new information. A given band spacing is found at increasingly lower crystallization temperatures as hexyl group content is increased. There appears to be a relatively linear relation between the observed temperature shift and the hexyl group content. Studies of a copolymer containing 4 hexyl groups per 1000 carbons permit a concurrent study of all three growth regimes. The reciprocal band spacing versus crystallization temperature plot shows two changes of slope coincident with the two changes of regime. Hence there appears to be a very clear connection between regime plots, and hence growth rate, with band spacing, which has not been reported before.

TABLE OF CONTENTS

SECTION **PAGE**

1. **INTRODUCTION**.....1

2. **THEORETICAL BACKGROUND**.....5

2.1 Melting Behavior.....5
2.1.1 Equilibrium Melting Point.....6
2.1.2 Pressure Effect on Melting Temperatures.....10
2.1.3 Phase Diagrams.....12

2.2 Diffraction and Scattering Theory.....17
2.2.1 Wide Angle X-ray Diffraction (WAXD).....18
2.2.2 High Temperature X-ray Diffraction.....19
2.2.2.1 Thermal Expansion.....20
2.2.3 Small Angle X-ray Scattering (SAXS).....21
2.2.3.1 Correlation Function.....22

2.3 Crystallization Kinetics.....29
2.3.1 Crystallization Theories.....31
2.3.1.1 Secondary Nucleation Theory.....36
2.3.1.2 Criticism of Secondary Nucleation Theory..41
2.3.1.3 Andrews Theory.....42
2.3.2 Bulk Crystallization Kinetics.....44
2.3.2.1 Half-time Analyses.....45
2.3.3 Crystallization Kinetics at Elevated Pressures.....46

2.4 Morphology.....47
2.4.1 Axialites.....47
2.4.2 Spherulites.....48
2.4.2.1 Banded Spherulites.....48

3 **EXPERIMENTAL PROCEDURES**.....53

3.1 Materials.....53

3.2 Sample Preparation.....53

3.3 High Pressure Equipment.....55

3.4 Depolarized Light Microscopy.....59

3.5 Wide Angle X-ray Diffraction (WAXD).....61

3.6 Small Angle X-ray Scattering (SAXS).....62

3.7 Differential Scanning Calorimetry (DSC).....64

3.8 Scanning Electron Microscopy (SEM).....64

4 **RESULTS**.....66

4.1 Kinetics of Crystalllization.....66
4.1.1 Linear Growth Rates.....66
4.1.2 Bulk Crystallization Kinetics.....72

4.2 X-ray Analysis.....76
4.2.1 Wide Angle X-ray Diffraction (WAXD).....78
4.2.2 High Temperature X-ray Diffraction.....78
4.2.3 Small angle X-ray scattering (SAXS).....94
4.2.3.1 Theoretical Development for Estimating the Interfacial Layer Thickness Using SAXS.....102

4.3 Thermal Analysis.....110
4.3.1 Melting at Atmospheric Pressure.....110
4.3.1.1 Samples Prepared at Atmospheric Pressure.....110
4.3.1.2 Samples Prepared at Elevated Pressure.....119
4.3.2 Melting at Elevated Pressure.....122

4.4 Morphology.....122
4.4.1 Optical Microscopy.....123
4.4.1.1 Band Spacing.....125
4.4.2 Scanning Electron Microscopy (SEM).....130

5 **DISCUSSION**.....143

5.1 Melting Behavior and The Phase Diagram.....143

5.1.1 Thermal Analysis.....143

5.1.1.1 Melting Behavior of L-04 Copolymer.....144
5.1.1.2 Melting Behavior of L-11 Copolymer.....156
5.1.2 Phase Diagram.....161
5.1.3 Eutectoid Transformation.....168
5.1.3.1 Eutectoid Transformation in Alloys.....168
5.1.3.2 Eutectoid-Like Transformation in Copolymers.....173
5.1.4 The Monoclinic Phase in Thermodynamics.....178
5.1.4.1 The Thermodynamics of Phase Diagram...185

5.2 Morphological Studies.....198
5.2.1 WAXD.....198
5.2.2 Interfacial Layer Thickness.....201
5.2.3 Lamellar Thickness.....206
5.2.3.1 Gibbs-Thomson Equation.....209

5.3 Crystallization Kinetics.....224
5.3.1 Nucleation of ECC Under High Pressure.....233
5.3.2 Bulk Crystallization.....240

5.4 Band Spacing.....244
5.4.1 Cellulation in Polymers.....255

6 **CONCLUSIONS**.....259
6.1 Melting Behavior.....259
6.2 Phase Diagram.....259
6.3 Eutectoid-Like Transformation.....260
6.4 Crystallization Mechanism.....260
6.5 Band Spacing.....261

7 **FUTURE WORK**.....262
7.1 High Pressure Studies.....262
7.2 Diffraction Studies.....263
7.3 Mechanical Properties.....263
7.4 Electrical Studies.....263

REFERENCES.....265

VITA.....272

LIST OF TABLES

TABLE **PAGE**

3.1.1 Characteristics of the as-received linear PE (M-54) and ethylene-octene copolymers.....54

4.2.1 A summary of the expansion coefficients of L-04 and L-11 copolymers obtained by high-temperature x-ray diffraction.....89

4.3.1 A comparison of the melting temperatures of L-04 and L-11 copolymers obtained by using DSC and Light Intensity techniques. All conditions listed are for samples crystallized at atmospheric pressure.....115

5.2.1 A comparison between the average interfacial layer thickness of L-04 obtained at different pressures. The data was assumed to be independent of the crystallization temperature.....205

5.2.2 A Summary of the different parameters determined for L-04 copolymer at different pressures.....222

5.3.1 A comparison between the parameters obtained using linear growth kinetics and bulk crystallization for two pressure sets. (σ=11.8 erg/cm^2).....243

5.4.1 A comparison between the transition temperatures obtained using linear growth kinetics and reciprocal band spacing for different materials (P =1 atm).....251

LIST OF FIGURES

FIGURE **PAGE**

2.1.1 The phase diagram of linear PE as suggested by Bassett *et.al*.....14

2.1.2 The phase diagram of PE as suggested by Keller *et. al*.....16

2.2.1 Schematic graph of $K(z)$ showing the 'self-correlation triangle'.....27

2.2.2 Electron density distribution and correlation function $K(z)$.....28

2.2.3 The correlation function $K(z)$ and its second derivative $K''(z)$.....30

2.3.1 Polymer chain folding of the adjacent re-entry model in one lamella.....38

2.3.2 Schematic of regime analysis.....39

3.3.1 A simplified schematic diagram of the high-pressure equipment.....56

3.3.2 Simplified schematic of the high-pressure equipment.....57

3.3.3 A schematic diagram of the high-pressure cell.....58

3.3.4 Schematic diagram of the experimental steps used to crystallize, melt, and cool down.....60

4.1.1 The change in the size of spherulites versus time for L-04 copolymer crystallized, a) at 0.48kbar.....68

4.1.1 Continued, b) at 0.76kbar.....69

4.1.1 Continued, c) at 1.24kbar.....70

4.1.2 The effect of the crystallization temperature and pressure on the linear growth rate of L-04 copolymer.....71

4.1.3 T_c versus P at constant growth rate for L-04 copolymer using linear growth and bulk crystallization methods.....73

4.1.4 Schematic diagram of the measurements of half crystallization time.....74

FIGURE **PAGE**

4.1.5 The bulk crystallization of L-04 copolymer crystallized at different pressures using light intensity.....75

4.1.6 A plot of the inverse 'half-time' ($1/t_{1/2}$) versus temperature ofp L-04 copolymer at different pressures.....77

4.2.1 The crystallinity values of L-04 copolymer crystallized using different measurement techniques, a) at P=0.48kbar, b) at P=0.76kbar, c) at P=1.24kbar .79

4.2.2 Wide-angle x-ray diffraction of L-04 copolymer crystallized at Tc= 140 °C and P=0.76kbar.....82

4.2.3 X-ray diffraction pattern of L-04 copolymer as a function of temperature. (T_c=127 °C, P=0.76 kbar).....84

4.2.4 X-ray diffraction pattern of L-04 copolymer as a function of temperature. (T_c=145 °C, P=0.76 kbar).....85

4.2.5 X-ray Diffraction Pattern for L-04 copolymer as a function of temperature. (T_c=128 °C, P=1.24 kbar).....86

4.2.6 X-ray Diffraction Pattern for L-04 copolymer as a function of temperature. (T_c=148 °C, P=1.24 kbar).....87

4.2.7 The effect of crystallization temperature and heating process on the a-spacing of L-11 copolymer crystallized at atmospheric pressure.....90

4.2.8 The effect of crystallization temperature and heating process on the a-spacing of L-04 copolymer crystallized at 0.76kbar.....91

4.2.9 The effect of crystallization temperature and heating process on the a-spacing of L-04 copolymer crystallized at 1.24kbar.....92

4.2.10 The Effect of crystallization temperature on the original SAXS data, a) at constant pressure (P=0.48 kbar), b) at constant temperature (T_c= 128 °C).....95

4.2.11 Lamellar thickness ℓ (Å) versus T_c (C) for L-04 copolymer crystallized at atmospheric pressure.....98

4.2.12 Lamellar thickness ℓ (Å) versus T_c (C) for L-04 copolymer crystallized at P=0.47 kbar.....98

FIGURE **PAGE**

4.2.13 Lamellar thickness ℓ (Å) versus T_c (C) for L-04 copolymer crystallized at P=0.76 kbar.....99

4.2.14 Lamellar thickness ℓ (Å) versus T_c (C) for L-04 copolymer crystallized at P=1.24 kbar.....99

4.2.15 Normalized one-dimensional correlation function behavior for L-04 copolymer crystallized at T_c =134.2 °C and P=1.24kbar.....101

4.2.16 Linear-gradient model showing the effect of background intensity correction on estimating interfacial layer thickness 'E' of L-04 copolymer crystallized at T_c =136 °C and P=0.76 kbar.....104

4.2.17 Sigmoidal-gradient model showing the effect of background intensity correction on estimating interfacial layer thickness 'Δ' of L-04 copolymer crystallized at T_c =136 °C and P=0.76 kbar.....105

4.2.18 Linear-gradient model and background intensity correction of L-04 copolymer as a function of pressure and at constant crystallization temperature of 128 °C.....107

4.2.19 Linear-gradient model and background intensity correction of L-04 copolymer as a function of temperature and at constant pressure of 0.76 kbar.....108

4.3.1 The melting behavior of L-04 copolymer crystallized at atmospheric pressure and different temperatures using light intensity method.....111

4.3.2 The melting behavior of L-04 copolymer crystallized at T_c=130 °C and P=0.48kbar using light intensity and its derivative.....113

4.3.3 The DSC melting curves of L-04 copolymer crystallized at atmospheric pressure.....114

4.3.4 The melting behavior of L-11 copolymer crystallized at T_c=112 °C and P =1 atm using light intensity and its derivative.....117

4.3.5 The DSC melting curves of L-11 copolymer crystallized at atmospheric pressure.....118

4.3.6 Normalized light intensity plot of samples prepared at 1.24kbar and melted at atmospheric pressure.....120

FIGURE **PAGE**

4.4.1 A picture of L-04 copolymer crystallized at T_c=136.6 °C and P=0.76kbar was taken: a) during crystallization, and b) after cooling down.....124

4.4.2 A picture of L-11 copolymer taken *in-situ* at: a) 0.5h and b) 2.5h crystallization times.....126

4.4.3 Band spacing as a function of temperature and branch content of metallocene ethylene-octene copolymer and linear polyethylene.....127

4.4.4 Cellulation effect in L-11 copolymer at T_c=118 °C, P= 0.48kbar.....128

4.4.5 Cellulation effect in L-13 copolymer at T_c=104.5 °C.....128

4.4.6 Cellulation effect in H-17 copolymer at T_c=103 °C (M_n= 48,700).....129

4.4.7 SEM picture of L-04 copolymer crystallized at T_c=131 °C and P=0.76 kbar.....131

4.4.8 SEM picture of L-04 copolymer crystallized at T_c=140 °C and P=0.76 kbar.....132

4.4.9 A magnified SEM picture of the squared area of figure (4.4.8).....133

4.4.10 SEM picture of L-04 copolymer crystallized at T_c=140 °C and P=0.76 kbar.....134

4.4.11 SEM picture of L-04 copolymer crystallized at T_c=140 °C and P=0.76 kbar.....135

4.4.12 A magnified SEM picture of the squared area of figure (4.4.11).....136

4.4.13 SEM picture of L-11 copolymer crystallized at T_c=115 °C and P=1atm.....138

4.4.14 A magnified SEM picture of the squared area of figure (4.4.13).....139

4.4.15 SEM picture of L-11 copolymer crystallized at T_c=115 °C and P=1atm.....140

4.4.16 SEM picture of L-11 copolymer crystallized at T_c=115 °C and P=1atm. The sample was partially melted then quenched to retain only large structures.....141

4.4.17 A magnified SEM picture of figure (4.4.16) for L-11 copolymer crystallized at T_c=115 °C and P=1atm.....142

5.1.1 T_m vs T_c for L-04 copolymer crystallized at P=1atm and 0.48 kbar. Squares are the return to base line values, and circles are the peak values.....145

FIGURE **PAGE**

5.1.2 T_m vs T_c plot of L-04 copolymer crystallized at P=0.76 kbar, a) following path (A), b) following path (B). Crosses represent the return-to-baseline values and triangles are the peak values.....152

5.1.3 Changes in d-spacing values of ethylene-octene copolymer as a function of temperature at P=1.95kbar.....155

5.1.4 The T_m versus T_c plot for L-11 copolymer crystallized, a) at atmospheric pressure, b) at P=0.48kbar, c) at 1kbar 157

5.1.5 The morphological change of L-11 copolymer crystallized at T_c=115 °C, 1 atm. a) T=118 °C , b) T=129 °C only large lamellar structure survive.....162

5.1.6 The three-dimensional (T, P, 1/l) phase-stability diagram.....164

5.1.7 The effect of branch content on P-T phase diagram.....165

5.1.8 A plot of temperature versus pressure used to estimate the corrected equilibrium melting points of L-04 copolymer using growth rate kinetics.....167

5.1.9 The effect of crystallization temperature T_c on the P-T phase diagram of L-04 copolymer.....169

5.1.10 Iron-carbon phase diagram showing the austenite (γ Fe) and ferrite (α Fe) phase regions and eutectoid composition and temperature. Dotted lines represent iron-graphite equilibrium conditions and solid lines represent iron-cementite equilibrium conditions. Only the solid lines are important with respect to steel.171

5.1.11 Gibbs-Thomson plot as a function of pressure. All melting temperatures were measured at atmospheric pressure.....174

5.1.12 A schematic diagram of the eutectoid-like transformation where the rejection of branches converts the thick lamella to thinner stacked ones.....177

5.1.13 Schematic free energy G versus temperature plot, illustrating the stable orthorhombic and unstable monoclinic phases at atmospheric pressure.....181

5.1.14 The effect of pressure on the schematic free energy G versus temperature plot. The monoclinic phase becomes stable.....182

FIGURE **PAGE**

5.1.15 The effect of branch content on the schematic free energy G versus temperature plot. The monoclinic phase becomes stable but at lower temperatures.....183

5.1.16 Phase (crystal) growth as a temperature T versus reciprocal size $1/l$, phase stability diagram.....187

5.1.17 A schematic diagram of the expected effect of T_c on Gibbs free energy G at 0.48kabr.....189

5.1.18 schematic diagram of the expected effect of T_c on the Gibbs free energy G of L-04 at 0.76kbar. Empty circles represent the melting temperatures $T_c < T_{cr}$, while squares are for $T_c > T_{cr}$. Shaded circle represents the melting temperature at T_{cr}.....191

5.1.19 A schematic plot of T_m versus T_c at 0.76kbar using the thermodynamically predicted melting temperatures of figure (5.1.9).....194

5.1.20 A schematic diagram of the expected effect of T_c on the Gibbs free energy G of L-11 at 1 atm. Empty circles represent the melting temperatures $T_c < T_{cr}$, while squares are for $T_c > T_{cr}$. Shaded circle represents the melting temperature at T_{cr}.....197

5.2.1 A plot of the interfacial layer thickness (E, Δ) versus T_c for L-04 copolymer crystallized at atmospheric pressure, b) at 0.48kbar, c) at 0.76kbar, d) at 1.24kbar.....202

5.2.2 Comparison between the lamellar thickness of L-04 copolymer obtained at P=0.76kbar and 1 atm (T_m^o =150.88 °C).....212

5.2.3 Comparison between the lamellar thickness of L-04 copolymer obtained at P=0.76kbar and 1 atm. (T_m^o =155.88 °C).....213

5.2.4 Comparison between the lamellar thickness of L-04 copolymer obtained at P=1.24kbar and 1 atm. (T_m^o =168.55 °C).....214

5.2.5 The lamellar thickness of L-11 copolymer crystallized at atmospheric pressure (T_m^o =134.5 °C).....216

5.2.6 Gibbs-Thomson plot for L-04 copolymer crystallized at different pressures. Open and solid circles represent high and low supercoolings at 0.48kbar, respectively. (x) symbol represents the T_m values of P=0.48kbar obtained at atmospheric pressure. Squares represent the atmospheric pressure crystallization data.....217

5.2.7 Gibbs-Thomson plot for L-04 copolymer crystallized at P=0.76kbar. (x) symbol represents the T_m values obtained at the atmospheric pressure.....218

5.2.8 Gibbs-Thomson plot for L-04 copolymer crystallized at P=1.24kbar. (x) symbol represents the T_m values obtained at atmospheric pressure.....219

5.3.1 Logarithm of linear growth rate versus crystallization temperature for L-04 copolymer at different pressures.....225

5.3.2 Logarithm of linear growth rate versus supercooling temperatures for L-04 copolymer at different pressures.....226

5.3.3 The regime plot of L-04 copolymer as a function of pressure.....227

5.3.4 The effect of the glass transition T_g on the Lauritzen-Hoffman analysis.....229

5.3.5 The effect of activation energy U^* on the Lauritzen-Hoffman analysis.....230

5.3.6 Regime transition temperatures as a function of pressure for L-04 copolymer...232

5.3.7 A comparison plot of the effect of pressure on ($\sigma_e/\Delta H_f$) ratio using secondary nucleation theory and Gibbs-Thomson equation.....237

5.3.8 Regime plots of the bulk crystallization kinetics analyzed with half time ($t_{1/2}$) assuming a heterogeneous secondary nucleation (T_∞ = -155 °C, U^*=1500 cal/mole).....241

5.4.1 A plot of band spacing versus T_c shows the effect of applying an opposite shift of 1°C/hexyl/1000 C atom on the curves.....247

5.4.2 A plot of band spacing versus reciprocal supercooling of different materials...248

5.4.3 The effect of temperature, and branch content on the reciprocal band spacing ($1/S$).....249

5.4.4 The effect of supercooling temperatures, and branch content on the reciprocal band spacing ($1/S$).....253

5.4.5 A plot of the secondary nucleation theory versus reciprocal band spacing for different materials.....254

1 INTRODUCTION

The technique of copolymerizing ethylene and octene using single-site metallocene catalysts has produced very promising materials for the polymer industry. Metallocene LLDPE (mLLDPE) film resins have found their place in four important market areas: food packaging, stretched films (mainly cast films), heavy-duty sacks, and diaper sheets. Many polymeric products are manufactured using the injection molding method, where the pressure used exceeds sometimes 2kbar.

Since rheological and mechanical properties of a given copolymer are significantly controlled by its morphology, it is important to understand the morphological changes as a function of pressure. The correlation between melting behavior and morphological changes is very crucial to comprehending the crystallization kinetics of ethylene-octene copolymers.

The P-T phase diagram of PE was constructed decades ago reaching to pressures exceeding 5kbars. The triple point at which hexagonal, orthorhombic, and the molten phase intersect was found by Bassett to be around 3kbar and 220 °C. A recent study of *in-situ* x-ray diffraction has confirmed the shift of triple point to lower pressures and temperatures with decreasing lamellar thickness [1]. Similar effects are expected upon increasing the branch content. Based on the work of Rastogi *et al* [2], the triple point of ethylene-octene copolymers, at pressures lower than 3kbar, represents the intersection of the monoclinic, orthorhombic, and molten phase instead. The main goal of this study is to

construct the phase diagram of ethylene-octene copolymers with relatively low hexyl branches as a function of temperature and branch content, and to gain greater insight into the crystallization behavior of ethylene copolymers.

Using the light intensity technique, the melting behavior of ethylene-octene copolymers at elevated pressures showed complicated behavior. Depending on the pressure and branch content, ethylene-octene copolymers manifest two melting peaks, one of which is reflecting a very thick lamellar structure. The excessively high melting temperatures compared to the equilibrium melting point of orthorhombic ethylene-octene crystals at a specific pressure suggests the formation of extended-chain crystals. The behavior is not retained at atmospheric pressure for low-branched (4 CH_3 /1000 C atom) copolymer because of the occurrence of a eutectoid-like transformation upon reducing pressure and temperature. Copolymer with 11 CH_3 /1000 C atoms, on the other hand, exhibited thick lamellar structures at atmospheric pressure and high crystallization temperatures. Morphological studies using SEM and x-ray diffraction are consistent with the melting behavior.

Different postulates exist on how a random copolymer crystallizes. First: a total exclusion of all defects including chain ends and branches from the crystalline lattice as suggested by Flory. Second: a uniform inclusion of defects in the crystalline lattice as assumed by Sanchez and Eby. Third: a partial inclusion of defects in the crystalline lattice, as was reported by Kim and Phillips. Several parameters control the behavior of defects during crystallization, and hence cause the system to adopt a specific mechanism.

Crystallization at elevated pressures can significantly differ from that at atmospheric pressure. In some cases, extended-chain morphology, rather than folded-chain morphology, is produced at high pressure and high temperature. By studying the melting behavior, morphology, and kinetics, the crystallization mechanism of ethylene-octene copolymer can be deduced.

Strobl *et al* [3] have suggested in some recently published papers a different crystallization mechanism. According to their *in-situ* SAXS experiments on ethylene-octene copolymers, crystallization from the melt always starts through the creation of a mesomorphic layer that spontaneously thickens to a critical value where it solidifies through a cooperative structural transition. The transition produces a granular crystalline layer, which transforms in the last step into homogeneous lamellar crystallites. This model, although consistent in a way with some of the results of this study, does not successfully expound the crystallization mechanism of ethylene-octene copolymers at elevated pressures. Another objective of this research is to scrutinize their conclusions based on the findings and interpretations of our results.

The crystallization kinetics of ethylene-octene copolymers has been studied extensively at atmospheric pressure. It is the objective of this study to investigate the behavior of the copolymers at higher pressures. Lauritzen-Hoffman secondary nucleation theory will be used in analyzing the radial growth rates. Its applicability at higher pressures will be assumed valid. The presence of the three regimes of crystallization in the copolymer with four hexyl branches per 1000 C atoms even at elevated pressures

made it an ideal system for exploring the effect of pressure on regime transitions. However, the critical dependence of regime plots on the equilibrium melting points necessitates first the study of melting behavior.

As is the case in many semi-crystalline polymers, ethylene-octene copolymers mainly crystallize in the form of spherulites, particularly at higher supercoolings. Spherulitic structure is very important industrially and scientifically because it is associated with mechanical weakness and cracking, as well as dominating electrical breakdown behavior and causing lack of optical clarity or the presence of haze in films. For this it is a common practice to add nucleating agents to reduce the spherulite size to the sub micron level. The effect of branch content, pressure, and crystallization temperature on the morphological details of ethylene copolymers, including band spacing, will be considered in this study. The morphology of isothermally and isobarically crystallized samples is studied using optical and electron microscopy, and wide- and small-angle x-ray scattering. The thermal behavior is mainly studied by means of transmitted and depolarized light intensities, and differential scanning calorimetry.

Banded spherulites characterize the orthorhombic morphology of ethylene-octene copolymers when crystallized at atmospheric pressure. For the first time a correlation between growth rate and reciprocal band spacing will be established. The change in slope of the reciprocal band spacing as a function of temperature resembles a regime plot, and occurs at temperatures that coincide with the regime transition temperatures of LPE, and the used copolymers.

2. THEORETICAL BACKGROUND

Isothermal and isobaric crystallization of ethylene-octene copolymers is crucial to understanding the mechanism behind its nucleation and growth kinetics. The observations of optical microscopy during the crystallization process indicated the formation of two different morphologies at certain conditions. A nonspecific morphological feature appears prior to the normal spherulitic structure, and exhibits different growth rates and melting temperatures from the spherulitic growth. A lack of knowledge of the nature of the two-phase system impedes the determination of equilibrium melting point that is important to the crystallization kinetics. Therefore, it was necessary to first investigate the melting behavior of ethylene copolymers and determine its phase diagram.

2.1 Melting Behavior

Melting of a polymer occurs when an ordered crystalline phase converts to a disordered amorphous (molten) phase. Thermodynamically, melting temperature is the temperature at which the thermal energy in a solid material is sufficient to overcome the intermolecular forces of attraction in the crystalline lattice.

The melting behavior of a lamellar polymer crystal is affected by several factors mainly, the lamellar thickness and the surface free energies. For this, it was important to derive an expression of the melting temperature as a function of lamellar thickness and

surface free energy. Melting temperature is strongly dependant on the lamellar thickness and hence the crystallization temperature. Therefore, the equilibrium melting temperature ($T_m°$), which can be defined as the temperature at which infinitely thick crystal will melt, was introduced as a characteristic parameter of the polymer at certain conditions.

2.1.1 Equilibrium Melting Point

In thermodynamics the free energy of formation of a single chain-folded crystal can be written as:

$$\Delta G_f = 4x\ell\sigma + 2x^2\sigma_e - x^2\ell(\Delta f) \tag{2.1.1}$$

where ℓ, x are the thin and large dimensions of the crystal, respectively. Lateral and fold surface free energy are represented, respectively, by σ, σ_e. Δf is the bulk free energy of fusion, and can be approximated at the near melting temperature to be:

$$\Delta f \approx \Delta H_f \frac{\Delta T}{T_m^o} \tag{2.1.2}$$

where the heat of fusion ΔH_f is assumed to be independent of temperature, and the supercooling equals to $\Delta T = T_m° - T_c$.

By substituting **equation (2.1.2)** at the melting point of the crystal into **equation (2.1.1)**, and assuming that x $\gg \ell$ and $\Delta G_f = 0$, Gibbs-Thomson equation is obtained and the melting temperature is defines as:

$$T_m = T_m^o \left(1 - \frac{2\sigma_e}{\Delta H_f \ell} \right) \qquad (2.1.3)$$

The upper equation indicates that a melting point depression from that of the infinite crystal will occur. The amount of depression equals ($2\ \sigma_e / \Delta H_f\ \ell$). By plotting T_m versus $1/\ \ell$ a linear behavior is expected with the intercept being $T_m{}^o$, and the σ_e value is determined from the slope.

Using the kinetic theory of lamellar crystallization from polymeric melts, the Hoffman-Weeks equation related the melting temperature to the crystallization temperature in the following way:

$$T_m = T_m{}^o (1 - 1/\gamma) + T_c/\gamma \qquad (2.1.4)$$

where γ is the fractional degree of thickening above the initial lamellar thickness ℓ_g^*. According to this equation, plotting T_m versus T_c should yield a nearly straight line at low and moderate ΔT [4], with γ^{-1} slope. The intercept of this line with the line $T_m = T_c$ will give an estimate of the equilibrium melting point $T_m{}^o$. It should be noticed that in practice

the lamellar thickening rate increases at higher temperatures and hence increases the value of the measured equilibrium melting points.

For random copolymers the equilibrium melting point depression equation, as derived by Sanchez and Eby [5], is given by:

$$\frac{1}{T_m^o} - \frac{1}{T_m^o(X)} = -\frac{R}{\Delta H^o}\left\{\frac{\varepsilon X_c}{RT_m^o(X)} + (1-X_c)\ln\frac{(1-X_c)}{(1-X)} + X_c \ln\frac{X_c}{X}\right\} \qquad (2.1.5)$$

where a uniform inclusion of defects in the crystalline phase was assumed. $T_m{}^o$, $T_m{}^o(X)$ are the equilibrium melting temperatures of the infinitely large crystal of a homopolymer and that of a copolymer with B counits in the crystalline lattice, respectively. 'X' and 'X_c' are the mole fractions of all B counits in the whole polymer and the mole fractions of the B counits incorporated into the crystalline phase, respectively. ΔH^o is the enthalpy of fusion of the homopolymer and 'ε' represents the excess free energy created by incorporating a B counit into the crystalline phase. 'R' is the universal gas constant.

For $X_c/X=\beta=1$ where all B counits are completely included in the crystalline lattice the upper equation becomes:

$$\frac{1}{T_m^o} - \frac{1}{T_m^o(X)} = -\frac{\varepsilon X}{\Delta H^o T_m^o(X)} \qquad (2.1.6)$$

For complete exclusion of B counits from the crystalline phase i.e.β=0, **equation (2.1.5)** becomes Flory's equation:

$$\frac{1}{T_m^o} - \frac{1}{T_m^o(X)} = -\frac{RX}{\Delta H^o} \qquad (2.1.7)$$

A different approach to the effect of lamellar thickness and branching content on the equilibrium melting temperature of copolymers was introduced by Strobl [6] *et al.* They assumed that for a growing polymer crystallite with a lateral growth face of area 'a' to proceed growing further by a step Δx, all co-units in front of the growth face within a volume '$a\ \Delta x$' have to be removed. This results in a work against the osmotic pressure exerted by the co-units, and is given by:

$$\Delta W = \rho_{osm} a \Delta x \qquad (2.1.8)$$

Assuming random distribution of the co-units along the chain **equation (2.1.8)** can be written as:

$$\Delta W = kTN_B \qquad (2.1.9)$$

where N_B is the number of co-units within the volume $a\ \Delta x$.

Using thermodynamics, and simple mathematical derivations Strobl *et al* expressed the equilibrium melting point depression equation as follow:

$$T_m^o - T_m^o(x_B, n) \approx \frac{k(T_m^o)^2}{\Delta h} x_B + \frac{2\sigma_e T_m^o}{\Delta h} \frac{1}{n} \qquad (2.1.10)$$

where Δh is the heat of melting per monomer, n is the number of monomers composing a stem. As can be noticed, the latter equation superposed the effects expressed by Raoult's law and the Gibbs-Thomson equation. The experimental results of this study suggested the invalidity of the Hoffman-Weeks procedure to determine the equilibrium melting points for copolymers.

2.1.2 Pressure Effect on Melting Temperatures

The effect of pressure on the melting behavior of polymers has not been extensively reported in the literature, although pressure is routinely used in plastics molding and has a significant effect on the growth behavior. Baer and Kardos [7] are one of the first groups to study the effect of pressure on the equilibrium melting temperature for polyethylene. They showed that the melting curve of PE rises indefinitely with pressure at a continually decreasing rate. The Clausius-Clapeyron equation thermodynamically expresses the change in temperature as a function of pressure as follow:

$$\left(\frac{dT}{dP}\right)_{eq}^{-1} = \frac{\Delta H}{T\Delta V} \tag{2.1.11}$$

where ΔH and ΔV are the changes in enthalpy and volume respectively. Clausius-Clapeyron equation could be rewritten as:

$$\left(\frac{dT_m}{dP}\right) = \frac{T_m \Delta V}{\Delta H} \tag{2.1.12}$$

To express the equilibrium melting temperature as a function of pressure the upper equation could be written as follow:

$$\left(T_m^o\right)_p = \left(T_m^o\right)_{atm} \exp\left[\Delta V / \Delta h_f (P-1)\right] \tag{2.1.13}$$

where $\Delta V = V_a - V_c$; V_a and V_c are the specific volumes of amorphous and crystalline material and P is the pressure in atmospheres.

Tseng and Phillips [8] studied the effect of pressure on linear polyethylene. Their results correlated with other studies. The melting and glass transition temperatures were found to be strong functions of pressure, increasing by approximately 20 °C per 1 kbar.

Elevated pressure tends to favor high-density forms leaving fold conformation to be possibly changed. This in turn will have a major effect on the fold surface free energy, and hence the rates of growth of the lamellae and the lamellar thickness [9]. Bassett *et al* [10, 11] showed that an increase in the annealing pressure to beyond the orthorhombic-hexagonal phase boundary, i.e. within the hexagonal phase, increases the lamellar thickness and hence the melting temperature dramatically. They also found that the annealing pressure required to produce a given lamellar thickness decreases as the molecular weight increases.

2.1.3 Phase Diagrams

Polymer crystallization under elevated pressures has been studied more widely in the past few decades. PE, in particular, gained the highest interest among other polymers due to its simple chemical structure, and the amount of significant information already available. The construction of phase diagrams is crucial in understanding and summarizing the changes in melting temperatures and morphology as a function of crystallization temperature and pressure.

The effect of crystallizing polyethylene at high pressures on morphology has been studied thoroughly and widely in the last few decades. Geil *et al* [12] have confirmed the presence of extended chain lamellae and suggested that molecular fractionation may take place during the growth of extended crystals.

Wunderlich *et al* [13,14] studied the formation of 'extended-chain' crystals of PE when crystallized from the melt under high pressures. They varied the pressure, supercooling, molecular weight, and crystallization time to obtain the best conditions for producing a near perfect crystal. The phenomenon of 'extended-chain' material attracted the attention of several people. This is because such altered molecular conformation, if existing, could be expected to produce important changes in electrical and mechanical properties. The reason behind such expected changes is the inherent anisotropy of extended chains, where the properties along the molecular chains vary significantly from those in the transverse directions. Studies, however, showed that crystallization under pressure is not a general mean of producing 'extended-chain' materials [15].

Bassett *et al* [10,11,15] extensively studied the pressure effect on the crystallization behavior of different polyethylene materials. They suggested that only two main solid structures could be formed under high pressure: orthorhombic and hexagonal phases. Based on the melting behavior and morphology they constructed the phase diagram of linear PE as shown in **figure (2.1.1)**. According to the figure the formation of solid orthorhombic structure from the melt occurs with continuity, i.e. there is no transferring phase in between, at pressures below the triple point, which was experimentally found to be about 3kbars. Above the triple point there are two possibilities available. For a very fast cooling rate from the melt, the polymer will show the orthorhombic structure without going into any intermediate phases. On the other hand, slower cooling rates allow the hexagonal phase to intervene.

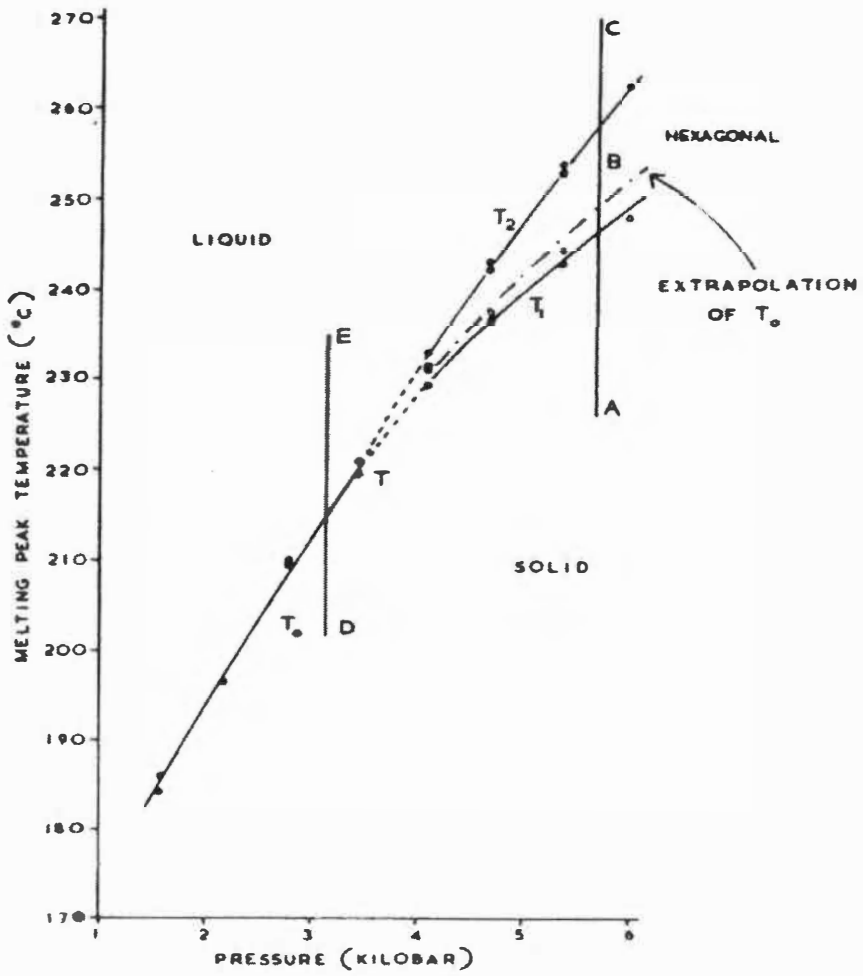


Figure (2.1.1) The phase diagram of linear PE as suggested by Bassett *et.al* [10].

Polyethylene formed in the hexagonal phase has higher melting temperatures, larger lamellar thickness (>1 μm), "cigar-shaped" crystals, and a **c**-axis that is always perpendicular to the hexagonal lamellae. Orthorhombic polyethylene shows the familiar spherulitic texture, with inclination of molecules to form lamellae.

On the other hand, a later study of the isothermal and isobaric crystallization of PE, conducted by Keller [16] *et al*, has shown that direct crystallization from the melt to the orthorhombic phase does not occur even in a region below the triple point. Instead, the liquid-crystal phase transformation always proceeds via the hexagonal phase, which is a metastable state. As a conclusion, the study showed that crystals can only grow in the hexagonal phase, and hence, the lateral growth rate of crystals is controlled by the supercooling temperatures corresponding to the hexagonal crystals, instead of the larger supercoolings from the orthogonal crystals that correspond to the state of thermodynamic equilibrium. This is true for both above and below the triple point regions, as illustrated in the phase diagram shown in **figure (2.1.2)**.

Wright et al [17] reported that aging highly branched ethylene-propylene copolymers at room temperature and pressure revealed a change in crystal structure from orthorhombic to hexagonal. Depending on the comonomer content, only hexagonal crystals were seen in some materials while both hexagonal and orthorhombic phases coexisted in other higher branched materials.

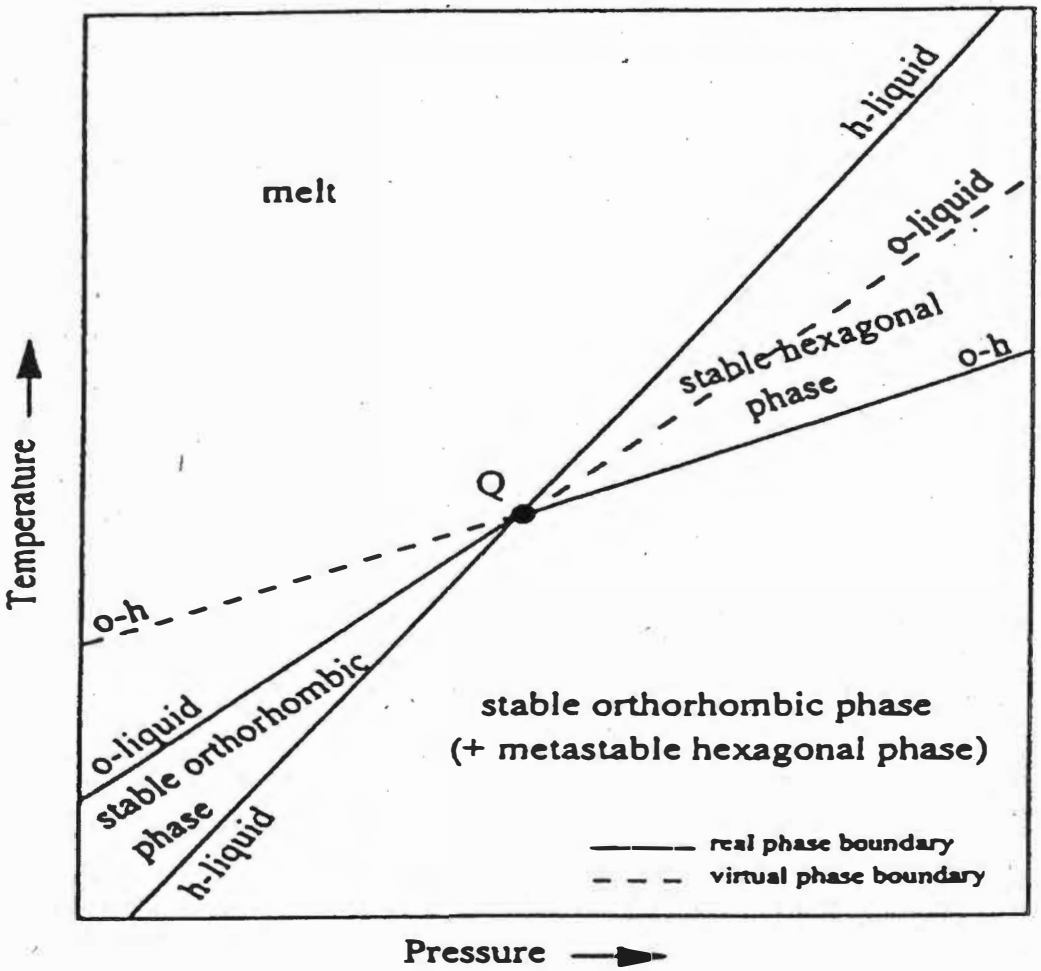


Figure (2.1.2) The phase diagram of PE as suggested by Keller *et. al* [16].

2.2 Diffraction and Scattering Theory

Diffraction and scattering methods are, in general, powerful techniques to reveal information regarding the internal structure of polymers. Two important and widely used techniques are wide-angle x-ray diffraction (WAXD) and small-angle x-ray scattering (SAXS). Wide angle x-ray diffraction (WAXD) describes the structure on an atomic scale, from 0.1-1 nm, and is used to determine the crystal structure of a crystalline polymer e.g. size and shape of the unit cell, crystal class, space group, and the position of individual atoms. In addition, WAXD is also used to determine the degree of crystallinity and crystal orientation of semicrystalline polymers. SAXS on the other hand, describes a structure with a characteristic length of tens to hundreds of nanometers and is used to estimate the long period and hence the lamellar thickness of semi-crystalline polymer, crystal size, and radius of gyration.

The principle of scattering in both techniques is the same. Atomic lattices i.e. regularly ordered three-dimensional periodic arrangements of atoms (crystal), scatter the incident x-ray beam in all directions in space. Scattering is assumed to be elastic and coherent. In elastic scattering the incident and scattered beam (photon) will have the same energy. Coherent scattering, that provides all information on the spatial distribution of atoms, assumes the interference of the scattered beams from different atoms. Constructive interference, where coherently scattered wavelengths are in phase, gives diffraction maxima and occurs at a high atomic density phases (crystals). Destructive interference, where scattered wavelengths are out of phase, results in cancellation of the

waves involved. Incoherent scattering, on the other hand, produces a background signal. Its main source is the Compton scattering and is assumed to be negligible for small angular ranges. The scattered intensity at small angles is usually larger than of those at higher angles [18,19].

2.2.1 Wide Angle X-ray Diffraction (WAXD)

One major application of WAXD is to determine the crystalline structure of a material using Bragg's law:

$$n\lambda = 2d_{hk\ell}\sin\theta \qquad (2.2.1)$$

where n is an integer and defines the order of diffraction, $d_{hk\ell}$ represents the distance between atomic planes of indices h, k, and ℓ. 'θ' is the Bragg diffraction angle. A change in the measured Bragg angle as a function of pressure or temperature, if noticed, indicates a change in the unit cell dimensions and hence, the crystal structure of the polymer.

Wide-angle x-ray diffraction, WAXD, is also used to determine the degree of crystallinity of a polymeric system. To determine the degree of crystallinity, the area under all peaks produced need to be measured. Since the diffraction pattern produced by this method is a result of the superposition of the diffraction pattern of both the amorphous and the crystalline regions, the amorphous peak is arbitrary drawn underneath

the prominent crystalline peaks. The degree of crystallinity can be determined using the following equation:

$$X_c = \frac{A_c}{A_{total}} = \frac{(A_{total} - A_a)}{A_{total}} = 1 - \frac{A_a}{A_{total}} \qquad (2.2.2)$$

where *A* represents the area under the peaks. The upper expression is modified by calculating the correction factors of each peak, as will be discussed in **section 3.5**.

2.2.2 High Temperature X-ray Diffraction

The scattering of the x-rays from an atom will suffer some destructive interference because of the size of the atom. Atoms vibrating about their lattice sites have a larger effective size, and hence the interference effect is larger. Debye and Waller [20] defined and related the parameter (*B*) to the vibrational amplitude of the atom as follow:

$$B=8\pi^2u^2$$

where (*B*) is called the Debye-Waller temperature factor, and u^2 is the mean-square amplitude of vibration of an atom. The temperature factor (*B*) is the same for all directions of vibration of an atom and is therefore called the isotropic temperature factor.

2.2.2.1 Thermal Expansion

The thermal expansion coefficient can be determined by measuring the increase of the lattice constant with increasing temperature. The use of x-ray diffraction to observe thermal expansion is known as 'x-ray dilatometry'. The accuracy of x-ray dilatometry is comparable to that of conventional dilatometry in giving information on thermal expansion. The coefficient of thermal expansion 'α' is given by:

$$\alpha = \frac{1}{a}\frac{\Delta a}{\Delta T} \tag{2.2.3}$$

where 'a' is the initial lattice constant (usually at room temperature), and Δa is the change in the lattice constant when the temperature is changed by ΔT. A plot of the thermal expansion ($\Delta a/a$) versus ΔT or the temperature (T) is a straight line with α slope.

The above linear relationship does not accurately describe the real polymer systems, and **equation (2.2.3)** should be replaced by the polynomial expression:

$$a + \Delta a = a\left[1 + A\Delta T + B(\Delta T)^2 + C(\Delta T)^3 + \cdots\right] \tag{2.2.4}$$

Although **equation (2.2.4)** provides a good mathematical fit to experimental data, the disadvantage of requiring more than one constant (i.e. A, B, C, etc) to describe the thermal expansion behavior demanded an alternative expression given by:

$$a + \Delta a = a\left(1 + R\right)^{\left(1+T/273\right)^{1.5}} \tag{2.2.5}$$

where R is an expansion constant that describes the thermal expansion behavior.

2.2.3 Small Angle X-ray Scattering (SAXS)

Due to the interaction of the incident x-rays with the electrons of an atom, SAXS is sensitive to inhomogeneities of the electron density. Since the lamellar texture formed in LLDPE can be viewed as a periodic fluctuation in electron density caused by the differences in the density of the amorphous and crystalline phases, SAXS is employed to measure the long period (L) parameter, which represents the average center-to-center distance of the stacked lamellae.

By applying Bragg's law to the intensity maximum at a specific angle, long period (L) can be estimated in real space using the following equation:

$$L = \frac{2\pi}{q_{peak}} \tag{2.2.6}$$

Since the thickness of the amorphous layers separating the lamellae is not known, the long period value calculated using the upper equation is only an index of the periodicity caused by the lamellar texture.

Bragg's law assumes a regular repeat of planes in only one direction. This is not the case in semi-crystalline polymers where the repeating planes do not align parallel and generate a different reflection condition. Because of this, the Lorentz correction is applied where the intensity is multiplied by a factor q^2. The long periodicity can hence be obtained from the maximum in the plot of $I(q).q^2$ against q. Lamellar thickness (l) is then determined by multiplying the long period by volume crystallinity obtained using DSC, density measurement, or using WAXD and density measurements.

The fundamental law in scattering methods is based on that the amplitude of the scattered wave $A(\boldsymbol{q})$ is the Fourier transform of the electron density distribution $\rho(\boldsymbol{r})$ in the sample. The scattering vector $\boldsymbol{q}$ defines the geometry of the system and is defined as $\boldsymbol{k}=\boldsymbol{k}_o + \boldsymbol{q}.\boldsymbol{q}$, where $\boldsymbol{k}$ is the wave vector of the incident wave, and $\boldsymbol{k}_o$ is the wave vector of the wave scattered at an angle 2θ. The previous formula means that the amplitude in a direction defined by vector $\boldsymbol{q}$ is related to one term of the Fourier expansion of $\rho(\boldsymbol{r})$. The absolute value of the scattering and wave vectors, respectively, are given by, $q=|\boldsymbol{q}|=(4\pi/\lambda)\ sin2\theta$, and $k= k_o= |\boldsymbol{k}|= 2\pi/\lambda$, where 2θ is the scattering angle.

2.2.3.1 Correlation Function

Assuming that the scattering particles are thin and laterally extended lamellae, the Lorentz corrected scattering intensity I_{LC} (q) can be related to the one-dimensional electron density correlation function $K(z)$ defined as:

$$K(z) = \langle \delta\rho(\xi - z)\delta\rho(\xi) \rangle_{\xi} \tag{2.2.7}$$

where $\delta\rho$ denotes the local fluctuations in the electron density, i.e. the difference between the average and the local electron density, 'z' is the coordinate in the direction perpendicular to the surfaces of the lamellae.

The correlation function can be obtained by the Fourier transform of the Lorentz corrected scattering curve:

$$K(z) = \frac{1}{2\pi^2} \int_0^{\infty} I_{abs}(q).q^2.\cos(qz)dq \tag{2.2.8}$$

where I_{abs} (q) is the measured absolute intensity and equals to the ratio of the scattered intensity to the intensity of the primary beam (or the intensity of single electron) per unit volume:

$$I_{abs}(q) = \frac{I(q)}{I_e(q)V} \tag{2.2.9}$$

For z = 0, the $K(z=0)$ will be equal to the average of the square of the local electron density fluctuations as shown from **equation (2.2.7)**, and the cosine function in **equation (2.2.8)** will equal to one. By dividing **equation (2.2.8)** by the correlation

function at $z = 0$, $K(0)$, along with the definition of the Lorentz corrected intensity, a normalized one-dimensional correlation function, $K(z)$, is obtained:

$$K(z) = \frac{\int_0^\infty q^2 I_{abs}(q)\cos(qz)dq}{\int_0^\infty q^2 I_{abs}(q)dq} \qquad (2.2.10)$$

The measured intensity $I(q)$ in the normalized correlation function do not need to be absolute to hold.

The second derivative of the correlation function, $K''(z)$, shows the distribution of distances between interfaces [21]:

$$K''(z) = \frac{O_s}{2}\Delta\rho^2[h_a(z) + h_c(z) - 2h_{ac}(z) + h_{aca}(z) + h_{acc}(z)...] \qquad (2.2.11)$$

where O_s represents the specific inner surface, which is simply the surface area divided by the volume, and $\Delta\rho$ gives the electron density difference between the crystalline and amorphous regions. The upper equation describes the distribution of the lengths of all chords that can be drawn between the interfaces in a two-phase system. Only the first three terms are of practical importance. They give the distribution of the thickness of the amorphous and the crystalline layers (h_a and h_c), and of the sum of both resulting in the

long period 'L' (h_{ac}) [22]. If the system possesses sharp phase boundaries, the asymptotic behavior of $I(q)$ is described by Porod's law:

$$P = \lim_{s\to\infty} I(q).q^4 \qquad (2.2.12)$$

Porod's coefficient 'P' is directly related to the interface area per unit volume, O_s. Fitting a horizontal line to $I(q).q^4$ versus q (Porod plot) in the correct region yields a constant which is proportional to the internal surface. The validity of Porod's law breaks down for distances smaller than r_o, of the order of the interfacial thickness, and consequently it will deviate from q^{-4} dependence at some $q \approx r_o^{-1}$. **Equation (2.2.11)** can be written in an integral form as follow:

$$K''(z) = -4\pi^2 \int_0^\infty \left[\lim_{q\to\infty} \left(I(q).q^4 \right) - I(q).q^4 \right] \cos(qz)dq \qquad (2.2.13)$$

Strobl *et al* [22,23,24] reported that the application of a graphical extrapolation procedure to the one-dimensional correlation function, $K(z)$, and its second derivative, $K''(z)$, permits direct determination of the following structure parameters: crystallinity, the specific inner surface, the average lamellar thickness, the long spacing, and the electron density difference if absolute values of the scattering intensities were measured. This procedure can be used to treat a periodic two-phase system or lamellar systems with low degree of order.

A summary of the information derived from the schematic graph of $K(z)$ is shown in **figure (2.2.1)**. **Figure (2.2.2)** shows the electron density distribution and its corresponding correlation function $K(z)$ for somewhat more physically realistic systems. The slope of the straight line forming the "self-correlation triangle" is related to the specific inner surface O_s as follow:

$$\frac{dK}{dz} = -\frac{O_s}{2}(\eta_c - \eta_a)^2 \tag{2.2.14}$$

where η_c and η_a represent the crystalline and amorphous electron densities, respectively. Extrapolating the straight line to $z = 0$ the invariant Q is obtained:

$$Q = w_c(1 - w_c)(\eta_c - \eta_a)^2 \tag{2.2.15}$$

where w_c represents the crystallinity. The invariant Q defines the 'ideal two-phase structure' with sharp boundaries. To determine the number-average lamellar thickness, an extrapolation of the same straight line to the other side is required. The extrapolated line cuts the horizontal line at $z = l$, and the abscissa $K = 0$ at:

$$z_0 = l(1 - w_c) \tag{2.2.16}$$

The base-line coordinate is:

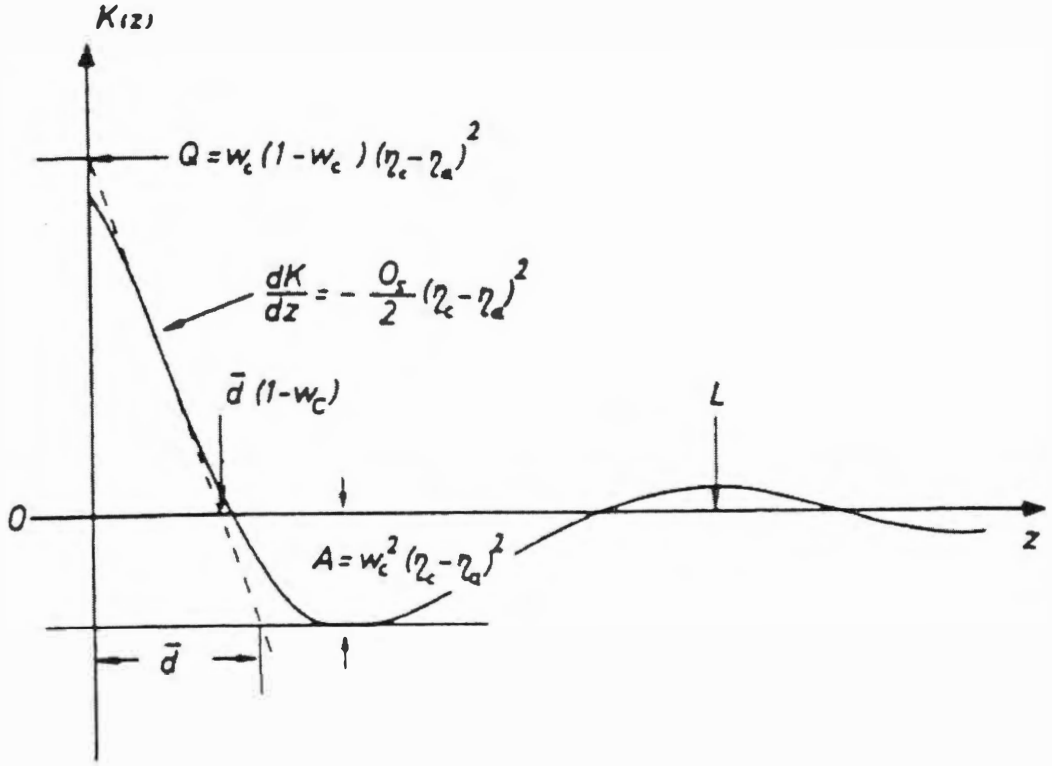


Figure (2.2.1) Schematic graph of $K(z)$ showing the 'self-correlation triangle'.

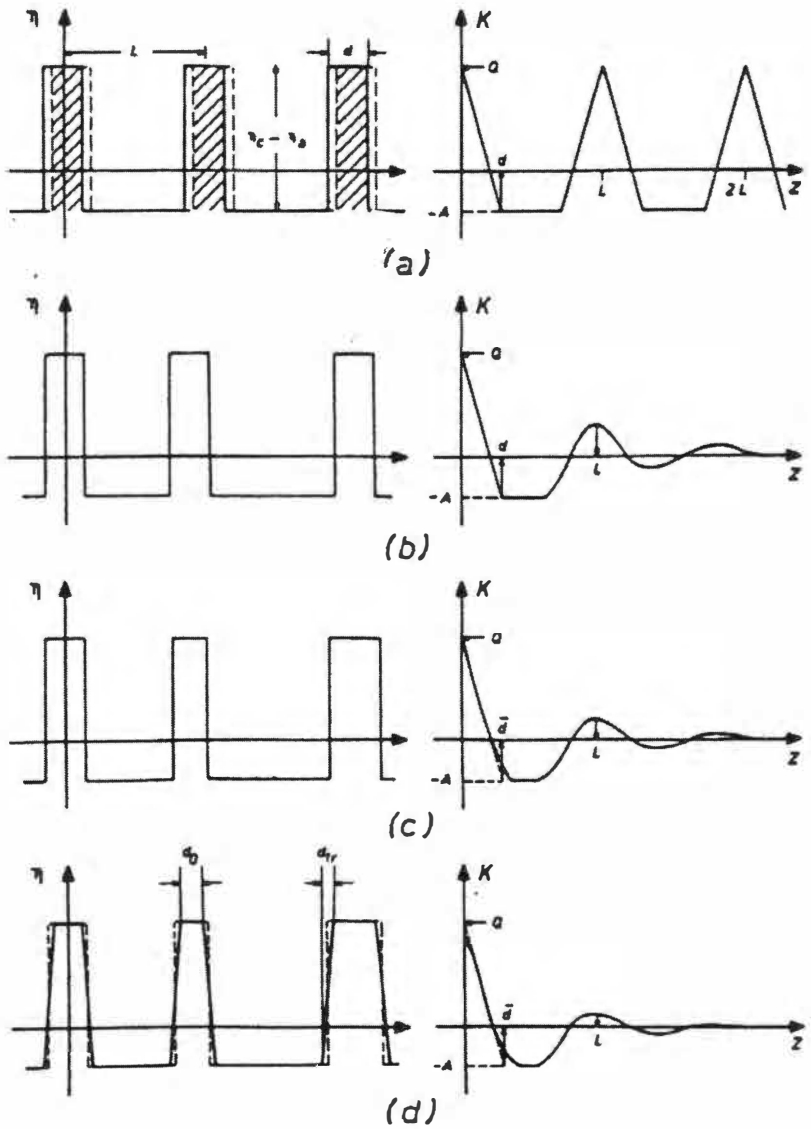


Figure (2.2.2) Electron density distribution and correlation function $K(z)$.

$$A = -w_c^2(\eta_c - \eta_a)^2 \tag{2.2.17}$$

SAXS results can be used to determine the "Linear crystallinity", where:

$$w_l = \frac{B}{Q+B} \tag{2.2.18}$$

where, $-B$, denotes the ordinate of the 'base line' of $K(z)$ and Q is the integral scattering power equal to $K(z=0)$. For a sample densely filled with stacks of laterally extended lamellae 'w_l' equals the global volume fraction crystallinity 'w_v'. For lamellae containing a certain portion of non-crystalline material, and a heterogeneous system, $w_v < w_l$. A plot of the second derivative, $K''(z)$, will give information about the thickness of the amorphous and crystalline layers denoted by 'd_a' and 'd_c', respectively, according to Strobl *et al* (**figure 2.2.3**).

2.3 Crystallization Kinetics

Interest in studying the nucleation and growth kinetics of polymers crystallized from the melt has risen in the past few decades. This interest was driven by the massive application of the melt-crystallized polymers in industry. Isothermal and non-isothermal crystallization of polymers were extensively studied both theoretically and experimentally. A brief introduction to the theory of crystallization is presented in this section.

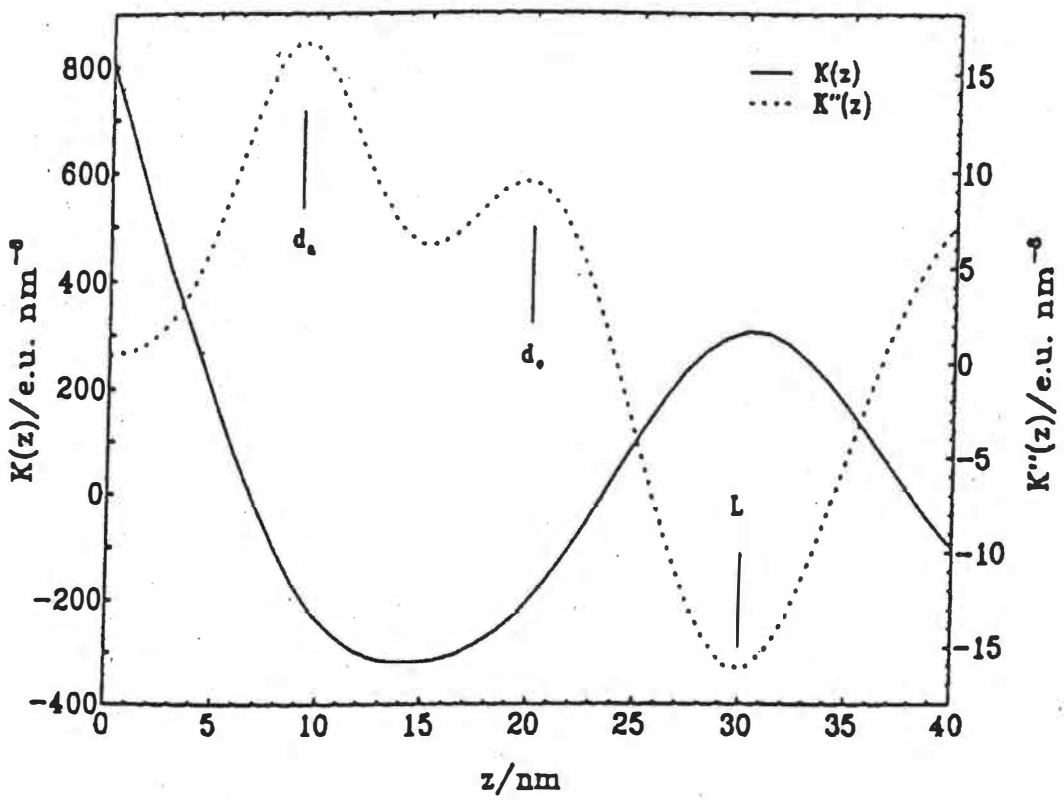


Figure (2.2.3) The correlation function $K(z)$ and its second derivative $K''(z)$.

Melt-crystallized PE exhibits a lamellar morphology with a considerable degree of chain folding of some type on the upper and the lower surfaces of each lamella. This model replaces the old model of 'fringed micelle', which describes the polymer crystallization in a way similar to crosslinks.

Although chain folding is a widely accepted phenomenon, the nature of the fold surface is still a controversial issue. The idea of solely adjacent re-entry folding as the means of incorporating a molecule into a crystal is ideal and oversimplified. Flory [25] suggested a 'random switchboard' surface with only accidental adjacency i.e. the probability that a lamella executes a transit to an adjacent site is near zero. This model does not consider the consequences for surface packing of the emerging stems, which generates surface densities larger than the known values [26]. To solve the problem of overcrowding it should be assumed that the stems are inclined at an angle to the lamellar surface. Although this improved the values of the surface densities determined by the model, some discrepancies still exist.

2.3.1 Crystallization Theories

Mandelkern *et. al.* [27] developed a specific theory for the rate of crystallization of chain molecules and concluded that the rate of nucleation and rate of spherulite growth should both pass through a maximum as temperature varies. They predicted that the maximum rate of crystallization should be observed between 0.8 and 0.9 T_m. The bell-shaped dependence of the lamellar growth rate on temperature is typical of a system in

which there is nucleation control at high temperatures, and diffusion control at low temperatures.

Hoffman *et. al.* [4] modified the original Lauritzen-Hoffman [28,29] nucleation approach several times to extend its range of applicability. The current version of the secondary nucleation theory included among several parameters the treatment of regime III and the nucleation-based treatment of the onset of 'quantized' chain folding at low and moderate molecular weights. The fundamental concept of the secondary nucleation theory is that the critical nucleus must be formed by condensation of stems of approximately equal length on the substrate crystal. The theory differs from the classical nucleation theory applied to elemental systems in which the freedom of action of individual molecules or atoms is not present in the secondary nucleation theory. The main mathematical expressions of the theory are listed in the following section.

Sadler *et al* [30,31,32] has developed a model of polymer crystallization based on the surface roughening of the growth faces, where roughness produced microscopically at high temperatures was generated by thermal fluctuations in equilibrium. According to this model, nucleation of a new layer, suggested by secondary nucleation theory, is not required. In order to understand the effect of loops created at the growth surface, Sadler *et al* has introduced the concept of 'pinning points', which represent the points on the crystal boundary that cannot extend. Stems formed at the crystal edge are shorter than the lamellar thickness and are generally pinned due to the existence of additional stems in the growth direction. Pinned stems can only be freed by fluctuations that remove some of the

material in the edge. The saddle point on rough surfaces, as was concluded by Sadler's model, is a state of low entropy instead of the high-energy state of nucleation. The low entropy depends on the crystal thickness, similar to that of the high enthalpy state in secondary nucleation.

Keller *et al* [33] described the crystallization from the melt process as a transformation from an isotropic phase (melt) to a one unit, two or more anisotropic phase variants. The latter phases formed could be in the form of a poly-morphic crystal structure or mesomorphic state, including liquid crystals. The stability of these phases with respect to each other cannot be achieved, for this reason one of the phase variants produced will need to be meta-stable. They have introduced the idea of 'thickening growth' which is different from the 'lamellar thickening' that usually corresponds to rearrangements within already crystallized material as illustrated by the secondary nucleation theory.

Hikosaka *et al* [34,35] proposed a new kinetic theory named 'Chain sliding diffusion theory'. The theory shows that the lamellar thickening growth rate is large when polymers crystallize into the mobile phase (meta-stable phase, e.g. hexagonal phase) where sliding diffusion is distinguishable. As a result extended chain single crystal ECSC is formed. On the other hand, polymers crystallize into the immobile phase (e.g. orthorhombic phase) where sliding diffusion is low will form a folded chain single crystal. Hence, 'lamellar thickening growth' mechanism based on chain sliding diffusion is not similar to the 'lamellar thickening' behavior. The former is a crystallization process

of a single lamella within the melt where new chains can be supplied easily from the melt. The latter is a recrystallization process of the stacked lamellae where no chains can be supplied and each lamella will thicken due to thermodynamic driving force.

Imai *et al* [36,37] investigated the ordering process in the induction period of crystallization from the viewpoints of orientation fluctuations, chain conformation, and the structure size. According to their experimental results, crystallization process is composed of two steps: 1) the induction period where density fluctuation appears, and 2) the growth of density fluctuation reaches certain value where crystallization starts and the stacked lamellae are formed.

The induction period is the step where randomly entangled polymer chains transform to the regular aligned process. It could be divided into two stages: i) The early stage, where its scattering behavior conforms to Cahn's linearized theory for spinodal decomposition [38], predicts that the wavelength of density fluctuations keeps a constant value and the amplitude of the fluctuations increases exponentially with annealing time. ii) The late stage, where the scattering behavior agrees with Furukawa's scaling theory [39] predicting that the amplitude of the density fluctuations grows with annealing time while it keeps self-similarity.

Imai *et al* concluded that, the increase in the persistence length, which might be caused by the conformational changes from gauche to trans form, induces the parallelization of the polymer chains having the spinodal decomposition kinetics, and

hence 'longitudinal adjustment' occurs. As a result a more efficient packing of the parallel oriented chains is produced to form the crystal nucleus. Nucleation starts at regions with localized fluctuations of density if the nuclei are larger than a critical size. Chain flexibility is the controlling parameter to this mechanism.

Using simultaneous small- and wide- angle X-ray scattering method Wang *et al* [40] studied the early stages of melt crystallization in PE and have observed a lack of any increase in the spacing or invariant with time. This evidence argues against the idea of that, the spinodal decomposition acts as a precursor to the crystallization process. Instead, they suggested that the early stages of crystallization follow the classical nucleation and growth behavior with a simple Avrami expression.

Strobl *et al* [41] gave a different explanation to the crystallization process from the melt for homopolymers and copolymerized derivatives. They used, beside other materials, two ethylene/octene copolymers similar to the ones used in this study and suggested, instead of the nucleation and growth mechanism, a two-step process. The first step is building up an initial form of lower order at the crystallization line. This initial structure could be composed of crystal blocks in planar assemblies, with a size represents the minimum necessary to retain intrinsic stability. The second step is the stabilization of the initial structure that ends up in the state with a layer-like morphology that melts at T_m. Stabilization results from the merging of the crystal blocks into a continuous lamella without a change in the lamellar thickness.

2.3.1.1 Secondary Nucleation Theory

The Lauritzen-Hoffman theory is a widely accepted theory that describes, kinetically, the linear growth rates of polymers. According to this theory, growth rates are functions of crystallization temperatures and depend on some combination of the net surface nucleation rate and the layer thickness. The dependence of the surface nucleation process on supercooling temperature results in producing three different regimes of crystal growth denoted as regimes I, II, and III.

A general expression of crystal growth as described by Lauritzen and Hoffman may be written as;

$$G = G_0 \exp\left\{\frac{-U^*}{R(T_c - T_\infty)}\right\}\exp\left\{\frac{-K_g}{T_c \Delta T f}\right\} \qquad (2.3.1)$$

where G is the growth rate, G_o is the growth rate constant, U^* is the activation energy of polymer diffusion and is independently estimated, R is the universal gas constant, T_c the crystallization temperature, T_∞ = T_g -30 (K) is a hypothetical temperature where all motions associated with viscous flow cease, the supercooling ΔT is equal to T_m^o-T_c, and 'f' is a correction factor to compensate for the error in ΔH_f^o at high supercooling. ΔH_f^o is the heat of fusion per unit volume of crystal at the equilibrium melting point. The correction factor can be written as:

$$f = \frac{2T_c}{\left(T_m^o - T_c\right)} \tag{2.3.2}$$

The nucleation rate constant K_g is given as:

$$K_g = \frac{jb_o\sigma\sigma_e T_m^o}{k\Delta H_f} \tag{2.3.3}$$

'b_o' is the width of the chain **(figure 2.3.1)**, σ and σ_e are the lateral and fold surface free energy, respectively. 'k' represents the Boltzmann constant. The constant 'j' equals to '4' in regimes I and III, and '2' in regime II. Phillips and Vatansever [42] were the first to report experimental observations of the three regimes of *cis*-polyisoprene fraction. For 314 000 molecular weight fraction, the slope ratio of regime I-regime II transition was equivalent to the 2.0 theoretical value and equaled to 1.86.

Lauritzen-Hoffman theory introduced the rate of secondary nucleation, denoted by ***i***, and the lateral spreading ***g***, as two competing rates resulting in three different regimes **(figure 2.3.2)**. Regime I occurs at lower supercoolings when $i \ll g$; in regime II '***i***' is of the order of ***g***, and regime III occurs at higher supercoolings where **i >g**. In terms of these variables the growth rate is proportional to **i** in regimes I and III, and to $(ig)^{1/2}$ in regime II. This difference in dependence is because of the free energy term in the nucleation exponential, which in regime II is half of that in regimes I and III.

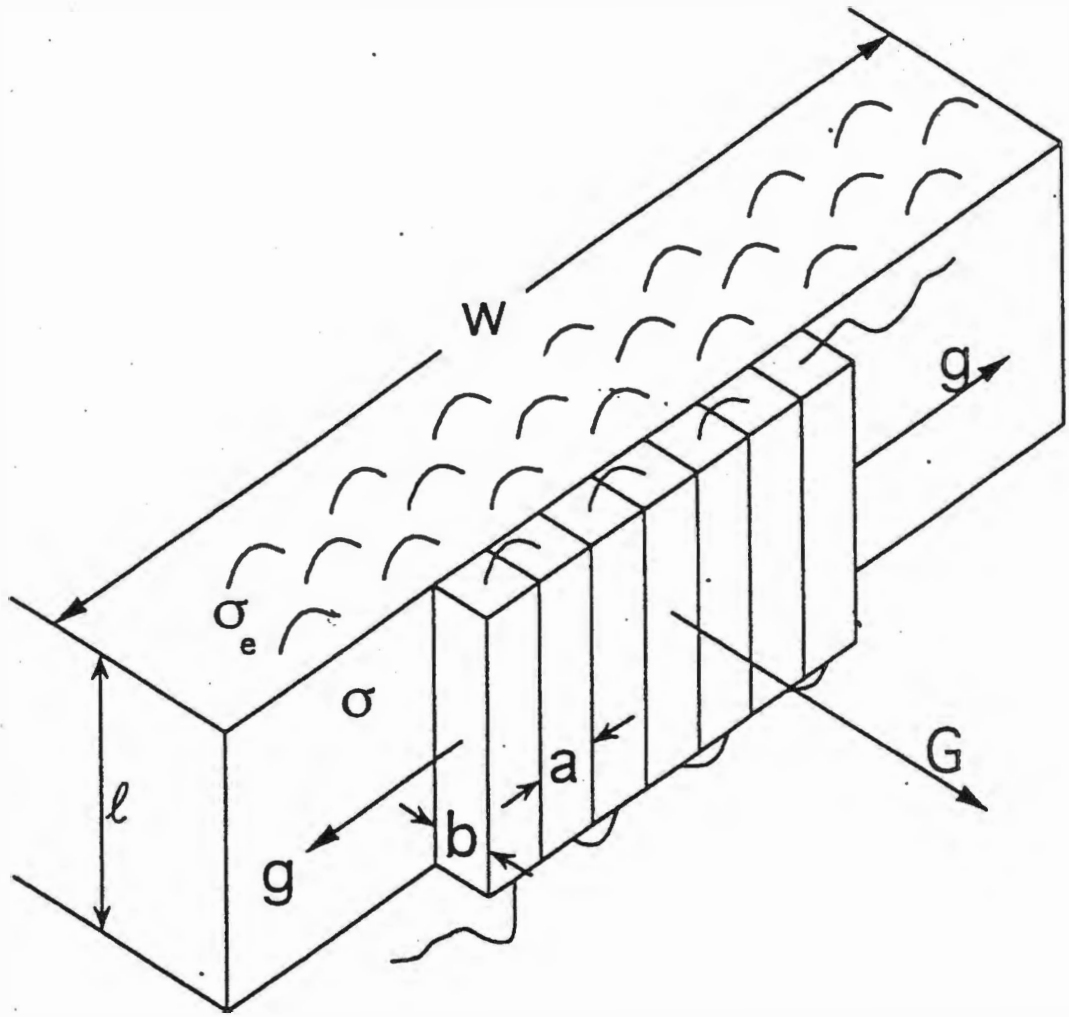


Figure (2.3.1) Polymer chain folding of the adjacent re-entry model in one lamella.

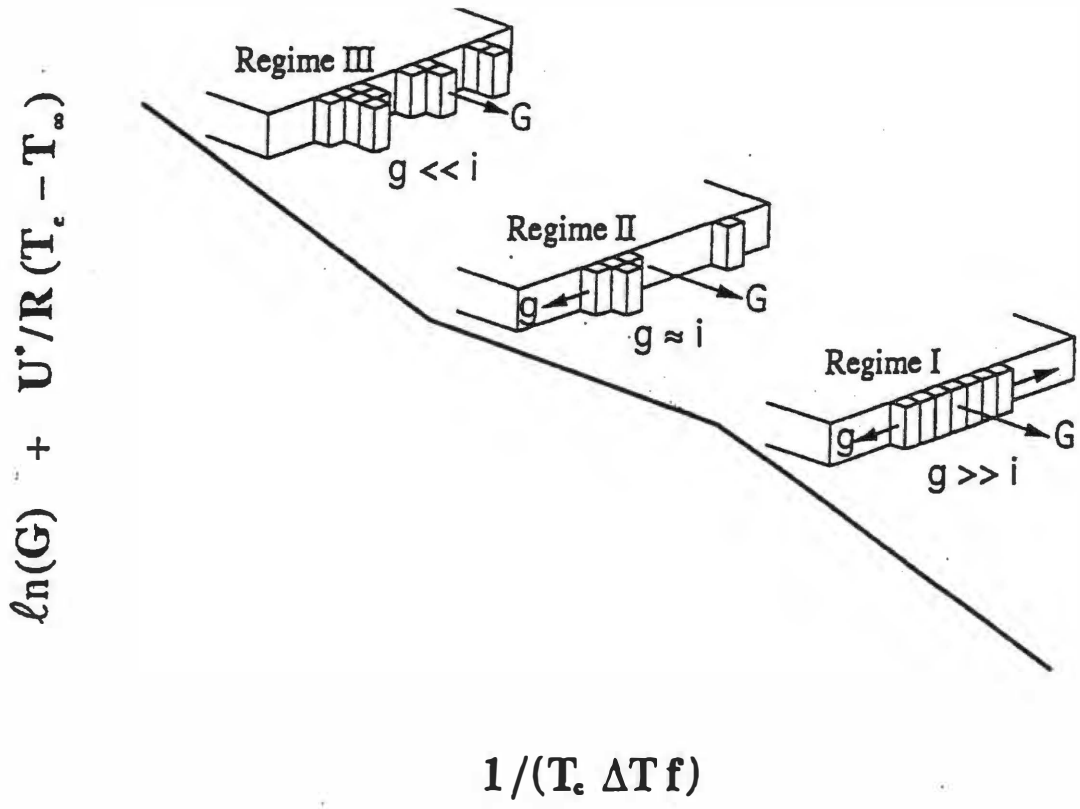


Figure (2.3.2) Schematic of regime analysis.

Hoffman and Miller [4] discussed the concept of reptation theory in polymers and used secondary nucleation theory and experimental results to estimate the secondary nucleation, i, rate of lateral spreading, g, substrate width, L, reeling time, r, and initial lamellar thickness, l_g^*. Regime behavior varies from one polymer to another. For example ethylene-octene copolymer, used in this study, shows all three regimes at atmospheric and elevated pressures. Similar material with higher branch content shows only regimes II and III [43]. High molecular weight isotactic polypropylene showed regimes II and III when crystallized at atmospheric pressures. At 150 Mpa, on the other hand, all three regimes appear [44]. PET crystallized at atmospheric pressure showed only regimes I and II, as reported by Tseng [45].

By plotting $log\ G+(U^*/R\ (T_c-T_\infty))$ versus $(1/\ T_c\ \Delta T\ f)$ a linear behavior is observed, where $\sigma\sigma_e$ can be obtained from the slope. The equilibrium melting point has to be determined in a separate experimentation. The slope represents the nucleation constant K_g defined by **equation (2.3.3)**, where j is 4 for regimes I and III, and 2 for regime II. The heat of fusion ΔH_f =2.80x10^9 erg.cm^{-3}, the Boltzman constant k=1.3806x10^{-16} erg.molecule^{-1}.deg^{-1}. The calculated lateral and fold surface free energies for PE are 11.8 and 90erg.cm^{-2}, respectively. The layer thickness b_o was 4.15x10^{-8} cm.

An estimated value of σ can be calculated using the Hoffman modification of the Thomas-Stavely relation:

$$\sigma = \alpha \Delta h_f \sqrt{a_o b_o} \tag{2.3.4}$$

where $\alpha \approx 0.1$ for most polymers. The work done by the chain, denoted by 'q', to form a fold can be calculated using the following equation:

$$q = 2a_o b_o \sigma_e \tag{2.3.5}$$

2.3.1.2 Criticism of secondary nucleation theory

Lauritzen-Hoffman theory was based on the assumption of adjacent re-entry chain folding, where all successive stems belong to one molecule. This assumption was used to simplify the theory and reduce calculations. Using 'Gambler's Ruin' method, Hoffman *et al* [46] reported a probability of adjacent re-entry '$\mathbf{P_{ar}}$' close to 0.7 in regime I. They noticed a 'quantized' chain folding effect, where an abrupt change in the fold surface free energy occurs with the increase of the chain length. This 'quantized' folding highly suggests the high degree of adjacent re-entry. In regime III the adjacency is less, and $\mathbf{P_{ar}}$ is typically 0.3-0.4.

The formation of extended chain materials under certain conditions, discussed in **section (2.1.2)**, contradicts with the basic assumption of LH theory of having large number of folded chain stems.

As mentioned earlier, Sadler has developed a model for polymer crystallization based on the concept of surface roughening. Consequently, roughening forms straight as well as smoothly rounded (curved) crystals. Straight and curved edges exhibit (110) and (200) growth faces, respectively. The kinetically dominant growth front in PE, according to LH theory, is the {110} faces, which is also the most densely packed. The {200} fronts grow slower than {110} ones.

Experimentally observed curved crystals raised some challenges to the validity of the standard nucleation model. To solve this problem Mansfield [47] proposed the idea of strained crystals. The strain results from the mutual repulsion of the folds in the {200} sectors, and can produce values of the substrate completion rate near the rate of advancement of the adjacent sector. Miller and Hoffman suggested that the lattice strain was a major source of additional retardation factor and embodied this effect in the parameter σ_s. This modification enabled them to explain the presence of the curved edges.

2.3.1.3 Andrews Theory

According to the secondary nucleation theory, the formation of a coherent monolayer nucleus on a complete growth face helps the rapid completion of a new layer of crystal. A modified view was introduced when Andrews *et al* [48] suggested the incorporation of a whole single molecule into the growing crystal, which implies the

elimination of all molecules containing fewer than a certain number of monomer units from the crystalline phase. As a result, the expression 'secondary nucleus' is replaced by 'molecular nucleus' as suggested by Wunderlich. The latter view is wholly consistent with the reported work of Andrews.

The minimum number of crystallizable units required in sequence to form a secondary nucleus, N, can be found using the following equation:

$$\ln G \cong -(N-1)\beta + \ln G_o \qquad (2.3.6)$$

where G is the growth rate of the polymer containing imperfections, G_o is the growth rate of an infinite homopolymer, and β is the fractional content of foreign units. A plot of *ln G* versus β should be linear up to $\beta \approx 0.1$, with a negative slope of (1-N) and an intercept at $\beta = 0$ of *ln G*. Using the upper equation Andrews *et al* calculated a minimum of three stems required to form a 'nucleus' in the *cis*-polyisoprene.

Using Andrews theory, Phillips *et al* [49] have studied the effect of crosslinking of linear PE on its crystallization kinetics. They applied Andrews analysis over the region in which the crosslinks are excluded, and found that the slope of the produced line increased with increasing the crystallization temperatures; indicating an increase to the size of the critical nucleus as a function of crystallization temperature. In agreement with Andrews model, the number of stems found for different gel fractions suggested that the nucleus

consists of multiple stems, although, the number of stems calculated in both studies are different. This is true for regime III. Regime II, on the other hand, gave a number of stems equals to one.

Phillips *et al* concluded that, the controlling factor of lamellar thickness is the chain length between crosslinks and not temperature. They also postulated that the II-III regime transition is the result of a change in nucleation mechanism from a single-stem nucleus to a multiple–stem nucleus.

Another model, suggested by Fischer [50], used the concept of widely spaced stem clusters, where the molecule tends to form clusters of a few stems, each of which are joined by amorphous sections of the same molecule. Obtaining the nature of the fold will be of concern while conducting this study.

2.3.2 Bulk Crystallization Kinetics

Various techniques were employed in bulk crystallization measurements. Earlier studies used dilatometric methods to measure volume changes. Less laborious techniques used are, 1) Differential scanning calorimetry (DSC), which measures the released energy due to crystallization as a function of time. 2) Transmitted polarized light intensity, which measures light intensity as a function of time. The latter technique was used in this study because of its convenience.

Data obtained from the bulk growth kinetics are usually handled in two ways: 1) Avrami analysis, which produces data of morphological relevance, and 2) Half-time analyses, which produce data of kinetic signification. The latter was used in this study for comparison purposes.

2.3.2.1 Half-time Analyses

Half time is the time needed for the crystallization process to be half complete, and denoted by ($t_{1/2}$). Substitution of 'G' by '$t_{1/2}$' in **equation (2.3.1)** allows an estimation of the homogeneous or sporadic influence.

Homogeneous nucleation occurs when the nuclei form spontaneously, where the number of nuclei increases with time. A linear relationship is obtained for this nucleation when plotting

$$\ln (t_{1/2}) + U^*/2.3R(T_c-T_\infty) \text{ versus } 1/T_c\,(\Delta T)^2 f^2$$

Heterogeneous (or instantaneous) nucleation takes place when a foreign surface such as impurity, motes, and wall of container already exists in the system. The number of nuclei remains constant with time. Plotting

$$\ln (t_{1/2}) + U^*/2.3R(T_c-T_\infty) \text{ versus } 1/T_c\,(\Delta T) f$$

will give a linear relationship for this kind of nucleation.

2.3.3 Crystallization Kinetics at Elevated Pressures

Phillips *et al* [51,52,53,54] conducted the first extensive studies of the influence of pressure on growth kinetics. They studied the lamellar growth kinetics of *cis*-polyisoprene at pressures up to 4kbar. The two main conclusions determined were (a) Lauritzen-Hoffman theory would be applicable, for the pressure considered, provided that, all parameters (e.g. glass transition, and equilibrium melting temperatures) were corrected for the effect of pressure. This can be true for all polymers. (b) At about 0.75kbar a sudden increase in the surface free energy was observed. This increase was explained in terms of a change in the conformational energy of the fold different from that encountered at atmospheric pressures.

Tseng [8,45] studied the radial growth kinetics for linear polyethylene. Results obtained in this study showed no change in the fold free surface energy as a function of pressure up to 2kbar, which implies that the folds produced under these conditions are short, uniform, and tight.

Measuring the equilibrium melting temperature of a polymer crystallized under elevated pressures can be obtained from **equations (2.1.3)** and **(2.1.4)**. The equations are assumed to be valid for high-pressure crystallization provided that the measurements of melting points and lamellar thickness are conducted *in-situ.* According to **equation**

(2.1.3), a decrease in the lamellar thickness at higher pressures will increase the equilibrium melting point depression, and hence increase the supercooling temperatures.

2.4 Morphology

Polymer morphology has gained a significant importance in the last four decades due to the wide information it reveals about the formation of crystals in the polymeric materials. It is considered as the past history record of the polymer and is a determinant of the materials properties. Studies in the past concentrated on the solution-crystallized polymers. New techniques of sample preparation and powerful electron microscopes eased the way to investigate the melt-crystallized polymers. Molecular chain folding underlying the lamellar habits is the remarkable phenomenon of solution- and melt-crystallized polymers.

Melt-crystallized polyethylene was reported to form two main morphological structures: axialites and spherulites. The formation of any one of the structures is controlled by several parameters e.g. crystallization temperature, pressure, molecular weight, and branch content in copolymers.

2.4.1 Axialites

Formation of axialites occurs usually at low supercooling temperatures, where less frequent lamellar branching is allowed and lamellae are organized into a rod like

entities. Tie molecules or crystals as suggested by Hearle [55] may limit the extent of splaying in the axialites. In certain conditions axialitic structure is a result to the formation of extended-chain crystals.

2.4.2 Spherulites

Hoffman [4] has reported three types of spherulites: non-banded spherulites, highly banded spherulites, and irregular spherulites where irregular coarse bands were observed. This irregularity is due to the separation of fingers of crystalline polymer by regions that contain a poorly or non-crystalline material and is called cellulation [56].

The formation of spherulites starts with a small fibrous nucleus followed by the formation of a sheaf-like embryo, gradually developing a spherulite. In a fully developed spherulite the crystal lamellae are oriented in the radial direction (outward direction) parallel to the b-axis, and fill the interior space by branching. Frequency of branching will affect the space filling and determine what structure will be formed, where significantly frequent branching will form spherulites, otherwise axialites will be formed. The chain direction (c-axis) is found to be perpendicular to the radius of the spherulite.

2.4.2.1 Banded Spherulites

Banded spherulites were first reported in 1952 when Jenckel [57] observed them in polyamides, and attributed their formation to eutectic-like variations in composition

along the spherulite radius. Keller [58] has reported them in PET and more correctly attributed their appearance to the helical rotation of the optic axes of the crystallites.

The mechanism of formation of banded spherulites is still debatable. Although it is agreed that in the *S*-shaped lamellae the molecular c-axis spirals about the b-axis when traveling along the radius of a banded spherulite, no general agreement has been reached on how crystalline orientation twists or what causes it to do so. Most of the studies were conducted on polyethylene, which is considered as a prototypical material, and hence generalizing the theories of how banding occurs in other materials need to be thoroughly investigated first.

Two main schools of thought were formed in the past few decades. Bassett *et al* [59] stated that for twisting molecular orientation to happen, a sudden quasi-discontinues rotation and splitting between originally untwisted *S*-shaped dominant lamellae should occur. Splitting is generated at isochiral screw dislocations, where daughter lamellae will splay sharply away from the parent lamellae. Such dislocations will all have the same handedness and are related to the direction of the chain inclination in the lamellae [60]. The identical handedness of consecutive spiral terraces could give rise to the periodically varying orientation constituting the banded spherulites. The cause of divergence of daughter lamellae can be attributed to the short-range repulsive forces building up between lamellae due to trapping non-crystallized cilia or other amorphous polymer in the areas of contact.

Keith and Padden [61] reported that giant screw dislocations generated in twisted lamellae are predominantly isochiral and have a positive contribution to twisting. This contribution, however, has a secondary effect compared to the overall torsions observed, in contradiction to the Bassett's opinion. According to them the leading lamellae twist smoothly (not suddenly) back from growth tips while they are still relatively narrow. Upon this, widening shoulders impinge onto each other and lamellae become mutually transfixed by continuing interpenetrating growth. The difference in the two opposing fold surfaces in a given lamellae enhances compression in one surface compared to the other. This will generate unequal stresses along the two opposing fold surfaces within a given lamella leading to a twist, which constitute the periodic orientation variation characteristic of the banded spherulites.

To prove the validity of their model, Keith and Padden studied the band spacing as a function of crystallization temperature and molecular weight for linear polyethylene and α-poly (vinylidene fluoride) (α-PVF_2). They found that log-log plots of band spacing S against $(1/\Delta T)$ behave linearly, and suggested that $log\ S \sim (n+2)\ log\ (1/\Delta T)$ with $n>1$. The decrease in band spacing with molecular weight, at a specific temperature, leads to the suggestion that band spacing responds to the molecular mobility of the crystallizing chain. The respond is stronger than the segregation of the amorphous polymer between lamellae. The study found that there is no simple correlation between relative rates of radial growth and corresponding band spacing. This contradicts recent data obtained in this study as will be illustrated in the discussion section.

Toda and Keller [60] tried to unify both models and asserted that the same stress unbalance which can produce the twist could also create screw dislocations all of identical handedness. The model links the geometrical description of Bassett *et al* with the model of Padden *et al*. Thus, all the raised features could retain their place without contradiction: consistently identical handedness of screw dislocations, unbalanced stresses, and S-shaped entities.

The effect of branch content on band spacing has not been reported anywhere in the literature so far. It is the goal of this study to examine the effect of this parameter on the morphology of LLDPE and compare the results with the preexisting models in a try to unveil some of the ambiguity that still exist.

The essential features that causes the spherulitic growth to occur was the focus of a recent study conducted by Bassett *et al* [56, 62]. They suggested that cellulation, which is visible as the onset of discontinuities of the internal banding, is not the primary cause of spherulitic growth as was predicted earlier by Keith and Padden, and is only a secondary mechanism that can be overlaid on spherulitic growth in suitable circumstances of high segregation. The concentration of segregants must be high enough to give a sufficient depression of growth rate.

According to them, the phenomenon of cellulation can be explained as follow: since lamellae are close packed in raw structure, the more-branched species (segregants) that are preferentially rejected, because of the exclusion of branches from the lattice, will

accumulate ahead of the planar growth front. Increasing concentrations of more-branched sequences will lower the local equilibrium melting temperature and with it the isothermal supercooling for growth, and hence the growth rate. This morphological instability will also form a progressive coarsening of the texture with a modest lamellar thickening.

When sufficient material has segregated, fluctuations in the local concentration produce regions at the growth front that have slower growth rate than the others. Those areas will continue to grow tending to become protuberances (swellings) ahead of their laggard surroundings with a limited width. Lateral diffusion will then concentrate further segregants between fingers as their extension proceeds.

3. EXPERIMENTAL PROCEDURES

3.1 Materials

Ethylene/1-octene random copolymers with branch content, molecular weight, and polydispersity (M_w/M_n) controlled by homogeneous metallocene catalyst were used in this study.

Table (3.1.1) summarizes the, as received, molecular structure data, densities, and branch contents of the investigated copolymers. The '*L*' and '*M*' symbols stand for low and medium molecular weight, respectively. The molecular weights of the copolymers are considered equal. Although the molecular weight of the linear polyethylene is twice larger, it will be assumed to be of no significant effect unless specified otherwise. The numbers represent the amount of methyl groups per 1000 carbon atoms (i.e. branch content). Materials were all kindly supplied, as pellets, by Dow Chemical Co.

3.2 Sample Preparation

Thin films were prepared by melting and pressing the, as received, pellets in the FP-82 model hot stage. The thickness of the samples produced was 0.5-1.0 mm for X-ray studies, and 20-50 μm for all other experiments. Discs of 0.375inch diameter were punched from these films for 'high pressure' experiments. Samples were dipped

Table (3.1.1) Characteristics of the as-received linear PE (M-54) and ethylene-octene copolymers.

Code	M_w (g/mole)	M_n (g/mole)	M_w/M_n	Density (g/cm^3)	CH_3/1000C	T_m (C)
M-54	101,300	53,900	1.88	0.954	0.5	142.7
L-04	59,900	27,300	2.19	0.9365	3.98	118.81
L-11	43,700	21,200	2.06	0.9195	10.86	
L-13	51,800	25,000	2.07	0.9110	12.93	105.00

In Acetone before any use to assure its cleanliness.

3.3 High Pressure Equipment

A simplified schematic of high-pressure equipment is illustrated in **figure (3.3.1)**. The experimental unit is composed of: high-pressure control, temperature control, and a recording system **(figure 3.3.2)**. The polymer sample was placed between two quartz windows and inserted into a tight Teflon tube. Silicon sealant with high temperature durability was applied to the outer edges of the windows to prevent any unwanted oil leak to the sample. Sample and windows are then put inside the high-pressure cell **(figure 3.3.3)**. The high-pressure cell was mounted on a trinocular-microscope under cross-polar conditions.

Using trinocular-microscope made it possible to, simultaneously: I) measure the growth rates using camcorder, TV, time generator and VCR; II) to record the bulk crystallization using photo-multiplier and chart recorder (not shown in **figure 3.3.2**); III) and to directly observe the growth mechanism using the eyepiece.

Small pressure was initially applied to adjust the system. The sample was then melted at a certain temperature for 10 minutes to remove any thermal history and allow the temperature to equilibrate. Once thermal equilibrium was attained, the required pressure was applied. This procedure assures the isothermal and isobaric crystallization of the specimen, and resembles the processing conditions used in industry. Initially

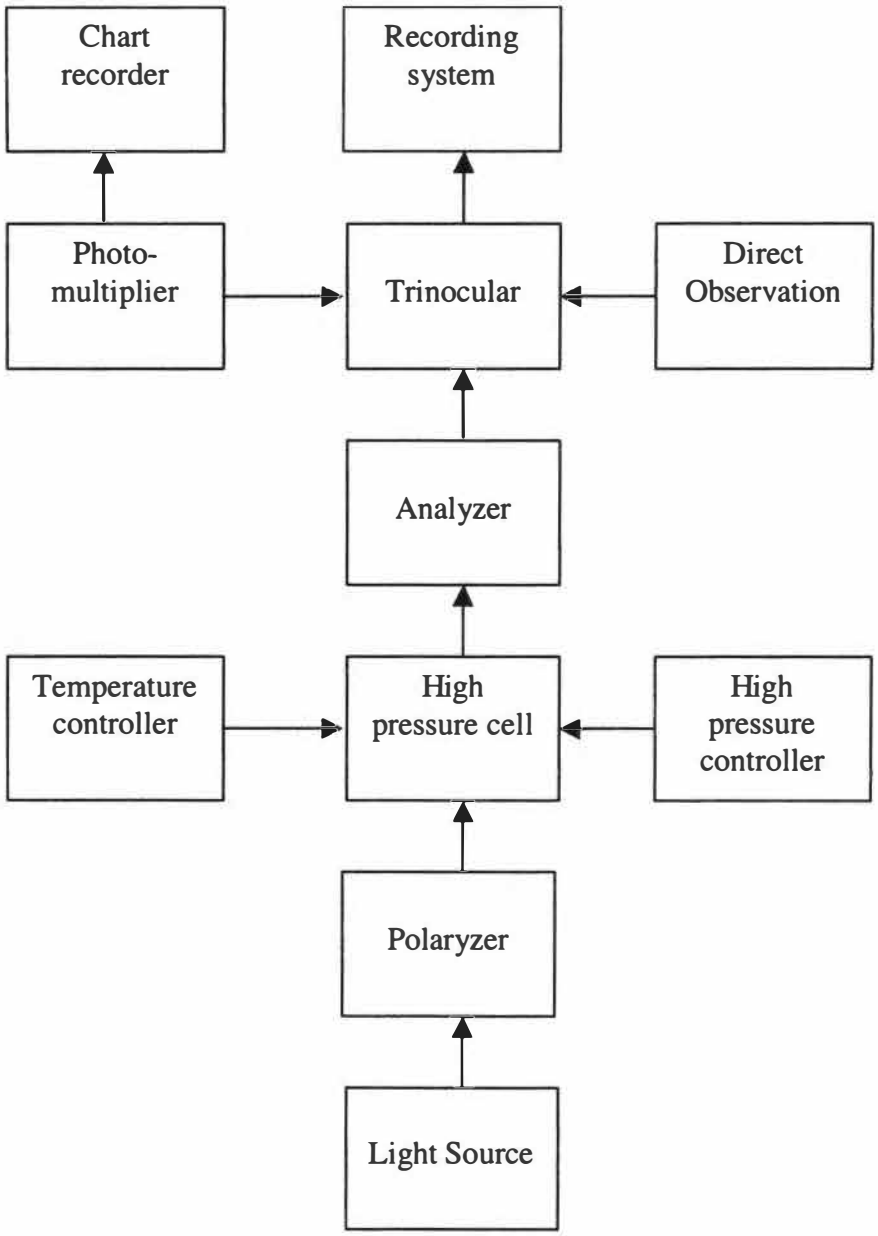


Figure (3.3.1) A simplified schematic diagram of the high-pressure equipment.

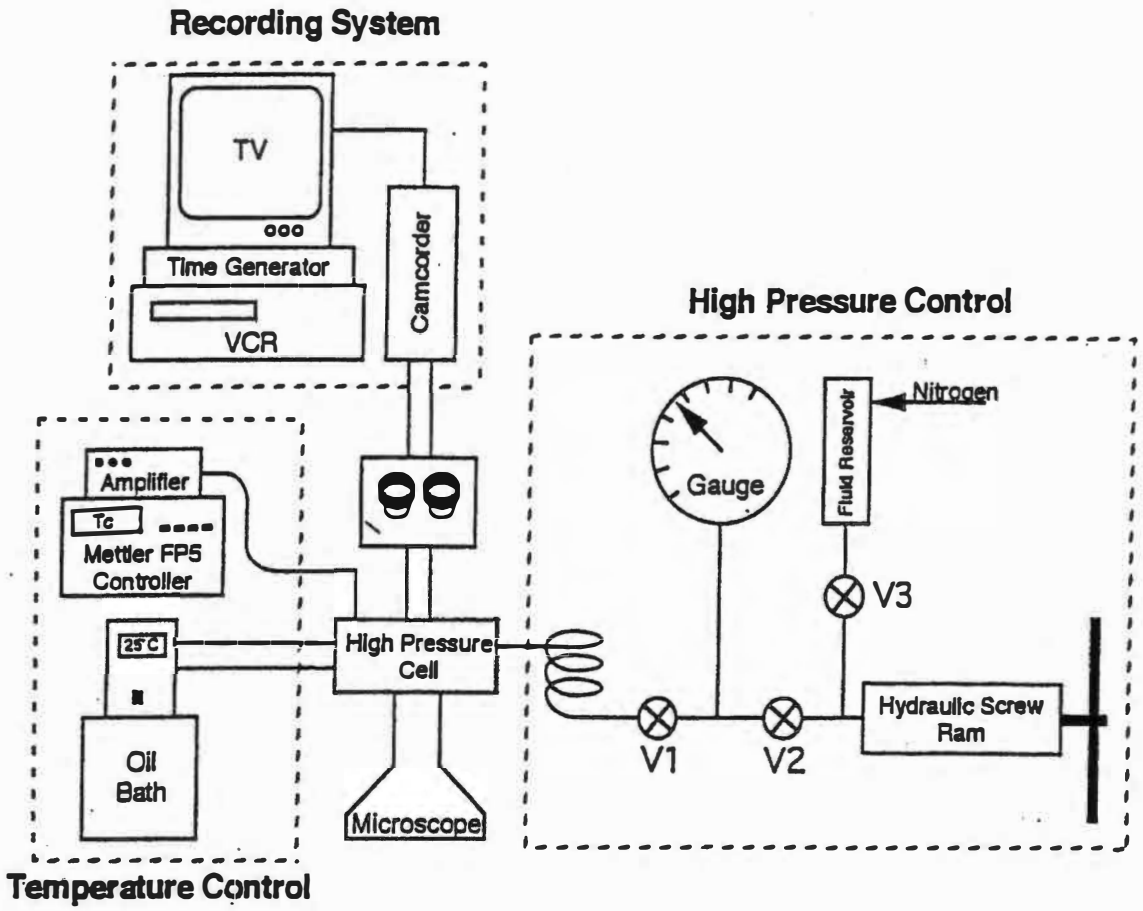


Figure (3.3.2) Simplified schematic of the high-pressure equipment.

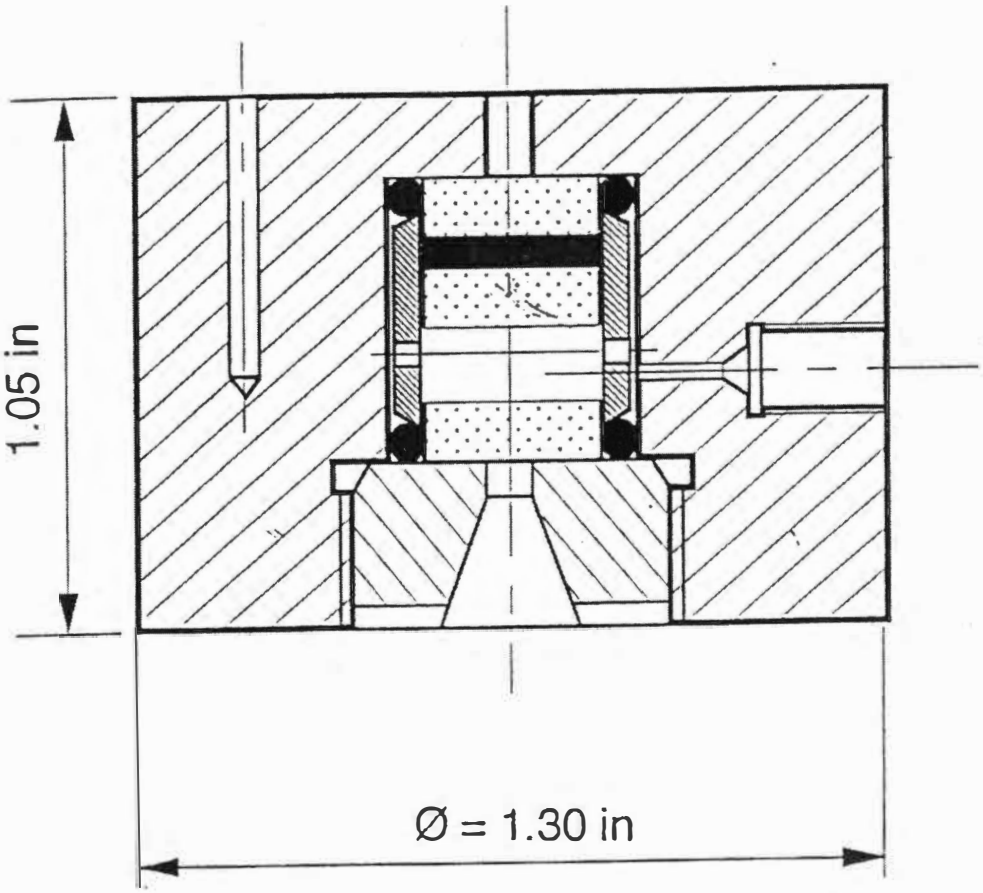


Figure (3.3.3) A schematic diagram of the high-pressure cell.

applied pressure was slightly increased at larger crystallization temperatures to prevent any sample degradation.

In-situ melting studies at elevated pressures have been conducted using the transmitted depolarized light intensity method. The crystallized sample was heated at a rate of 10 °C/min using a Mettler controller. Samples prepared for morphological and x-ray studies were first cooled down to room temperature using HAAKE D8 oil bath before releasing the pressure. The schematic diagram in **figure (3.3.4)** illustrates the steps followed in crystallizing and melting.

3.4 Depolarized Light Microscopy

For isothermal crystallization experiments at atmospheric pressure, transmission polarized Nikon (Optiphot-Pol) microscope and two FP-82 Mettler hot stages were employed. The first hot stage was used to melt the sample for 10 minutes to prevent any thermal history, sample was then rapidly transferred to the other hot stage that was previously set to the designated crystallization temperature using FP-80 Mettler temperature controller and was mounted on the microscope. Nitrogen gas may be flown over the sample during crystallization to prevent any degradation.

Depolarized transmitted light intensity was recorded as a function of time for studies of bulk crystallization rate, and as a function of temperature for studies of melting behavior. A silicon photo-sensor was used for this purpose where it was connected to a

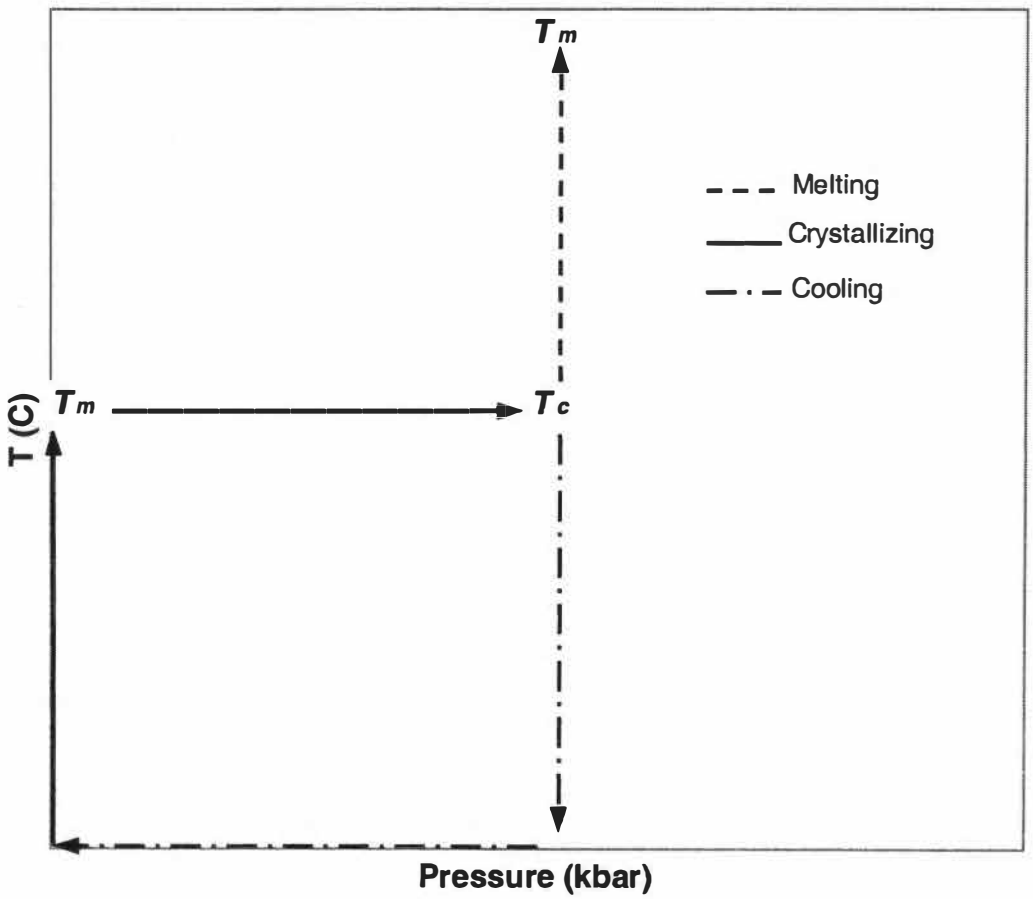


Figure (3.3.4) Schematic diagram of the experimental steps used to crystallize, melt, and cool down.

Metro-logic Radiometer 60-530 photometer. The analog output, of 3V full scale, was fed to a Speedomax W strip-chart recorder through a voltage divider. Simultaneous recording of light intensity and optical micrographs was possible using this technique. This allowed one to correlate the morphological changes during crystallization or melting with the thermal transitions. The analog data produced was digitized for easier processing.

3.5 Wide Angle X-ray Diffraction (WAXD)

WAXD studies were carried out using Philips and Rigaku Diffractometers in the reflection mode. Cu$K\alpha$ radiation, λ=1.542 A° was used with an operating voltage and current of 35 kV and 40 mA, respectively. Calibration is usually done using a silicon standard (2θ =24.465°).

Changes in the crystalline structure and degree of crystallinity can be identified using WAXD. The latter was determined by using the following equation [63]:

$$W_{c,x} = \frac{A_{110} + 1.42A_{200}}{A_{110} + 1.42A_{200} + 0.68A_a} \qquad (3.5.1)$$

where 'A' represents the area under the peak of the (110) and (200) planes. Amorphous phase is represented by 'a', and the correction factors for the crystalline and amorphous peaks were calculated.

X-ray patterns as a function of temperature was recorded using the Philips Difractometer at Oak Ridge National Laboratory, with operating voltage and current of 40 kV and 45 mA, respectively. Position Sensitive Detector (PSD) was employed, with a scanning time of 60 seconds for each temperature setting. The advantage of the PSD method is the ability to detect and measure the scattered x-rays at more than one point in the diffraction space simultaneously. The diffraction pattern was collected for the angles between 16° and 26°. To minimize any temperature overshooting, the heating rate used in all experiments was 5°C/min. Using higher heating rates will cause an overshooting of about 5-10°C depending on the rate used.

3.6 Small Angle X-ray Scattering (SAXS)

Small angle x-ray scattering, SAXS, was used to study the morphological parameters of the copolymer. It was carried out at the center for small angle scattering research at Oak Ridge National Laboratories using a sample to detector distance (SDD) of 5.119 m. The x-ray source is a rotating anode with CuKα (1.54 A°) wavelength. The detector is a 2-dimentional position-sensitive proportional counter with resistance wire mesh of a 20cmX20cm dimension.

All collected data was corrected by subtracting the instrument background and the dark current which both will be collected under the same conditions used for the samples and in separate runs. The dark current is measured by placing a lead sample in the path of the beam to block it. Thus, the collected data will be only due to the originating cosmic

radiation and electronic noise in the room. The instrument backgrounds were measured with no sample in the beam path. The net corrected scattering intensity 'I_{corr}' will be defined as follow:

$$I_{corr} = \frac{1000}{Mon_s T_{m,s} S_{i,j} F_{abs} t}\left\{\left[I_s - \frac{t_s}{t_{DC}} I_{DC}\right] - \left[\frac{Mon_s}{Mon_{MT}} I_{MT} - \frac{t_s}{t_{MT}} I_{DC}\right]\frac{T_{m,s}}{T_{m,MT}}\right\} \qquad (3.6.1)$$

where Mon_s and Mon_{MT} are the monitor counts of sample and empty background runs, respectively. I_s and I_{MT} are the scattering intensity measurements of the sample and the empty beam, respectively. t_s, t_{Dc}, and t_{MT} represent time in seconds for sample scattering, dark current, and empty beam measurements, respectively. $T_{m,s}$ and $T_{m,MT}$ are the transmission coefficient of sample and empty beam, respectively. 't' is the sample thickness, $S_{i,j}$ means 64X64 data array which is related to detector resolution, and F_{abs} represents the absolute intensity conversion factor derived from standards. The 1000 is an arbitrary normalization constant.

The transmission coefficient of each sample '$T_{m,\ s}$' was calculated using the following equation

$$T_{m,s} = \frac{(I_{gcs} - I_{DC}) - 0.686(I_s - I_{DC})}{(I_{gc} - I_{DC}) - 0.686(I_{MT} - I_{DC})} \qquad (3.6.2)$$

where I_{gcs}, I_{DC}, I_s, I_{gc}, and I_{MT} represent the intensity of glassy carbon and sample, dark current, sample alone, glassy carbon alone, and nothing in the beam, respectively. The sensitivity of the detector can be determined by collecting data of a radioactive material such as iron-55 isotope.

3.7 Differential Scanning Calorimetry (DSC)

Standard DSC measurements were performed under a nitrogen atmosphere on Perkin-Elmer DSC 7. The sample temperature and heat flow rate were calibrated using, respectively, the onset of melting and the heat of fusion of Indium (T_{onset} =156.6 °C, ΔH_f =28.45 J/g) with a heating rate of 10 °C/min. The peak temperature in the DSC thermogram was chosen to be the melting temperature.

3.8 Scanning Electron Microscopy (SEM)

Pictures for the morphology of samples prepared at different pressures were taken using LEO 1525 field emission high-resolution scanning electron microscope. All samples were etched for 35 minutes using permanganic acid solution. The procedure steps followed for etching and cleaning were similar to the ones reported in literature [64]. The electron microscope used was designed to run at high vacuums and low electron beam voltages (≤1 kV in our case). This protects fragile samples like LLDPE from being damaged by the electron beam, and reduces the possibility of charging the sample even at

high magnifications. Because of this no sample coating were needed to get pictures, and hence more structural details were observed.

4. RESULTS

4.1 Kinetics of Crystallization

Crystallization kinetics was studied by calculating the linear growth rates of both L-04 and L-11 copolymers as a function of pressure and temperature. The crystallization half time of L-04 copolymer was also studied. The technique of transmission depolarized optical microscopy was used in both studies. For bulk crystallization kinetics light intensity measurement was additionally employed.

Both techniques showed two different morphological structures during the crystallization of L-04 and L-11 copolymers at certain conditions. Morphology with unclear features and a very fast growth rate appears before the spherulitic structure. The existence of two-phase system requires extra precaution when measuring the linear growth rates. Since the spherulitic structure normally grows in the orthorhombic phase, and its slower growth rates are slow enough to measure compared to the first appearing structure, only the growth of spherulites will be discussed in the consequent sections.

4.1.1 Linear Growth Rates

Isothermal crystallization of L-04 and L-11 copolymers at elevated pressures showed different morphological structures at certain conditions, as will be explained later. Spherulitic and some irregular morphological structures were observed in most of

the conditions applied. In addition, an axialitic structure was also observed. For linear growth rate studies only the spherulitic and axialitic structures were considered.

The diameter of the spherulite was measured instead of the radius to minimize the amount of error produced in measuring the size of the spherulite. The spherulite size was taken to be the diameter divided by two. Fringes surrounding the spherulites, if they exist, are the result of focusing problems, and are not associated with the polymer morphology. This problem is more evident at high supercooling temperatures and was avoided during diameter measurements.

The size of the spherulite is linearly dependent on time and the slope represents the growth rate. The slope average of a minimum of three different spherulites was taken at all conditions. **Figures (4.1.1a-c)** show the linear change in the spherulite size for L-04 copolymer as a function of time at different pressures. All data were normalized to zero growth rate at t=0 for comparison. **Figure (4.1.2)** shows the effect of crystallization temperature and pressure on the growth rates of L-04 copolymer. The atmospheric pressure data included in this report are essentially those reported in preliminary publications [43,65]. As expected a very fast growth rate is observed at high supercoolings, i.e. at high pressures and low temperatures, while in the vicinity of the equilibrium melting point T_m^o growth rate becomes very slow.

The horizontal dashed line drawn in **figure (4.1.2)** represents a constant growth rate value. A plot of the crystallization temperature, intersected by the dashed line, versus

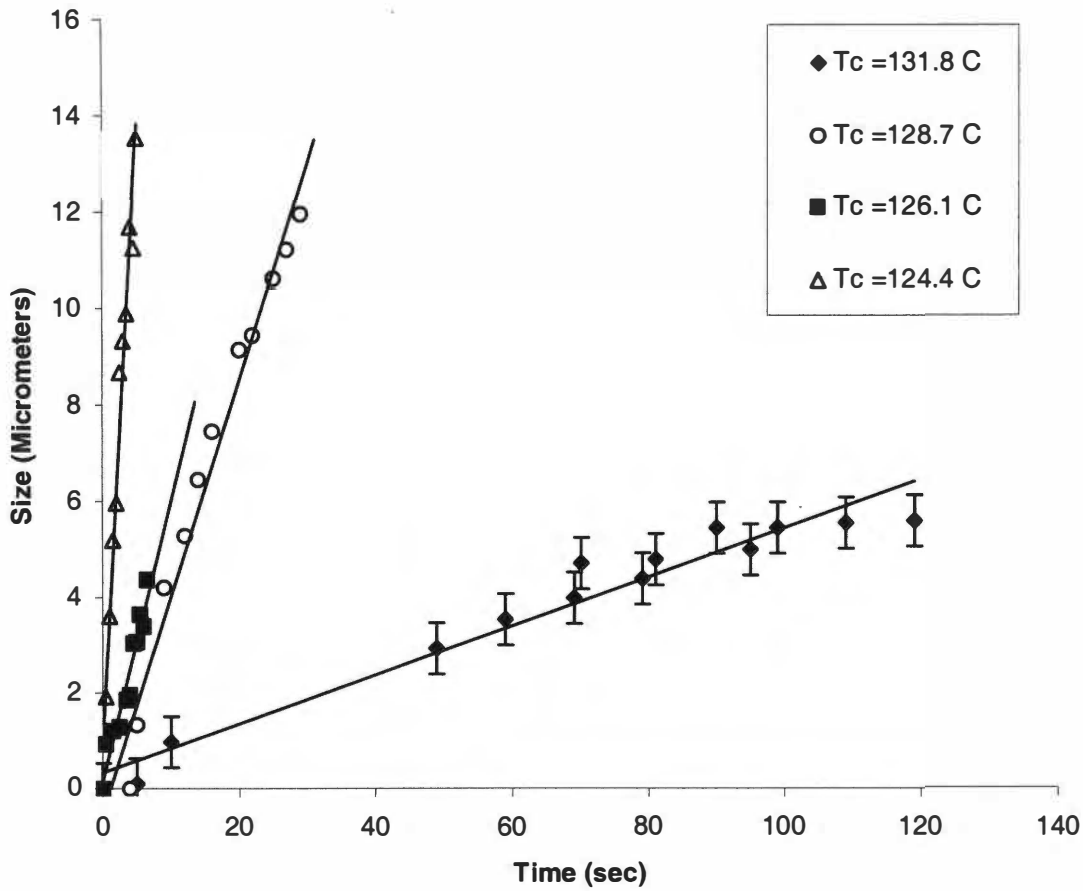


Figure (4.1.1) The change in the size of spherulites versus time for L-04 copolymer crystallized, a) at 0.48kbar.

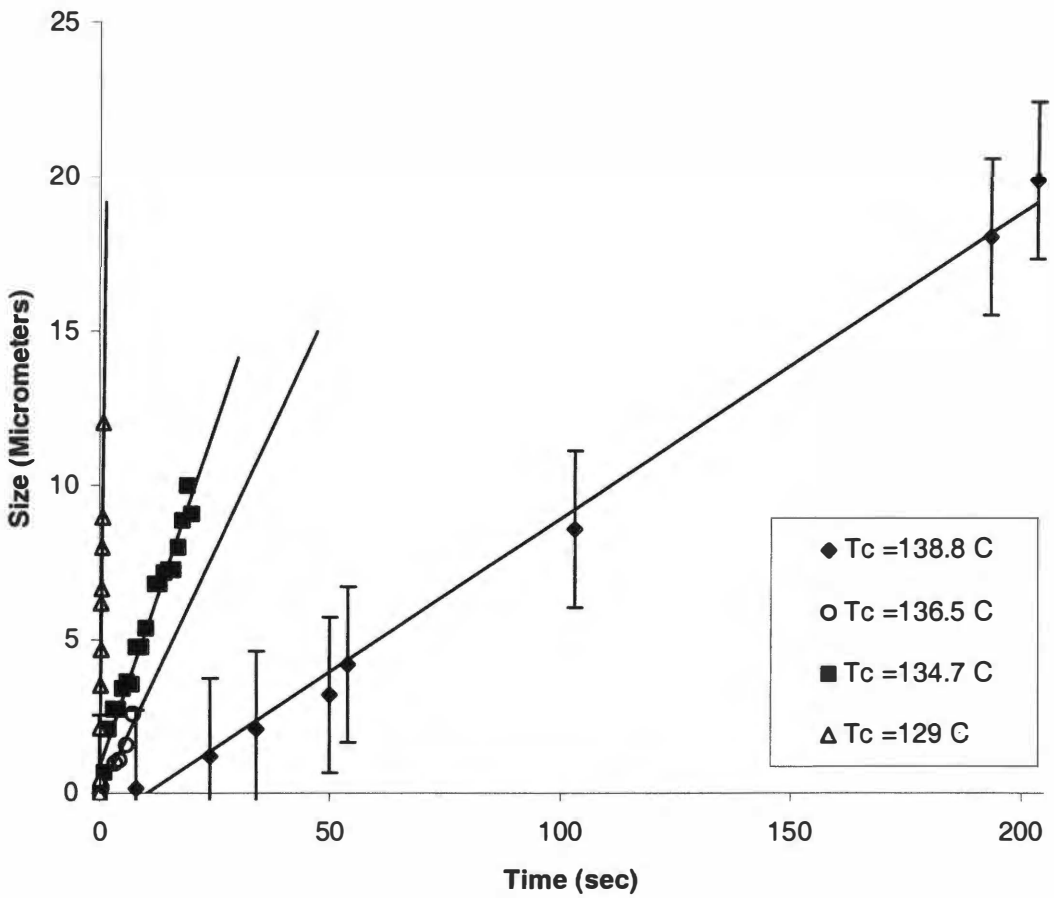


Figure (4.1.1) Continued, b) at 0.76kbar.

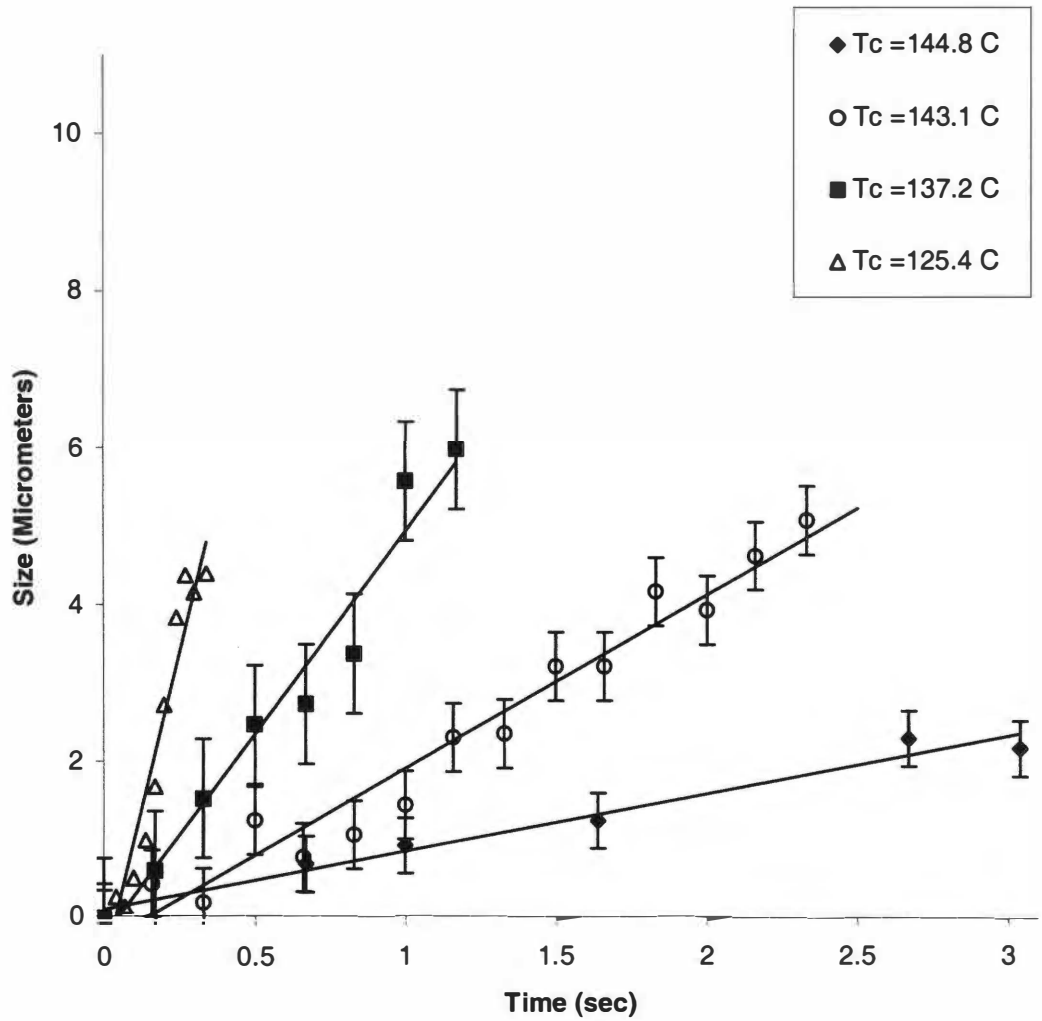


Figure (4.1.1) Continued, c) at 1.24kbar.

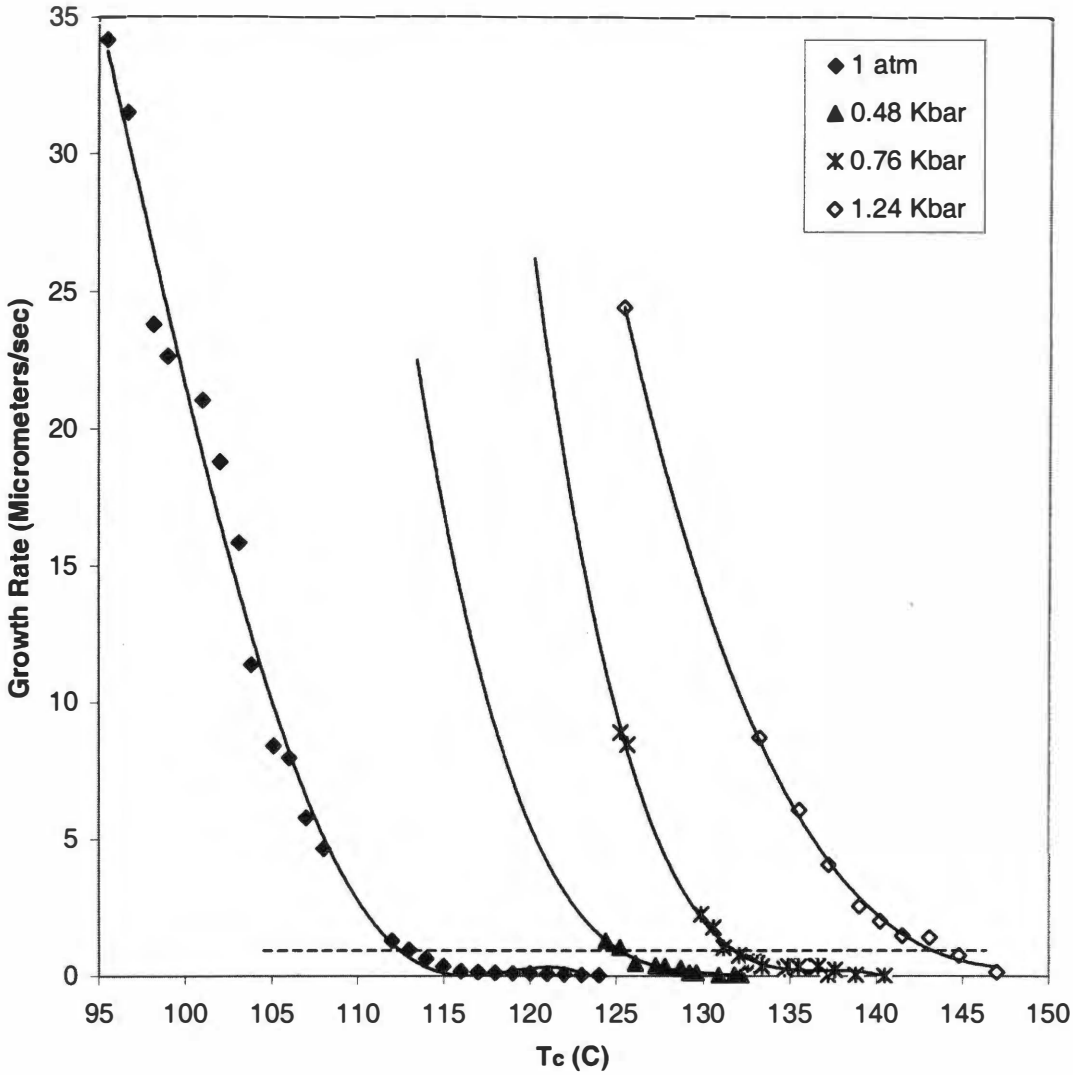


Figure (4.1.2) The effect of the crystallization temperature and pressure on the linear growth rate of L-04 copolymer.

pressure gives a linear relationship of average slope dT_c/dP~24.5 °C/kbar as shown in **figure (4.1.3)**. This value will give an additional credibility to the phase diagram as will be discussed in **section 5.1.2**.

4.1.2 Bulk Crystallization Kinetics

Isothermal bulk crystallization of a polymer usually follows a sigmoidal pattern. **Figure (4.1.4)** illustrates schematically a typical isothermal crystallization. Position 'A' in the figure represents the time when the sample reached the preset temperature and pressure. Initial detection of crystallization occurs at position 'B'. After that, crystallization proceeds at an accelerated rate, which is almost autocatalytic in character. Finally, primary crystallization reaches a pseudo-equilibrium level at position 'C'. The time required for crystallization to reach its 50% value is called 'half-time $t_{1/2}$' and is measured for L-04 as a function of pressure and temperature.

The transmitted light-intensity pattern changes for samples prepared at elevated pressures. **Figure (4.1.5)** compares the light intensity behavior of some of the L-04 copolymer samples crystallized at different pressures. The pseudo-equilibrium level could not be reached in most cases due to the slower continuing crystallization or the lamellar thickening at larger times. At 0.76 and 1.24kbar two distinct slopes i.e. two crystallization rates, can be observed. The two different crystallization rates could be attributed to the existence of two populations or phases in the system, as will be seen in

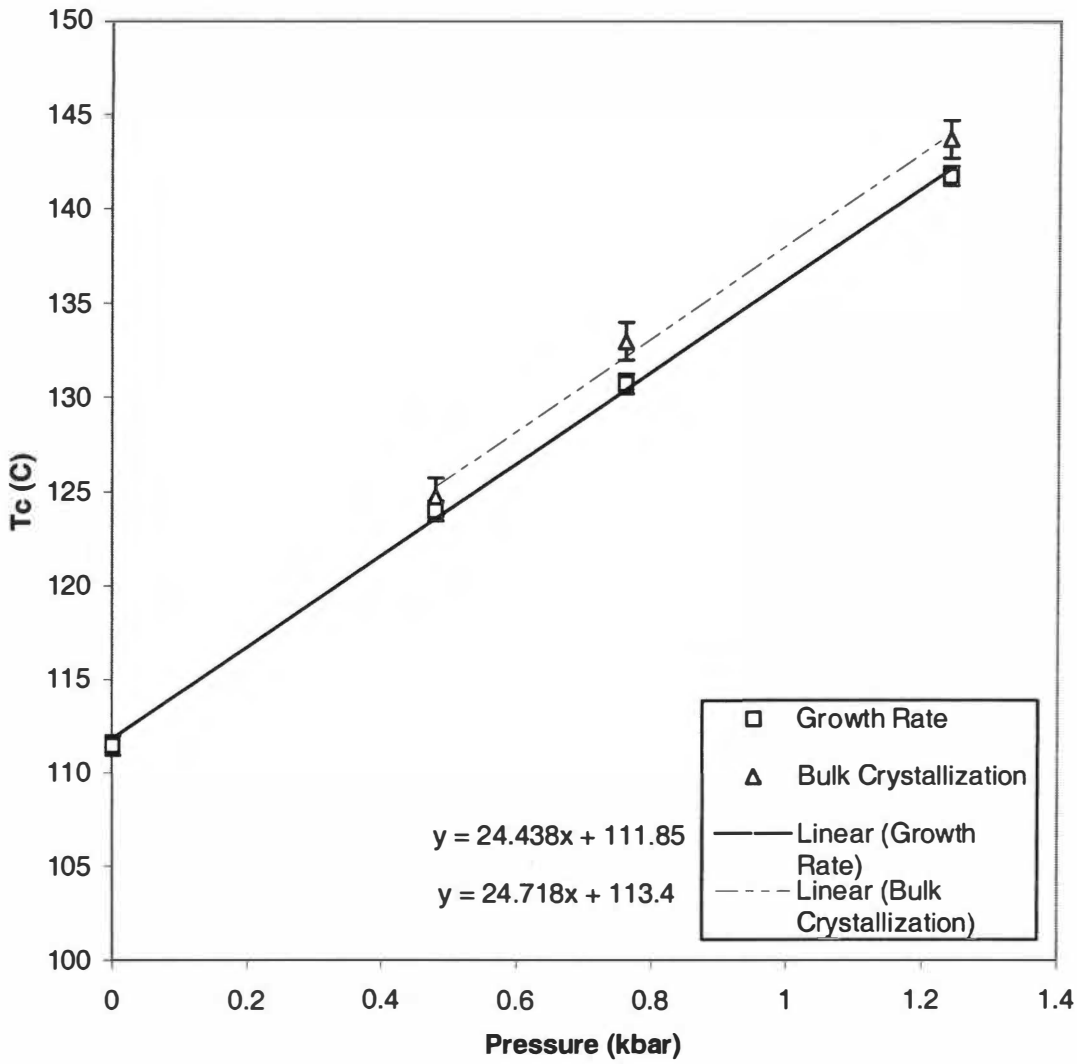


Figure (4.1.3) T_c versus P at constant growth rate for L-04 copolymer using linear growth and bulk crystallization methods.

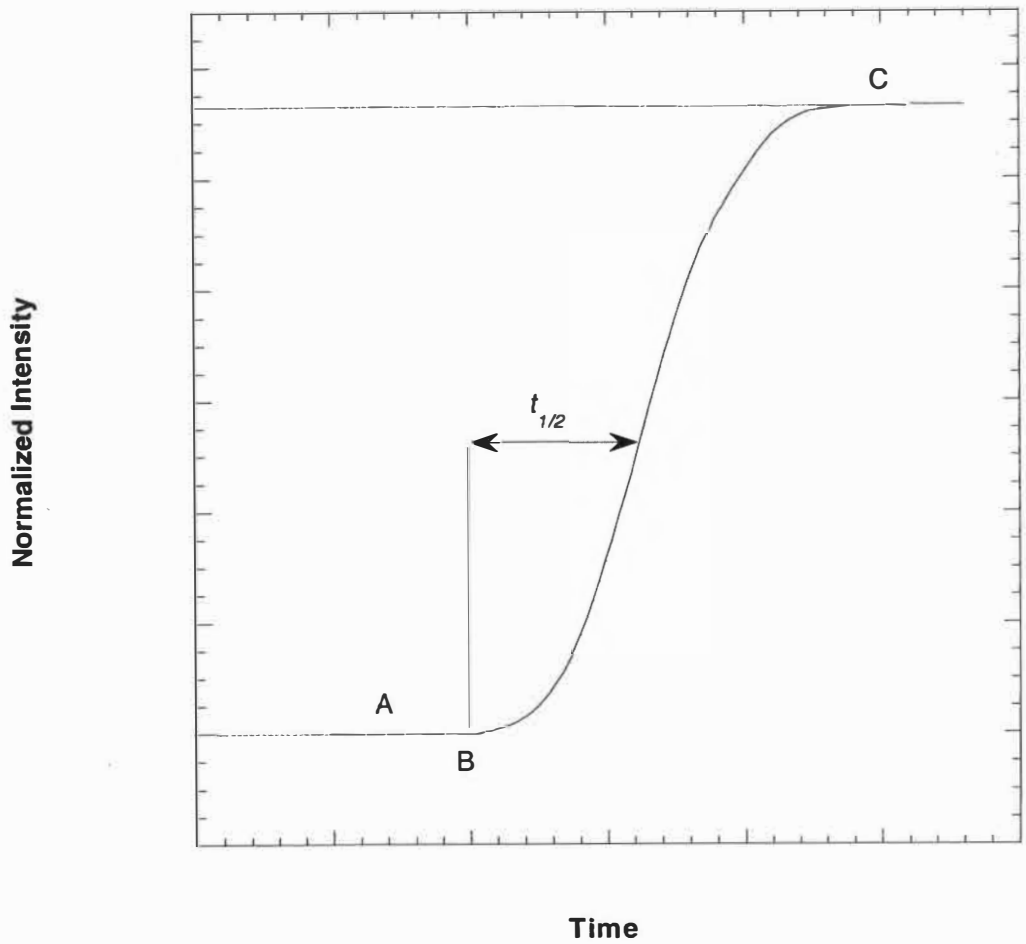


Figure (4.1.4) Schematic diagram of the measurements of half crystallization time.

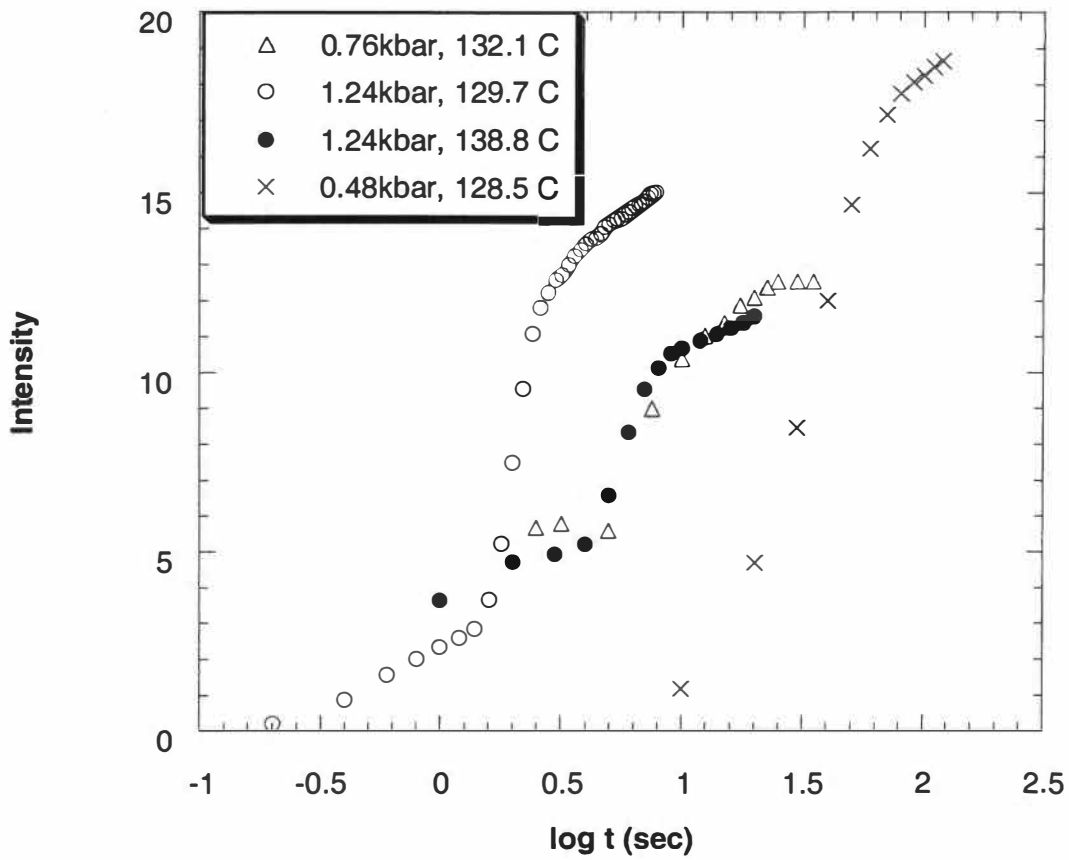


Figure (4.1.5) The bulk crystallization of L-04 copolymer crystallized at different pressures using light intensity.

a later discussion. In general, the phase that appears earlier has a faster growth rate and corresponds to the appearance of disordered entities under the microscope. The second phase, however, is slower and corresponds to the appearance of spherulites. Accordingly, only the latter crystallization rate should be considered in the studies of bulk crystallization and growth kinetics. The appearance of the second phase, as observed from the optical microscope, does not completely terminate the other phase but co-exists with it.

The accuracy in calculating the 'half-time' ($t_{1/2}$) values becomes very questionable when two phases co-exist. In **figure (4.1.6)**, plotting the reciprocal of the 'half-time' ($1/t_{1/2}$) as a function of temperature shows similar behavior to the growth rate (see **figure 4.1.2**). The rate of crystallization decreases as T_c increases, while at constant T_c the rate of crystallization increases with pressure. For a fixed $1/t_{1/2}$ value (as represented by the horizontal line) the dT_c/dP~24.7 °C/kbar is in a good agreement with the linear growth rate result (**figure 4.1.3**). The value, however, is much larger than the 17 °C/kbar value expected for LLDPE and the 20 °C/kbar value for linear PE reported in literature. The interference of the second phase in the crystallization process cannot be ignored and could be the reason behind this behavior as will be shown in the next section.

4.2 X-ray Analysis

X-ray studies were carried out for L-04 and L-11 copolymers using Rigaku Denki and Phillips diffractometers. All x-ray experiments were conducted at atmospheric

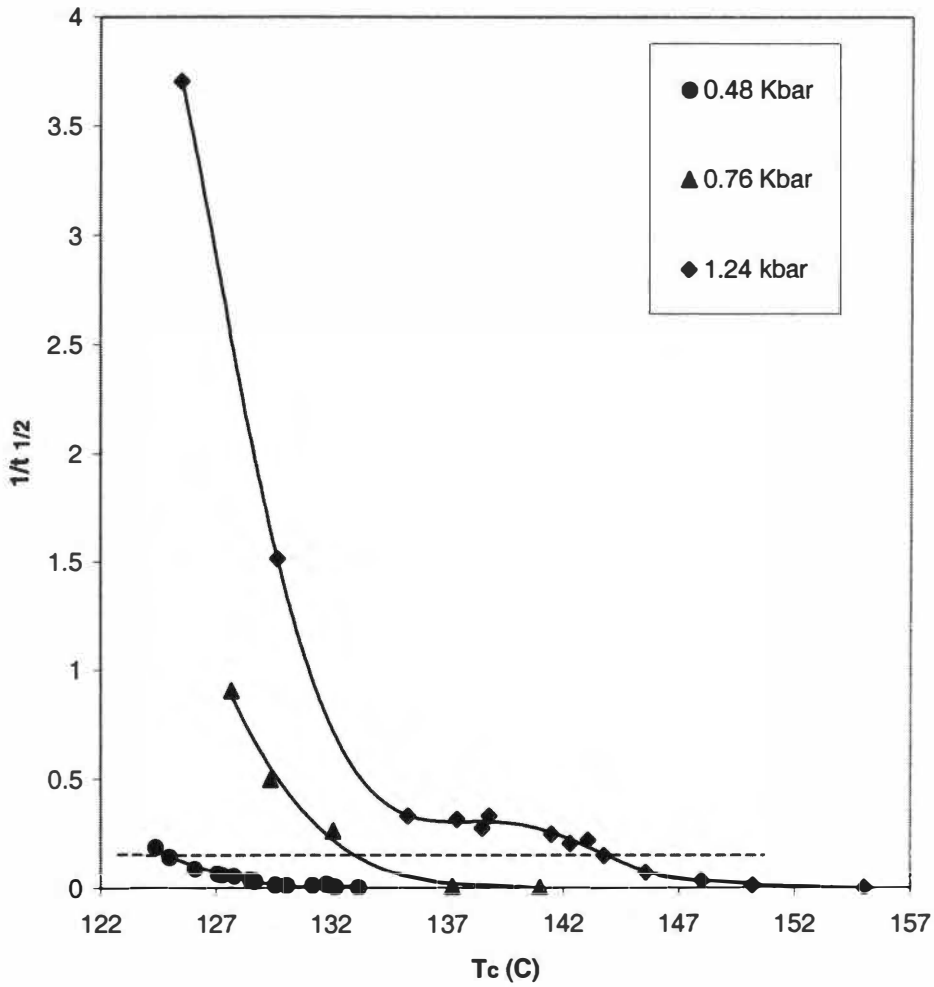


Figure (4.1.6) A plot of the inverse 'half-time' ($1/t_{1/2}$) versus temperature of L-04 copolymer at different pressures.

pressure. Samples, to be analyzed, were first prepared at atmospheric and high pressures before quenching them to room temperature and atmospheric pressure (see **section 3.3**).

4.2.1 Wide Angle X-ray Diffraction (WAXD)

WAXD studies were conducted on L-04 copolymer to determine the effect of crystallization temperature and pressure on the material structure and the degree of crystallinity. The latter was calculated using **equation (3.5.1)**. For L-04 copolymer the small increase in crystallinity as a function of temperature is negligible for all pressures applied as shown in **figures (4.2.1a-c)**. Crystallinity obtained by SAXS and WAXD are in a good agreement, while that of DSC shows lower crystallinity values. Crystallinity value is almost unchanged at 0.48 and 0.76kbar pressures, but increases significantly for 1.24kbar. **Figure (4.2.2)** illustrates the diffraction patterns of L-04 copolymer crystallized at certain pressure and temperature. The (110), (200), (210) and (020) reflections of the orthorhombic phase of polyethylene are obviously present. The diffraction pattern taken at room temperature and for 2θ between 10^{o} and 50^{o} is the same for all samples, regardless of the crystallization conditions used. The arrowed peaks belong to the aluminum in the sample holder.

4.2.2 High Temperature X-ray Diffraction

Atoms, in general, undergo thermal vibration about their mean positions even at the absolute zero temperature. As temperature increases the amplitude of this vibration

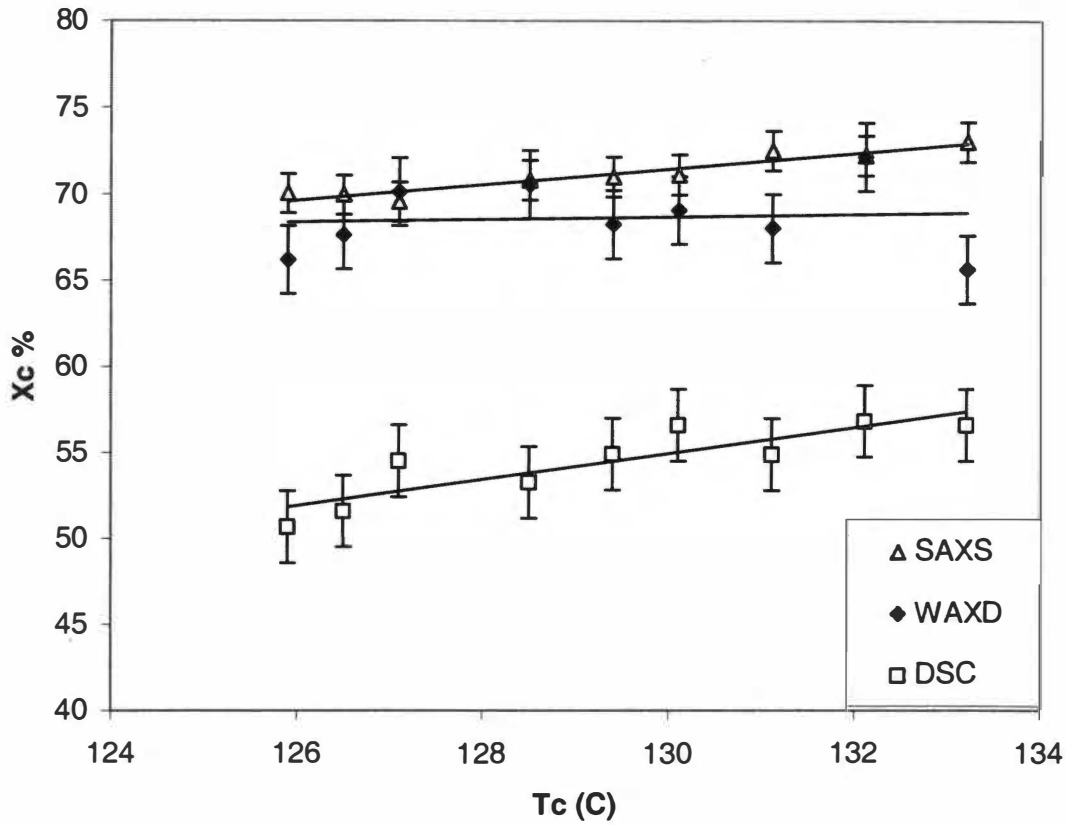


Figure (4.2.1) The crystallinity values of L-04 copolymer crystallized using different measurement techniques, a) at P=0.48kbar.

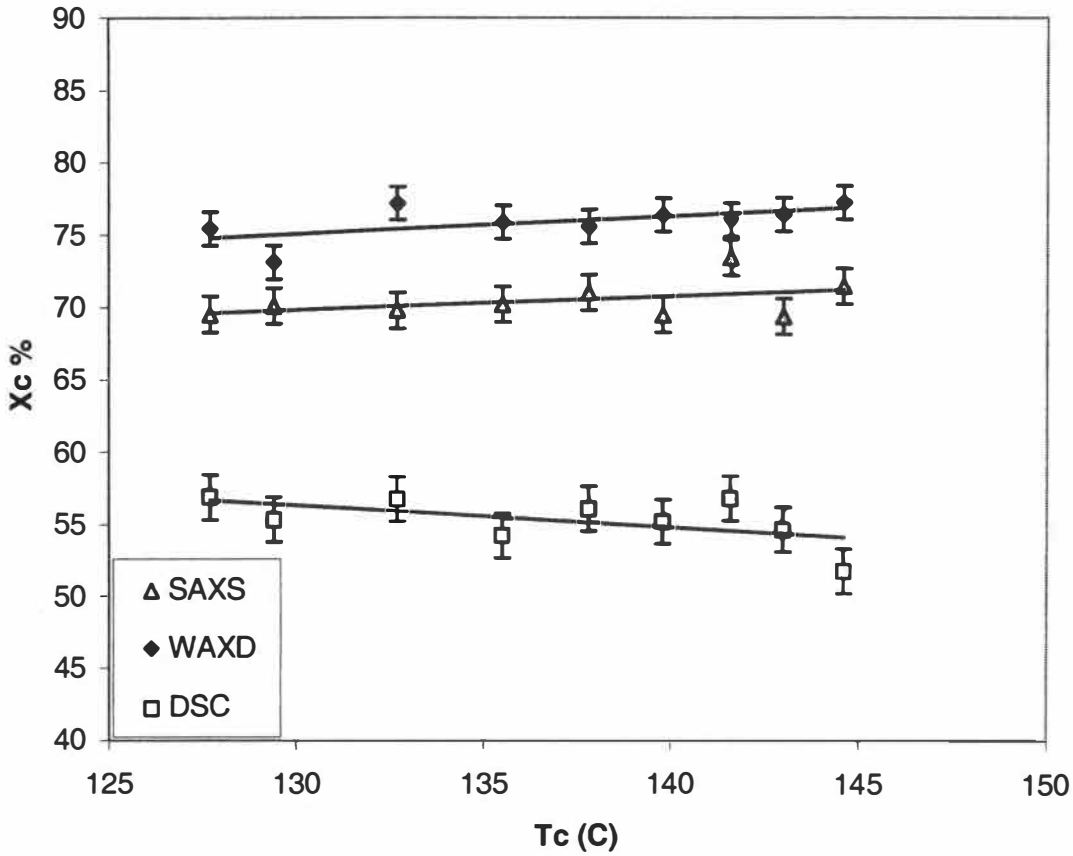


Figure (4.2.1) Continued, b) at P=0.76kbar.

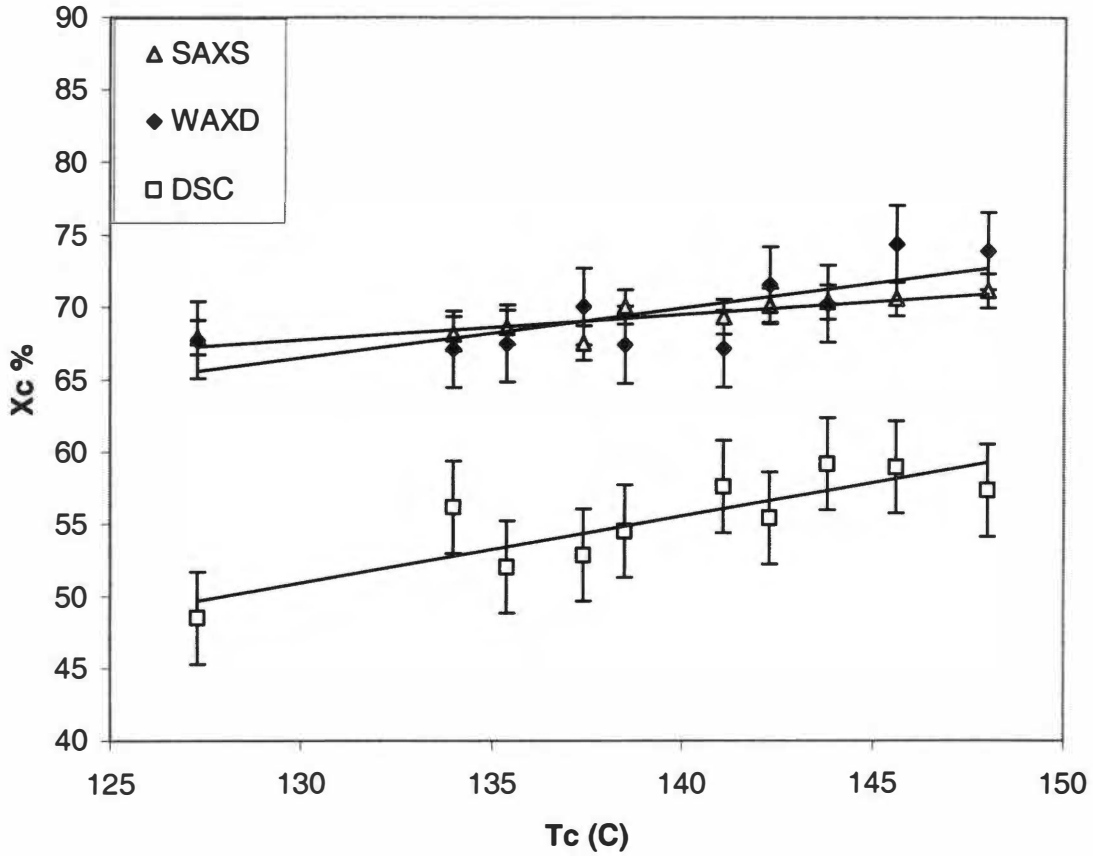


Figure (4.2.1) Continued, c) at P=1.24kbar.

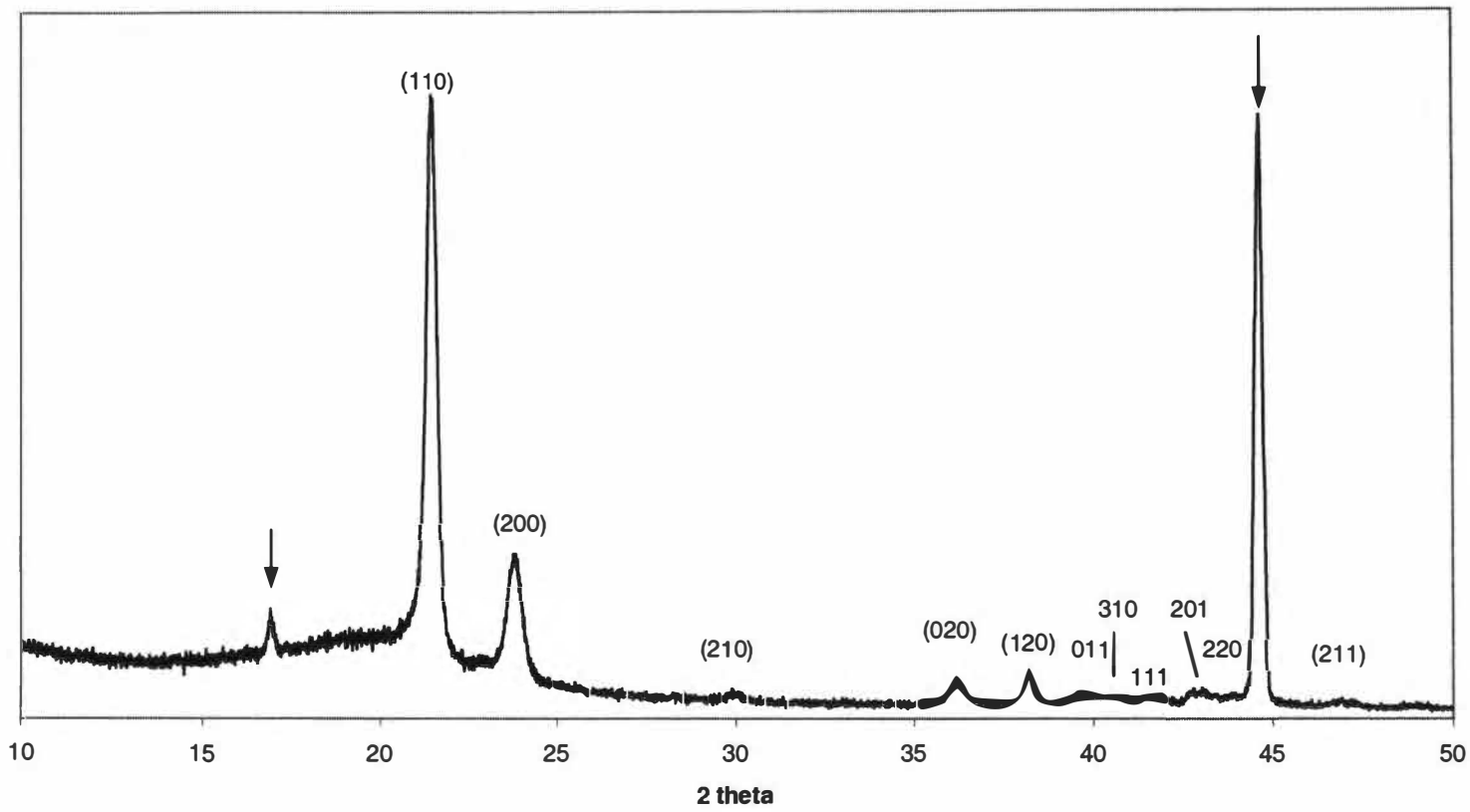


Figure (4.2.2) Wide-angle x-ray diffraction of L-04 copolymer crystallized at Tc= 140 °C and P=0.76kbar.

increases. The increase of the thermal vibration of the atoms will have three main effects on the x-ray diffraction patterns that were taken for the quenched high-pressure samples. All effects can be clearly noticed in **figures (4.2.3-6)** and are:

- The expansion of the unit cell, which causes changes in the planar spacings and therefore shifts the 2θ positions of the diffraction lines. By measuring the amount of shift of the peak position as a function of temperature, one can obtain the thermal expansion coefficient of the specimen used.
- The decrease of the intensities of the diffraction peaks.
- The increase of the intensity of the background scattering as a result of the temperature-diffuse scattering effect.

Figure (4.2.3) shows the x-ray diffraction of L-04 copolymer crystallized at T_c =127 °C and P = 0.76kbar during heating. The Bragg d_{200} spacing value has shifted from 3.75 Å at room temperature to 3.84 Å just before melting. The consistent shift of the orthorhombic (200) peak towards smaller 2θ values results from the thermal expansion of space lattice in the direction of a-axis. The shift was accompanied with a drop in the peak intensity, as expected. The average displacement of a molecule from its mean position calculated for the above example was about 0.18 Å in the direction of a-axis, or 2.4% expansion from its original lattice size. The (110) peak has also shifted to a lower 2θ value, however this shift is very small and is expected to be a reflection of the expansion in the a-axis direction. The calculated average displacement in the b-axis direction showed almost a zero change at all conditions. The negative expansion values

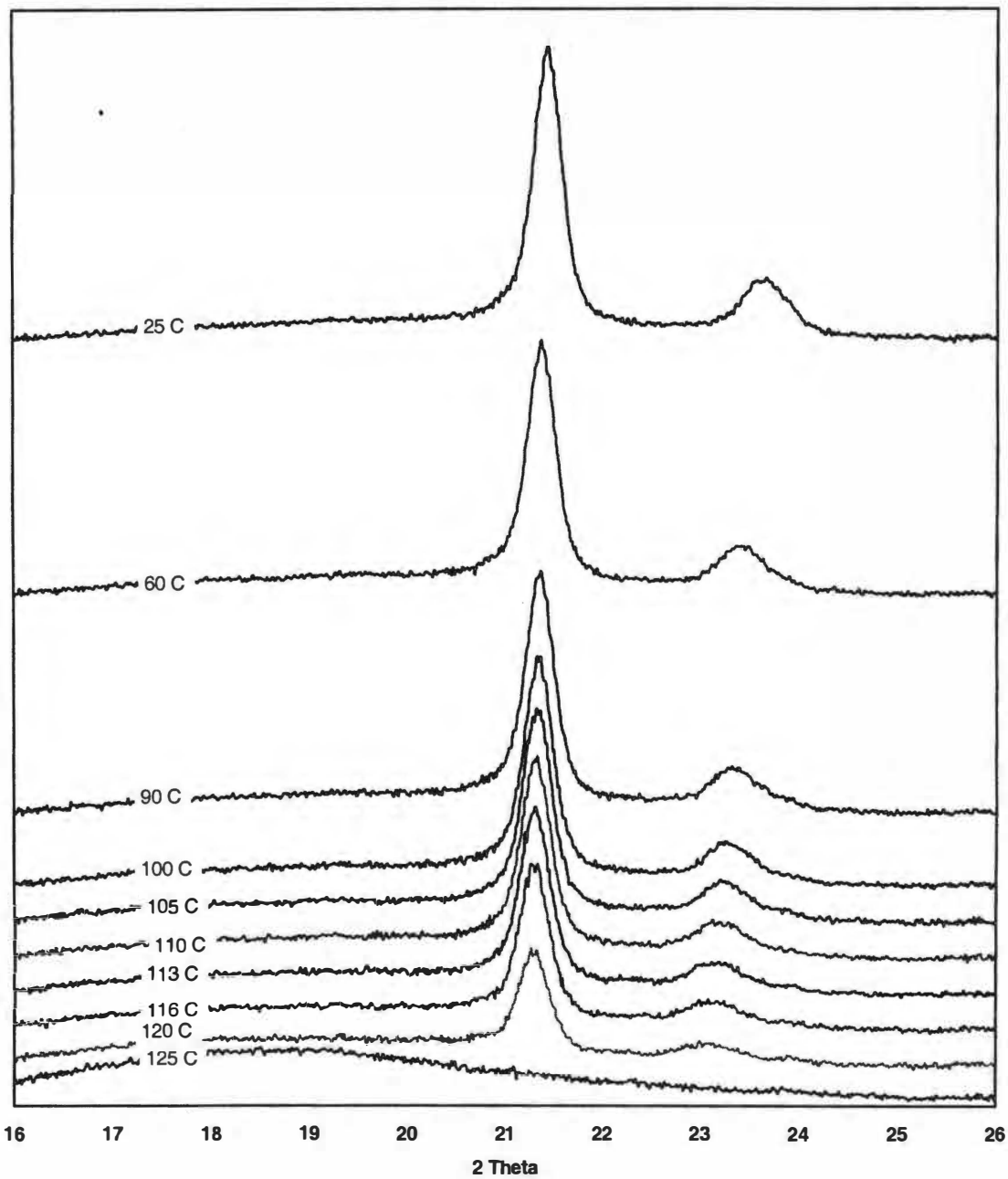


Figure (4.2.3) X-ray diffraction pattern of L-04 copolymer as a function of temperature. (T_c=127 °C, P=0.76 kbar).

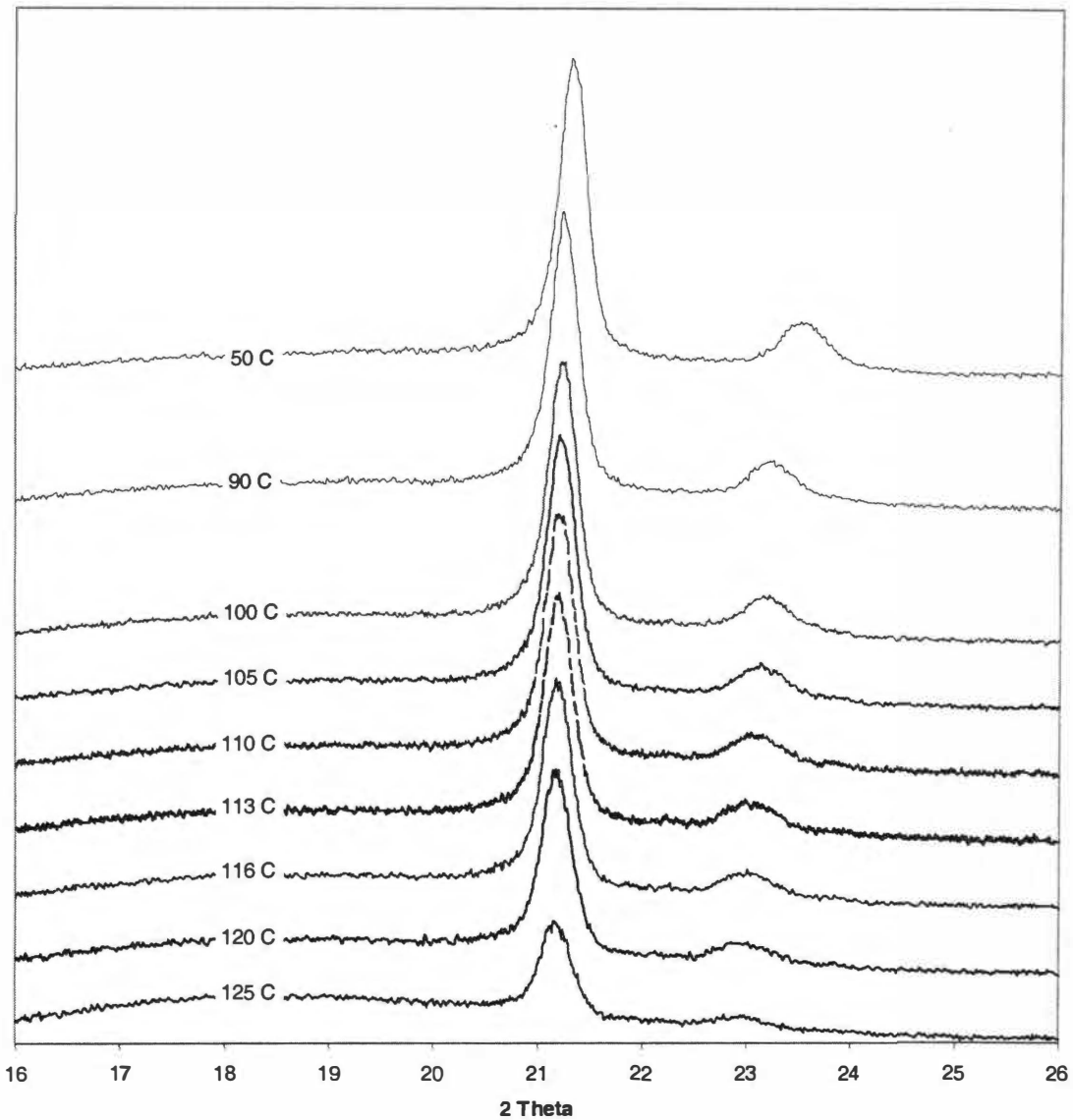


Figure (4.2.4) X-ray diffraction pattern of L-04 copolymer as a function of temperature. (T_c=145 °C, P=0.76 kbar).

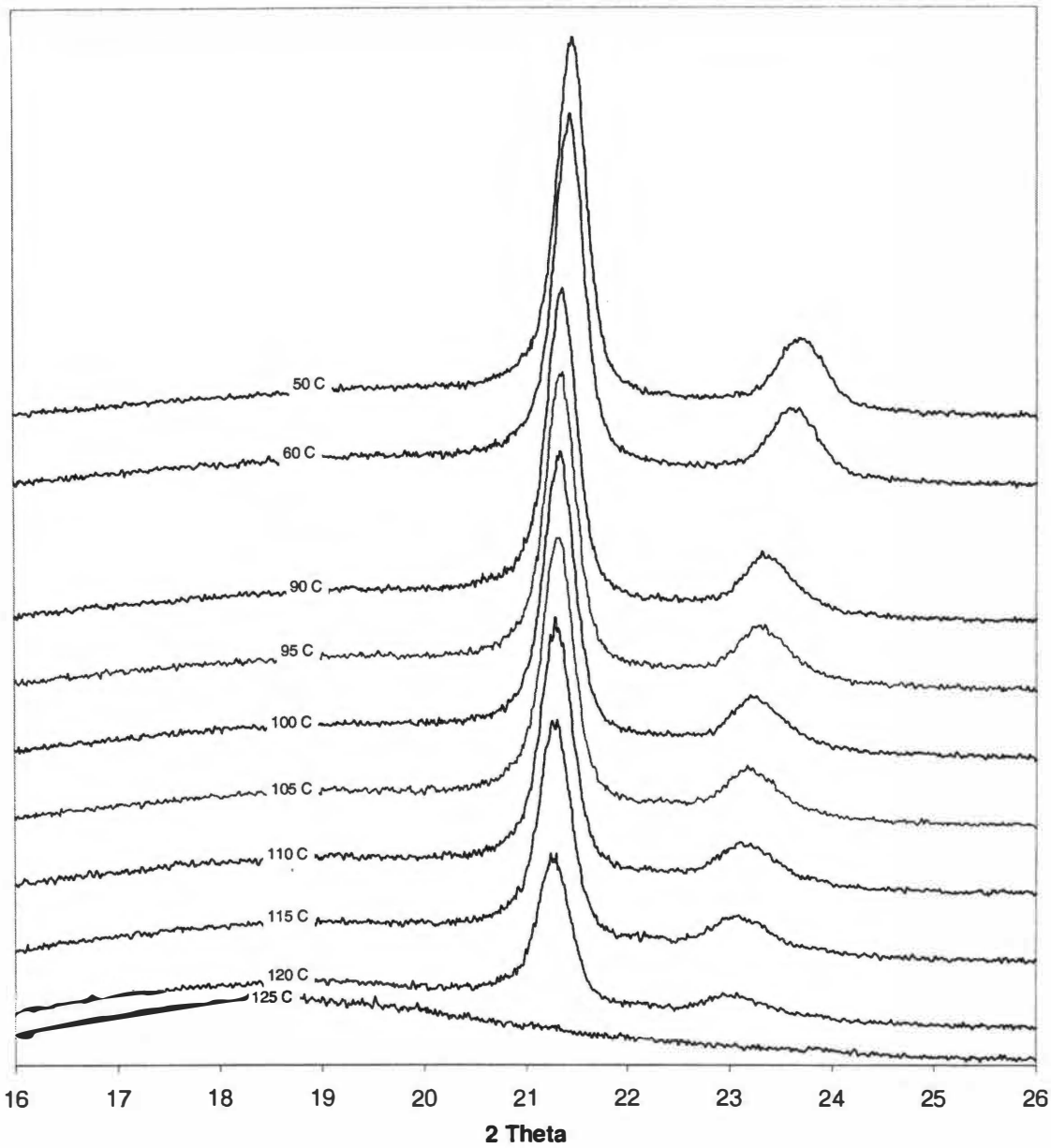


Figure (4.2.5) X-ray Diffraction Pattern for L-04 copolymer as a function of temperature. (T_c=128 °C, P=1.24 kbar).

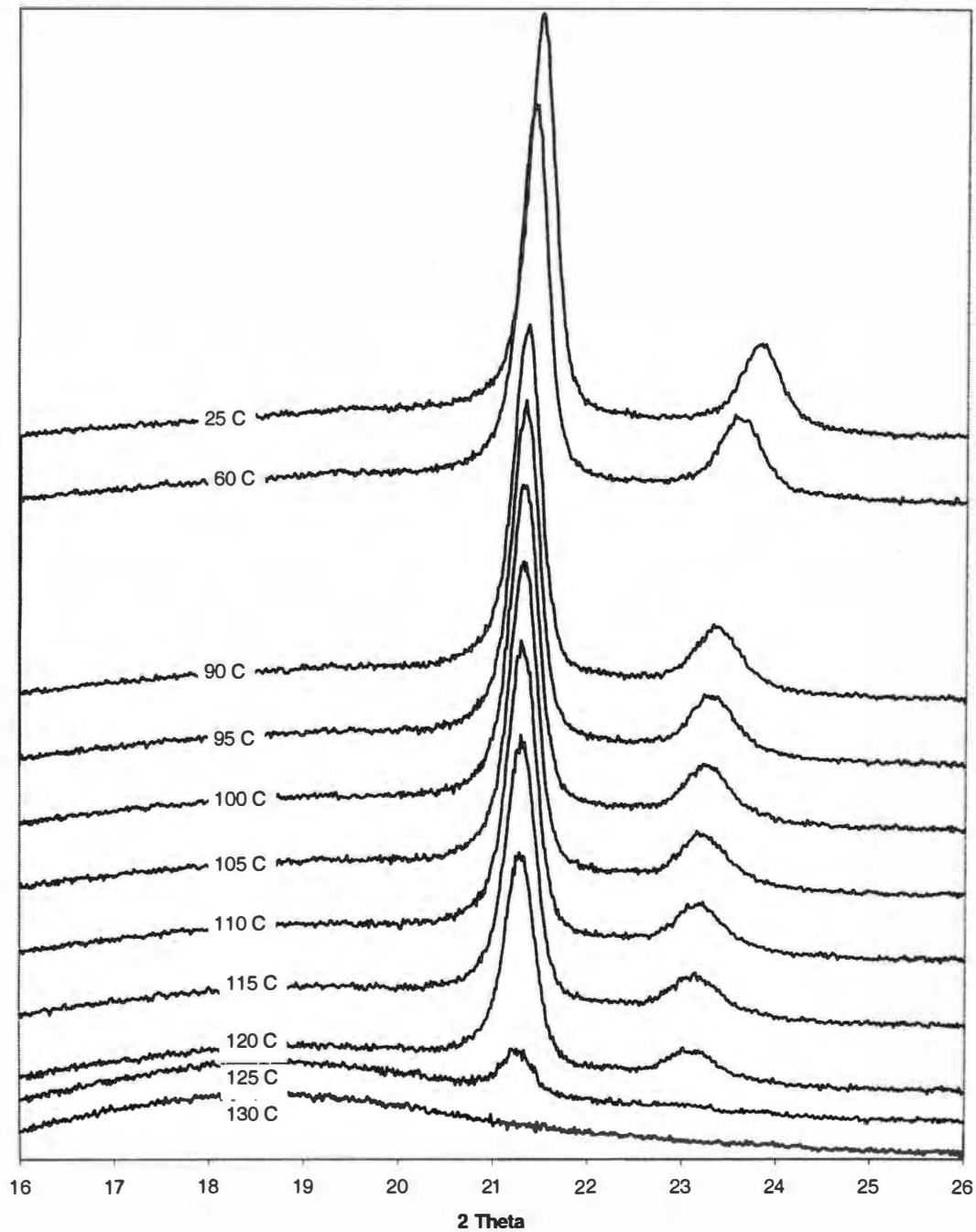


Figure (4.2.6) X-ray Diffraction Pattern for L-04 copolymer as a function of temperature. (T_c=148 °C, P=1.24 kbar).

reflect a decrease in the unit cell size. The behavior is repeated for other conditions (see **figures 4.2.4-6**). Peeters *et. al.* have reported similar behavior to the strong increase in a-axis, while b-axis remained almost constant [66]. When correcting for thermal expansion using densities of polyethylene crystalline phase they found a slight increase in the mass density of ethylene-octene copolymers as a function of temperature. They attributed their results to the melting of less perfect, less stable, and hence, less dense crystals, which leaves the most perfect crystals intact and results in a higher mean crystalline density.

Table (4.2.1) summarizes the maximum expansions of the crystals in the a- and b-directions. It is noticed from the table that the amplitude of the molecular vibrational motion in the a-axis (i.e. lattice expansion) is always larger than that of the b-axis. This could be due to the larger displacement between two adjacent molecular chains in the a-axis direction, and hence its larger degree of freedom. Accordingly, if branches were to be included in the crystalline phase, due to its increase of solubility when heating, they would be more favorably placed parallel to the a-axis.

A plot of the thermal expansion a-spacing versus temperature '*T*' for selected conditions is shown in **figures (4.2.7-9)**. Using **equation (2.2.3)** the thermal expansion coefficient 'α' can be measured from the slope of linear portion of the plot. All measured values are listed in **table (4.2.1)** and was found to agree with literature [67].

Table (4.2.1) A summary of the expansion coefficients of L-04 and L-11 copolymers obtained by high-temperature x-ray diffraction.

Material	Tc (^{o}C)	P (kbar)	Δ (a-axis) Å	Δ (b-axis) Å	Linear Thermal Expansion Coefficient K^{-1} ($X10^{-5}$)
L-04	127	0.76	0.18	-0.007	17
L-04	145	0.76	0.18	0.001	21
L-04	128	1.24	0.22	0.002	29
L-04	148	1.24	0.23	0.021	27
L-11	100	atm	0.17	-0.013	40
L-11	114	atm	0.15	-0.017	30

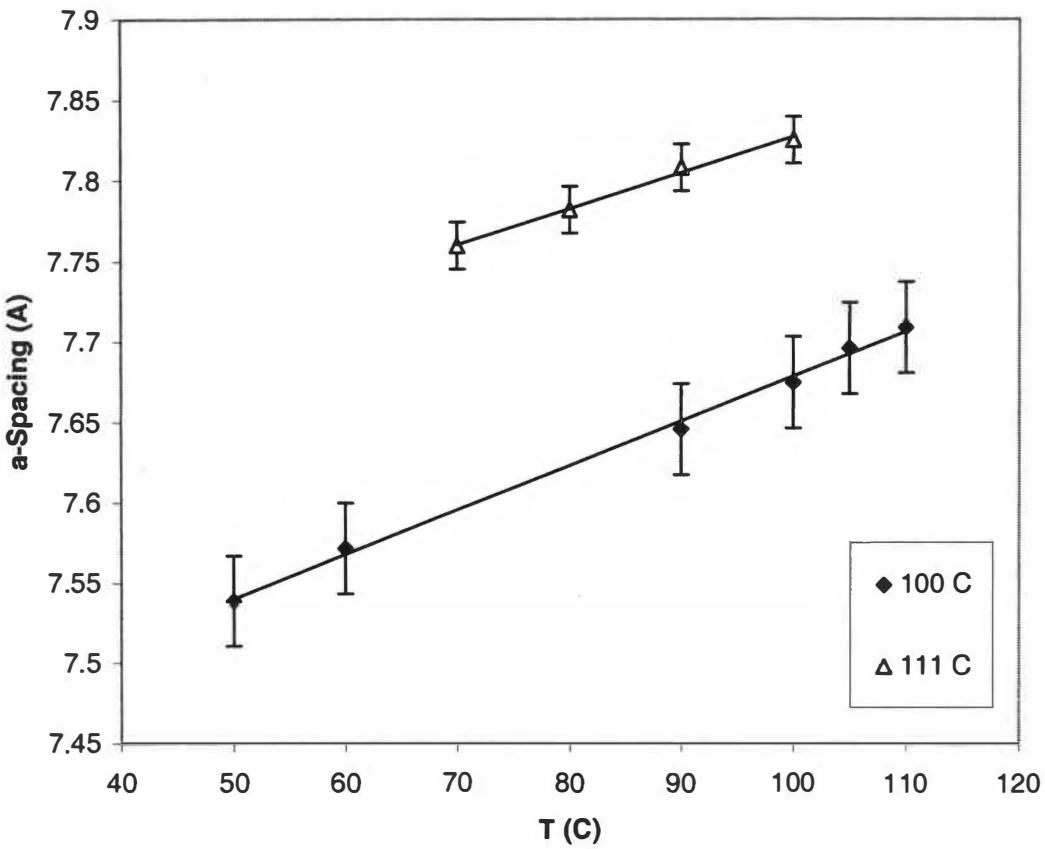


Figure (4.2.7) The effect of crystallization temperature and heating process on the a-spacing of L-11 copolymer crystallized at atmospheric pressure.

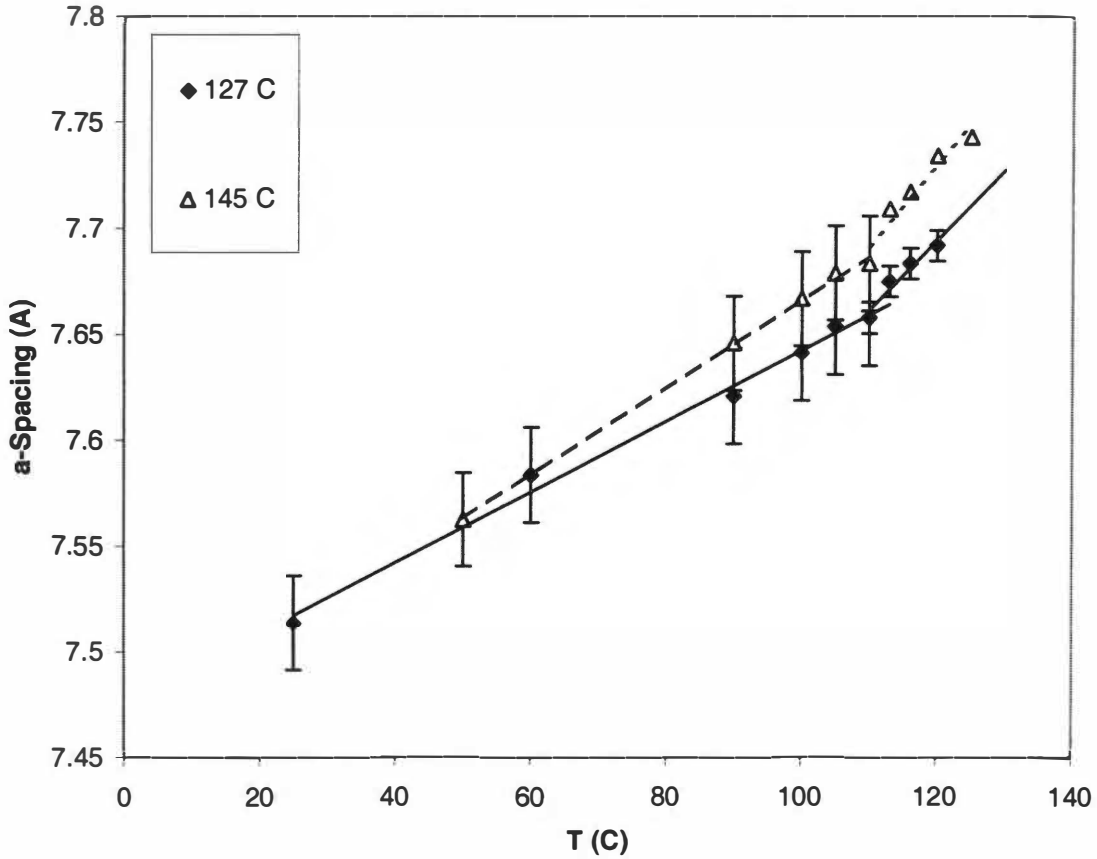


Figure (4.2.8) The effect of crystallization temperature and heating process on the a-spacing of L-04 copolymer crystallized at 0.76kbar.

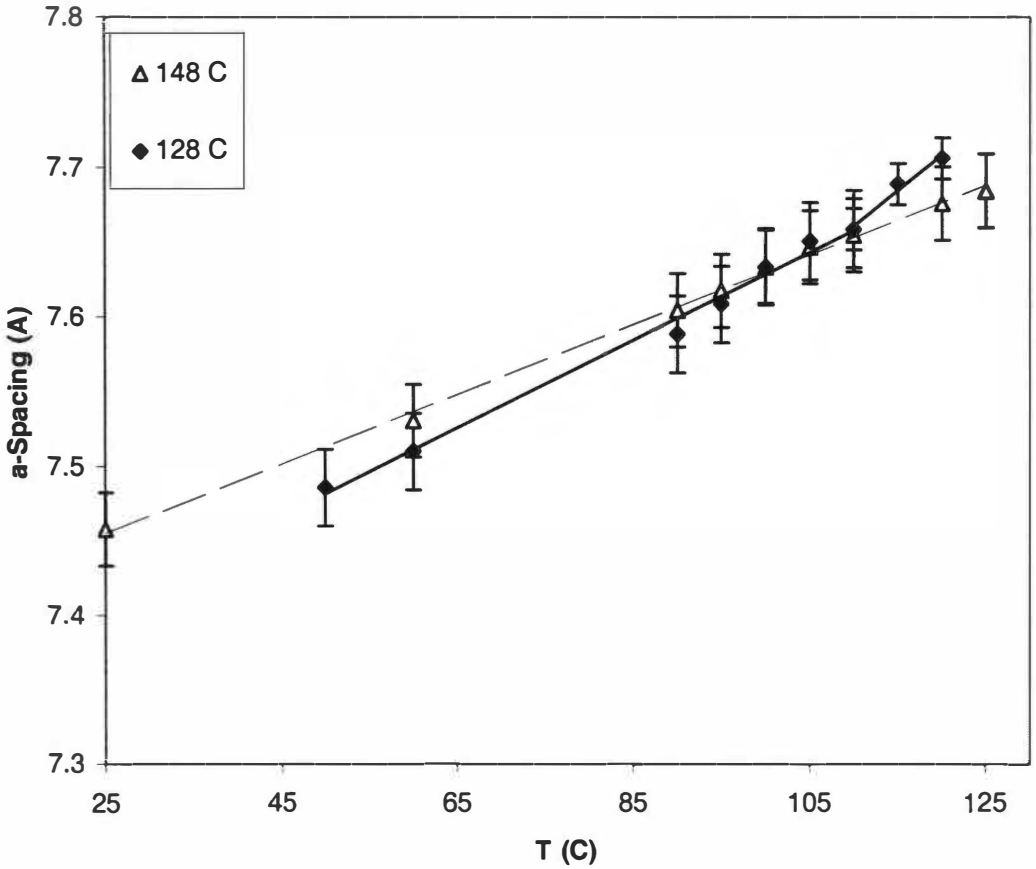


Figure (4.2.9) The effect of crystallization temperature and heating process on the a-spacing of L-04 copolymer crystallized at 1.24kbar.

The lattice dimensions of L-11 copolymer crystallized at atmospheric pressure show clear dependency on the crystallization temperature as shown in **figure (4.2.7)**. From the figure, the a-spacing value obtained just before melting is close to the theoretical value of the monoclinic crystal (a=8.09Å). One possible explanation to this behavior is the attempt of the hexyl branches to dissolve in the crystalline phase, which requires larger crystal size. The larger lattice dimension of the sample prepared at higher crystallization temperature could indicate a partial inclusion of the hexyl branches into the crystalline phase.

The change in the expansion rate of the lattice observed in **figures (4.2.8-9)** is attributed to the change in the solubility parameter as a function of temperature. The change cannot be seen for samples prepared at T_c =148 °C and P =1.24kbar. The lattice dimensions of the high-pressure samples are almost equal at room conditions but depart from each other at higher temperature depending on their original crystallization temperatures. It appears that although the history of the sample is not significant at room temperature, it has certain effect on its melting behavior.

Theoretically, thermal vibration of the atoms causes a very slight increase in the breadth of the diffraction peaks. The increase was not clear in this study, however, the tip of the peak started to show some flatness at higher temperatures.

4.2.3 Small Angle X-ray Scattering (SAXS)

SAXS profiles were mainly produced to determine the effect of pressure and temperature on the lamellar thickness of L-04 copolymer. By measuring the peak's parameter 'q_{peak}', the long period 'L' can then be calculated using **equation (2.2.6)**. Once the long period and degree of crystallinity (from WAXD) are known, lamellar thickness can be calculated. The lamellar thickness (l) obtained by this method was employed in Gibbs-Thomson plots.

Figures (4.2.10a-b) show the effect of temperature and pressure on the original SAXS data. The general shape of SAXS profiles does not change with changing conditions. In general, the peak shifts to lower 'q' values with increasing intensity at higher crystallization temperatures **(figure 4.2.10a)**. The introduction of pressure at constant crystallization temperature should behave similarly to increasing the supercooling temperatures where a drop in the degree of crystallinity is expected. In contrary, **figure (4.2.10b)** shows a peak shift towards lower (q_{peak}) values, i.e. larger long periods, accompanied with increasing peak intensity. This sign of increasing crystallinity indicates the formation of a larger crystalline system at elevated pressures. Apparently, the system does not depend on the supercooling temperature when crystallized at high pressures. This behavior resembles that of extended chain crystals 'ECC' as will be discussed in the next chapter.

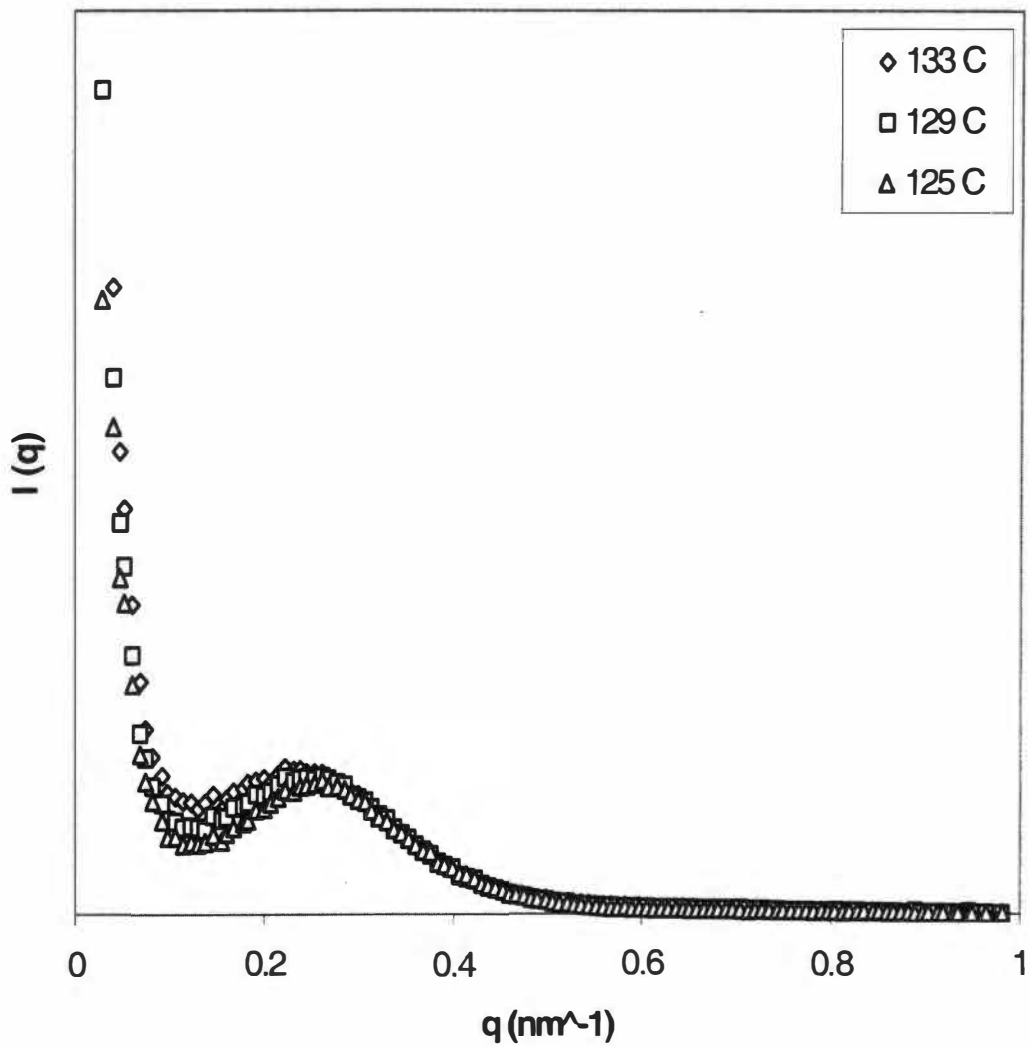


Figure (4.2.10) The Effect of crystallization temperature on the original SAXS data, a) at constant pressure (P=0.48 kbar).

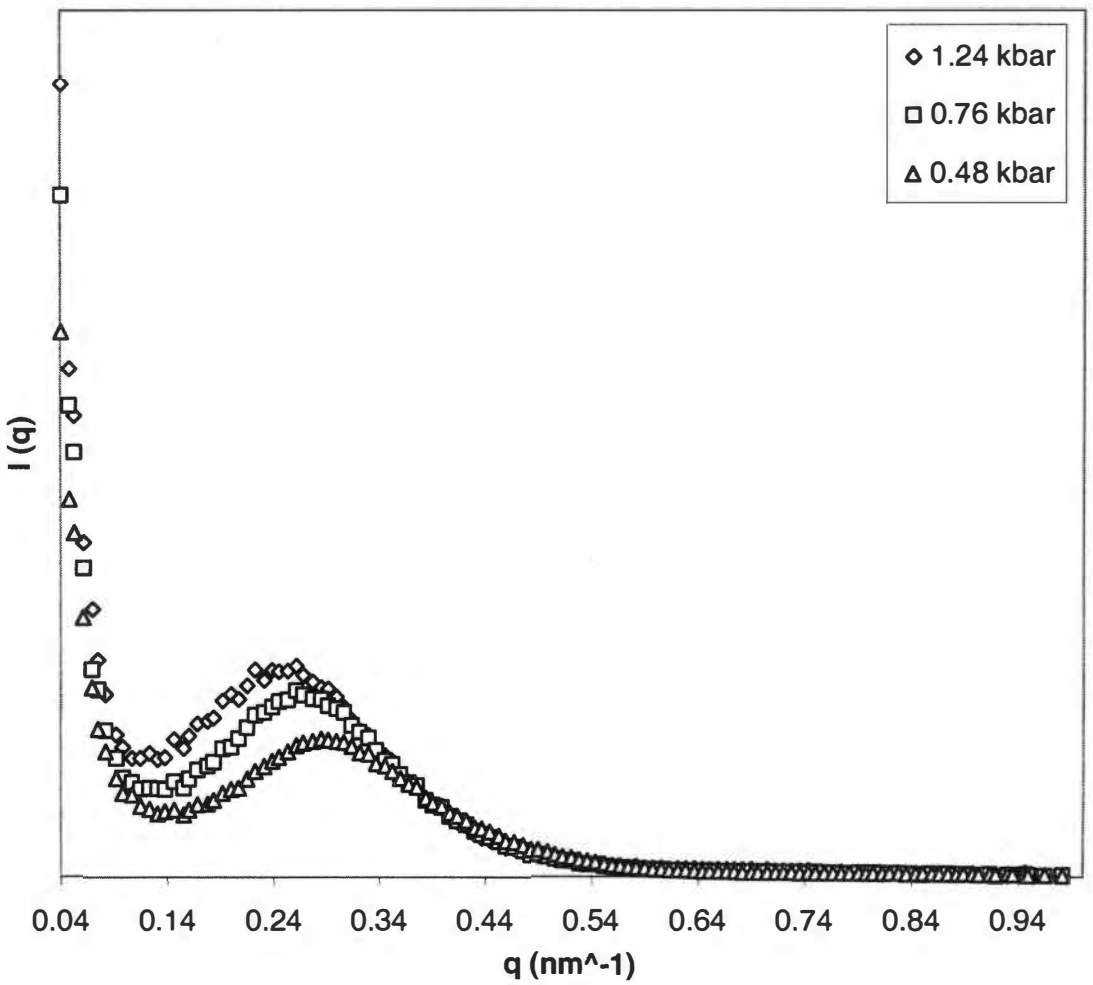


Figure (4.2.10) Continued, b) at constant temperature (T_c= 128 °C).

Since the scattered beam was collected using a linear detector, the Lorentz correction was applied to the original SAXS data. By determining the peak position, the weight average of the long period can be obtained. **Figures (4.2.11-14)** compare the lamellar thickness values calculated using the original SAXS data, Lorentz corrected data, and 1-D correlation function. For samples prepared at P =0.76 and 1.24 kbar (see **figures 4.2.13-14)** one can observe an increase in the lamellar thickness before it starts to decrease at higher temperatures. The inversion started at about 140 °C for samples prepared at P =0.76 kbar and around 150 °C for the 1.24 kbar set. Both temperatures exceed the regime I-II transition temperature.

It could be argued that the upper behavior is caused by the time of crystallization used. Growth rates at high temperatures are very slow, and very long time is required before reaching a near complete crystallization. Reading lower lamellar thickness values at this region could indicate that the time taken to crystallize the sample was not enough. However, the long crystallization times used in these experiments are believed to be sufficient for the crystallization to be near complete. It will be seen later that this deflection is real and should not be ignored when determining the equilibrium melting point.

The Lorentz corrected data show a second peak that appears at larger (q_2) values in the shape of a shoulder. The ratio of the q_{peak}/q_2 is ≈2.2 in average. This peak could be a result of scattering problems and it is not believed to carry any real information about the material's structure.

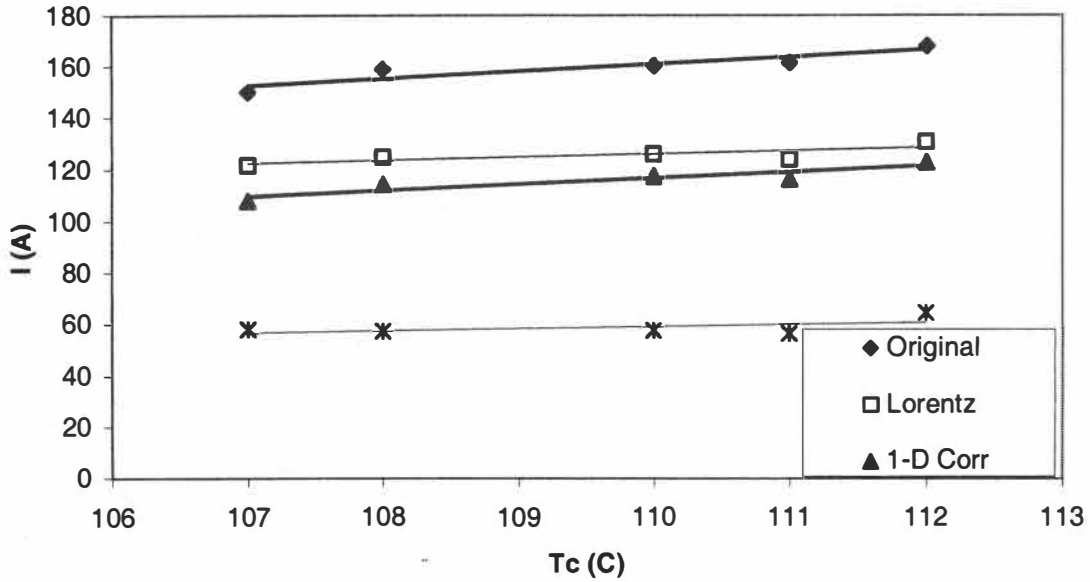


Figure (4.2.11) Lamellar thickness ℓ (Å) versus T_c (C) for L-04 copolymer crystallized at atmospheric pressure.

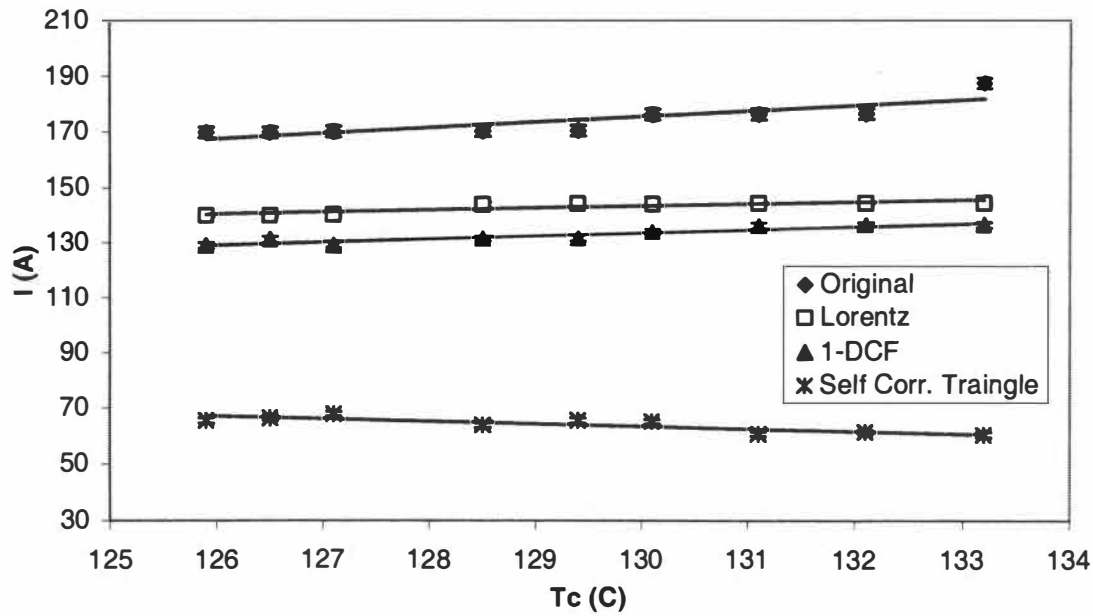


Figure (4.2.12) Lamellar thickness ℓ (Å) versus T_c (C) for L-04 copolymer crystallized at P=0.47 kbar.

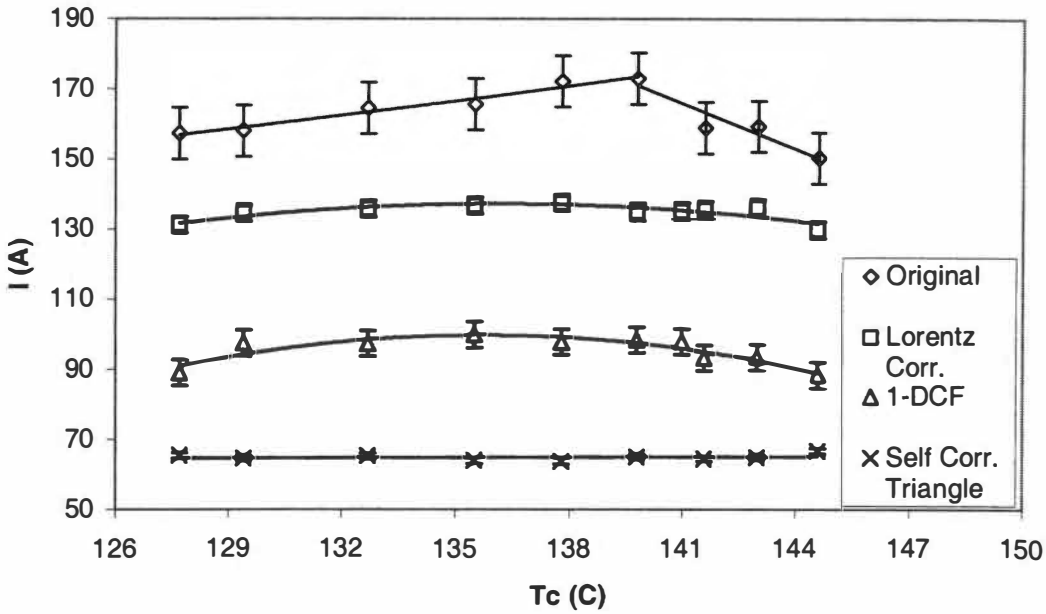


Figure (4.2.13) Lamellar thickness ℓ (Å) versus T_c (C) for L-04 copolymer crystallized at P=0.76 kbar.

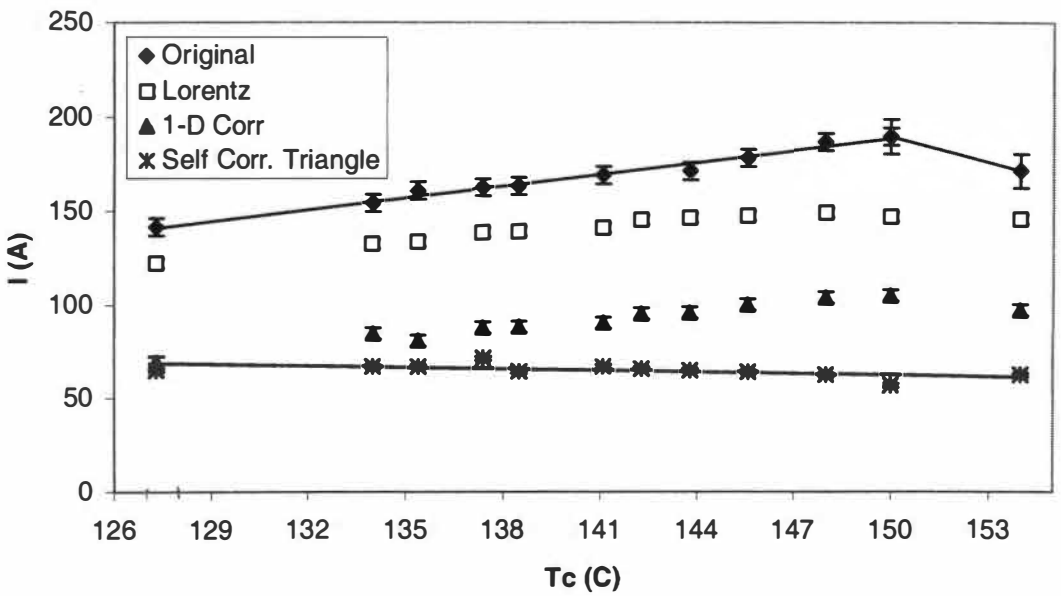


Figure (4.2.14) Lamellar thickness ℓ (Å) versus T_c (C) for L-04 copolymer crystallized at P=1.24 kbar.

Lorentz correction method assumes that lamellae are separated by the same amount of the amorphous material, and each long period represents the summation of the amorphous phase length (l_a) and the crystalline phase length (l_c) for a two-phase system with sharp phase boundary. In real polymer system this assumption is very ideal. For this reason the one-dimensional correlation function was used. This method considers a three-phase model with diffuse transition boundary. The long period (L) is expressed as $L=l_a+l_c+2l_{intf}$, where l_{intf} is the interfacial (or diffuse transition) layer thickness between the crystalline and amorphous phases. Calculating the interfacial layer thickness can be done using two main methods: the modified Porod's law suggested by Ruland, and the one-dimensional correlation function based on the linear gradient of electron density. The values determined using both methods were in a very good agreement as will be shown in **section (5.2.3)**. **Section (4.2.3.1)** explicates the mathematical steps behind both methods. **Figure (4.2.15)** shows the results of the normalized one-dimensional correlation function of L-04 copolymer crystallized at T_c =134.2 °C, and P =1.24kbar. The shape of the curve is typical for all conditions. Only values obtained by the 1-D correlation function method will be used throughout the rest of this study. The crosses in **figures (4.2.11-14)** represent the number average lamellar thickness obtained from the self-correlation triangle of the 1-D correlation function.

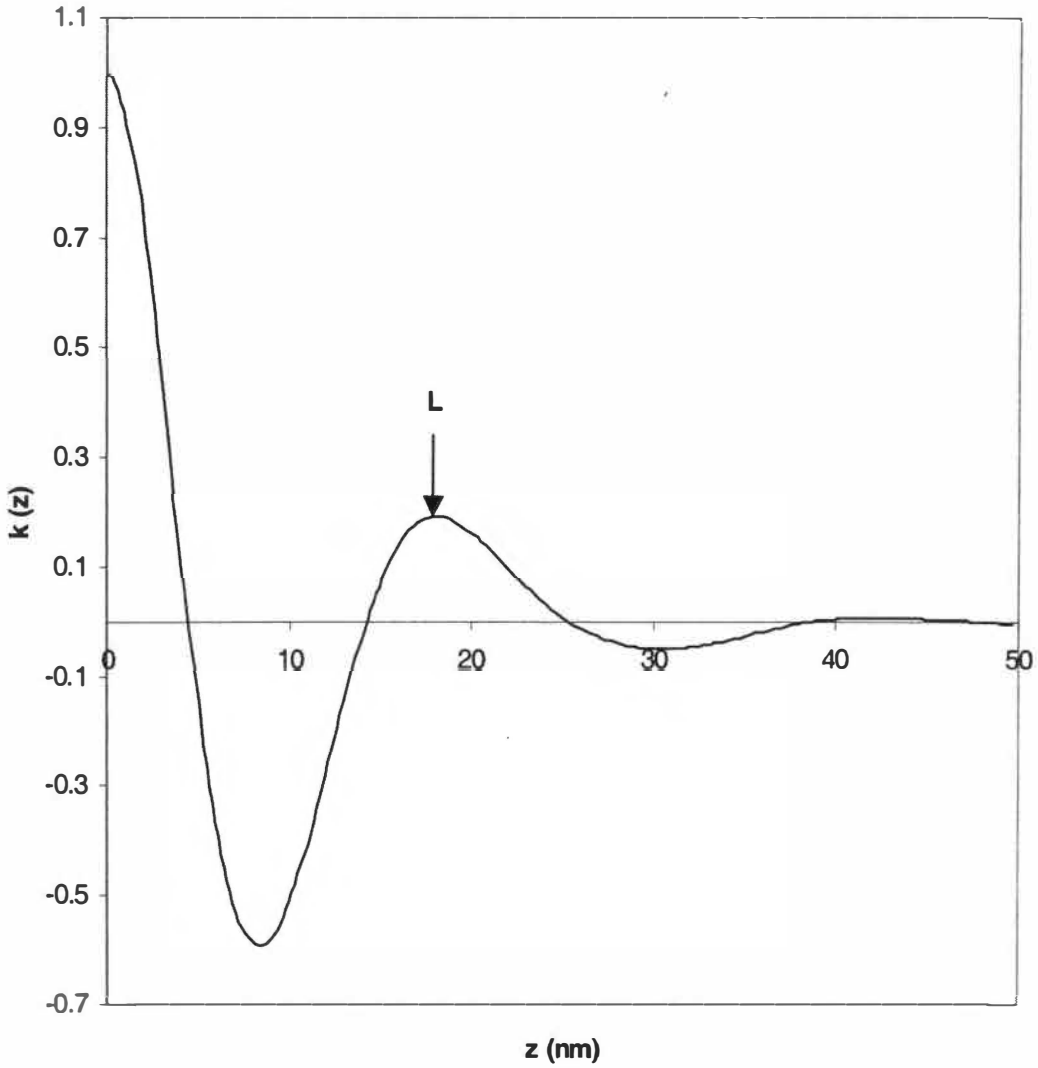


Figure (4.2.15) Normalized one-dimensional correlation function behavior for L-04 copolymer crystallized at T_c =134.2 °C and P=1.24kbar.

4.2.3.1 Theoretical Development for Estimating the Interfacial Layer Thickness Using SAXS.

Porod's Law

Electron density fluctuation, known to cause the positive deviation from Porod's law, can be calculated using the empirical equations of Vonk and Ruland.

Vonk's expression for slit-smeared intensity is:

$$I_{Fl}(q) = Fl + b.q^2 \qquad (4.2.1)$$

where Fl is the thermal density fluctuation constant at $I_{Fl}(0)$, 'b' is a constant, and 'n' is an even number.

Ruland's expression is:

$$I_{Fl}(q) = Fl.\exp(b.q^2) \qquad (4.2.2)$$

Following few mathematical derivations (see details in ref. (68)) the observed scattering intensity corrected thermal density fluctuation can be expressed as:

$$\lim_{q\to\infty}\left[I_{FIcor}(q).q^4\right]=\lim_{q\to\infty}\left[K_p^{'}\left(1-\frac{E^2q^2}{12}\right)\right] \qquad (4.2.3)$$

where 'E' is the transition layer thickness and could be obtained from the negative slope of $I_{FlCor}(q).q^4$ versus q^2 plot.

Using the Fourier transform of the autocorrelation of a Gaussian function the upper equation becomes:

$$\lim_{q\to\infty}\left[I_{FlCor}(q).q^4\right]=\lim_{q\to\infty}\left[K_p^{'}\exp\left(-\Delta^2.q^2\right)\right] \qquad (4.2.4)$$

By expanding the exponential function, **equation (4.2.4)** could be written as:

$$\lim_{q\to\infty}\left[I_{FlCor}(q).q^4\right]=\lim_{q\to\infty}\left[K_p^{'}\left(1-\Delta^2.q^2\right)\right] \qquad (4.2.5)$$

where 'Δ' is the standard deviation of the Gaussian function, and is equivalent to the transition layer thickness. From the above the determination of the diffuse transition layer thickness (Δ) can be calculated from the negative slope of the plot $ln(I_{FlCor}(q).q^4)$ versus q^2 of **equation (4.2.4)** under the assumption of a sigmoidal-electron density gradient across the boundary, or the linear plot of $I_{FlCor}(q).q^4$ versus q^2 of **equation (4.2.5)**. For calculating the crystalline lamellar thickness (l_c) the former method was used to avoid the truncation effect. The calculated value represents the l_{intf} value. **Figures (4.2.16-17)** are

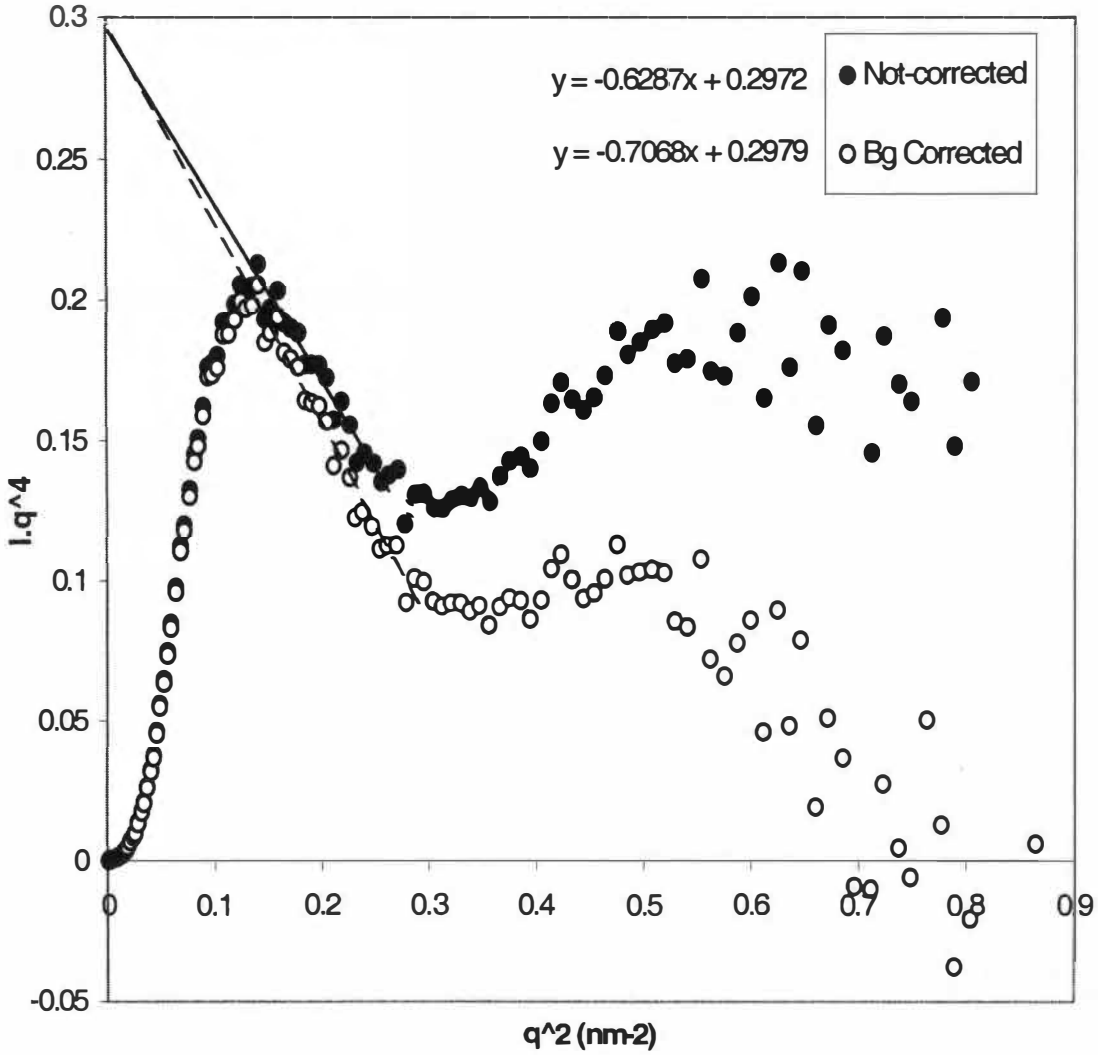


Figure (4.2.16) Linear-gradient model showing the effect of background intensity correction on estimating interfacial layer thickness '*E*' of L-04 copolymer crystallized at T_c =136 °C and P=0.76 kbar.

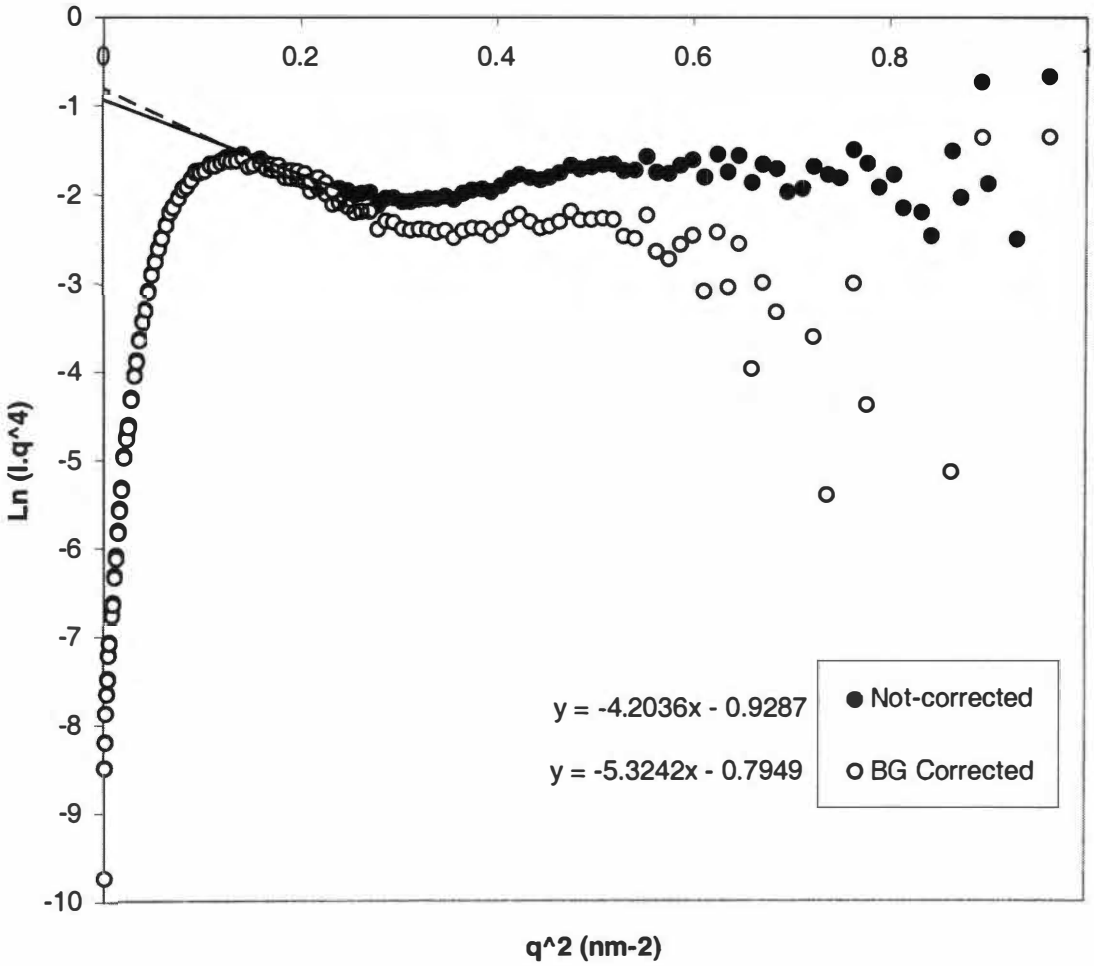


Figure (4.2.17) Sigmoidal-gradient model showing the effect of background intensity correction on estimating interfacial layer thickness 'Δ' of L-04 copolymer crystallized at T_c =136 °C and P=0.76 kbar.

good examples of the sigmoidal- and linear-gradient techniques. In both cases, the background intensity correction always gives a larger interfacial layer thickness value. The correction will be applied to all data.

Figures (4.2.18-19) show the effect of pressure and temperature on the estimation of the interfacial layer thickness '*E*' obtained by using linear-gradient model and background intensity correction. A negligible increase in the negative slope, hence the interfacial layer thickness, is observed with increasing pressure (**figure 4.2.18**). On the other hand, there is no consistent change of the interfacial layer thickness as a function of temperature (**figure 4.2.19**). The average amount of change is within a constant value. The independency of interfacial layer thickness on pressure and temperature will be clearly illustrated when a comparison between '*E*' and 'Δ' values is established in the discussion section.

One-Dimensional Correlation Function

The extrapolated line in **figure (2.2.1)** (dashed line) is represented by the following equation:

$$K(z) = -\frac{w_c}{d}(\eta_c - \eta_a)^2 z + w_c(1 - w_c)(\eta_c - \eta_a)^2 \qquad (4.2.6)$$

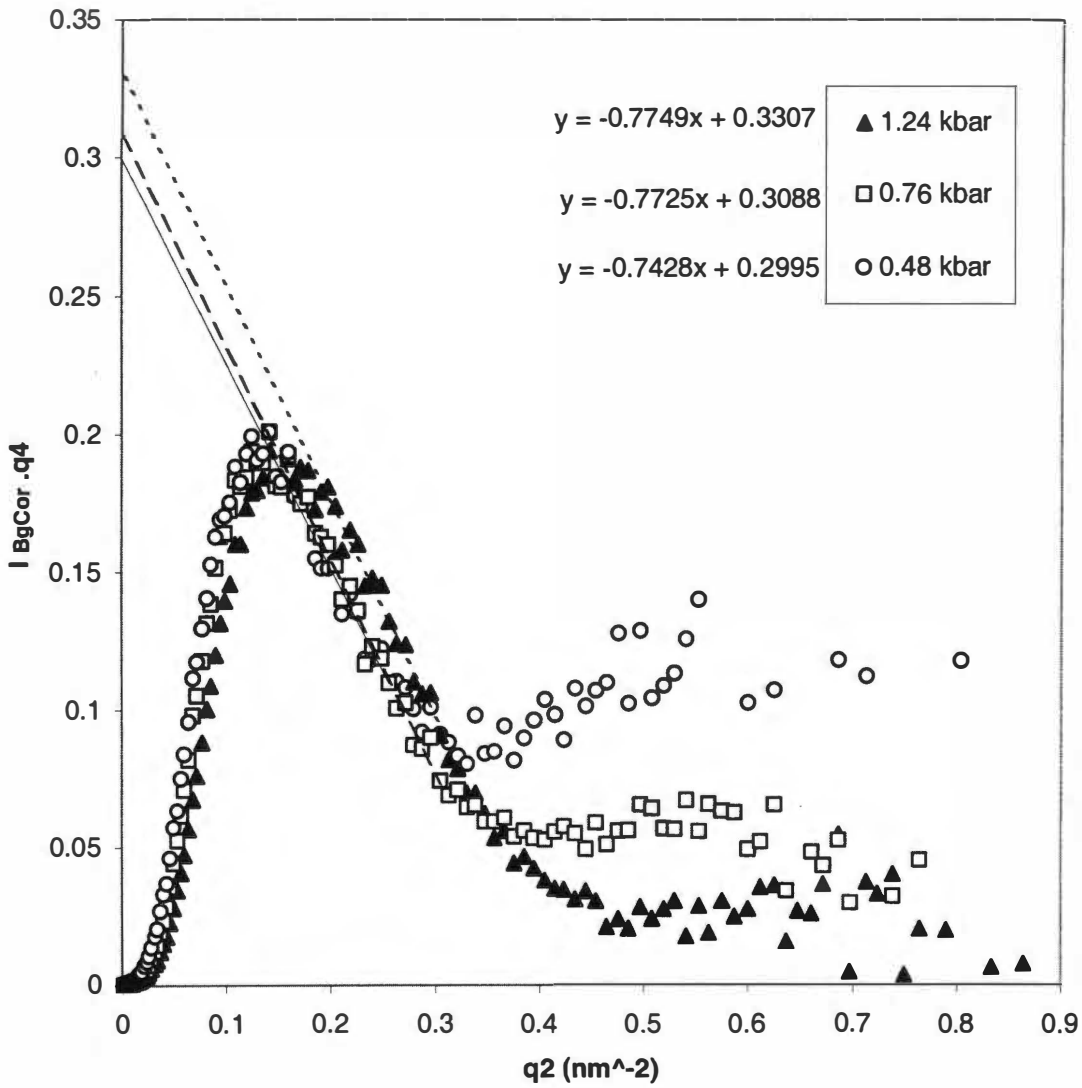


Figure (4.2.18) Linear-gradient model and background intensity correction of L-04 copolymer as a function of pressure and at constant crystallization temperature of 128 °C.

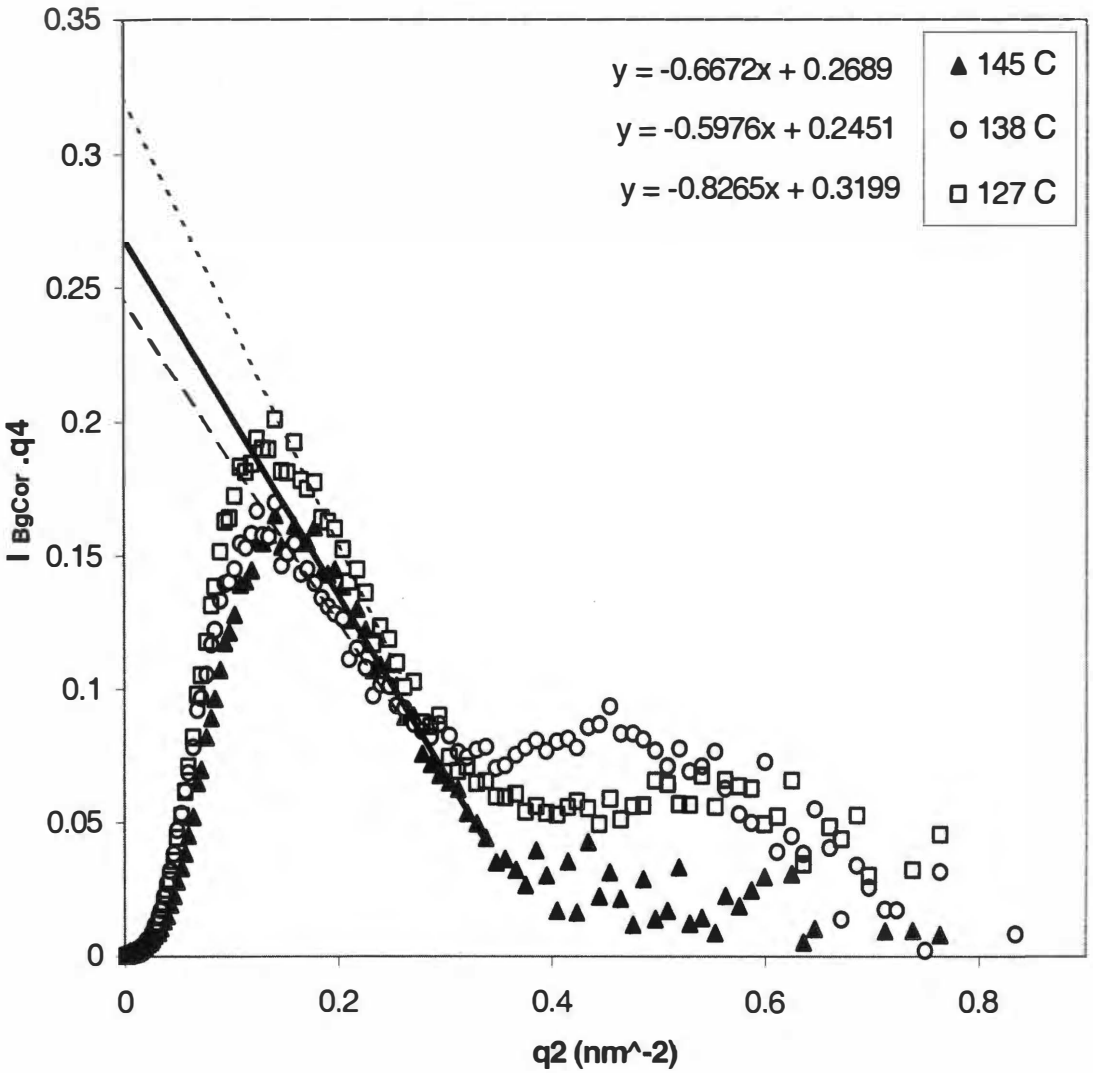


Figure (4.2.19) Linear-gradient model and background intensity correction of L-04 copolymer as a function of temperature and at constant pressure of 0.76 kbar.

where symbols used here are the same as in **section (2.2.3.1)**. The line forms the hypotenuse of what is known as the 'self-correlation triangle'. The derivations used by this method are based on the crystallinity being less than 50%, i.e. w_c<0.5. For systems with higher crystallinity, as is the case in this study, the equations can easily be adjusted by switching w_c to $w_a = (1 - w_c)$ and η_a to η_c. In order to have a flat section before the first maxima the crystallinity should be either less than 30% or more than 70%. By applying the above modifications the interfacial lamellar thickness can then be expressed as follow:

$$\Delta = \frac{E\left(w_c - 1/3\right)}{w_c} \tag{4.2.7}$$

for w_c>0.5, 'E' can be written as:

$$E = -4\left(\frac{dK(z)}{dz}\right)\frac{\int_0^\infty q^2 I(q)dq}{\int_0^\infty q^4 I(q)dq} \tag{4.2.8}$$

The difference in the measured interfacial lamellar thickness obtained by the two methods will be the subject of **section 5.2.3**.

4.3 Thermal Analysis

The melting behavior of L-04 and L-11 copolymers under high pressure was studied using the transmitted light intensity technique. DSC and Light intensity methods were used to study the melting behavior of the quenched high-pressure samples and samples prepared at atmospheric pressure. All melting experiments were run at a melting rate of 10 °C/min.

4.3.1 Melting at Atmospheric Pressure

4.3.1.1 Samples prepared at atmospheric pressure

L-04 and L-11 copolymers were crystallized at atmospheric pressure and different crystallization temperatures. Kim [68] has studied the thermal behavior of those materials thoroughly at atmospheric pressure using DSC technique. Light intensity technique was not considered in his study. A comparison between the equilibrium melting temperatures 'T_m^o' obtained by this study and Kim's study will be established later in the next section.

Similar to the isothermal bulk crystallization, transmitted light intensity in melting experiments generates a sigmoidal pattern when measured as a function of time or temperature. **Figure (4.3.1)** shows a typical melting behavior of L-04 copolymer that was crystallized at different temperatures before melting it at atmospheric pressure. Complete melting is reached when the light intensity reaches zero. For easier analysis the derivative

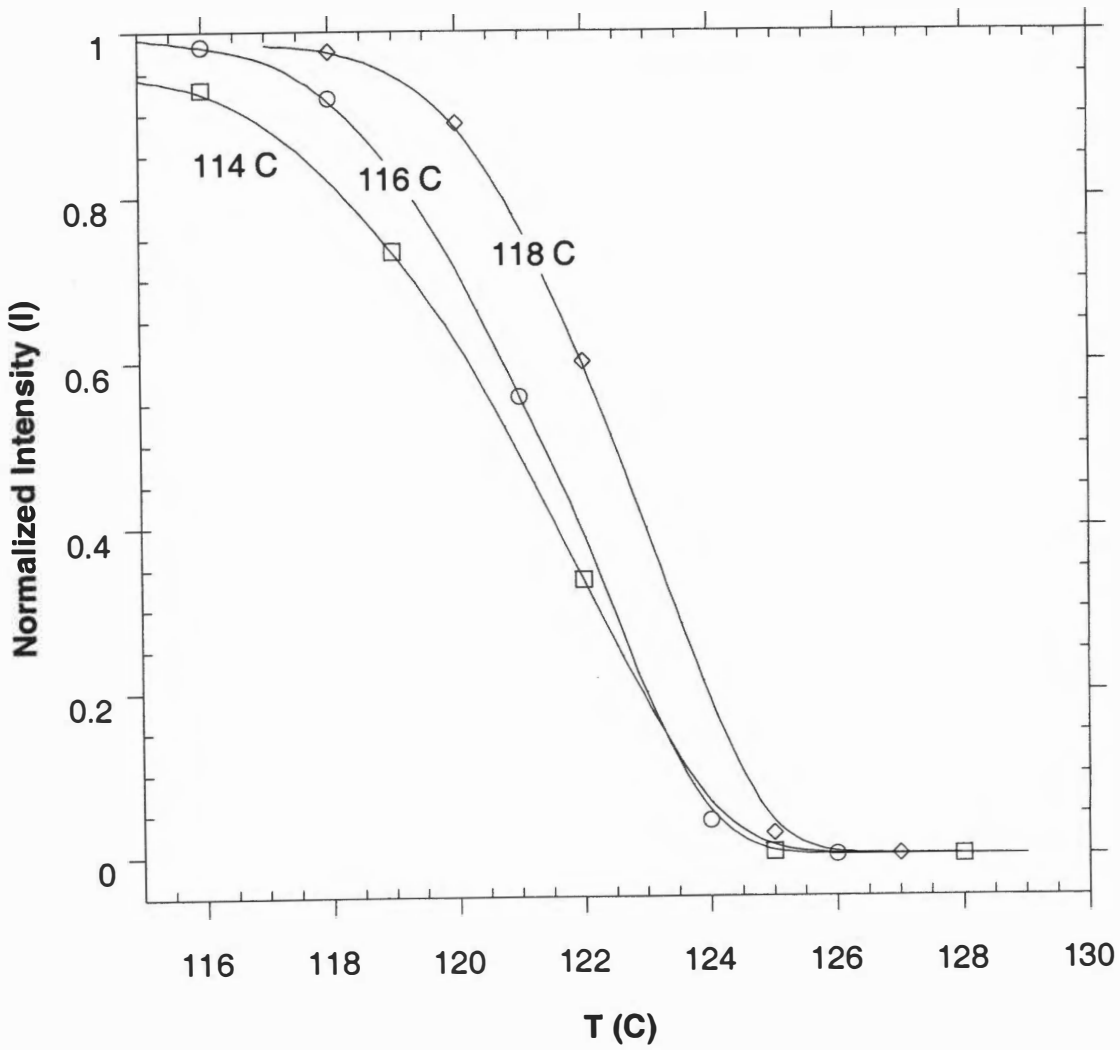


Figure (4.3.1) The melting behavior of L-04 copolymer crystallized at atmospheric pressure and different temperatures using light intensity method.

of the intensity with respect to temperature '*dI/dT*' was plotted versus temperature, as shown in **figure (4.3.2)**, resulting in a behavior similar to the DSC melting curves. The peak position, which resembles the endotherm peak in DSC, represents the temperature at which the intensity drop occurs at its highest rate. In other words, it represents the average melting point compensated by the distribution of spherulite sizes, and hence, reflects the thickness of the lamellae. The temperature at which intensity reaches zero could be referred to as the return-to-the-baseline (RTB) temperature.

DSC melting behavior was studied for the same material at selected temperatures as shown in **figure (4.3.3)**. A sharp single endotherm peak was produced for the three selected conditions. The heat of fusion increases with temperature and a small shoulder that developed to a small hump is observed. The hump formed at temperatures lower than the crystallization temperature disappeared completely when the sample was crystallized and melted without quenching it. This behavior is believed to be a result of the annealing-recrystallization of the crystalline fraction at room temperature.

The three crystallization temperatures, used in the DSC experiments, were chosen in a way to cover a wide range of temperatures. Although this number of points is not sufficient to determine the equilibrium melting temperature, but it could be used for comparison purposes with the ones obtained from light intensity. A comparison between the melting points obtained by light intensity and DSC techniques for the same conditions are listed in **table (4.3.1)**. The reasonable match achieved between the two techniques adds more credibility to the results of the light intensity technique.

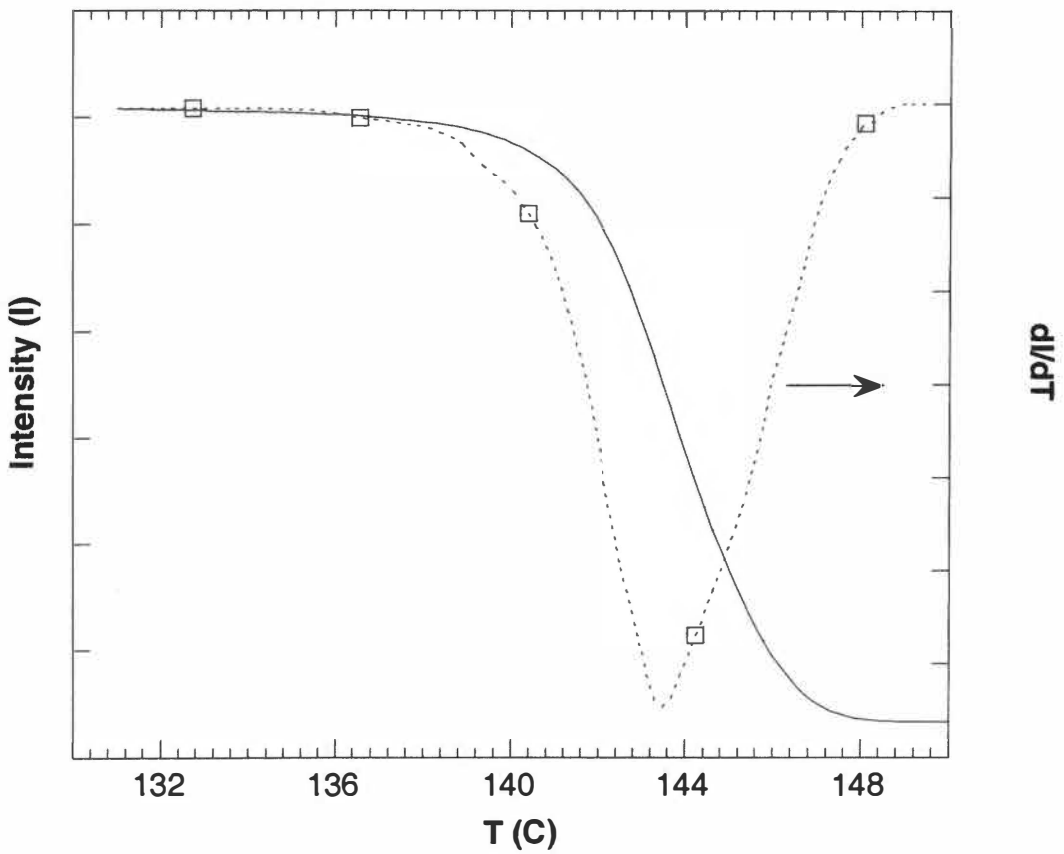


Figure (4.3.2) The melting behavior of L-04 copolymer crystallized at T_c=130°C and P=0.48kbar using light intensity and its derivative.

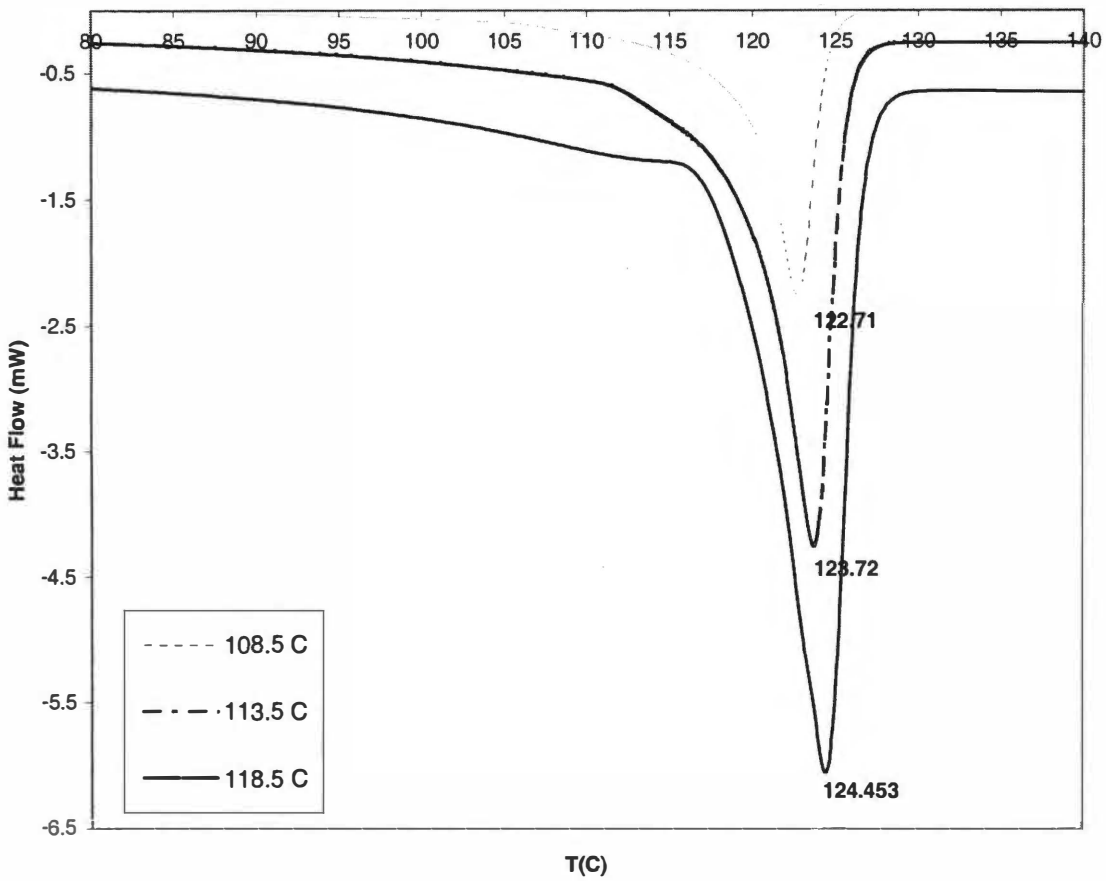


Figure (4.3.3) The DSC melting curves of L-04 copolymer crystallized at atmospheric pressure.

Table (4.3.1) A comparison of the melting temperatures of L-04 and L-11 copolymers obtained by using DSC and Light Intensity techniques. All conditions listed are for samples crystallized at atmospheric pressure.

Material	T_c(C)	T_m(C) DSC	T_m(C) L.I.	ΔT_m(C)
L-04	108.5	122.71	122.0	0.71
	118.5	124.45	124.26	0.19
L-11	100	102.83	103.75	0.92
	100	109.67	110.09	0.42
	105	107.69	108.40	0.71
	105	111.48	111.00	0.48

Melting behavior studies of L-11 copolymer were handled similarly. However, all light intensity profiles of this material showed two different slopes with a small plateau region or a shoulder between them. The plateau region becomes clearer at lower temperatures. A plot of '*dI/dT*' versus *T* represents the two slopes as two different peaks as shown in **figure (4.3.4)**.

The two peaks are obvious in the DSC melting curves as shown in **figure (4.3.5)**. It is important to notice that the heat flow of the peaks is temperature dependent. For lower crystallization temperature the heat flow of the higher melting temperature peak is larger than the lower melting temperature peak. At higher crystallization temperature both peaks tend to have equivalent heat flow values. When crystallization temperature is further increased, the order is switched and the heat flow becomes larger for the lower melting peak. Heat of fusion and hence crystallinity for each peak is also following the same pattern. The small peak appeared at temperatures lower than the crystallization temperatures disappeared for samples prepared at higher crystallization temperature. Instead, the sharp peak formed at lower melting temperature became broader. Detailed comments on this behavior will be included in the discussion section. **Table (4.3.1)** shows the reasonable agreement between the melting temperatures of L-11 copolymer obtained by both DSC and light intensity methods.

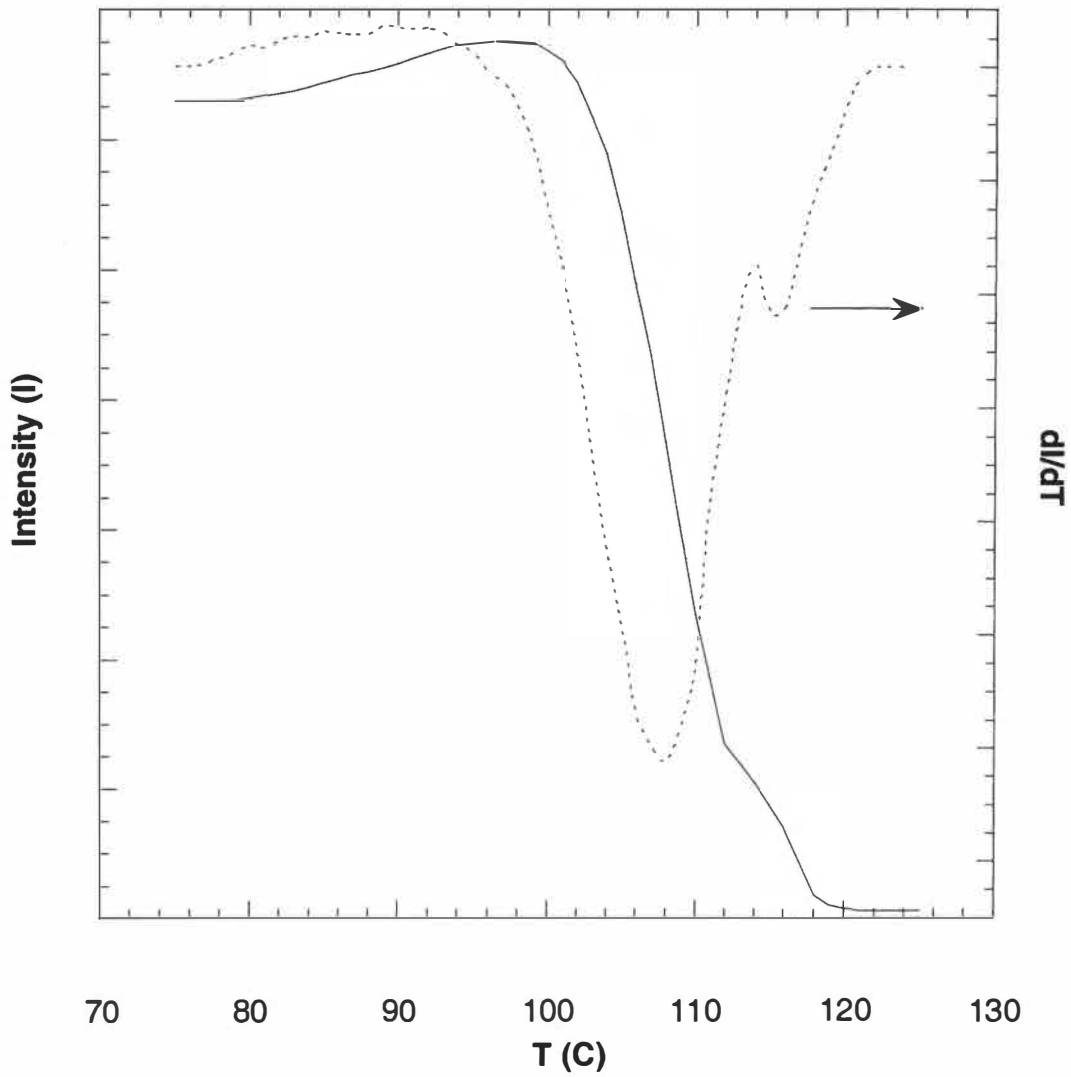


Figure (4.3.4) The melting behavior of L-11 copolymer crystallized at T_c=112 °C and P =1 atm using light intensity and its derivative.

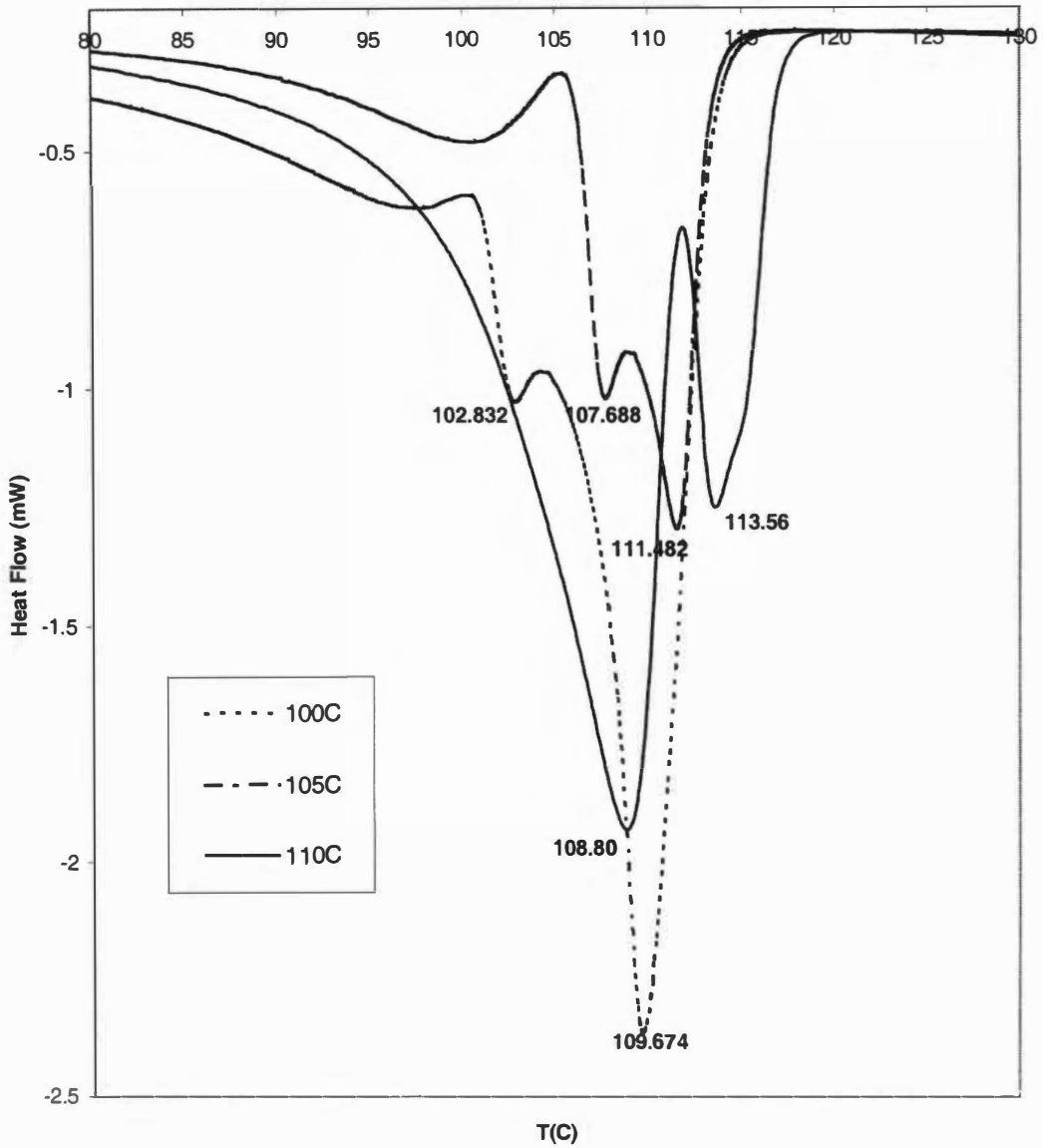


Figure (4.3.5) The DSC melting curves of L-11 copolymer crystallized at atmospheric pressure.

4.3.1.2 Samples Prepared at Elevated Pressures

To study the effect of pressure on the material's thermal behavior, L-04 copolymer was first crystallized at specific temperatures and pressures for enough time, then cooled down to room temperature before releasing the pressure. Quenched samples were reheated at a rate of 10°C/min tell it melted. An example of the light intensity measurements taken during the heating process is shown in **figure (4.3.6)** for samples crystallized at P =1.24kbar. From the figure, samples crystallized at temperatures lower than the regime II-III transition temperature show an increase in intensity before melting starts. No corresponding event was observed by the DSC for the same condition. In addition, no sign of double peak formation was observed. The peak positions obtained by both methods were very consistent. The behavior is repeatable for all different pressures applied.

A possible explanation of the upper phenomenon could be related to the thermal expansion of the material, or to the change in the internal structure of the spherulites [69]. The melting behavior of isotactic polypropylene showed similar results [70], where the presence of thin lamellar branches, that are inclined at 80° to the dominant radial lamellae, is believed to be the reason behind the reported increase of the birefringence. Observing the increased birefringence by light intensity, but not DSC, supports the explanation of thermal expansion of the material. At low T_c, the crystallization process is very rapid and less packed structure is formed. Consequently, the expansion of the

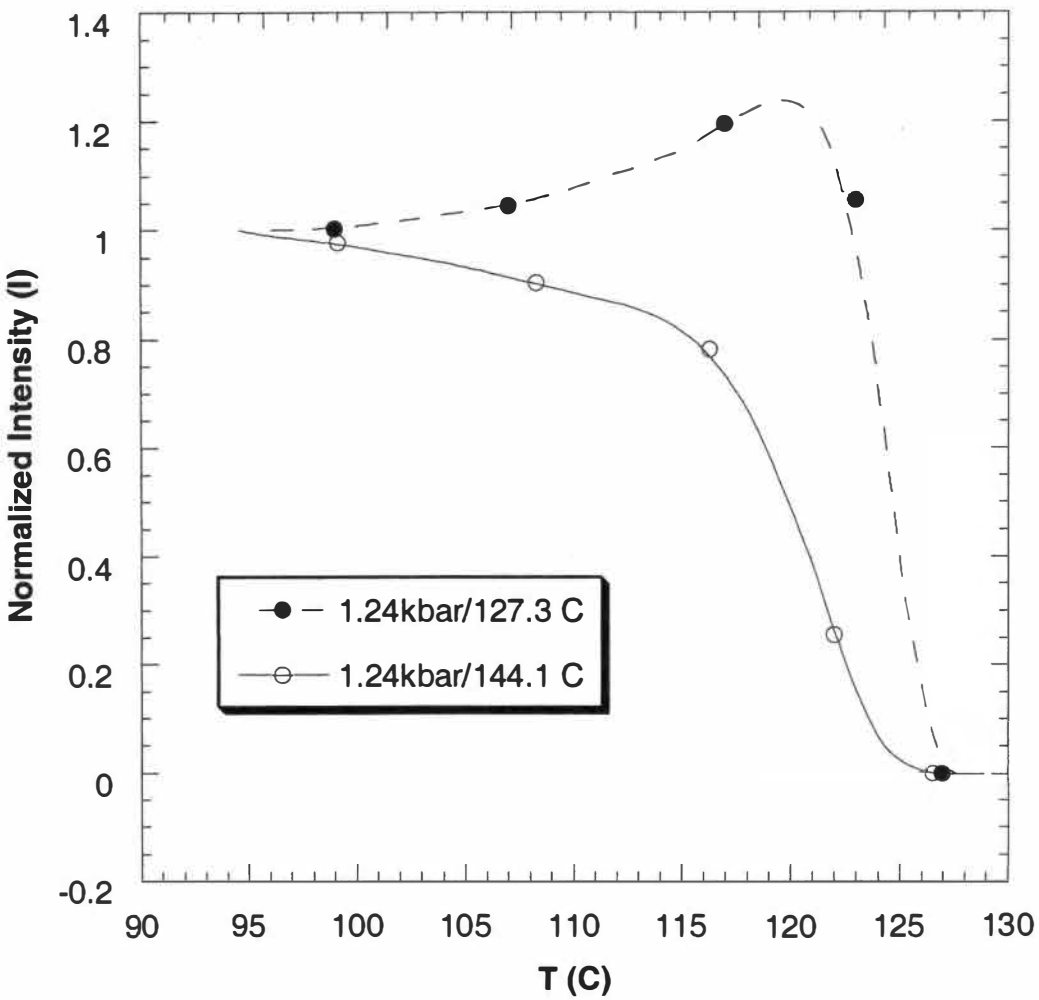


Figure (4.3.6) Normalized light intensity plot of samples prepared at 1.24kbar and melted at atmospheric pressure.

material is more favorable on heating. Crystallization at higher T_c, on the other hand, produces less amorphous material and highly packed structure therefore thermal expansion cannot be observed. The formation of a highly packed structure is consistent with the formation of extended-chain crystals as will be discussed later.

It is very important to notice that the melting points obtained for high-pressure samples are very low compared to the expected high melting temperatures observed at elevated pressures even after correcting for the expected 17 °C/kbar increase. For example, the melting temperature of the sample crystallized at T_c =125.9 °C and P =0.48kbar is about 141 °C under pressure. Removing the pressure should drop the melting point by 8.2 °C and give a melting point of 132.8 °C. However, DSC and light intensity methods gave a value of ~125 °C. In conclusion, the structure or phase that co-exists with the known stable orthorhombic phase at high pressures and temperatures is meta-stable and cannot be detected at atmospheric conditions. It appears that thick crystals are produced at elevated pressures, but they decay to thinner crystals when pressure is reduced.

All high-pressure samples when studied by DSC where run twice. In the first run, samples were cooled down to –50 °C using DSC and heated at a rate of 10°C/min. till a complete melt is reached. In the second run, samples were kept in the molten state at 150 °C for 10 minutes to assure the removal of any thermal history. Samples were then crystallized at a rate of 10°C/min. before heating started again at the same rate. All DSC thermograms showed a surprising coincidence between the two different runs of DSC.

This implies that severe changes to the crystalline structure must have occurred to the sample when it was transferred from the high pressure-temperature environment to the room pressure and temperature. In other words, the final structure of the high-pressurized samples resembles the ones prepared at atmospheric pressure, which confirms the occurrence of phase transformation.

4.3.2 Melting at Elevated Pressures

Melting samples at the crystallization pressure, *in-situ* melting, was conducted to understand the real effect of pressure on the thermal behavior of the copolymers. Melting starts from the assigned crystallization temperature ($T_c \geq T_m$ of the sample at atmospheric pressure). For all crystallization temperatures applied, L-04 copolymer showed a single melting peak when crystallized at P = 0.48kbar (**figure 4.3.2**). At larger pressures two melting peaks started to appear similar to what was observed in **figure (4.3.4)** for L-11 copolymer. In all cases no increase in intensity was observed before melting started. Since *in-situ* melting experiments start at relatively high crystallization temperatures and before quenching the material, thermal relaxation is not expected. This confirms that the observed increase in intensity is a result of the thermal relaxation of the material.

4.4 Morphology

Any method yielding quantitative or qualitative structural data involving features larger than the unit cell is usually deemed 'morphological'. Two main morphological

methods were used in this study to achieve wider understanding of the behavior of ethylene-octene copolymers crystallized at elevated pressures and temperatures. Optical microscopy was used for the spherulitic level analysis, while scanning electron microscopy was used on the lamellar level.

4.4.1 Optical Microscopy

The relatively small size of spherulites associated with ethylene-octene copolymers, and the limited magnification of the objective lenses used, made it a difficult task to produce good pictures while crystallizing under pressure. The design of the pressure cell discussed in **section 3.3** allows the minimum working distance of the objective to be 18 mm. This, as a result, forced us to work with only 200x total magnification, that is not enough for detailed pictures as seen in **figure (4.4.1)**.

To detect any morphological changes, at the spherulitic level, of the high-pressure samples during quenching, pictures at the same position of the sample were taken *in-situ* i.e. while pressure and temperature are applied, and after cooling down and releasing the pressure. **Figures (4.4.1a-b)** show no detectable changes, at this scale, to the morphology of the spherulitic structure of the L-04 copolymer, crystallized at T_c =136.6 °C and P =0.67kbar, because of quenching. The figures clearly show two distinctive crystal populations, one have the normal spherulitic crystals (circled area), while the other population has a nonspecific morphological feature that includes some axialitic-like structure (squared area).

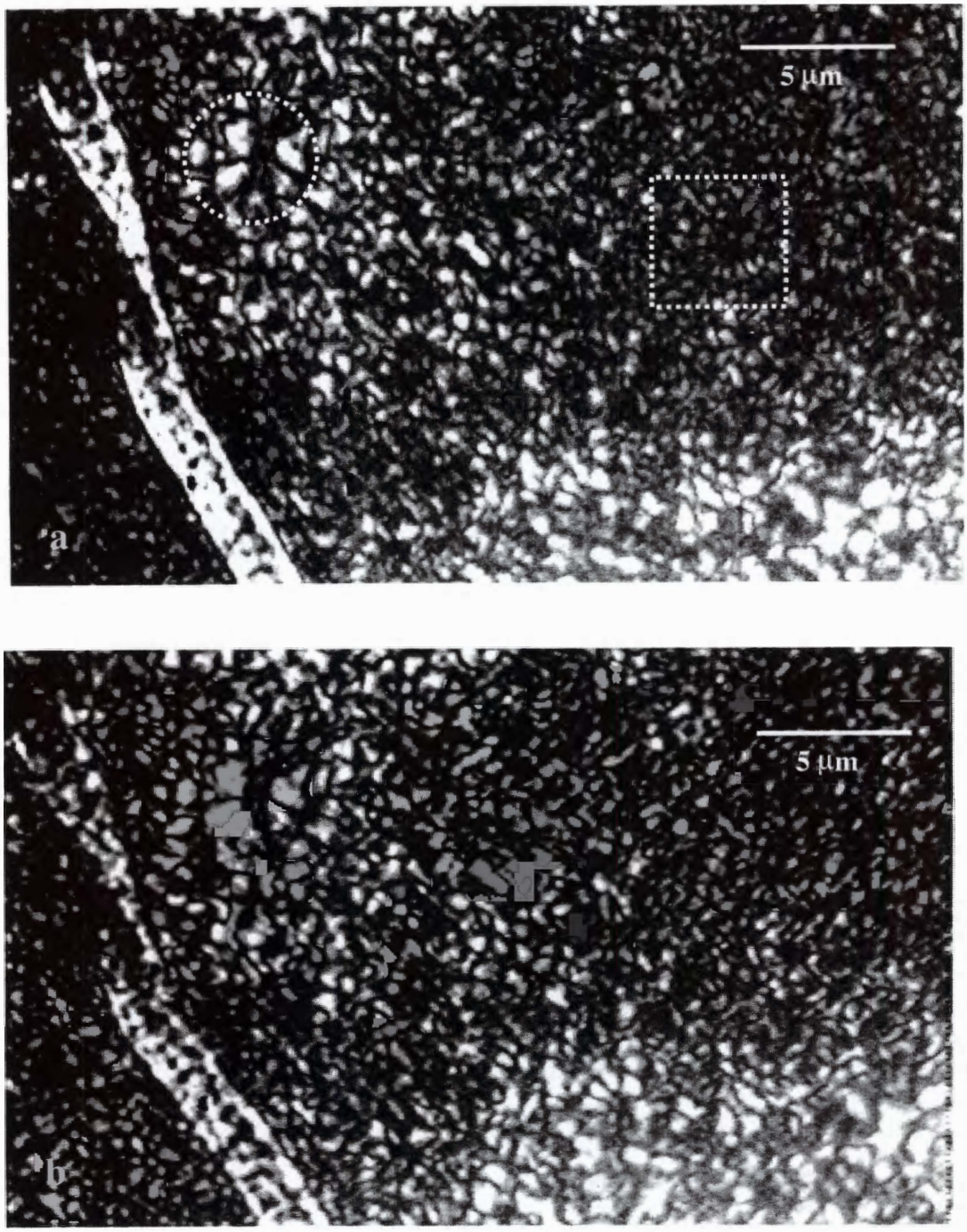


Figure (4.4.1) A picture of L-04 copolymer crystallized at T_c=136.6 °C and P=0.76kbar was taken: a) during crystallization, and b) after cooling down.

In agreement to **figure (4.3.4)**, **figure (4.4.2)** shows the crystallization process of L-11 copolymer crystallized at T_c =121.3 °C and P =0.48kbar. Although the detailed structure of the spherulites formed is not clearly seen, it is obvious that in the early stages of crystallization (t_c =30 minutes) small crystallizable entities grew very fast to form the background seen in **figure (4.4.1a)**. Spherulites (arrowed structure) started to grow later at slower rate as seen in **figure (4.4.1b)** (the picture was taken for the same position after 2.5 hours). Similar to the above example, the morphology of the background does not have any regular shape, and does not change during quenching.

4.4.1.1 Band Spacing

The size of the band spacing was measured using optical microscopy. The band spacing was measured for all available spherulites to obtain reasonable statistical data. The average band spacing for each condition was determined and plotted as a function of temperature and branch content as represented by **figure (4.4.3)**. Larger crystallization temperatures and branch content increase the separation between bands in which extinction bands become 'blotchy' and fade out. **Figures (4.4.4-6)** show the banded spherulites formed at different conditions. The separation of fingers of crystalline polymer by regions containing poorly or noncrystalline material is defined as cellulation. The cellulation effect appears as a discontinuity in the concentric rings without interrupting the periodicity of bandings (see the arrowed structure). The effect is more obvious for higher branched materials as can be seen from the figures.

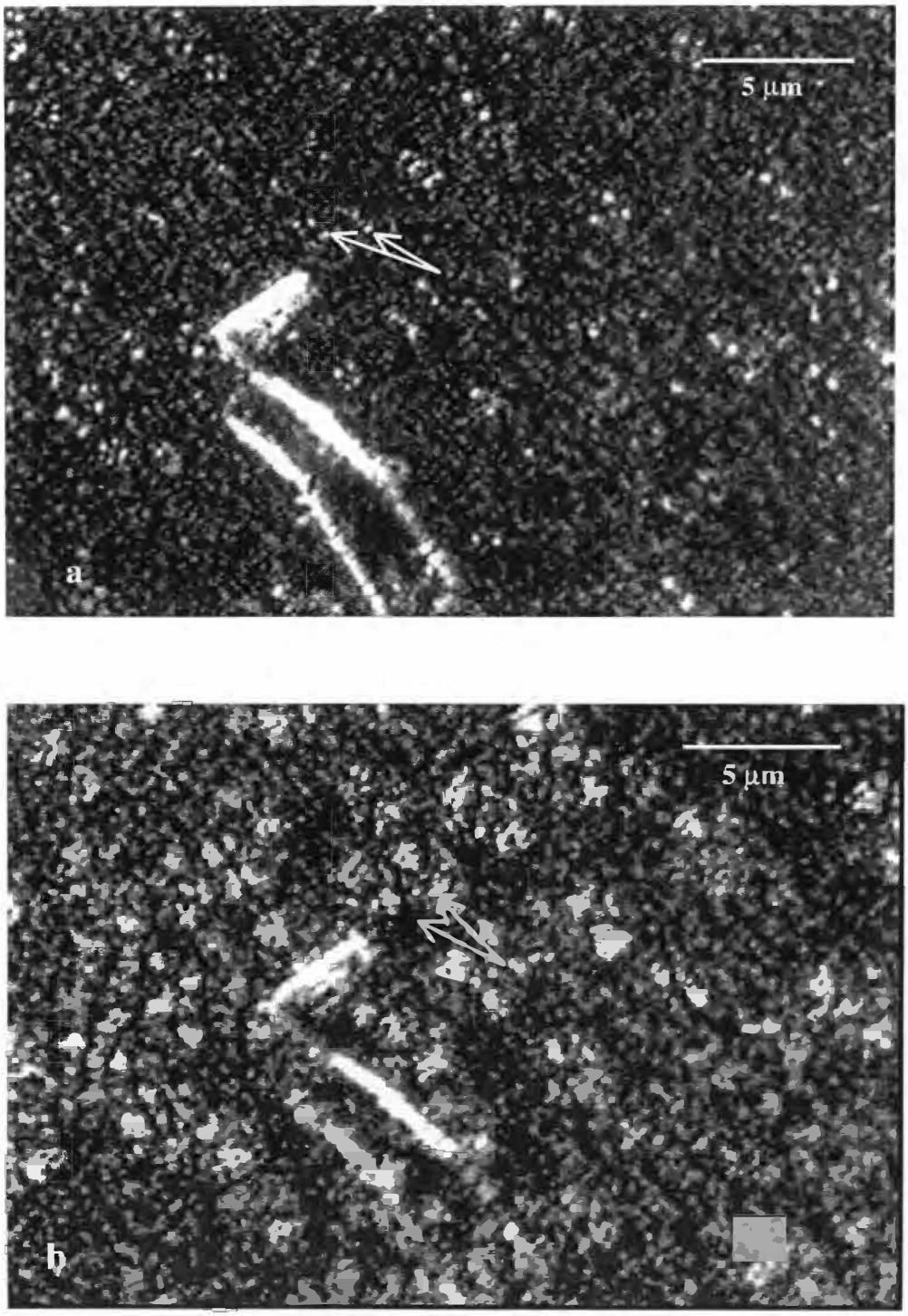


Figure (4.4.2) A picture of L-11 copolymer taken *in-situ* at: a) 0.5h and b) 2.5h crystallization times.

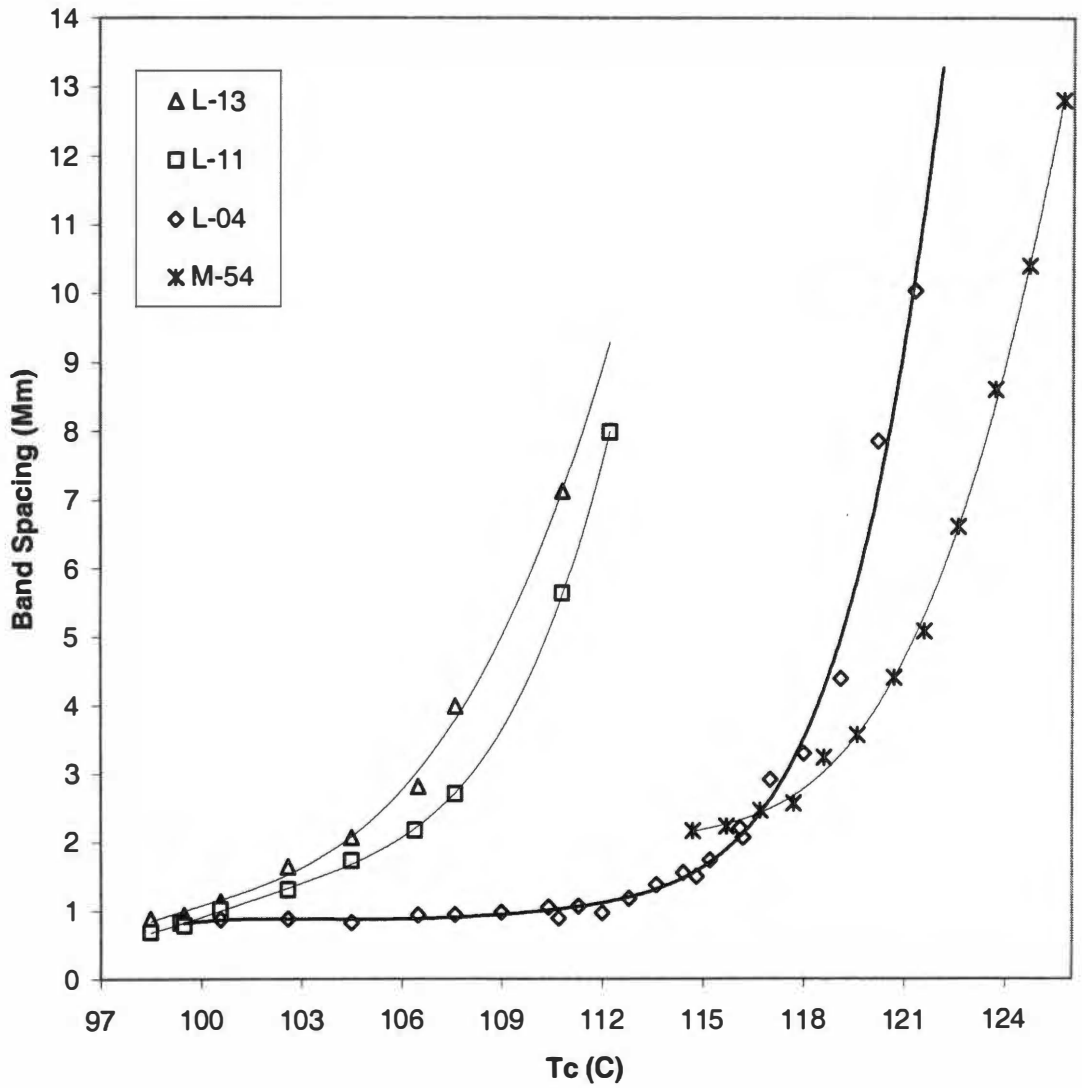


Figure (4.4.3) Band spacing as a function of temperature and branch content of metallocene ethylene-octene copolymer and linear polyethylene.

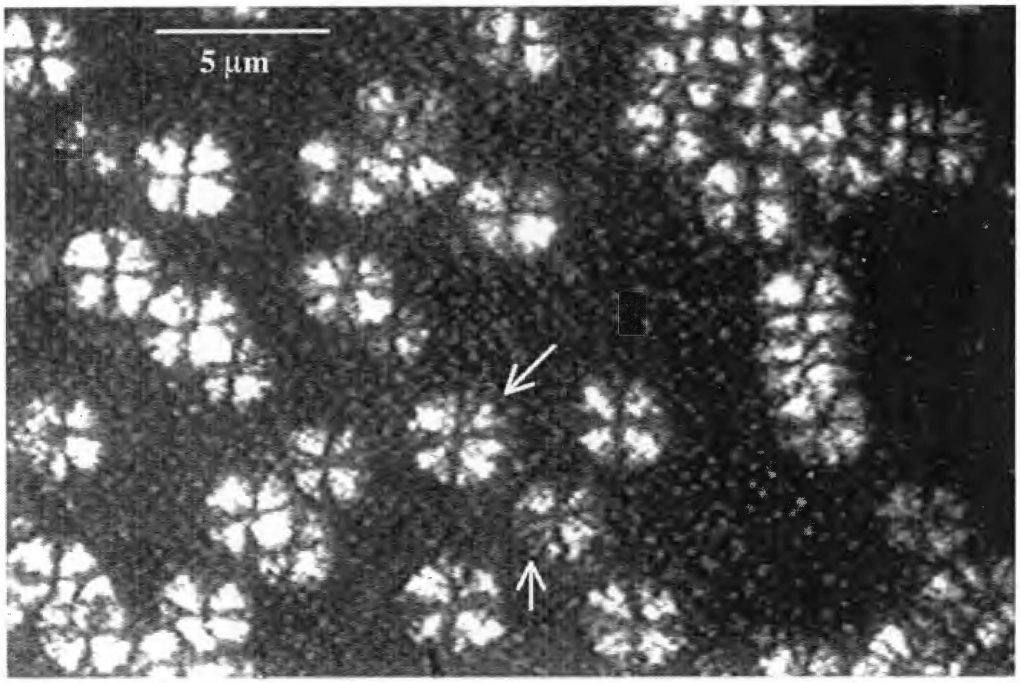


Figure (4.4.4) Cellulation effect in L-11 copolymer at T_c=118 °C, P= 0.48kbar.

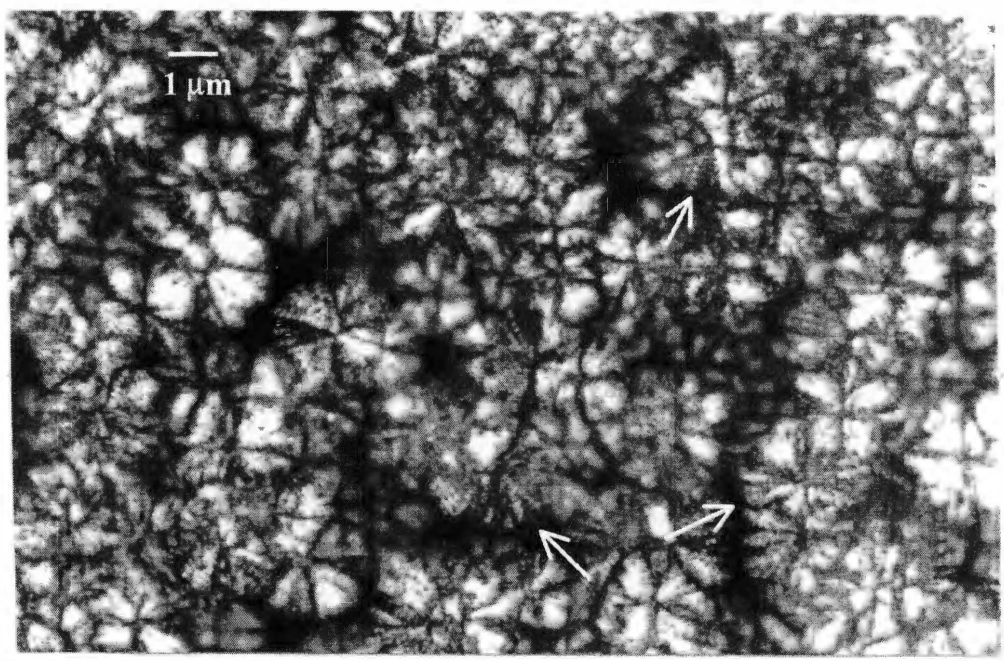


Figure (4.4.5) Cellulation effect in L-13 copolymer at T_c=104.5 °C.

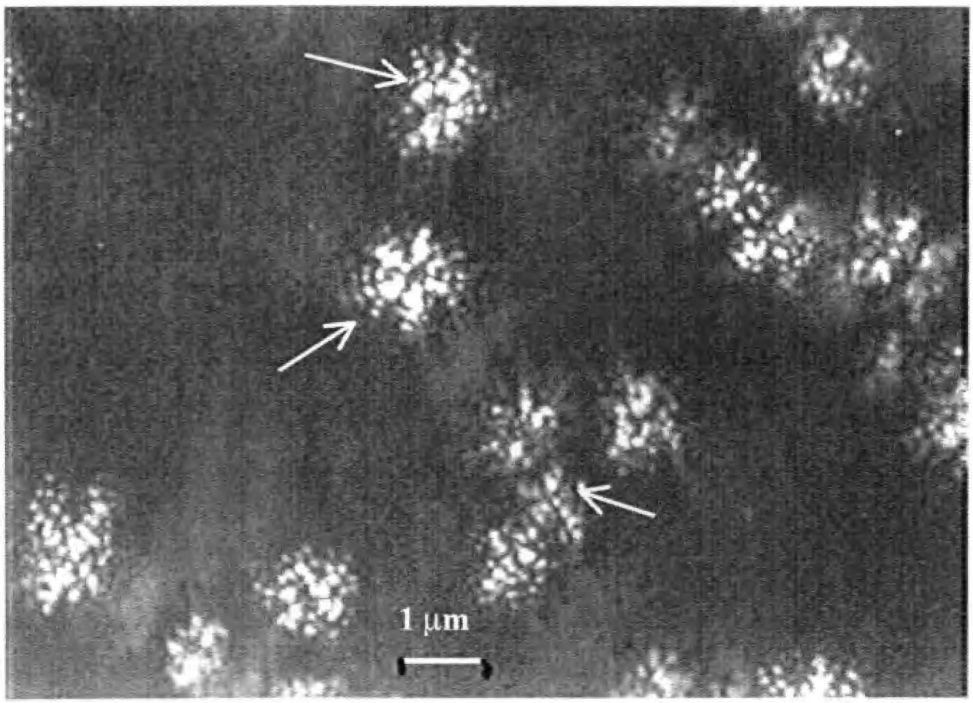


Figure (4.4.6) Cellulation effect in H-17 copolymer at T_c=103 °C (M_n= 48,700).

4.4.2 Scanning Electron Microscopy (SEM)

The morphology of ethylene-octene copolymers was studied using SEM technique. All pictures shown below were taken at room temperature. Two populations of lamellae can be observed for L-04 copolymer prepared at T_c=131 °C and P=0.76 kbar as shown in **figure (4.4.7)**: A) banded spherulites similar to those observed in the orthorhombic phase at atmospheric pressure, and B) thicker lamellar structure that appear as chunks. The two lamellar populations were reported in literature for linear low-density polyethylene [71]. **Figures (4.4.8-12)** demonstrate the SEM pictures of L-04 copolymer crystallized at T_c=140 °C and P=0.76kbar. All the pictures were taken for the same sample. As temperature exceeds the regime II-III transition of the assigned pressure banded spherulites disappear, and are substituted by an axialitic structure as shown in **figure (4.4.8)** and more clearly in **figure (4.4.10)**. In addition, the population density of the large structure increases with temperature. In **figures (4.4.8 and 4.4.10)**, an axialitic crystal (denoted '**A**') and the large features (e.g. squared area) are randomly distributed in a matrix of unordered thin lamellae of an average thickness of 200Å. The latter structure is believed to occur upon cooling. **Figure (4.4.9)** is a magnified picture of the squared area shown in **figure (4.4.8)**.

The axialitic structure (denoted '**A**') is very clear in **figure (4.4.10)**. The arrowed features in **figures (4.4.9-12)** illustrate tight lamellar stacks that contain a number of stacked thinner lamellae each with an average thickness of 100-200Å. The total thickness of each chunk is between 200~500 nm.

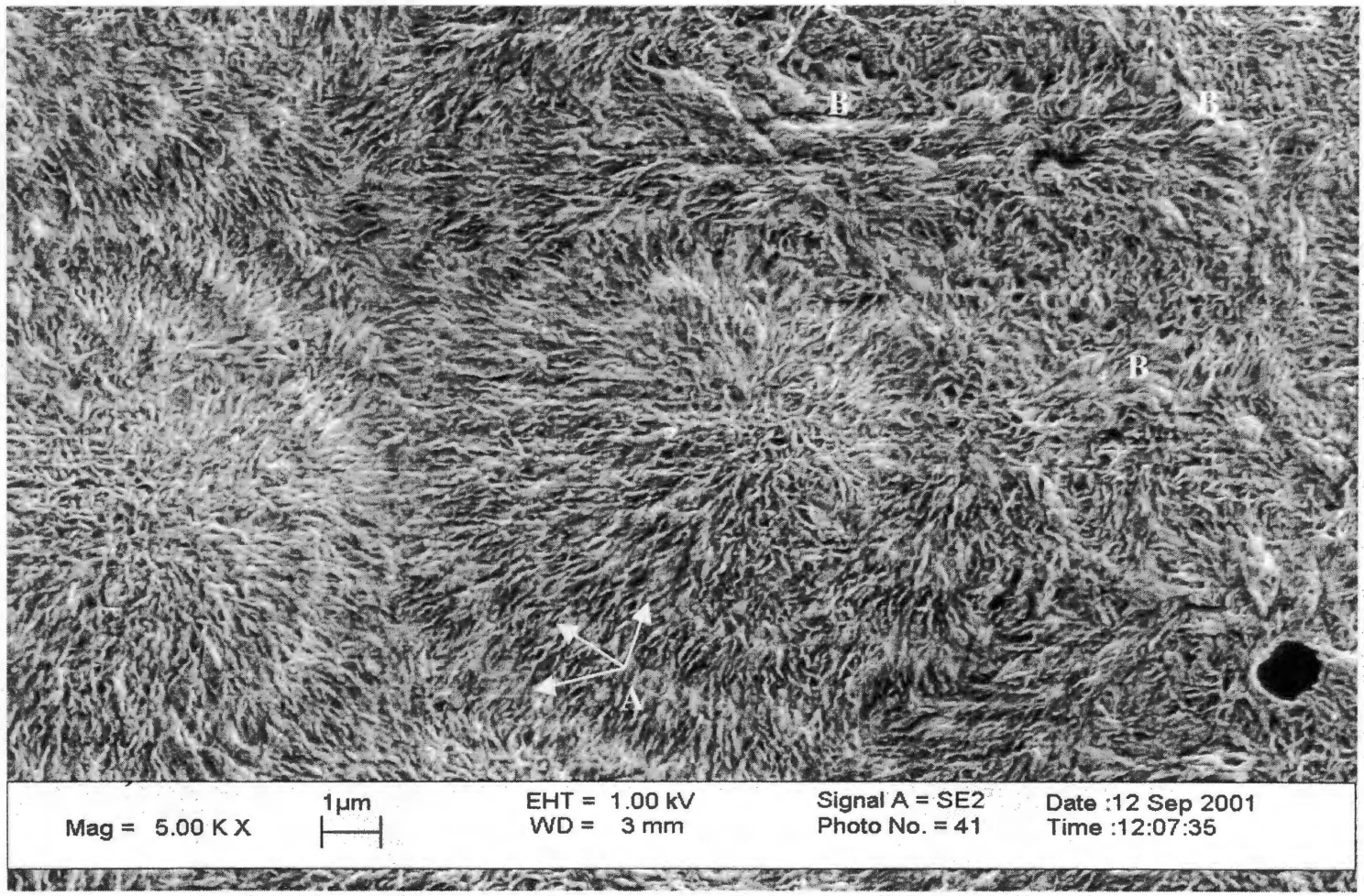


Figure (4.4.7) SEM picture of L-04 copolymer crystallized at T_c=131 °C and P=0.76 kbar.

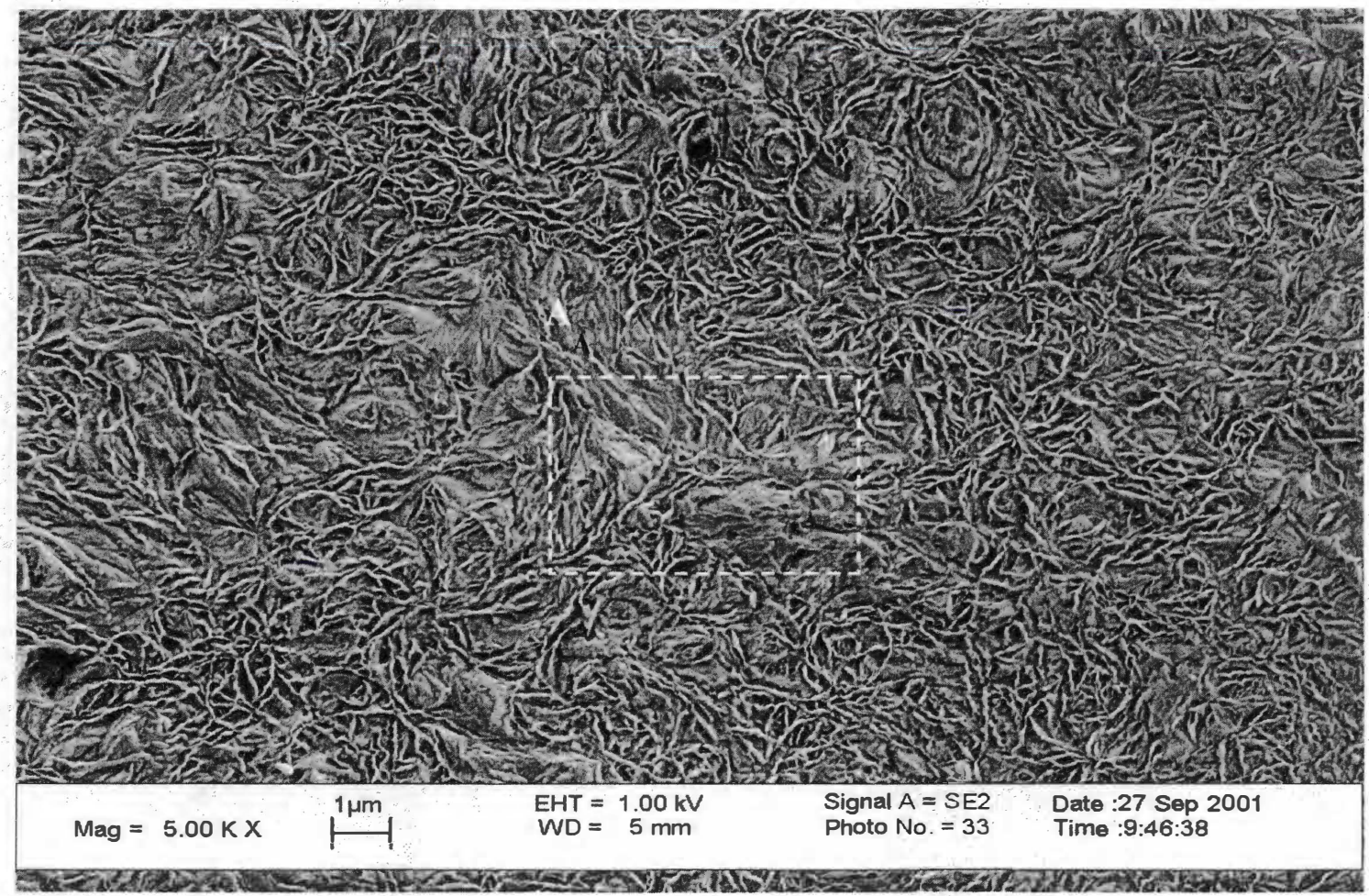


Figure (4.4.8) SEM picture of L-04 copolymer crystallized at T_c=140 °C and P=0.76 kbar.

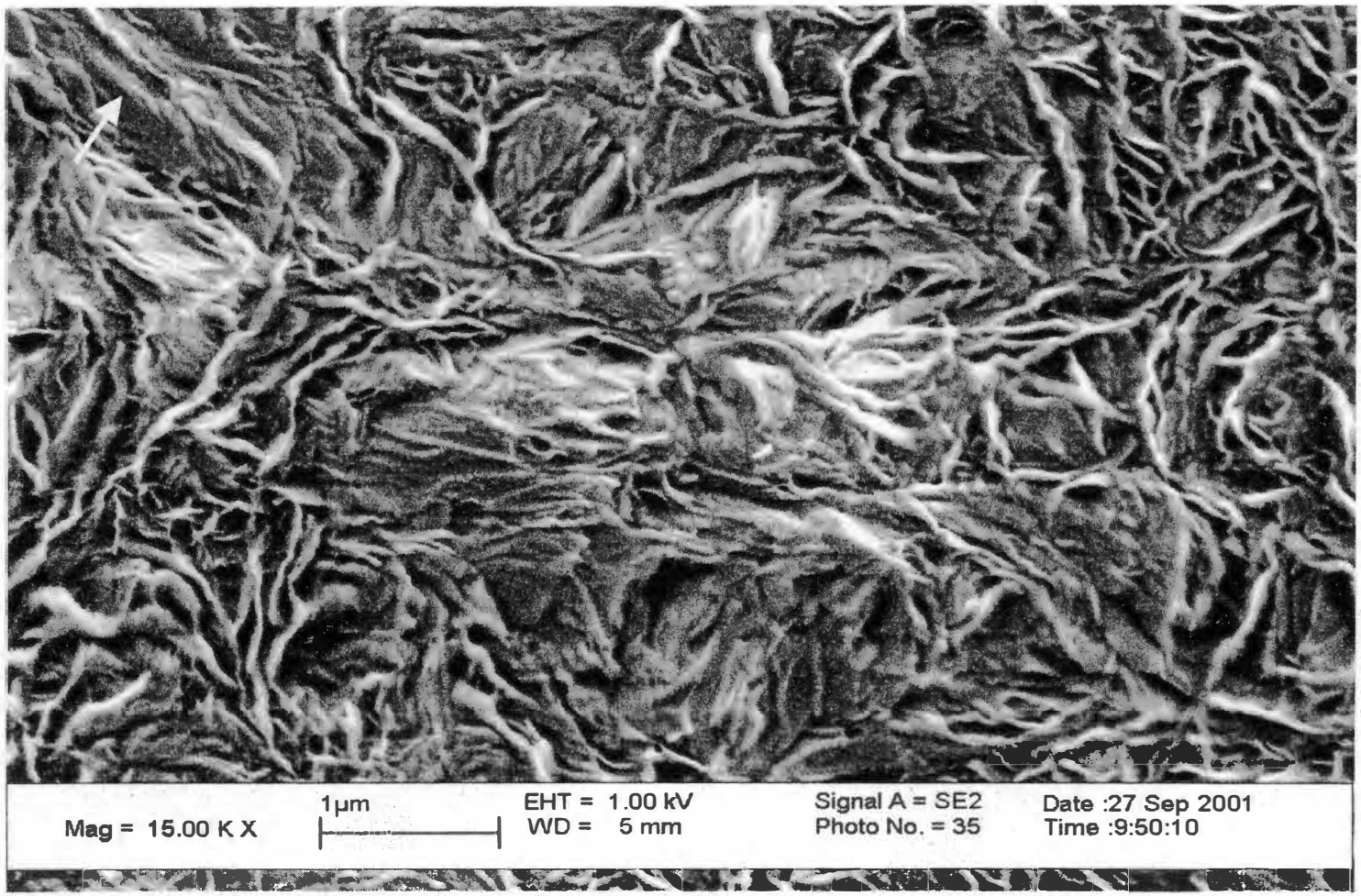


Figure (4.4.9) A magnified SEM picture of the squared area of figure (4.4.8).

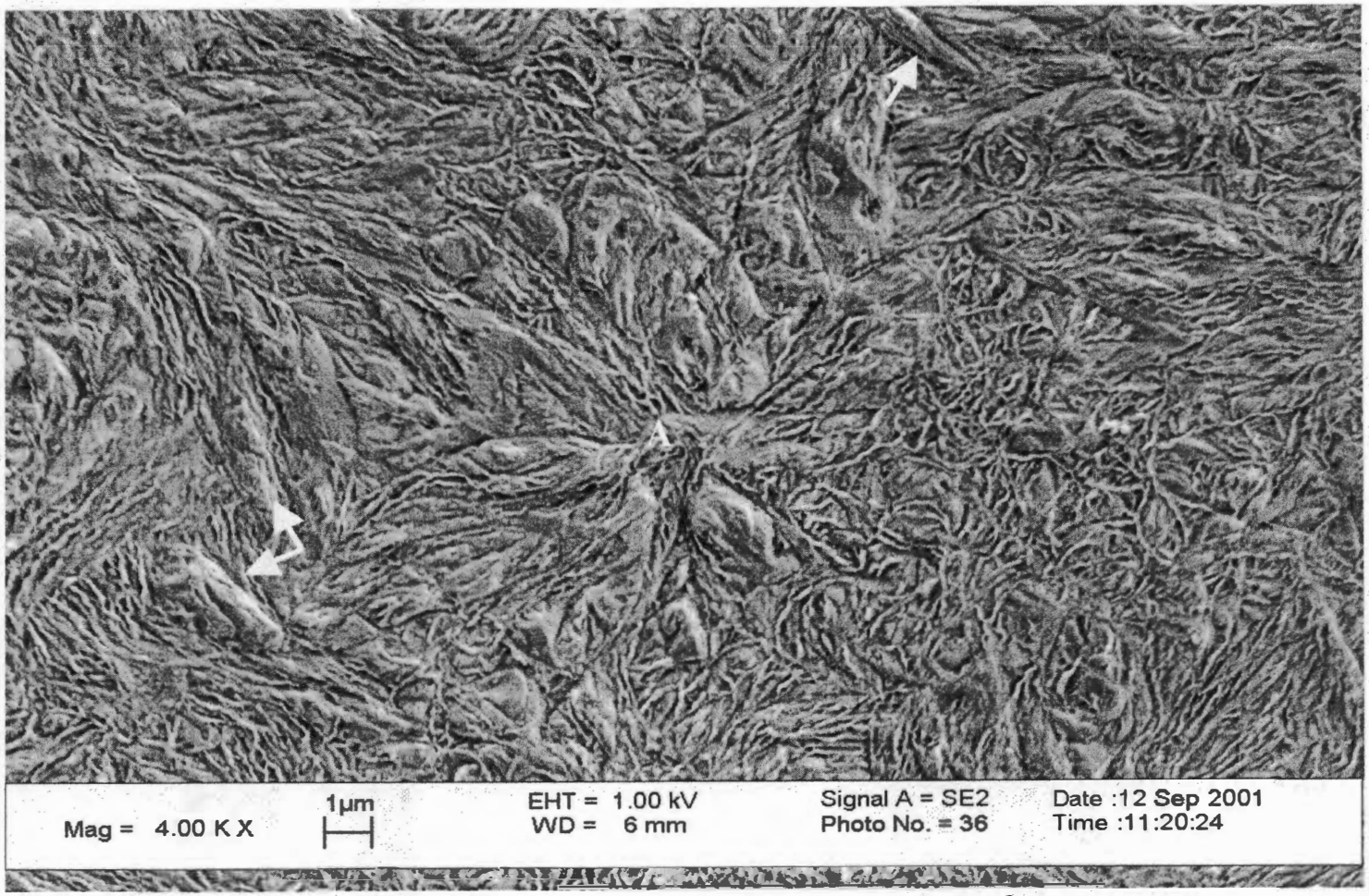


Figure (4.4.10) SEM picture of L-04 copolymer crystallized at T_c=140 °C and P=0.76 kbar.

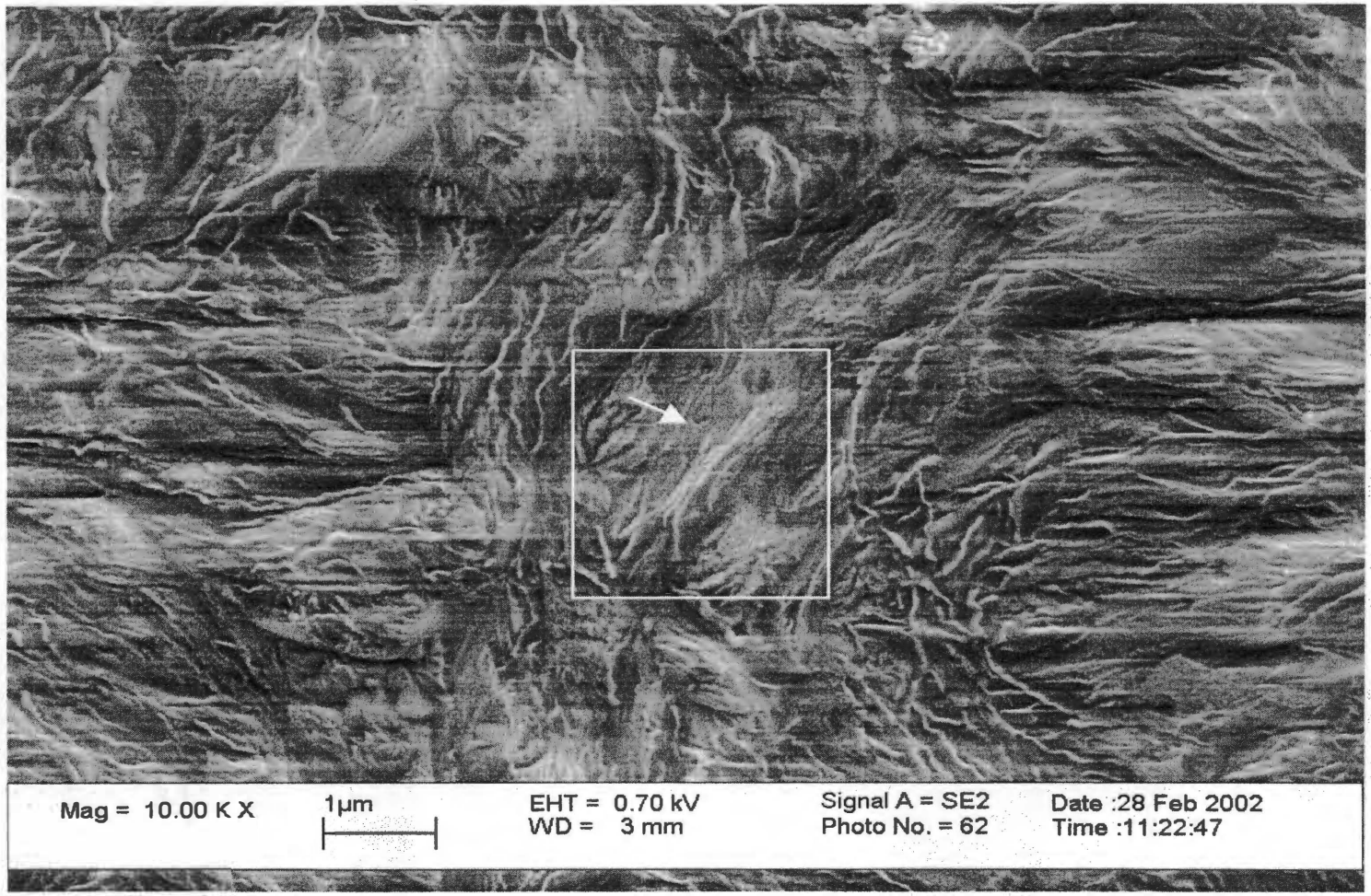


Figure (4.4.11) SEM picture of L-04 copolymer crystallized at T_c=140 °C and P=0.76 kbar.

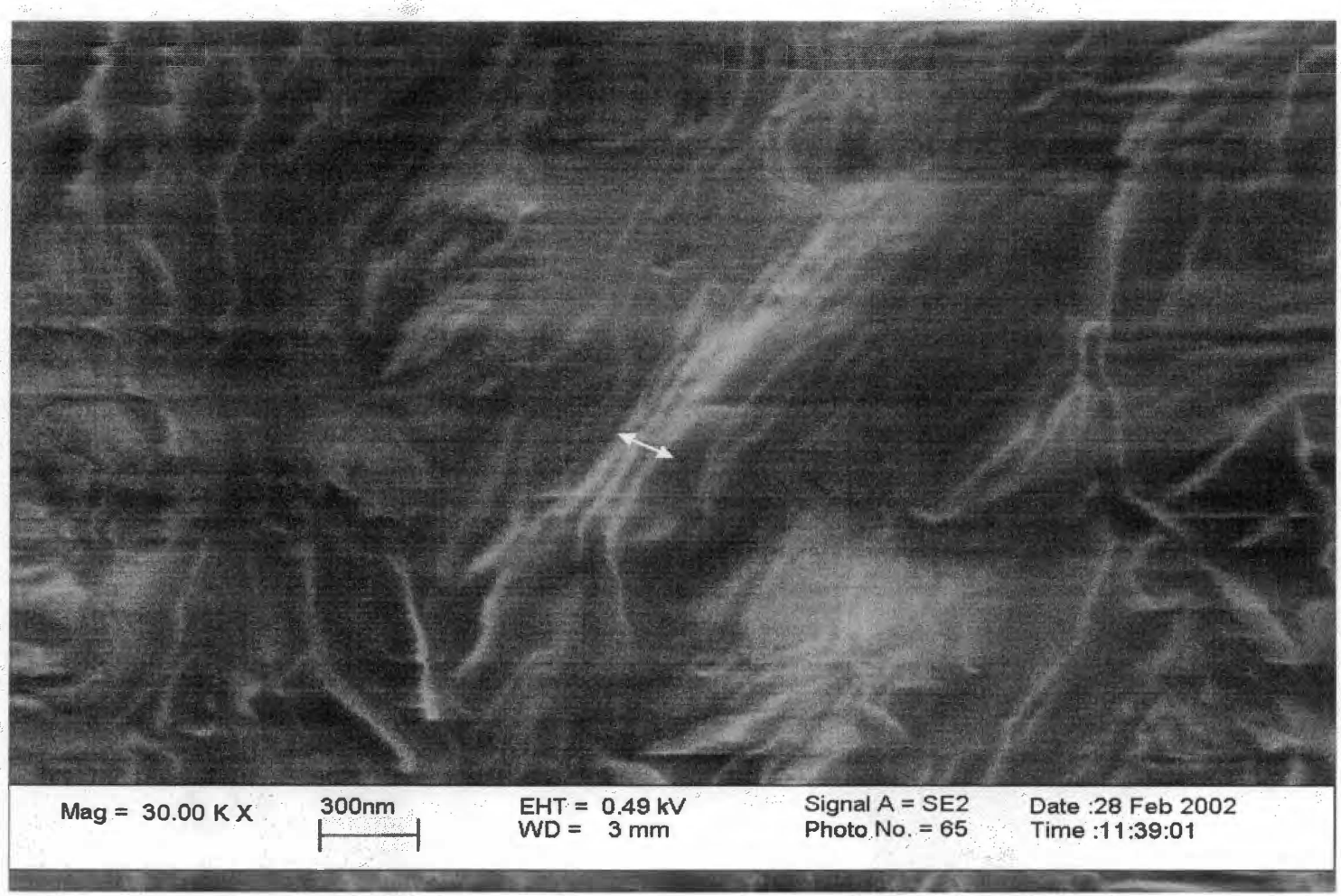


Figure (4.4.12) A magnified SEM picture of the squared area of figure (4.4.11).

Figures (4.4.13-17) illustrate the morphological structure of L-11 copolymer crystallized at T_c=115 °C, and atmospheric pressure. **Figures (4.4.13-14)** clearly show very thick lamellae of an average thickness of ~200 nm. The surface structure (denoted '**A**') in **figure (4.4.14)** is believed to be the result of etching process. Stacked lamellae (arrowed) can obviously be seen in **figures (4.4.15-16)**. **Figures (4.4.16-17)** represent the partially melted sample. Samples crystallized at the above conditions were melted partially to reserve only the higher melting phase (details will be reported in the next section). The selectivity in the figures is very clear (the arrowed structure), where very orderly stacked lamellae survived the etching process.

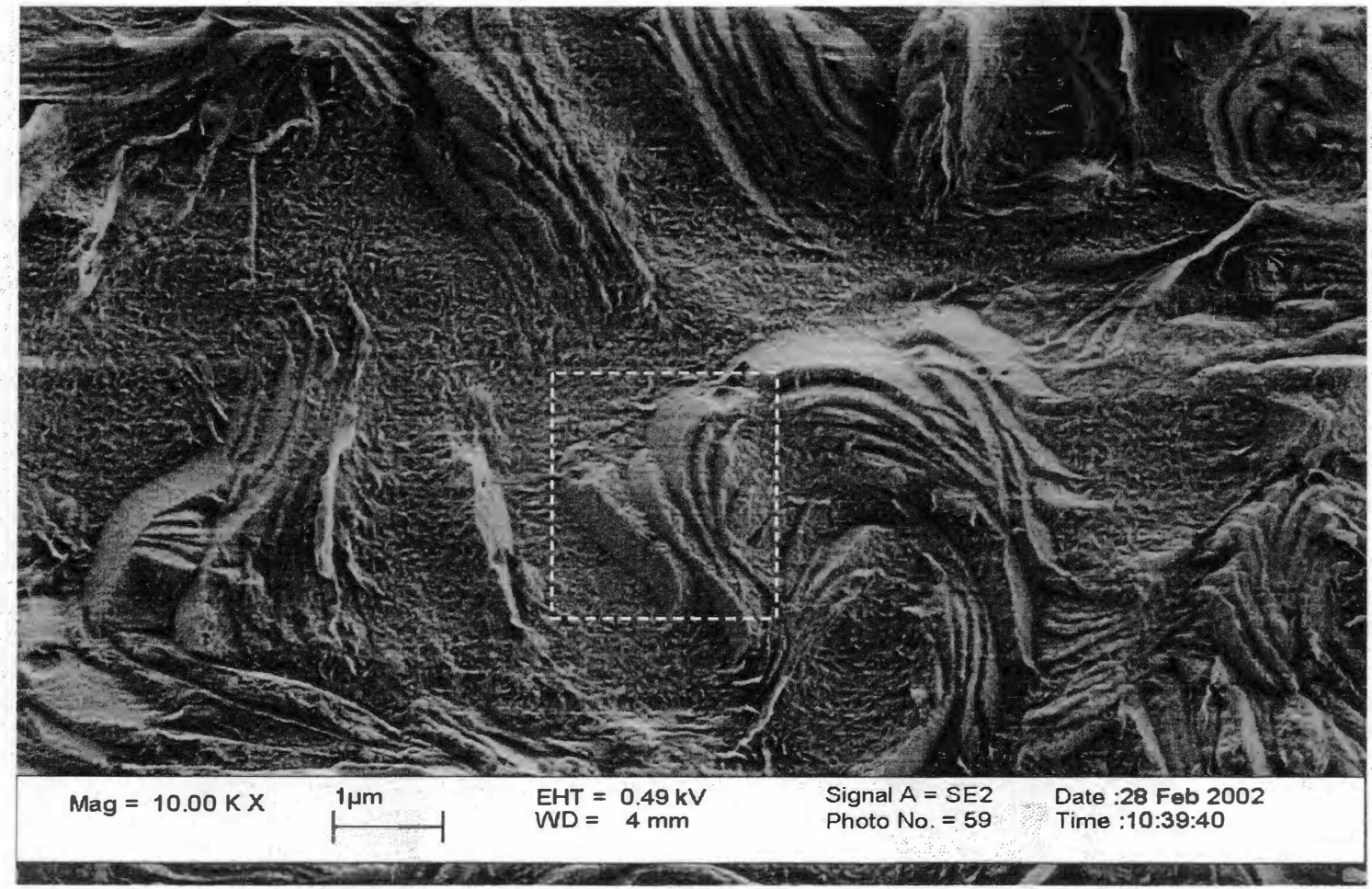


Figure (4.4.13) SEM picture of L-11 copolymer crystallized at T_c=115 °C and P=1atm.

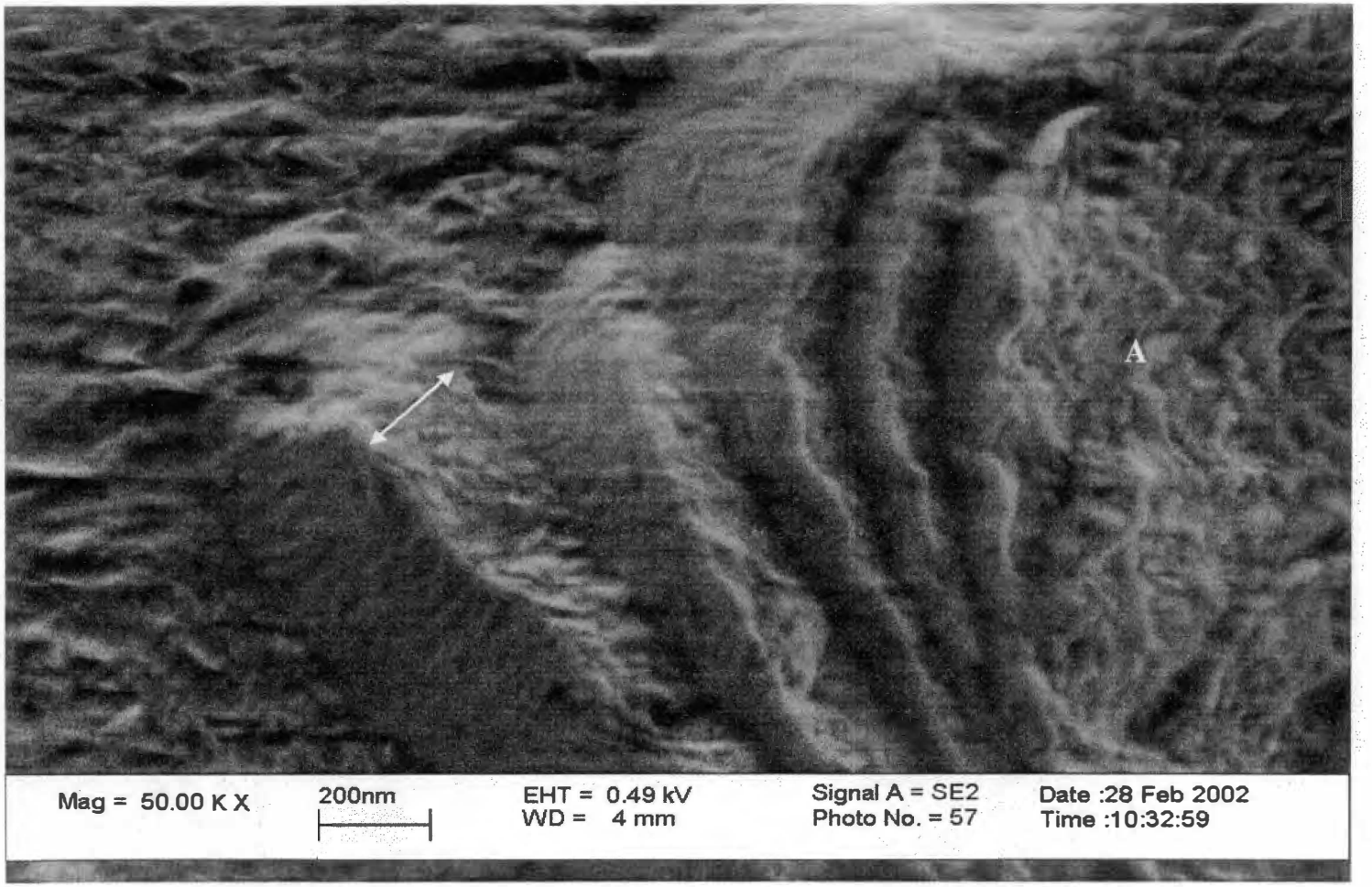


Figure (4.4.14) A magnified SEM picture of the squared area of figure (4.4.13).

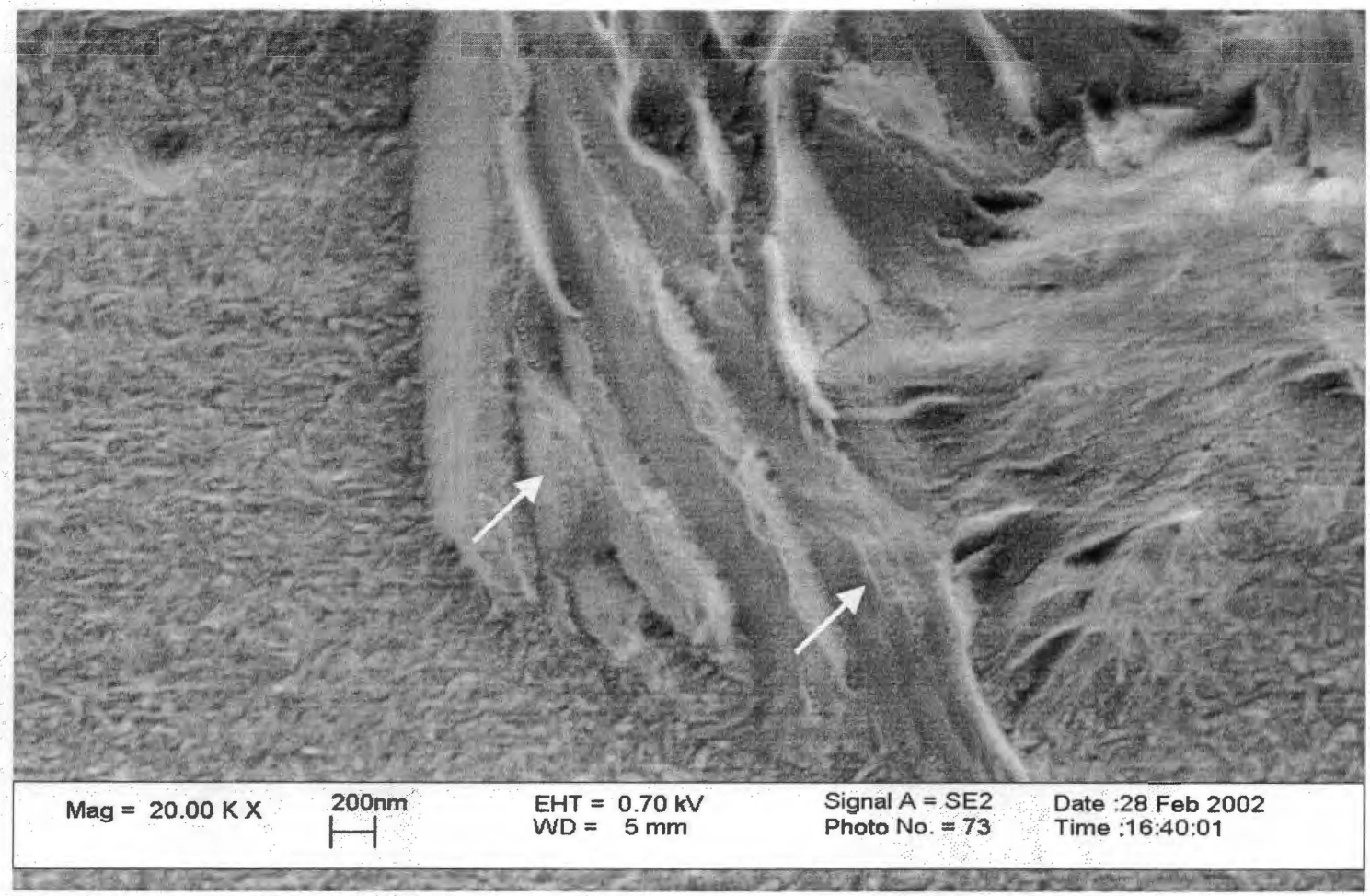


Figure (4.4.15) SEM picture of L-11 copolymer crystallized at T_c=115 °C and P=1atm.

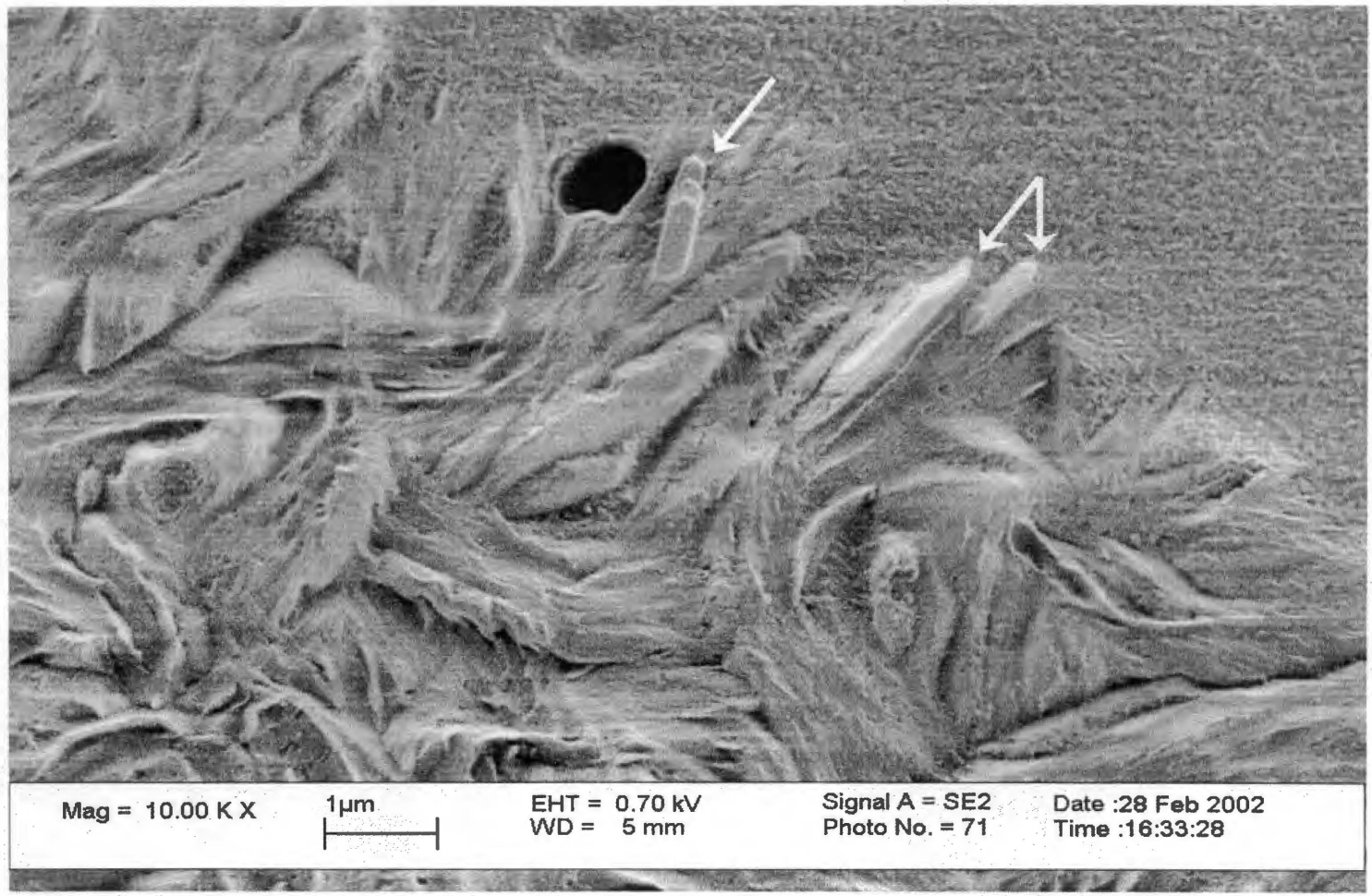


Figure (4.4.16) SEM picture of L-11 copolymer crystallized at T_c=115 °C and P=1 atm. The sample was partially melted then quenched to retain only large structures.

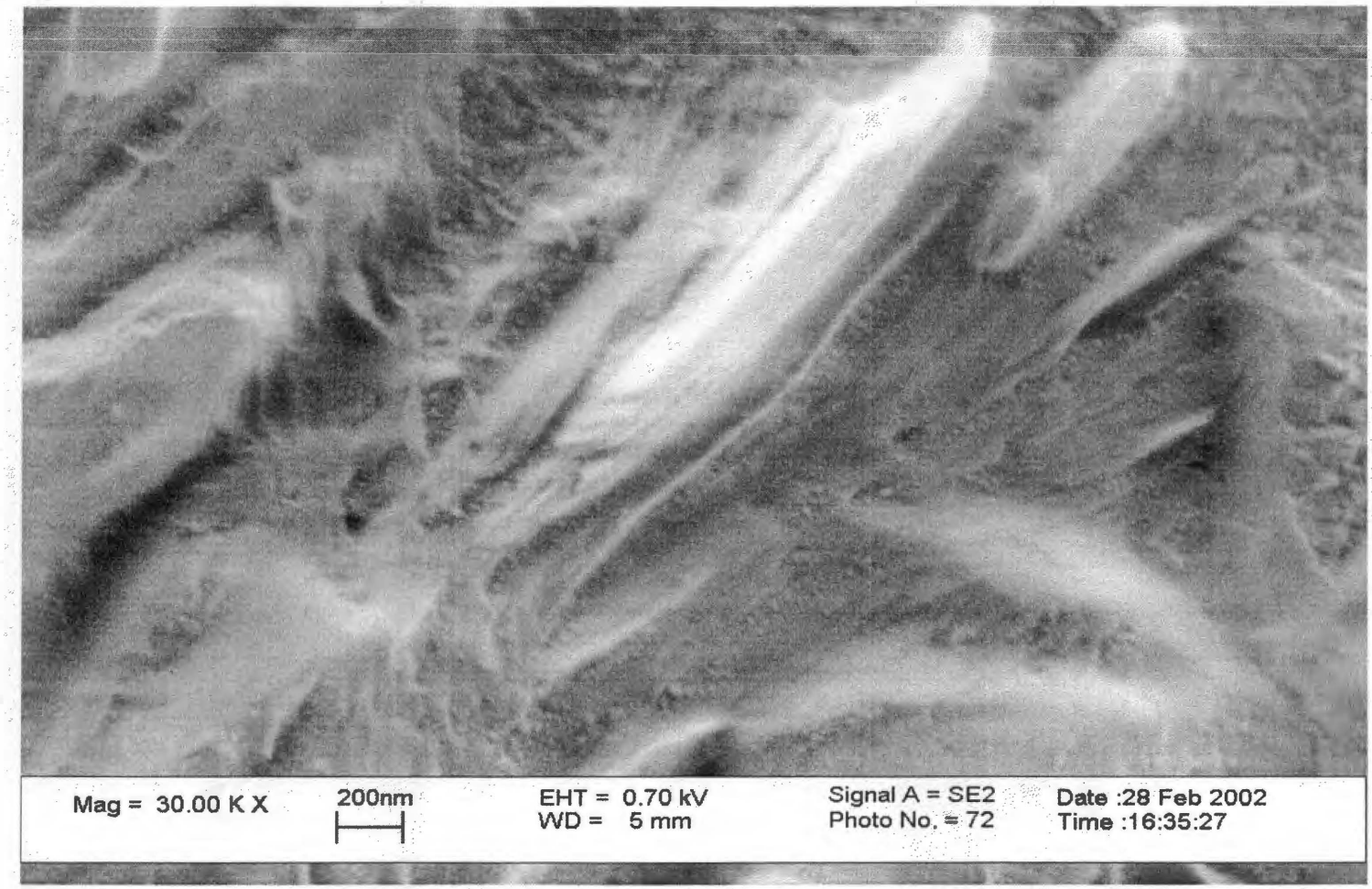


Figure (4.4.17) A magnified SEM picture of figure (4.4.16) for L-11 copolymer crystallized at T_c=115 °C and P=1atm.

5. DISCUSSION

5.1 Melting Behavior and The Phase Diagram

5.1.1 Thermal Analysis

The melting behavior of copolymers, in general, and ethylene-octene copolymers in particular, have exhibited complicated behavior. The appearance of multiple melting peaks during the melting process could carry different explanations. Several studies [72,73] referred to it as the presence of a broad distribution of crystal sizes, where a highly heterogeneous structure results from a non-random incorporation of the comonomer inter-molecularly, and possibly intra-molecularly. This molecular heterogeneity, mainly obtained from a heterogeneous catalyst like the classical Ziegler-Natta catalyst, is also considered to be the reason behind producing a single broad melting peak. In this study all copolymers used are metallocene-catalyzed materials and are theoretically homogeneous copolymers with a narrow molecular weight distribution. The homogeneity of the materials used makes the above explanation doubtful and not expected.

Other studies [17,74,75] explained the existence of two or more melting endotherms in PE material as a change in its crystalline structure from the orthorhombic to the hexagonal phase. Villar *et al* [76] have found that for copolymers with α-olefin concentration lower than 14mol% a thermo-rheologically complex behavior is observed.

To explain the observed complexity of these materials, they suggested the presence of a dendritic-like molecular structure with branches-on-branches morphology.

In addition, the molecular segregation by branch content that occurs during crystallization is another possible reason of the 'multiple melting peak' behavior [68,77,78]. According to Kim the segregation of low-branched polymers, similar to the ones used in this study, is dominated by the molecular weight. Morphological changes, discussed in **section 2.1.3**, are also expected to show similar behavior since folded and extended chain crystals require different thermal energies to melt.

Depolarized light intensity (DLI), as well as, DSC techniques have confirmed the existence of the double melting peaks for L-11 copolymer at all conditions and for the L-04 copolymer beyond certain applied pressures, as discussed in **section 4.3**.

5.1.1.1 Melting Behavior of L-04 Copolymer

Atmospheric Pressure

Figure (5.1.1) shows the melting behavior of L-04 copolymer at atmospheric pressure using light intensity technique. At high supercoolings, the melting temperatures decrease very slightly with crystallization temperature. The melting process is accompanied with an increase in the size of the spherulites before melting. This behavior could be attributed to superheating. The phenomenon appears only at low crystallization

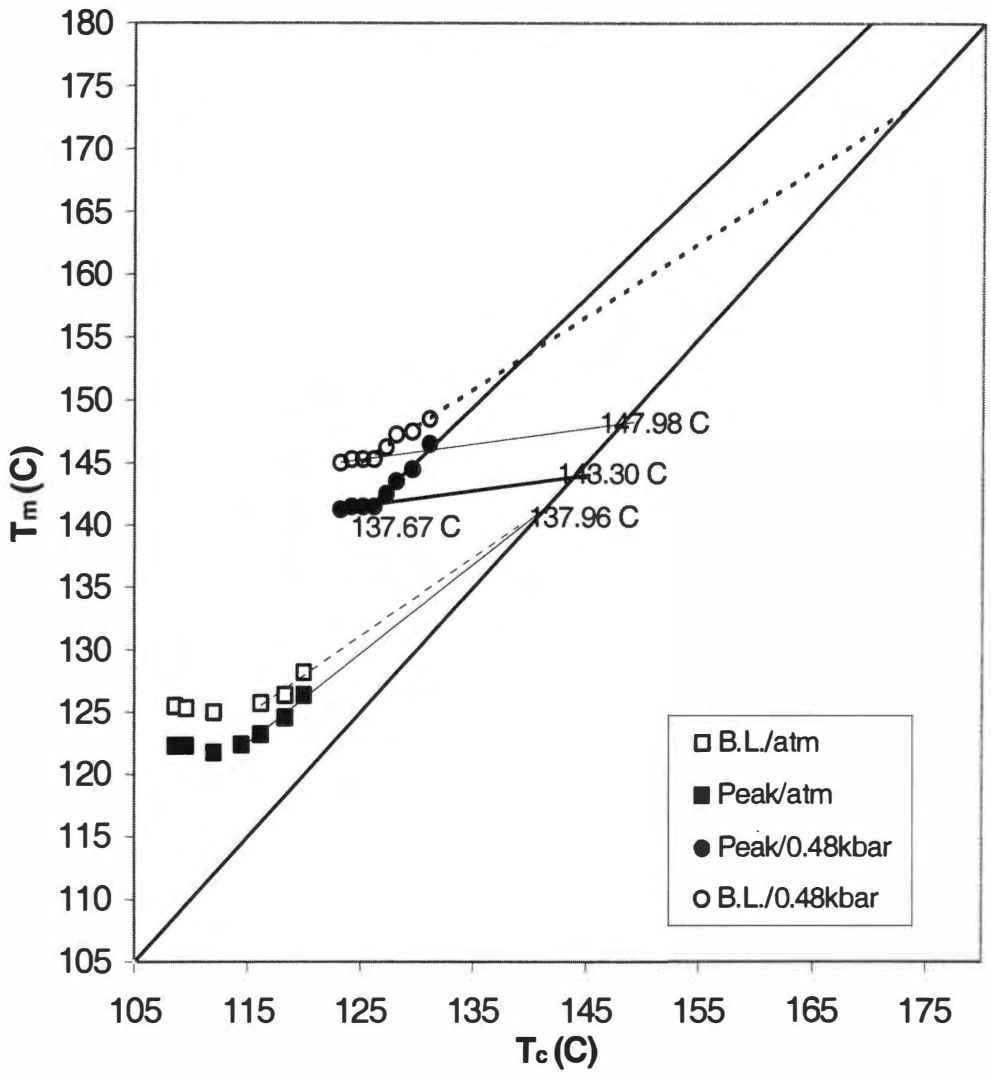


Figure (5.1.1) T_m vs T_c for L-04 copolymer crystallized at P=1atm and 0.48 kbar. Squares are the return to base line values, and circles are the peak values.

temperatures where crystal imperfection dominates. The negative slope is negligibly small and could be considered a straight line with a y-intercept of about 121.5 °C.

Keller *et al* [79] explained the independence of the melting and crystallization temperatures to the exclusive formation of extended chain crystals, since a zero slope line implies an infinite thickening coefficient value according to **equation (2.1.4)**. However, the relatively low melting temperatures of the atmospheric pressure specimens do not support the above explanation. All melting temperatures obtained at atmospheric pressure imply the formation of the expected orthorhombic crystals.

On the other hand, SAXS data obtained for samples prepared at high supercooling, where the zero slope region is observed, have shown a consistent increase in the lamellar thickness with crystallization temperature as shown in **figure (4.2.11)**. This contradicts the 'no-thickening' prediction of Hoffman-Weeks equation and leads to the conclusion that for high supercooling temperatures, i.e. regime III, the Hoffman-Weeks equation cannot be used to determine the equilibrium melting point.

According to the Gibbs-Thomson theory (see **equation 2.1.3**), higher melting temperatures indicate thicker lamellar structures, provided that the heat of fusion and surface free energy are constant. The increase in the lamellar thickness, while melting temperatures remain constant, indicates that either the surface free energy of the system is increasing or the latent heat of fusion is dropping; provided that the equilibrium melting point is still the characteristic parameter of the material and is constant at all times. The

change in both parameters should be equivalent to the amount of change in the lamellar thickness. Since the latent heat of fusion is defined as the amount of energy required to break the intermolecular forces when transforming the crystalline phase into amorphous phase, degree of crystallinity and crystal perfection are directly related to it. The fast growth rate in regime III is expected to reduce the crystallinity of the system. The reduction of the latent heat of fusion could be a result of the partial inclusion of hexyl branches into the crystalline phase, while the increase in the fold surface free energy could be a result of the crowding of the rejected side branches in the interfacial regions.

Based on the available morphological (**figure 4.2.11**) and melting (**figure 5.1.1**) results, the effect of increasing surface free energy is preferable if the multiple-stem (or bundle-like) nucleation was considered. For single-stem nucleation, however, no easy preference exists.

It is not until $T_c \approx 114.5$ °C when the deflection point is reached where the melting temperatures start increasing steadily with crystallization temperature. This deflection temperature occurs exactly at the regime II-III transition temperature of L-04 copolymer crystallized at atmospheric pressure, although, both experiments for thermal studies and kinetics were conducted separately using different samples. The melting process is accompanied by a gradual disappearance of the spherulites. The lateral spreading rate is larger than the rate of the secondary nucleation at this temperature range (regimes I and II). Accordingly, the lower growth rates will increase the selectivity of the crystallization

process. Therefore for T_c >114.5 °C, branches will more likely be excluded from the stems where thickening process causes the melting temperatures to rise.

A thickening coefficient of 1.45, using peak values, and 1.74, using the return-to-baseline values, were obtained at low supercoolings. The thickening coefficient measured at lower supercoolings using the Hoffman-Weeks equation is generally assumed to be a constant value, where the thinnest crystals produced at higher supercoolings have the larger lamellar thickening. However, since annealing and defect behavior depend on temperature, the thickening coefficient γ cannot be described by a simple function and is expected to be a complex function of temperature.

Elevated Pressures

Crystalline polymers are pressure-sensitive materials due to their weak interchain potential. Mandelkern [80] has suggested that the total entropy change on melting can be divided into two parts: volume change and change in the configurational entropy of melting. This can be expressed as follow

$$\Delta S_m = (\Delta S_m)_p + \left(dP/dT\right)_v \Delta V_m \qquad (5.1.1)$$

where ΔS_m is the total entropy of melting, $(\Delta S_m)_p$ is the configurational entropy, $\left(dP/dT\right)_v$ is the thermal pressure coefficient at constant volume, and ΔV_m is the volume

change on melting per mole of crystalline repeat unit. Baer *et al* [7] studied the melting behavior of PE under pressure and found that the volume entropy change decreases very slightly with pressure compared to the increase in the configurational entropy change. This brought the total entropy to a net increase and caused PE materials to exhibit the most melt disorder compared to other polyolefins.

The formation of extended chain molecules is the main element in the production of the hexagonal or monoclinic phases. Molecular chains of ECC are believed to have higher mobility than the folded chain molecules, due to its higher configurational entropy. This will cause the net entropy to rise, as discussed earlier.

The introduction of isobaric pressure, expectedly, raised the melting temperatures to higher values. **Figure (5.1.1)** shows the effect of 0.48kbar pressure on the melting temperatures of L-04 copolymer. Similar to the atmospheric pressure data, 'curved' melting temperatures are obviously seen. However, for higher supercooling temperatures, the melting points tend to increase with crystallization temperature, opposite to what was observed at atmospheric pressure. Deflection starts at $T_c \approx 126$ °C, where melting points became more affected by the crystallization temperatures. According to the regime plots, discussed in **section 5.3**, the deflection point coincides with the regime II-III transition temperature similar to what was observed at atmospheric pressure.

In addition to the increase of the melting temperature, the introduction of a pressure as small as 0.48kbar caused the melting temperatures at high supercoolings to be

more sensitive to the crystallization temperatures. The melting path of the L-04 copolymer in this pressure region shows two distinctive slopes, an indication of two different thickening coefficients, where the thickening coefficient at high supercoolings (γ=8) is about seven times larger than that of the low supercoolings. The shallow slope at high supercoolings indicates major thickening in the time between crystallization and melting point determination.

Based on the melting behavior it appears that the thickening process at high supercoolings is very limited compared to low supercooling conditions. It is possible that the lamellar thickness of the orthorhombic folded chains has reached the branch point separation where it becomes difficult for the thickening process to proceed. At low supercoolings the thickening process resumes, as obvious from the melting behavior, but apparently in another phase where the formation of extended chain crystals (ECC) is possible. Since dT_m/dP~17 °C/kbar for ethylene-octene copolymers, the equilibrium melting temperature of the orthorhombic phase at 0.48kbar is estimated to be around 147 °C. Obtaining melting temperatures equivalent to the expected equilibrium melting points is strong evidence for the formation of very thick lamellar crystallites. For example, at T_c =131.1 °C the melting temperature T_m=146.5 °C which is very close to the theoretical T_m^o value of orthorhombic PE crystals at the same pressure. Using the Gibbs-Thomson equation and the measured melting points has given extremely large lamellar thicknesses for all high-pressure materials as will be discussed in **section 5.2**. Although ECC is thermodynamically more stable than the folded-chain crystals (FCC), it appears that the

latter is kinetically more desirable and crystallization takes place faster through it, at least for high supercoolings.

The behavior of L-04 copolymer at P =0.48kbar gives the impression that some form of transition occurs under the applied conditions. In order to understand the possible cause of this behavior, it should be remembered that the melting process occurs at pressure. Applied pressure, although small, has a noticeable effect beyond a certain temperature, especially when the linear growth rate is slow enough, which is the case in regime I and to some extent in regime II. At low supercoolings the molecular chains in the crystalline phase gain some thermal energy during melting, i.e. the configurational entropy change increases, thus increasing the chain mobility of the system and hence produces a mobile phase (e.g. monoclinic). The applied pressure however generates an opposing effect by reducing the volume entropy change of the system and hence limits the mobility of the chains. If the temperature effect dominates, the effect of the lamellar thickening will dominate during the heating process and larger melting points are produced. In this case the melting behavior at the high supercooling temperatures does best reflect that of the orthorhombic phase instead of the mobile phase. On the other hand, when the pressure effect dominates at relatively high temperatures it is possible that the molecular chains become better packed and require more thermal energy to melt.

On increasing the isobaric pressure to 0.76kbar or higher, two melting peaks were formed at all crystallization temperatures used, as shown in **figures (5.1.2a-b)**. The melting point behavior could be described in two different ways: **A**) In route (1) (filled

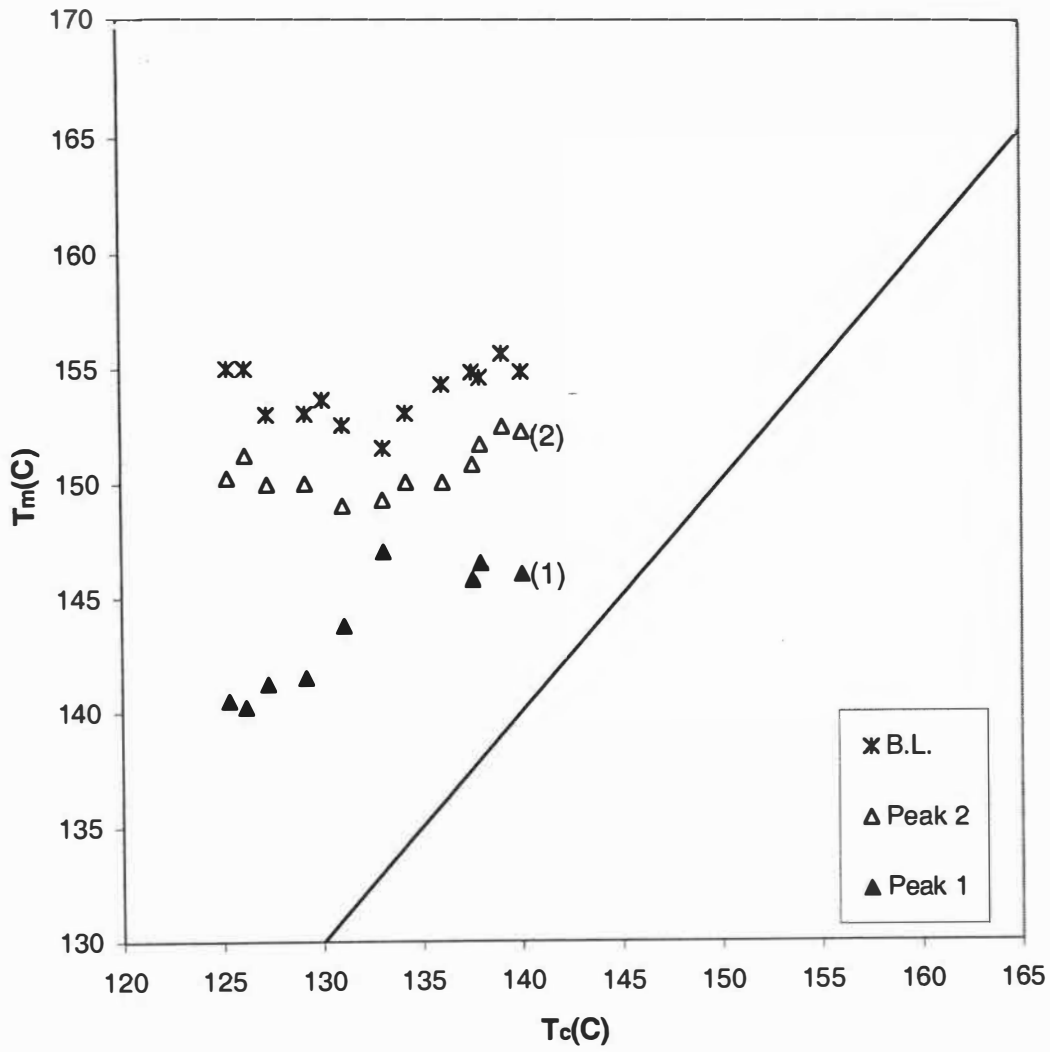


Figure (5.1.2) T_m vs T_c plot of L-04 copolymer crystallized at P=0.76 kbar, a) following path (A). Crosses represent the return-to-baseline values and triangles are the peak values.

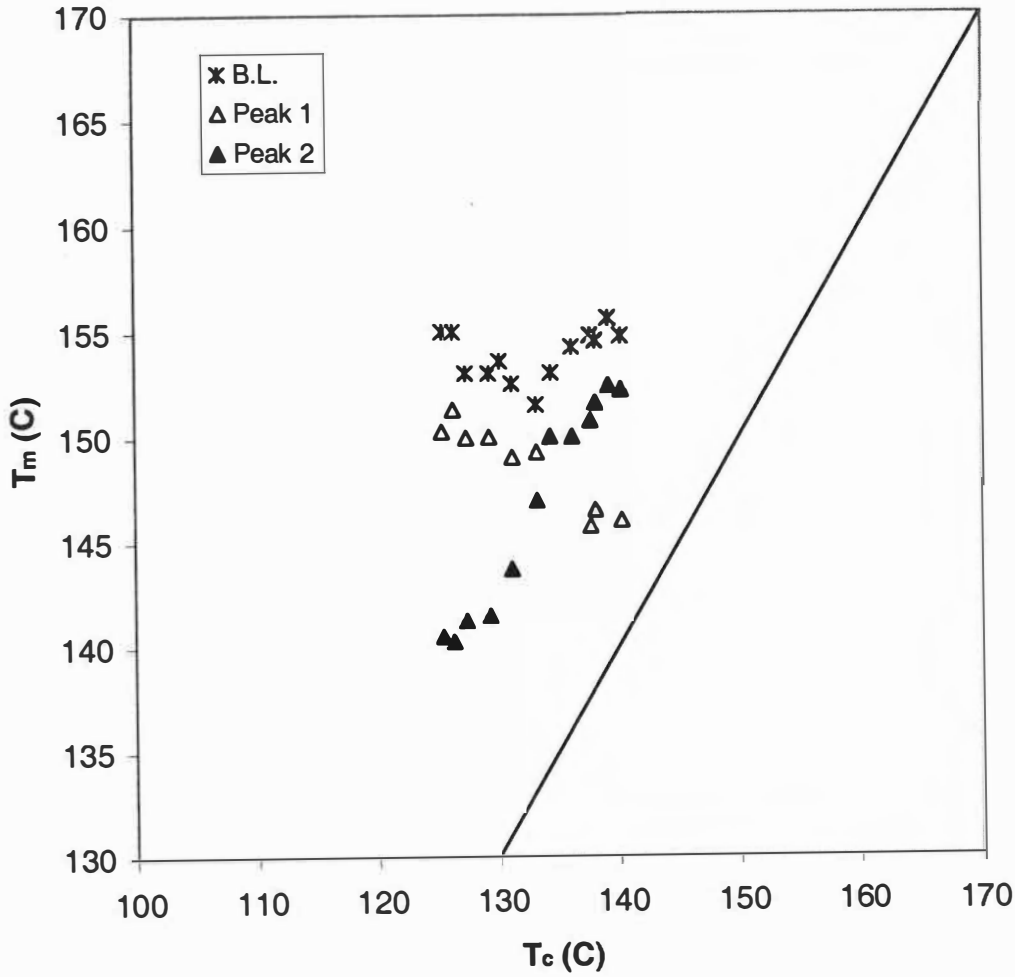


Figure (5.1.2) Continued, b) following path (B). Crosses represent the return-to-baseline values and triangles are the peak values.

symbols) the lower melting points stay constant at higher supercoolings then start to increase linearly, in a similar way to the atmospheric and 0.48kbar pressures. At a certain temperature the melting points started to level off producing what seems to be a discontinuity (or jump) in the melting temperatures. In route (2) (open symbols) the larger melting points showed a consistent decrease in value before reaching a transition temperature at $Tc \approx 133$ °C. Beyond the transition temperature, the melting points started to increase. The transition temperature coincides with the regime II-III transition obtained from kinetics. **Figure (5.1.2a)** illustrates this behavior.

A discontinuity (or jump) of the melting temperatures was reported in the literature for LPE [81]. It was interpreted as a change in the number of folds per chain, where the number of folds decreases with increasing temperature. Bragg *d* spacing values, as a function of crystallization temperature, were reported to have a similar behavior to **figure (5.1.2a)** at high pressures. In **figure (5.1.3)** the *d* spacing values that resemble route (1) were assigned to the orthorhombic (110) peak, while values behaving similar to route (2) were designated to either the hexagonal (100) for pressures beyond the triple point, the monoclinic (010) for pressures right below the triple point (similar to what is used in this study), or the amorphous peaks depending on the temperatures used [2]. The compatibility of the results of **figure (5.1.3)** and of those obtained in this study will be used to interpret our data.

B) Another less plausible view of the data could be explained as two intersecting lines, where one group of the melting temperatures increases with crystallization

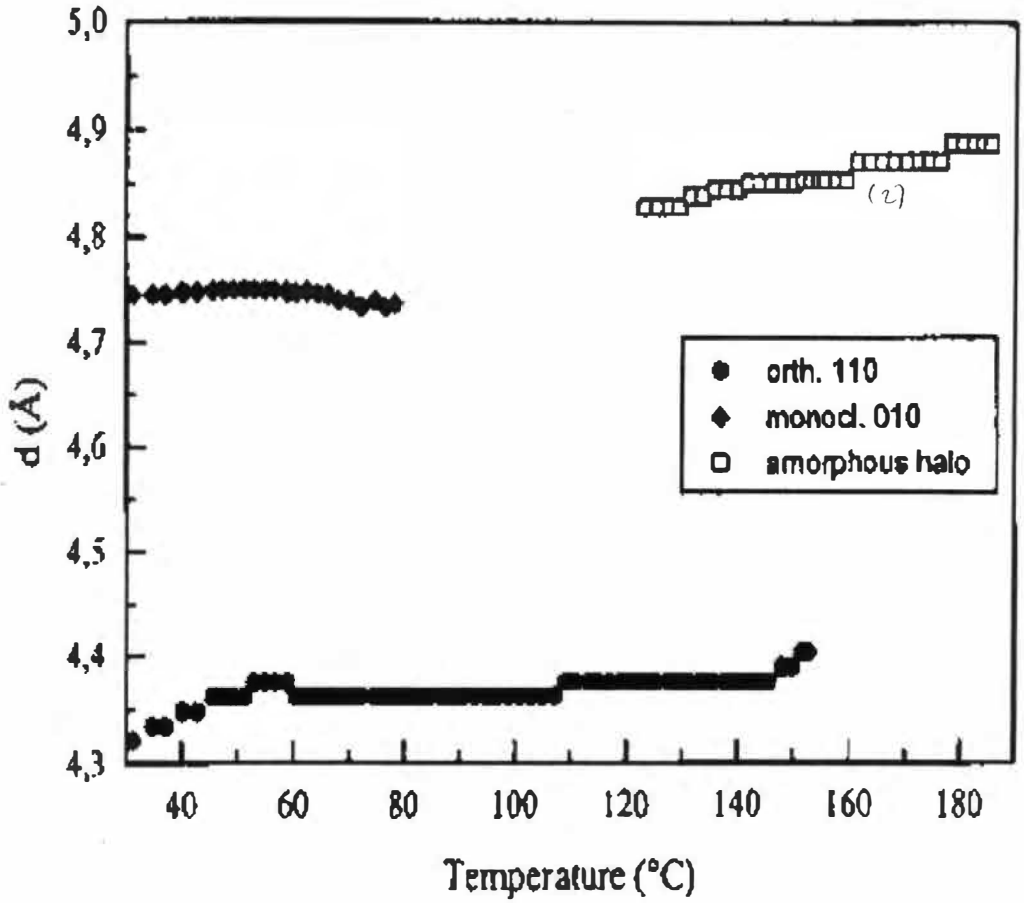


Figure (5.1.3) Changes in d-spacing values of ethylene-octene copolymer as a function of temperature at P=1.95kbar. (Rastogi *et. al.* [2])

temperature while the other one decreases with crystallization temperature. Each group can be assigned to the melting of either the orthorhombic or the second co-existing phase. Both routes are illustrated in **figure (5.1.2b)**. The continuous drop of the melting temperatures (empty symbols) over a wide range of crystallization temperature cannot be explained straightforwardly by thermodynamics. Unless there is a significant change in the surface free energy or the heat of fusion, the persistent drop of the lamellar thickness value at higher crystallization temperatures contradicts with the prediction of Gibbs-Thomson equation. In addition, the appearance of the thick lamellar structure at low and high crystallization temperatures (see **figures 4.4.7** and **4.4.10**) cannot be explained by **figure (5.1.2b)**, since thick lamellae require larger melting temperatures. Therefore, **figure (5.1.2b)** is not believed to represent the actual melting behavior of the ethylene copolymers and it should be ignored.

5.1.1.2 Melting Behavior of L-11 Copolymer

The thermal analysis of L-11 copolymer was similar to that of the L-04 copolymer crystallized at pressures ≥ 0.76kbar. The double melting peak behavior was observed at all conditions in L-11 copolymer, as illustrated in **figures (5.1.4a-c)**. The lower melting peaks (filled symbols) of the atmospheric pressure samples do not show a discontinuity even beyond the critical temperature of the regime II-III transition ($T_{II\text{-}III}$ =114 °C). The melting temperature at the deflection point (T_c=106 °C) corresponds to a lamellar thickness of ~100Å, which is equivalent to the average sequence length of L-11 copolymer. In contract to L-04, the temperature at which the slope of the melting points

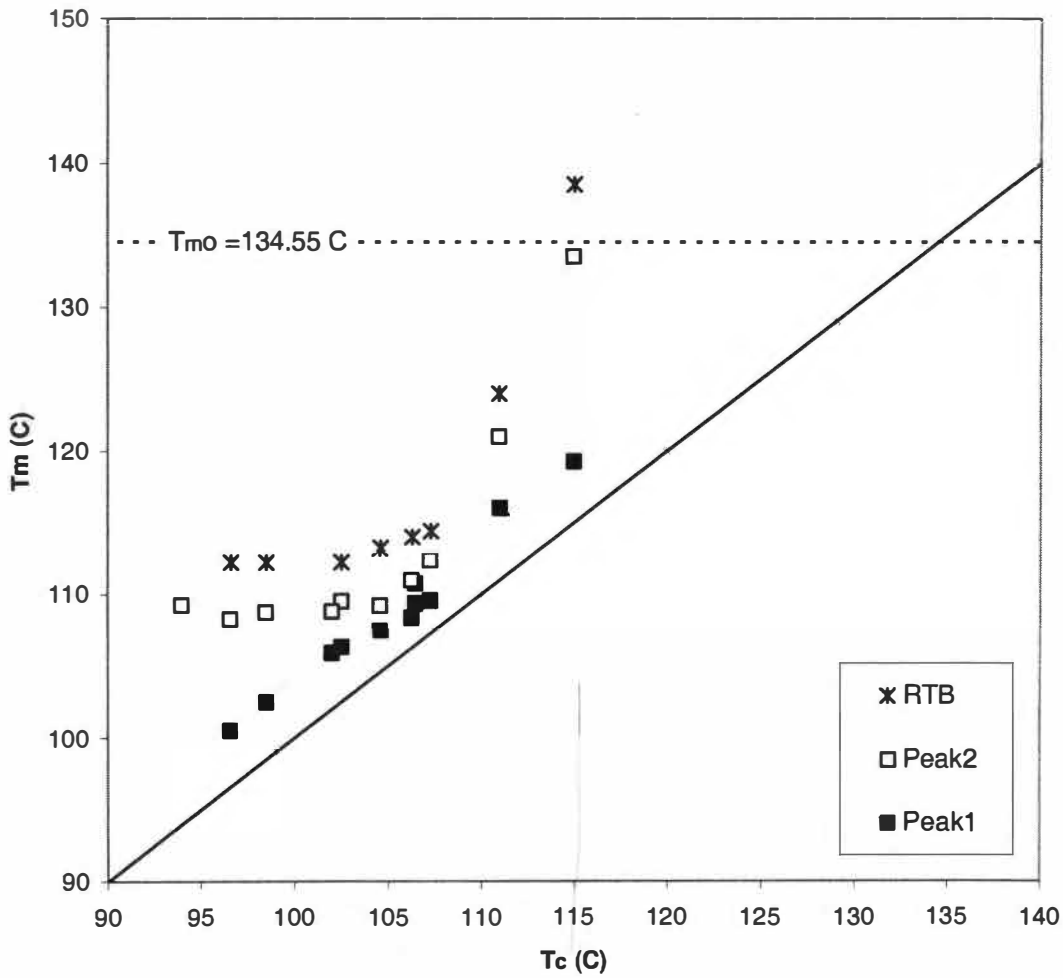


Figure (5.1.4) The T_m versus T_c plot for L-11 copolymer crystallized, a) at atmospheric pressure.

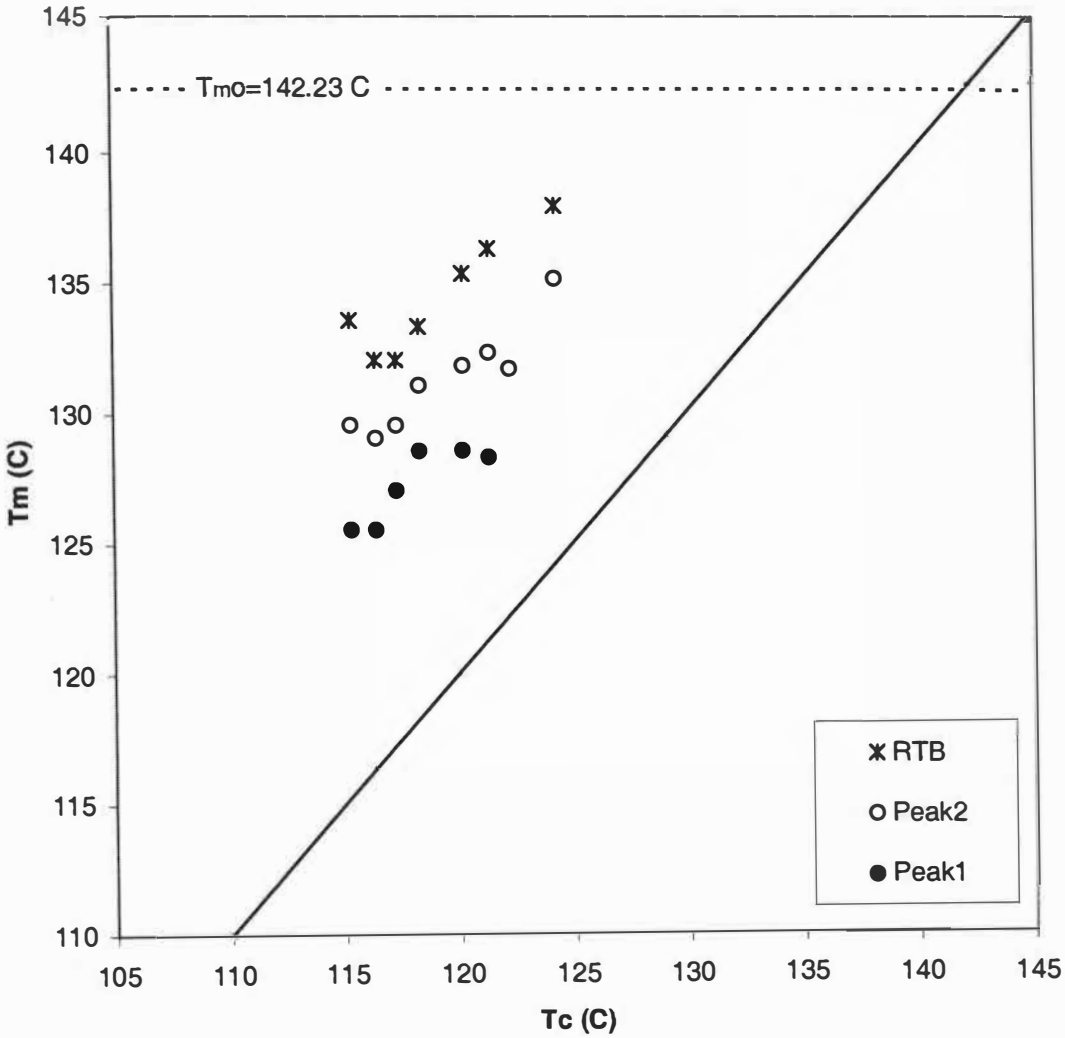


Figure (5.1.4) Continued, b) at P=0.48kbar.

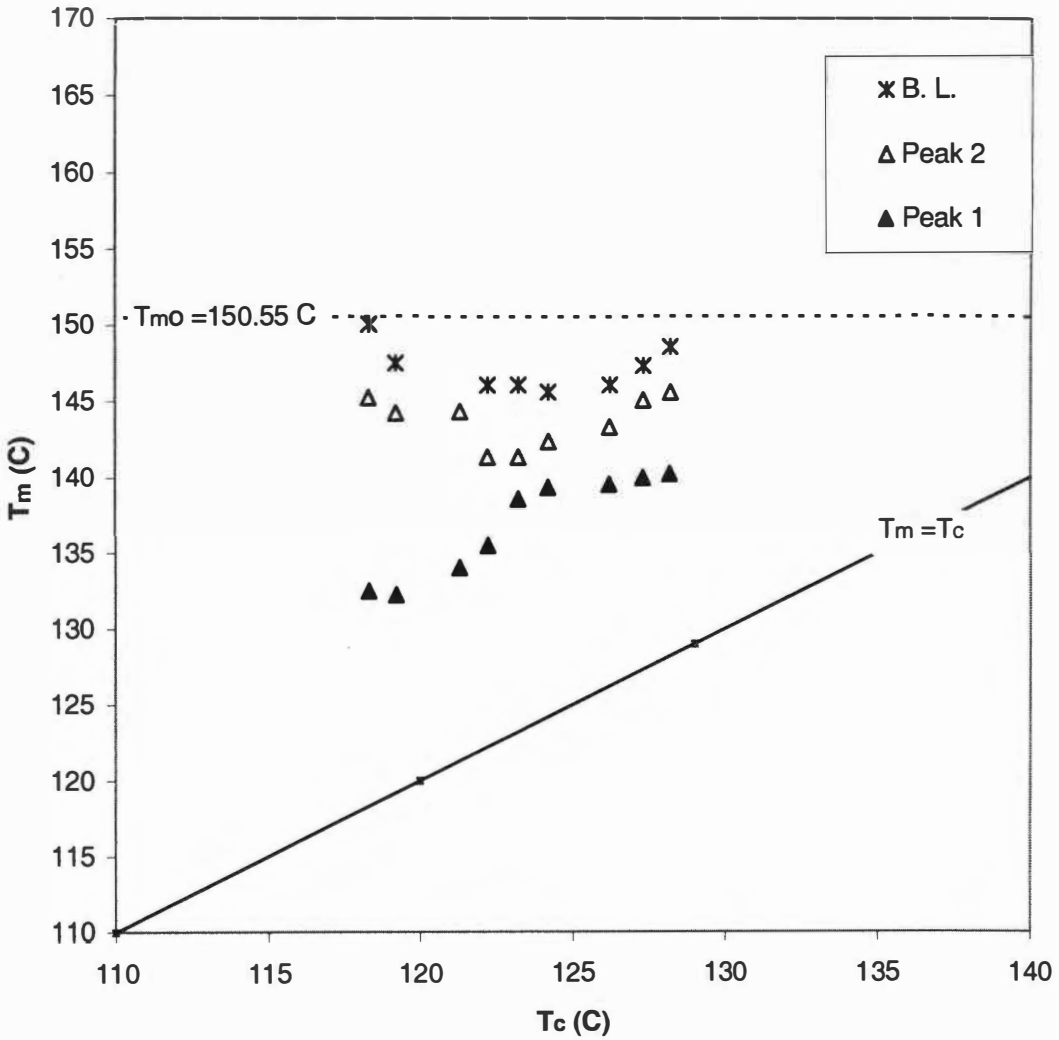


Figure (5.1.4) Continued, c) at 1kbar.

changes (the deflection point) does not correspond to the regime II-III transition temperature. At T_c>106 °C both melting points reflect a lamellar thickness that is larger than the sequence length, which implies the inclusion of hexyl branches into the crystalline phase. At T_c ≈115 °C i.e. regime II region, extensively high melting temperatures start to appear. The mechanism behind the co-existence of two phases, regardless of its nature, seems to be very sensitive to the branch content. Adding as little as 11 hexyl branches per 1000 C atom is enough to retain the two phases in a stable state hence shifting the triple point of the phase diagram to very low temperatures and pressures.

The extremely high melting temperature (T_m =133.5 °C) obtained at T_c=115 °C and 1 atm, corresponds to a lamellar thickness of 2496Å. The value was calculated using Gibbs-Thomson equation, where T_m^o=134.55 °C was obtained by Kim for L-11 copolymer, and the σ_e and ΔH_f values were obtained by Hoffman. This result confirms without any doubt the formation of extended chain crystals at atmospheric pressure in ethylene-octene copolymers of ≥ 0.1% branch content, and nicely agrees with the SEM pictures shown in **figure (4.4.13-17)**, and will be discussed in more detail in **section 5.2**. The lower melting point T_m=119.25 °C gives a value of 171 Å.

To understand the time dependence of melting of linear PE, Hellmuth and Wunderlich [82] have studied its superheating effect both qualitatively and quantitatively. They found that for a 10 °C /min heating rate, the melt-crystallized folded-chain crystals

do not exhibit any significant amount of superheating. However, extended-chain crystals produced at high pressure have shown 2 °C increase in the melting temperatures. Therefore, a correction for the superheating effect should be considered in the monoclinic phase.

The inclusion of hexyl branches into the crystalline phase cannot be explained by the crystallization model of orthorhombic folded chain crystals. Branches dissolved in the crystalline phase necessitate the expansion of the crystal lattice dimension to be accommodated in the crystalline phase. As a result, the introduction of the monoclinic phase is needed to explain the melting behavior of L-11 at high crystallization temperatures.

High-pressure results obtained in **figure (5.1.4)** show similar behavior to that of L-04 copolymer and similar comments could be used. **Figure (5.1.5)** illustrates the change in morphology accompanying the melting process of the above example. At lower melting temperatures the spherulitic structure disappears whereas only the axialitic structure survives the higher temperatures before a complete melt is reached at 133.5 °C.

5.1.2 Phase Diagram

Bassett and Turner [83] were the first to establish the phase diagram of polyethylene. They calculated that the triple point, where new high-pressure phase was formed, is around 3kbar as illustrated in **figure (2.1.1)**. However, the effect of the

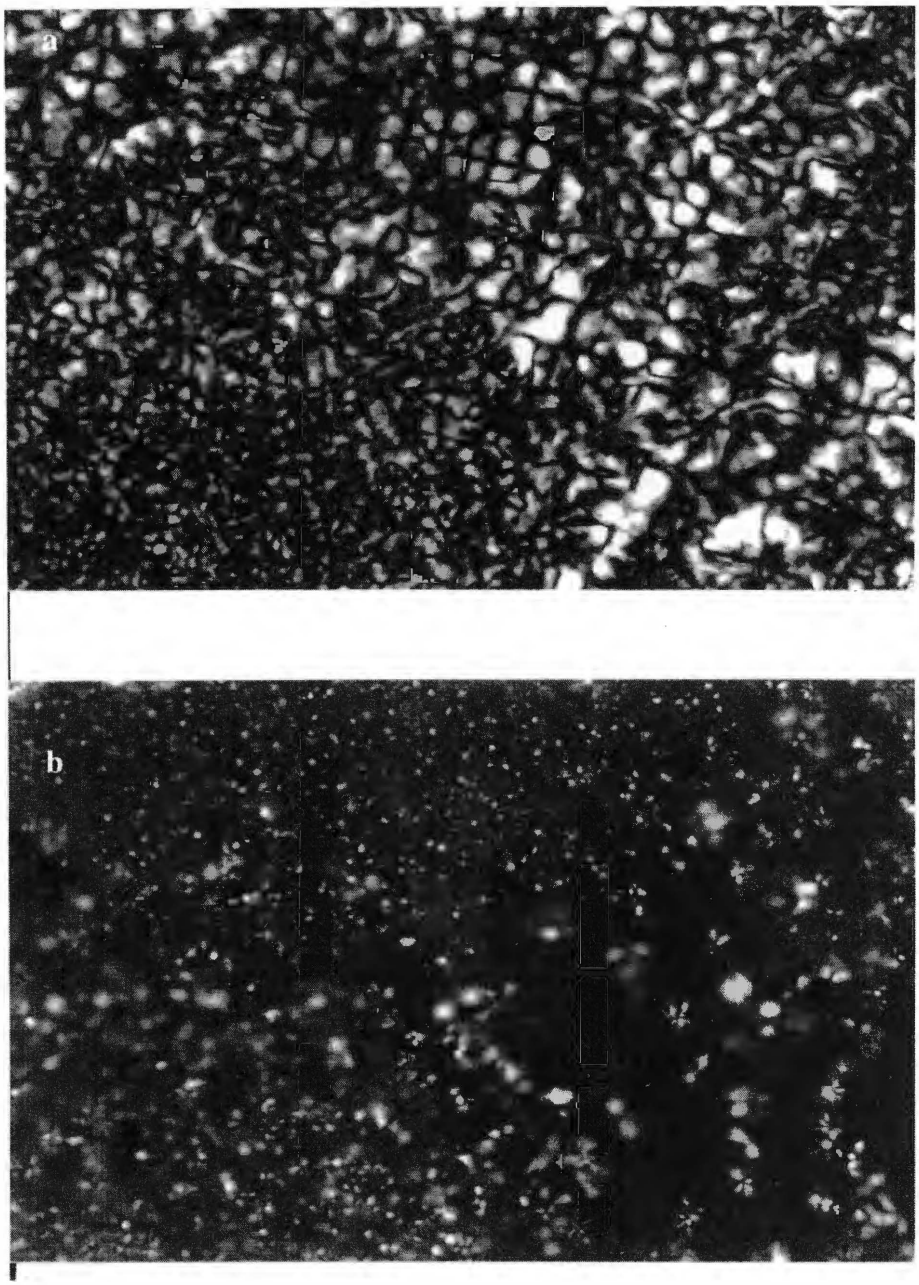


Figure (5.1.5) The morphological change of L-11 copolymer crystallized at T_c=115°C, 1 atm. a) T=118 °C , b) T=129 °C only large lamellar structure survive.

lamellar thickness on the phase diagram of the materials crystallized from the melt was not studied till later when Keller *et al* [84] established a three dimensional phase-stability diagram that demonstrates the effect of pressure, temperature, and lamellar thickness simultaneously. The 'temperature-pressure-reciprocal lamellar thickness' phase-stability diagram introduces the idea of triple line instead of the triple point, as shown in **figure (5.1.6)**. The plot suggests that a stable hexagonal phase can exist at pressures as low as atmospheric pressure. This is true for small crystal thicknesses, and appropriate crystallization temperatures. Crystals can also grow in the stable orthorhombic phase, then transform to the hexagonal phase upon heating.

Based on the melting behavior of L-04 and L-11 copolymers, and the findings of Rastogi *et. al.* it is believed that the extensively high melting temperatures which reflect thick lamellar structures, grow in the monoclinic phase. The lower melting points, on the other hand, represent the orthorhombic lamellar structure. Using the highest melting temperatures obtained in this study, P-T phase diagram of ethylene-octene copolymers can be constructed as a function of branch content as shown in **figure (5.1.7)**. The increase of branch content shifts the triple point significantly to lower pressures and temperatures. The triple point for L-04 copolymer appears at about 0.48kbar and 146 °C. For L-11 copolymer the triple point falls below atmospheric pressure. The triple point in this discussion represents the intersection of the melt, monoclinic and orthorhombic phases of the used systems. The difference in the melting temperatures between orthorhombic and monoclinic phases of L-04 is found to be ~5 °C for 0.76kbar and ~9 °C

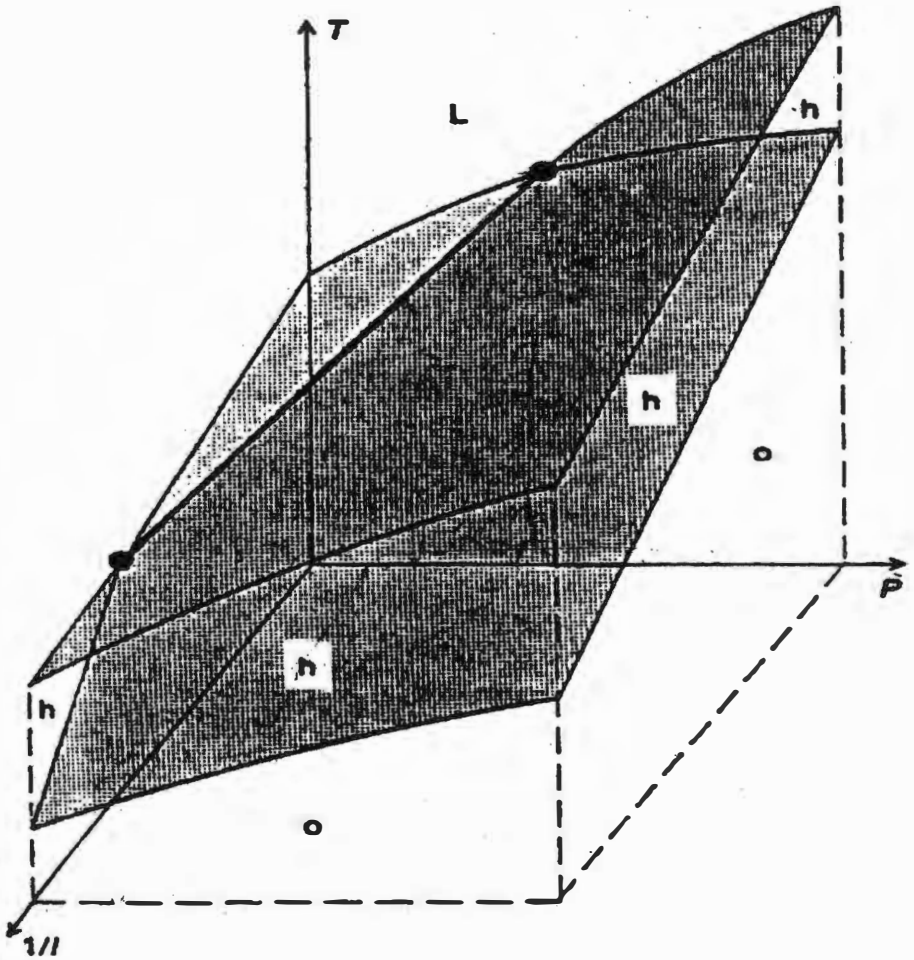


Figure (5.1.6) The three-dimensional (T, P, $1/l$) phase-stability diagram [84].

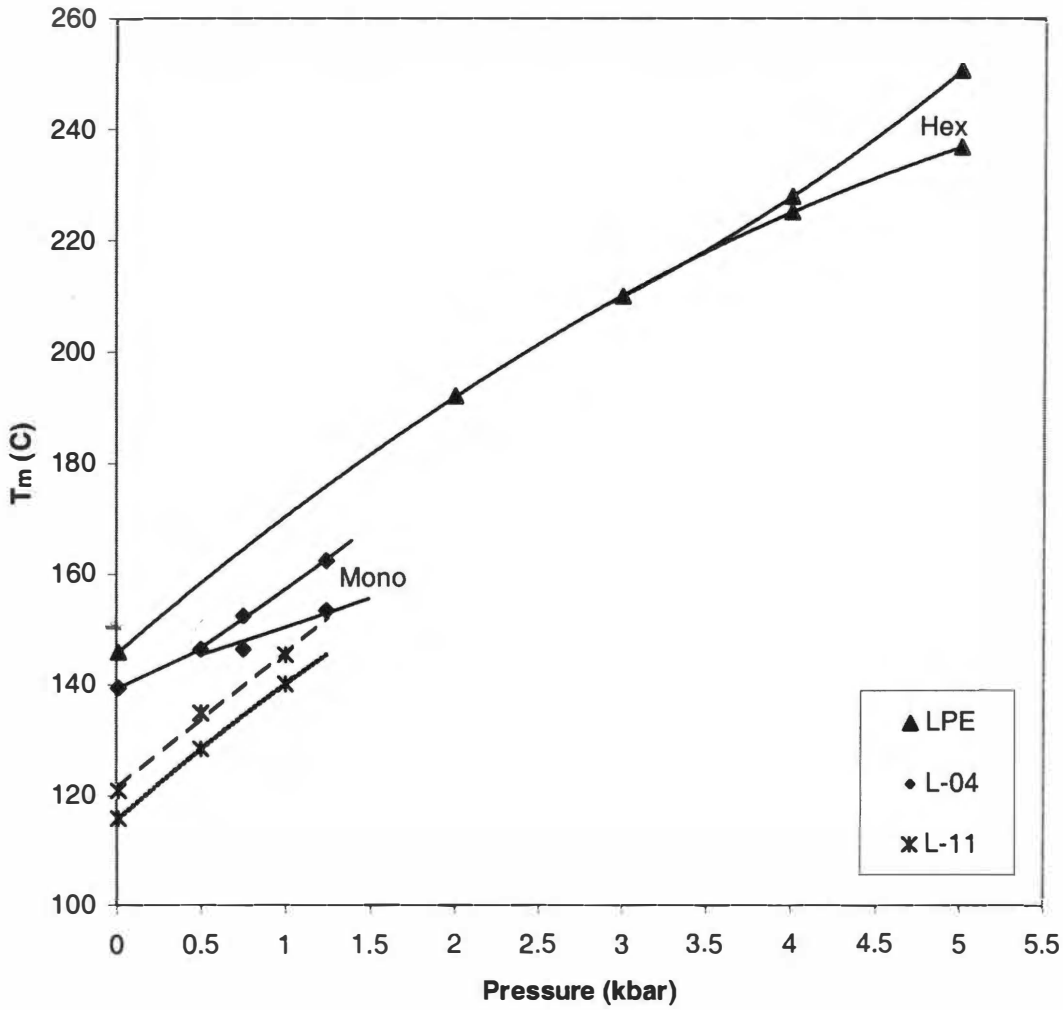


Figure (5.1.7) The effect of branch content on P-T phase diagram.

at 1.24kbar. These values are of crucial importance and will be used in **section 5.2** to estimate the corresponding lamellar thickness of the melting points at elevated pressures.

Similar values can be obtained indirectly using growth rate kinetics. In **figure (5.1.8)** the values obtained from **figure (4.1.3)** are shown as squares (■). They represent the crystallization temperature needed at each pressure to obtain a certain growth rate. The solid triangles (▲) represent the expected equilibrium melting points of the orthorhombic crystals as a function of pressure. The values were obtained using dT_m/dP~17 °C/kbar. The two solid lines are not parallel to each other and, interestingly, will intersect at T=202.98 °C and P=3.729kbar. The intersection point is equivalent to the triple point suggested by Bassett. Lines intersection suggests a fixed spherulitic growth rate value at zero supercooling.

To solve the upper discrepancy, a specific correction should be applied to the equilibrium melting points as demonstrated by the dashed line. To avoid lines intersection, the corrected melting points should form a parallel line with the crystallization temperatures. To obtain a parallel relationship, T_m^o must be shifted by ~5°C at 0.76kbar, and ~9 °C at 1.24kbar. The shift corresponds perfectly with the one obtained from the phase diagram.

The reduction of the initial lamellar thickness shifts the triple point to lower pressures and temperatures as reported by Rastogi *et al* [1]. The effect of crystallization temperature, hence, lamellar thickness on the phase diagram is crucial. However, it is

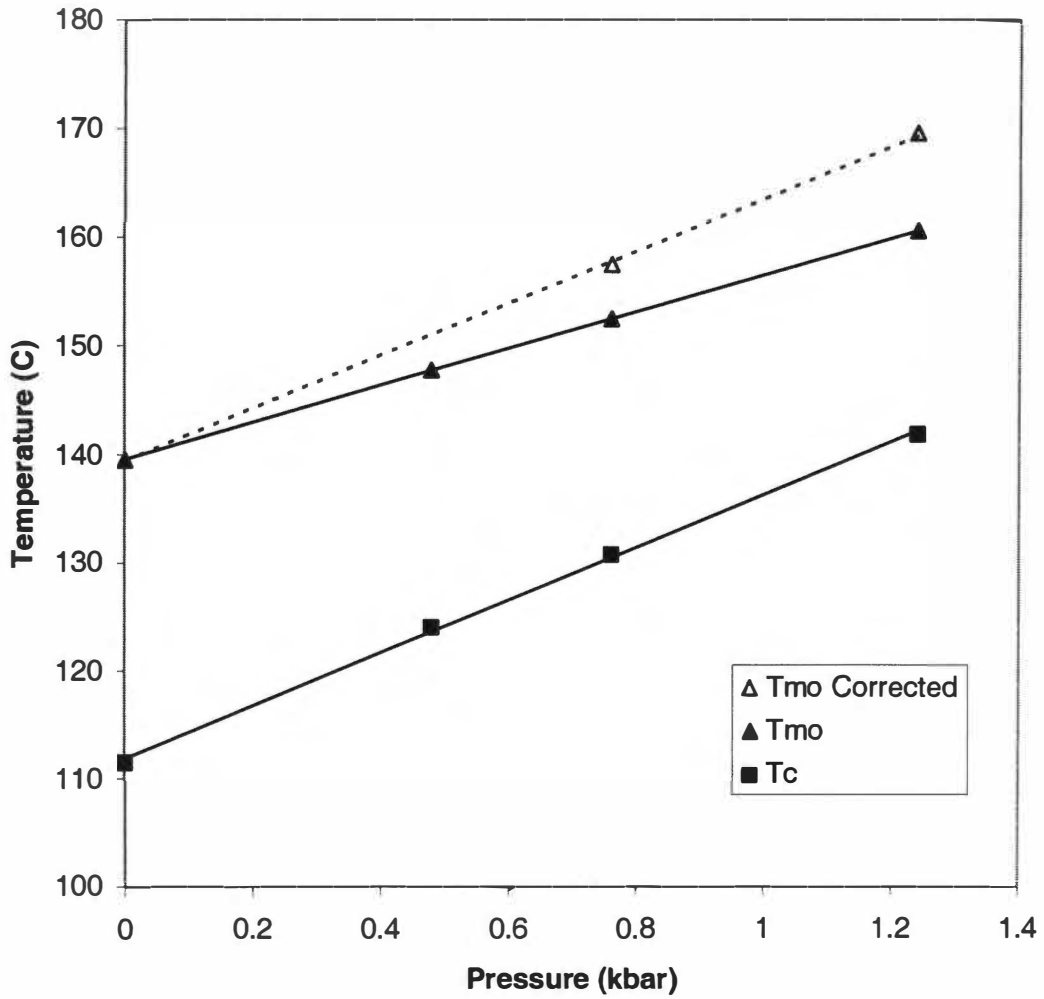


Figure (5.1.8) A plot of temperature versus pressure used to estimate the corrected equilibrium melting points of L-04 copolymer using growth rate kinetics.

difficult to implement it on a 2-dimensional phase diagram, and a 3-dimensional phase diagram is required to better visualize the effect of T_c. **Figure (5.1.9)** represents the effect of crystallization temperature on the P-T phase diagram of L-04 copolymer. At T_c=140 °C the melting temperature at atmospheric pressure is the reported equilibrium melting temperature of the L-04 copolymer. The almost linear relationship (line **a**) between the equilibrium melting point of the orthorhombic phase of L-04, and the highest melting points obtained for the monoclinic phase is more evidence of the formation of extended-chain crystals at elevated pressures.

5.1.3 Eutectoid Transformation

5.1.3.1 Eutectoid Transformation in Alloys

Eutectoid transformation is observed in alloys in which one phase decomposes, on cooling, into a mixture of two low-temperature phases at a temperature called the *eutectoid temperature*. The number of solids formed is the same as the number of components in the system [85]. An example of great practical importance is in low carbon steels where the relationship of its three phases is directly affected by the amounts of carbon.

Gamma phase (γ), also called austenite, is an allotrope of iron that is stable at intermediate-to-high temperatures, has a face-centered cubic crystal structure, and can dissolve considerable amounts of carbon. The transformation from gamma to alpha phase

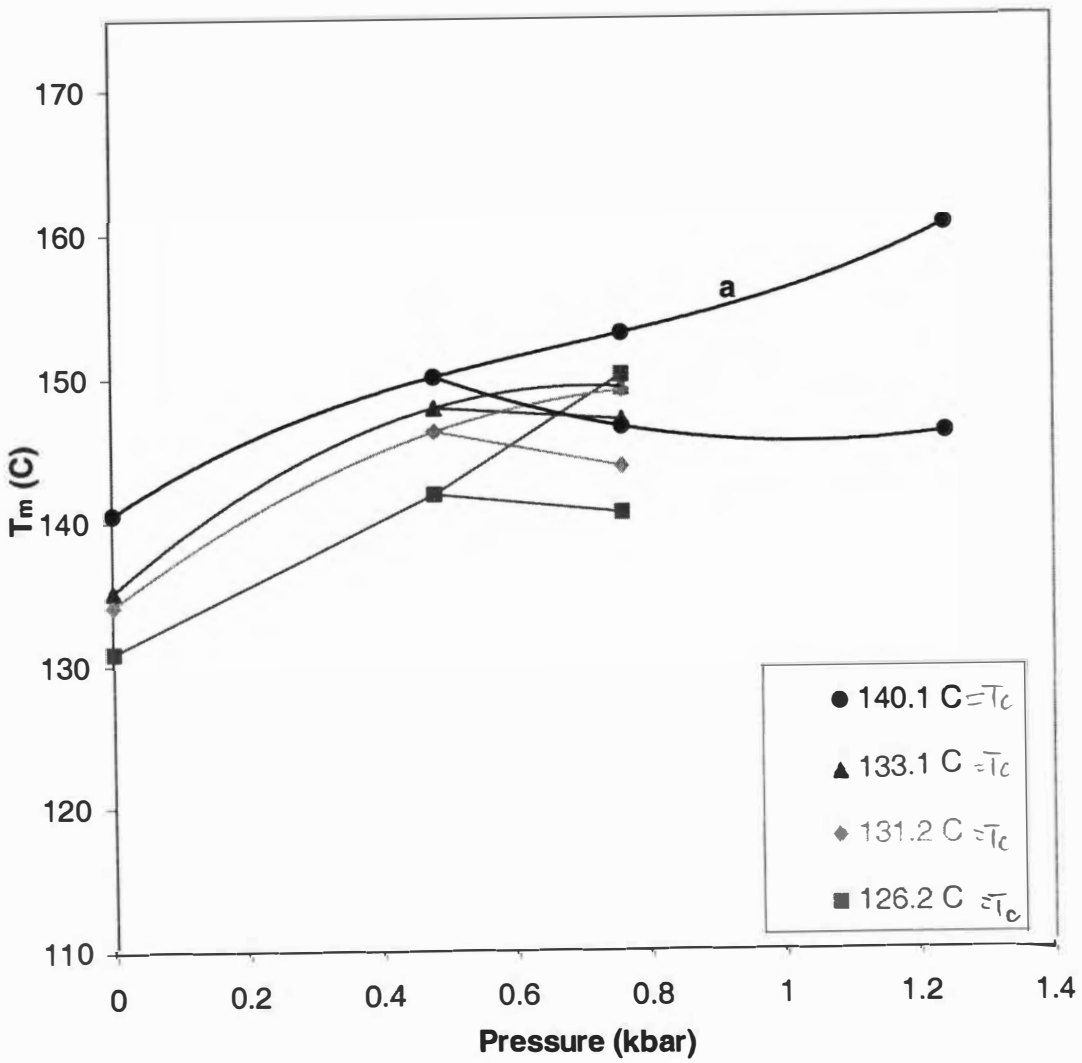


Figure (5.1.9) The effect of crystallization temperature T_c on the P-T phase diagram of L-04 copolymer.

occurs at a specified temperature 912 °C in pure iron, but over a range of lower temperatures when carbon present. Alpha phase (α) (or ferrite) is an allotrope of iron that is stable at intermediate-to-low temperatures, has a body-centered cubic crystal structure, and can dissolve only very small amounts of carbon. Cementite phase is a compound of iron and carbon that has the approximate composition Fe_3C and a complex crystal structure. The stable phase of the iron-carbon system is graphite, while cementite is its meta-stable phase.

Figure (5.1.10) illustrates the iron-carbon phase diagram, and shows that the lower temperature of the transformation range is constant for all carbon contents (the solid horizontal line in the figure). It is interesting to notice that at relatively low temperatures and carbon contents the co-existing phases (austenite and ferrite) transform to a single alpha phase, a behavior similar to our polymeric system. It can also be noticed that at certain temperature (727 °C) the simple allotropic transformation ceases. The remaining of austenite decomposes into a mixture of the low-temperature allotrope (ferrite) and cementite. This is called eutectoid transformation and occurs at a specific eutectoid temperature and composition. Eutectoid system is slightly different than the eutectic system in that all interactions among the phases in the former occur inside a solid i.e. between a solid crystal and a solid crystal rather than between a liquid and a solid as is the case in the eutectic system.

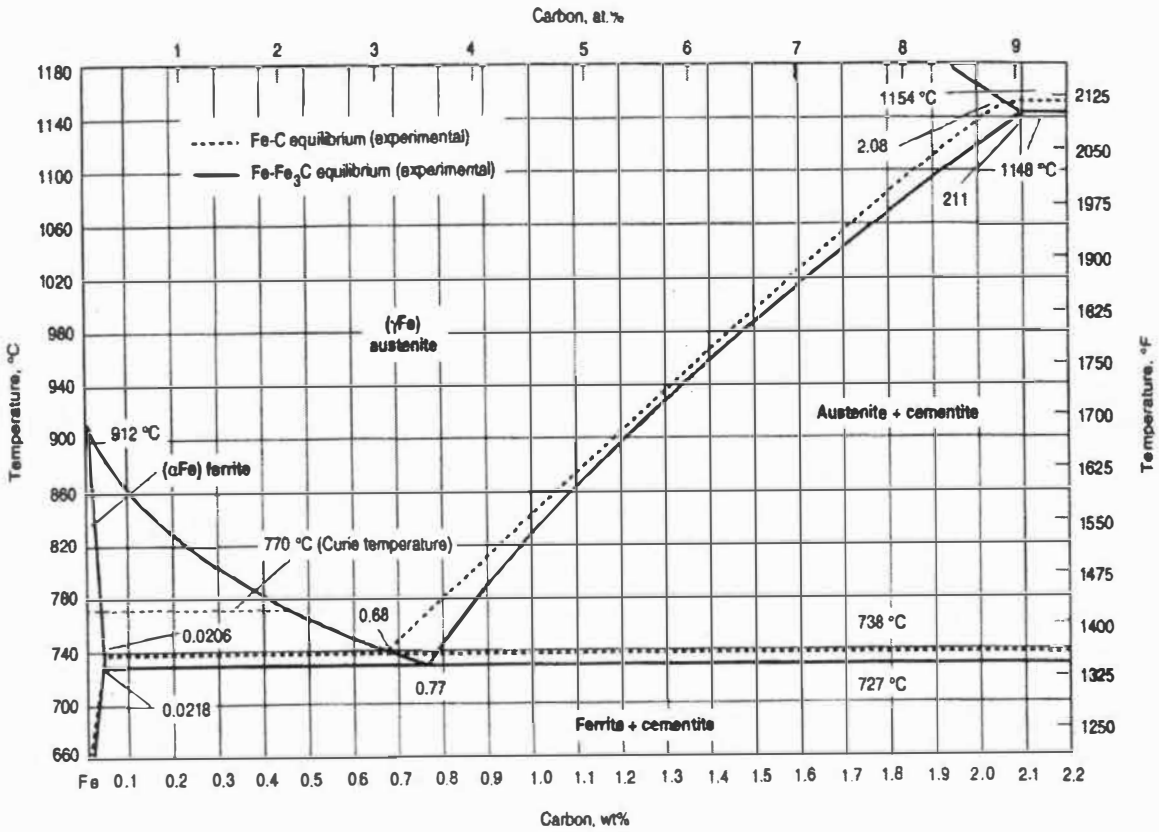


Figure (5.1.10) Iron-carbon phase diagram showing the austenite (γ Fe) and ferrite (α Fe) phase regions and eutectoid composition and temperature. Dotted lines represent iron-graphite equilibrium conditions and solid lines represent iron-cementite equilibrium conditions. Only the solid lines are important with respect to steel [86].

Eutectoid Transformation does not occur instantaneously. Nuclei for the two phases have to form adjacently in a certain period of time before the start of the diffusion-controlled growth process. Both phases are arranged in colonies of thin, roughly parallel plates. This structural constituent is known as pearlite. The time needed for a complete transformation to pearlite depends mainly on temperature and differs for different carbon composition.

Transformation also occurs during the continuous process. For slow cooling (e.g. cooling in furnace) transformation starts and finishes at comparatively high temperatures, and forms coarse pearlites. Faster cooling (e.g. cooling in liquid), in general, helps retaining the high-temperature phase at room temperature. However, for iron-carbon alloys the high-temperature phase transforms to a non-equilibrium phase, called martensite, before it reaches room temperature. It should be noticed that the design of the high-pressure cell limits our ability for a very rapid cooling. The maximum cooling rate obtained by this design is around 10~15 ^{o}C/min depending on the setting temperature. Since the effect of cooling rate is not considered in this study, one cannot judge its real effect on the polymeric system. It may be possible that similar to iron-carbon alloys, relatively slower cooling rates prohibit the stabilization of one of the high-pressure phases.

In conclusion, some phases produced in iron-carbon and similar alloys cannot be retained when cooling down to room temperature. There are several parameters that affect the final product. The very important parameters, beside the carbon composition,

that must be considered are the rate of cooling and the annealing time. The similarities in behavior between iron-carbon alloy and ethylene-octene copolymer are important and expected to successfully explain the melting behavior of the latter. It is very important to know which process is responsible for the transformation, the cooling process or the releasing of pressure

5.1.3.2 Eutectoid-Like Transformation in Copolymers

The melting temperatures of high-pressure samples obtained at atmospheric pressure were inconsistent with the ones obtained *in-situ*, as discussed in **section 4.3.1.2**. Melting at atmospheric pressure experienced the disappearance of the second melting peak in the 'two melting peak' system i.e. $P \geq 0.76$kbar. In addition, all pressurized samples exhibited a larger drop in the melting temperatures than what was expected when pressure was released. Another interesting observation is the relatively narrow range of melting temperatures even when the crystallization conditions varied significantly. For example the melting temperature of sample crystallized at $T_c = 126\ ^{o}C$ and $P = 0.48$kbar is around 125 ^{o}C at atmospheric pressure, while that of the one crystallized at $T_c = 126\ ^{o}C$ and $P = 1.24$kbar is about 122.2 ^{o}C. **Figure (5.1.11)** compares the atmospheric melting temperatures of L-04 copolymer crystallized at different pressures. The equilibrium melting points obtained for high-pressure samples are generally ~2.5 ^{o}C higher than those of the atmospheric pressure samples. The small difference in the melting temperatures of high-pressure samples implies that the final crystalline morphology is relatively similar regardless of the original crystallization conditions. The final lamellar structure of the

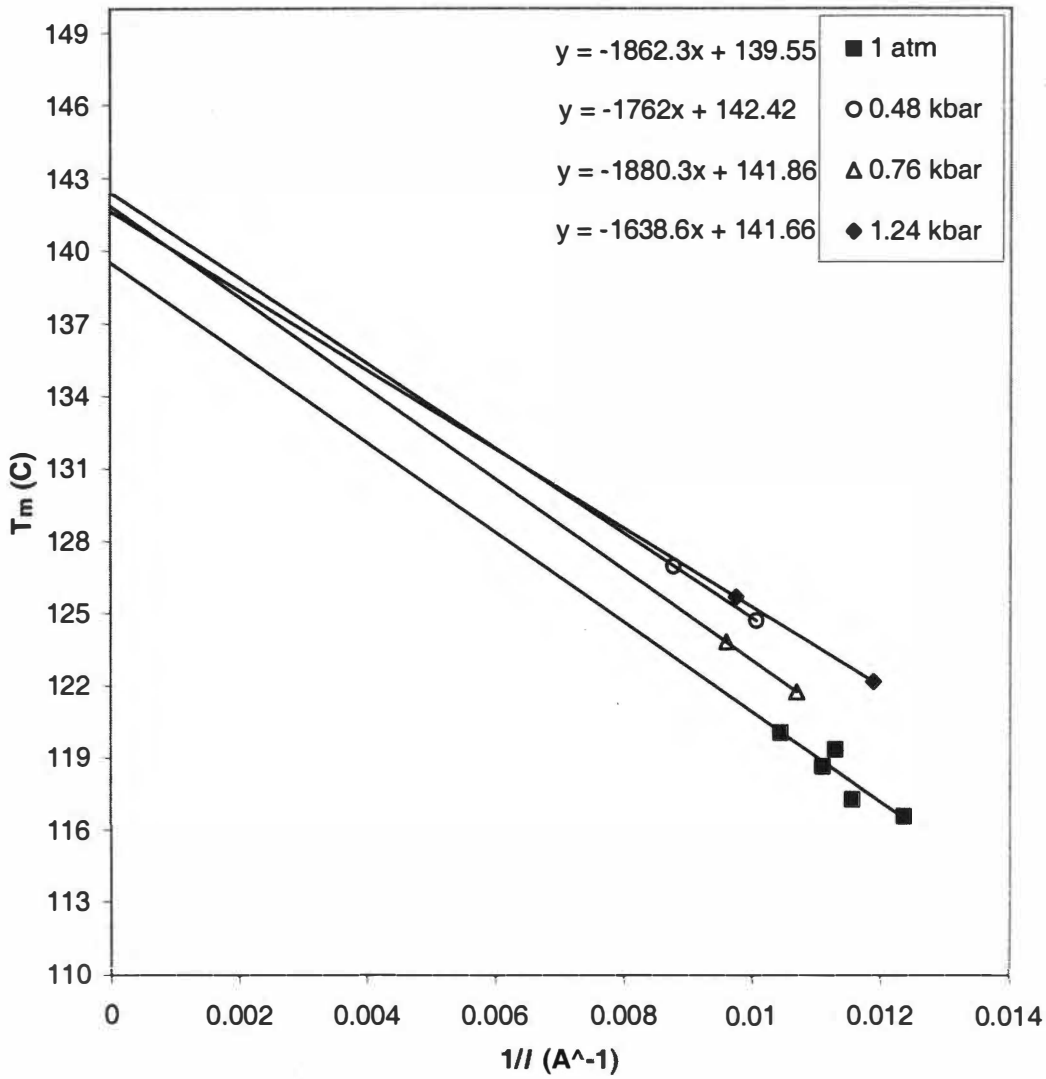


Figure (5.1.11) Gibbs-Thomson plot as a function of pressure. All melting temperatures were measured at atmospheric pressure.

high-pressure samples, on the other hand, always has thicker lamellae than that of the atmospheric pressure crystallization. In other words, the difference in lamellar thickness of the high-pressure samples is almost negligible and could be considered constant. This assumption consists in a way with what Strobl suggested about the granular crystalline layer that transforms to homogenous lamellar crystallites.

Based on the previous discussions it is believed that the formation of ECC in L-04 copolymer crystallized at elevated pressures occurs through the monoclinic phase. The solubility limit of hexyl branches in the monoclinic phase is higher than that of the orthorhombic phase. Therefore, hexyl branches can be dissolved in the crystalline phase. However, upon releasing pressure the hexyl branches are rejected from the crystalline phase into the amorphous material, due to the lower solubility in the orthorhombic phase, and generate a well-stacked lamellar structure. Consequently, the monoclinic phase transforms to the stable orthorhombic phase in a similar manner to a eutectoid-like transformation.

As a result of the transformation, high-pressure samples generate an almost constant T_m^o value at atmospheric pressure (**figure 5.1.11**). The stacked lamellae mentioned above should be of equal size to each other regardless of the original applied pressure. The slightly higher T_m of the high-pressure samples compared to the atmospheric pressure is a sign of better stacking crystals, therefore less amorphous material. The major influence on the final lamellar thickness will be the branch content

and distribution, not the pressure used. The schematic in **figure (5.1.12)** demonstrates the suggested eutectoid-like transformation in ethylene-octene copolymers. For L-11 copolymer, crystallization is believed to occur in the monoclinic phase before it transfers to the orthorhombic phase right behind the growth front.

The X-ray results, as will be discussed in **section 5.2**, did not show any convincing evidence of another stable co-existent phase beside the orthorhombic phase. Due to its high mobility the monoclinic, or hexagonal, phase is only identifiable at elevated pressures and temperatures and is expected to transform to the stable orthorhombic phase after cooling down and removal of pressure as discussed previously. *In-situ* high pressure and temperature x-ray diffraction is needed for definitive characterization of the phases produced.

SEM pictures shown in **section 4.4.2** demonstrate the ramification of eutectoid-like transformation on the morphology of ethylene-octene copolymers. **Figures (4.4.8-12)** represent the morphological features of L-04 copolymer crystallized at 140 °C and 0.76kbar. The pictures demonstrate two different morphologies of chunky pieces surrounded by randomly distributed thinner lamellae. The arrowed structures in **figures (4.4.9-12)** have an overall thickness of few thousands of angstroms and contains within it few stacked thinner lamellae each of a thickness of few hundreds of angstroms. **Figures (4.4.10-11)** better exhibit the phenomenon. The thickness of the arrowed area in **figure (4.4.11)** is about 1951Å while the thinnest individual lamella is about 160Å. The lamellar structure shown in the squared area of **figure (4.4.11)** resembles the suggested schematic

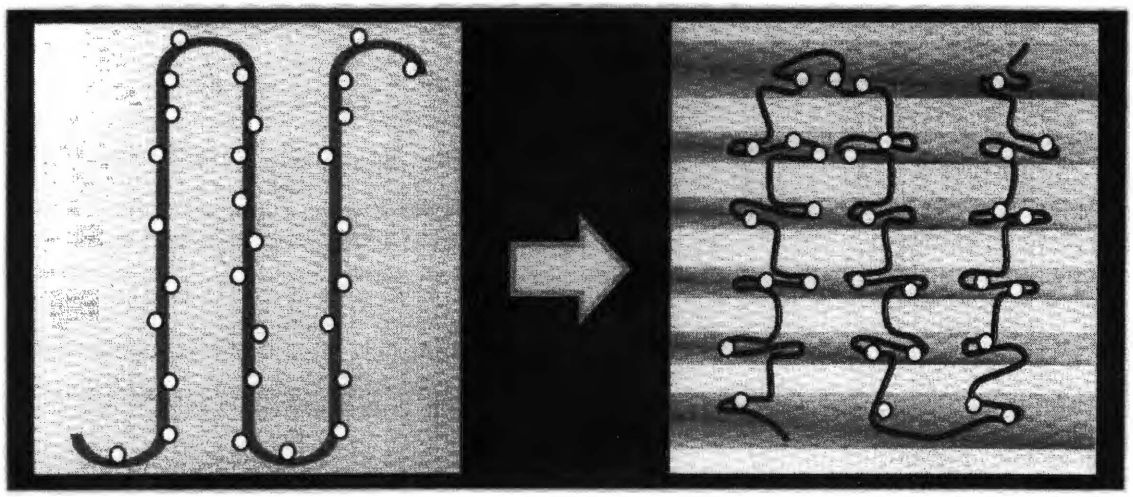


Figure (5.1.12) A schematic diagram of the eutectoid-like transformation where the rejection of branches converts the thick lamella to thinner stacked ones.

diagram of the eutectoid-like transformation shown in **figure (5.1.12)**.

Figures (4.4.13-17) display the thick lamellar structure of L-11 copolymer crystallized at atmospheric pressure and T_c=115 °C. Based on the melting behavior of this material and the phase diagram of **figure (5.1.7)**, the monoclinic phase does form at atmospheric pressure. The eutectoid-like transformation, however, may occur during crystallization right behind the growth front or on cooling. Crystallization and melting experiments under *in-situ* WAXD are required for a definitive judgment.

The very selective crystallization process can be observed in the figures. The thick lamellar structure shown in **figure (4.4.13)** is around 2000Å thickness. The structure shown in area '**A**' could be a result of the etching process. **Figures (4.4.16-17)** show a partially melted sample of L-11 copolymer. The partial melting process should discard the structure of the lower melting temperature, i.e. the orthorhombic structure, as illustrated in **figure (5.1.5)**. The lamellar structure pointed to by the arrows is another example to the stacked thin lamellae resulted from the eutectoid-like transformation.

5.1.4 The Monoclinic Phase in Thermodynamics

Giel *et al* [87] were one of the first groups to introduce the phenomenon of extended-chain crystals when they discovered that PE samples crystallized from the melt at about 5 kbar have a very high density and 100% crystallinity. ECC exhibit very thick

lamellae compared to the well known thin lamellar crystals formed in a folded-chain manner.

Fully extended chains are unlikely to form under normal conditions due to the very high-activation barrier, whether the barrier is entropic (low-deposition probability) or enthalpic (large surface free energy). However, the molecular length is usually longer than the crystal thickness of ECC in the chain axis direction as reported by Bassett [88]. This implies that the molecular chains in the ECC lamellae may be folded with their chain ends included in the lamellae. The large lamellar thickness of ECC is due to the relatively low entropy of fusion per unit volume. The fold surface free energy (σ_e) of the chain-folded crystals has lower value than that of the hexagonal phase, if folding the molecule did not introduce additional gauche bonds. In an unpublished work by Bassett *et al* it was found that the lamellar thickness, of both linear material and copolymers under high pressure, decreased in chain-extended growth of longer molecules. They attributed it to the transport problems necessarily associated with thickening.

According to the crystallization mechanism of lamellar thickening growth postulated by Hikosaka *et al* [89], the extended chain crystals (ECC) of polyethylene always arise through the mobile hexagonal phase irrespective of whether it is a stable or meta-stable phase. The meta-stable hexagonal crystals will eventually transform into thermodynamically stable orthorhombic crystals on cooling.

A numerical assessment of the crystallization of PE under atmospheric pressure indicated that there is a strong likelihood that crystallization may proceed via a meta-stable, mobile, hexagonal or monoclinic phase. The mobile phase is transiently stable at the smallest size where the crystal first appears. In order to understand the upper possibility Keller *et al* [84] constructed a simplified schematic plot of the free energy, G, versus temperature as shown in **figures (5.1.13-15)**. The lines denoted G_C, G_M and G_L represent the free energy of the stable crystal (orthorhombic), intermediate (monoclinic), and liquid states (molten), respectively.

Figure (5.1.13) represents a situation where the intermediate (monoclinic) phase is unstable ($G_M >$ both G_C and G_L) and the material is either stable crystalline phase (e.g. orthorhombic) or liquid i.e. melt (solid lines). The melting temperature ($T_{m,c}$) (points in bold) represents the melting of the crystalline (or orthorhombic) phase and increases with increasing the crystallization temperature T_c due to reduction in the free energies (the drop in G_M is not shown in the figure for simplicity).

Raising G_L as shown in **figure (5.1.14)** will bring the intermediate phase into the picture and shift the melting temperatures ($T_{m,\ c}$ becomes T_{tr}) to larger values. The transition temperature (T_{tr}) represents the temperature at which the crystalline phase transforms to the intermediate phase. Increasing G_L occurs when the enthalpy of the melt, H_L, is raised and/or its entropy, S_L, is lowered. Achieving this practically happens by applying an external pressure or increasing the chain stiffness of the material, physically or chemically.

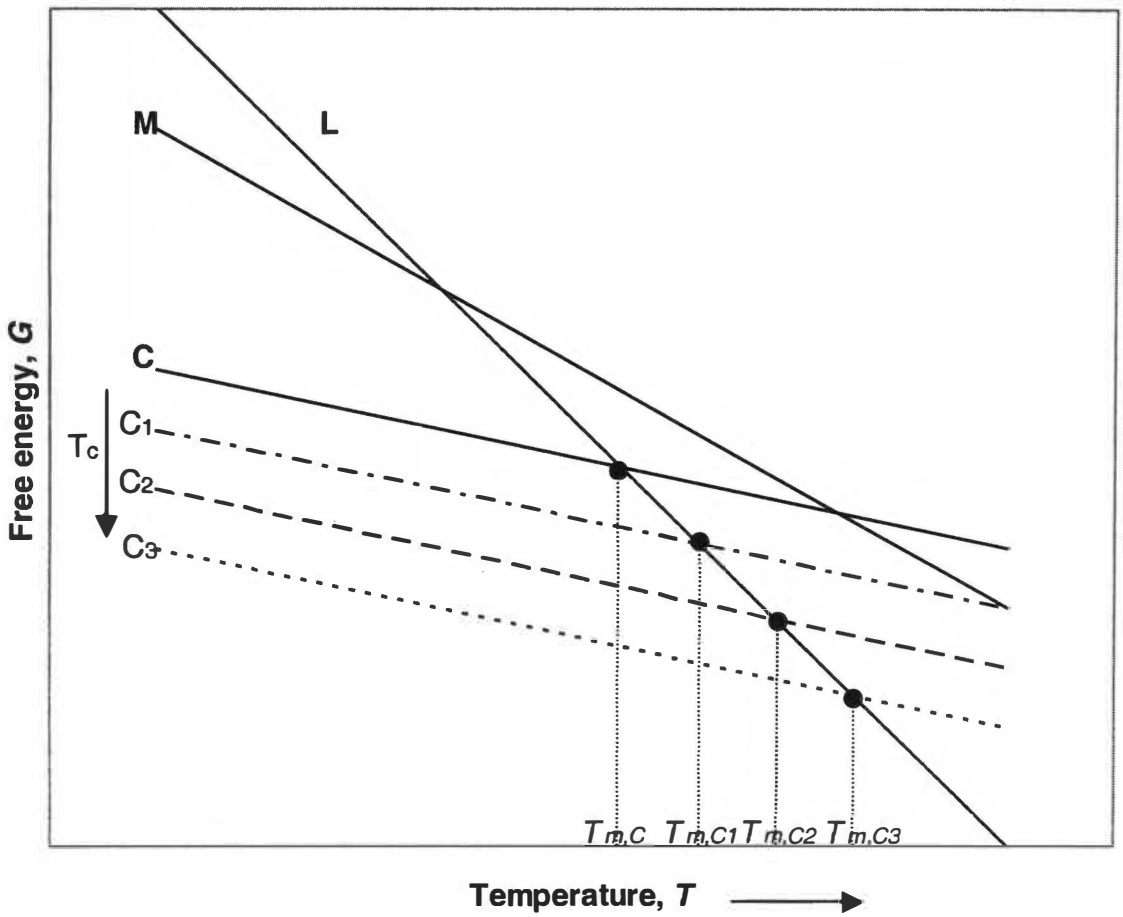


Figure (5.1.13) Schematic free energy G versus temperature plot, illustrating the stable orthorhombic and unstable monoclinic phases at atmospheric pressure.

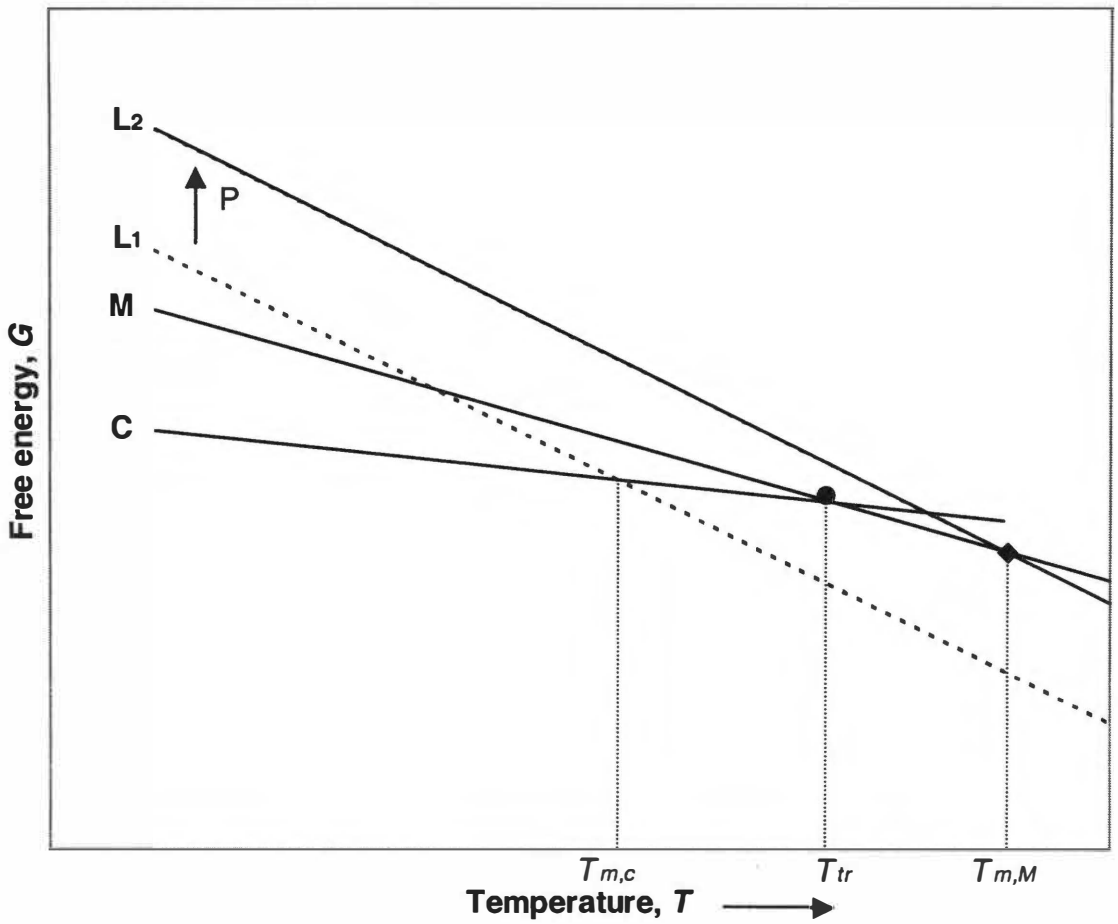


Figure (5.1.14) The effect of pressure on the schematic free energy G versus temperature plot. The monoclinic phase becomes stable.

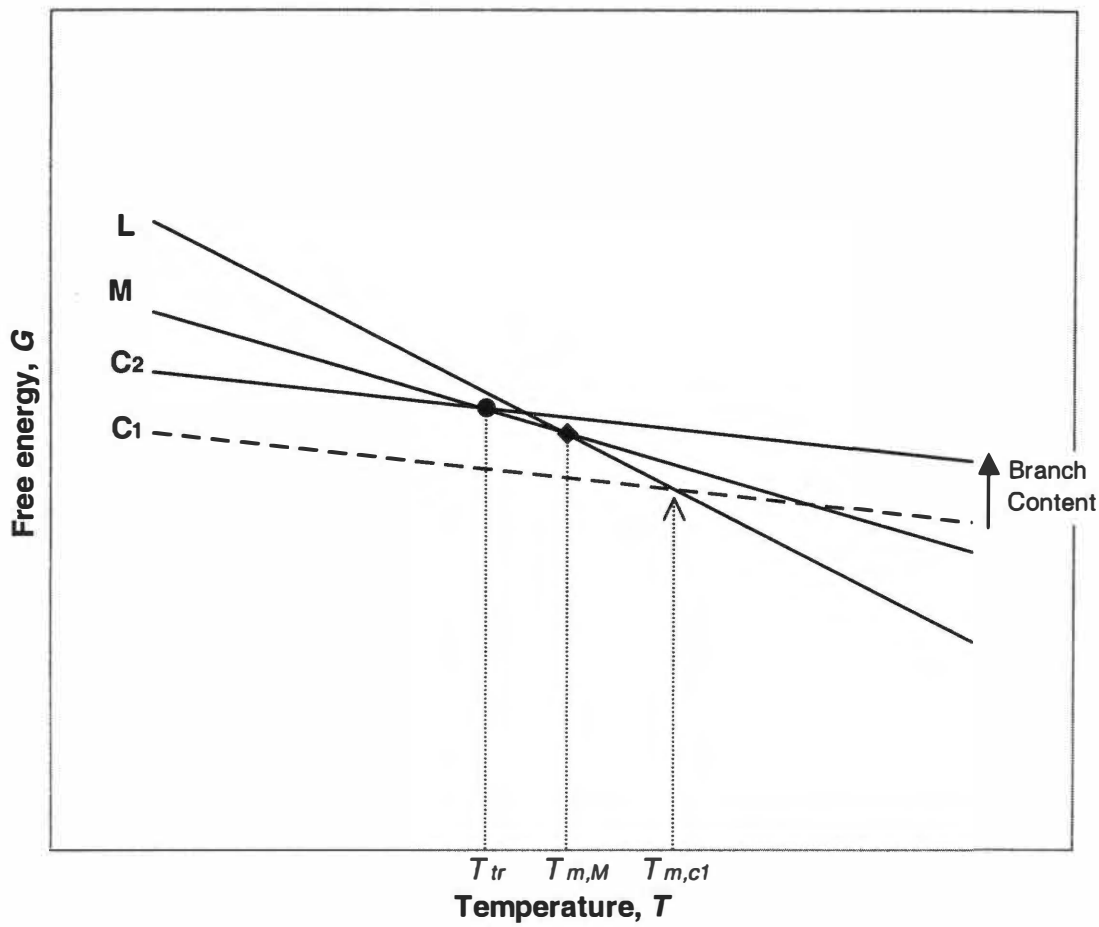


Figure (5.1.15) The effect of branch content on the schematic free energy G versus temperature plot. The monoclinic phase becomes stable but at lower temperatures

Another way to unveil the intermediate phase is by raising the G_C value. This, as seen in **figure (5.1.15)**, will not only introduce the intermediate phase, but will shift the transition and melting points to lower temperatures. Impairing the lattice order (e.g. introduction of defects) and the reduction of the crystal size are two main factors of raising G_C value. One practical example is the addition of powder particles of several tens of microns in size to UHMW-PE material which produced a sufficiently small initial crystal size with enhanced molecular chain mobility, and hence shifted the stability of the hexagonal phase to a much lower pressures (~1kbar) and temperatures [1]. Another example is by increasing the branch content.

Accordingly, the crystallization of ethylene-octene copolymers should raise the G_C value of the system depending on its branch content. Hexyl branches act as defects in the material and will reduce the lamellar thickness. The larger the branch content the higher the value of G_C and the lower the transition and melting temperatures. On the other hand, high-pressure crystallization of the copolymers will affect both G_L and G_C values, and will expand the range of the intermediate phase temperatures. This explains the observed shifting of the triple point in the P-T phase diagram.

When comparing with the results discussed in **sections 5.1.1-3** it can be stated that the existence of two melting peaks results from the formation of another intermediate phase beside the well-known stable orthorhombic phase. For L-04 copolymer a minimum pressure of 0.76kbar is needed to sufficiently raise the free energy of the liquid state and observe the intermediate state. The nature of the intermediate phase cannot be easily

identified especially if it is in the meta-stable state. However, the results collected in this study support the formation of thick crystals grown in the monoclinic phase. Increasing the branch content, and hence the number of defects, as in L-11 copolymer raised the free energy of the crystalline state, G_C, high enough to allow for the intermediate phase to appear even at atmospheric pressure. Applying pressure will, additionally, shift the G_L line upward and, hence, expand the area between $T_{m,\ M}$ and T_{tr}. The effect of the crystallization temperature, and hence the lamellar thickness, on the stability of the presented phases is discussed in the next section and will be used to explain the melting behavior of the observed lamellar thickness of L-04 at different pressures and temperatures.

5.1.4.1 The Thermodynamics of Phase-Diagram

According to the previous argument of **section 5.1.4**, an increase of the lamellar thickness depresses the crystalline free energy G_C and shifts the melting temperatures of the orthorhombic phase to higher values. The increase in the lamellar thickness by the same amount has less effect on dropping G_M, therefore the increase in the melting temperature of the monoclinic phase will not be significant. To better understand the effect of crystallization temperature or lamellar thickness on the free energy of the system, the change in Gibbs free energy at constant temperature is introduced as,

$$\Delta G_i = \Delta H_{f,i} - T\Delta S_i \qquad (5.1.1)$$

The change of entropy (ΔS_i) can be determined when the equilibrium state is reached where ΔG_i=0 and $T = T_m^o$.

$$\Delta S_i = \frac{\Delta H_{f,i}}{T_m^o} \tag{5.1.2}$$

The subscript '*i*'= '*c*' for the crystalline (or orthorhombic) phase, or '*M*' for the intermediate (or monoclinic) phase, where the parameters ΔS_i, $\Delta H_{f,i}$ and ΔG_i are not equivalent for the different phases.

At larger crystallization temperatures molecules in the orthorhombic phase become more mobile due to its increased entropy. This reduces the total free energy ΔG_C of the solid phase as can be observed from **equation (5.1.1)**. On the other hand, the mobile phase (e.g. monoclinic or hexagonal) is not expected to increase its entropy significantly as temperature increases, in addition its larger solubility parameter allows for the defects to be included into the crystalline phase hence reducing the heat of fusion. Therefore, the total drop in the free energy of the mobile phase is expected to be slim.

Based on the above demonstration Keller *et al* have plotted the melting temperature versus reciprocal lamellar thickness ($1/l$) phase diagram as shown in **figure (5.1.16)**. Although their model managed to explain some of the results reported in this section, there was some difficulty in explaining the melting behavior at elevated

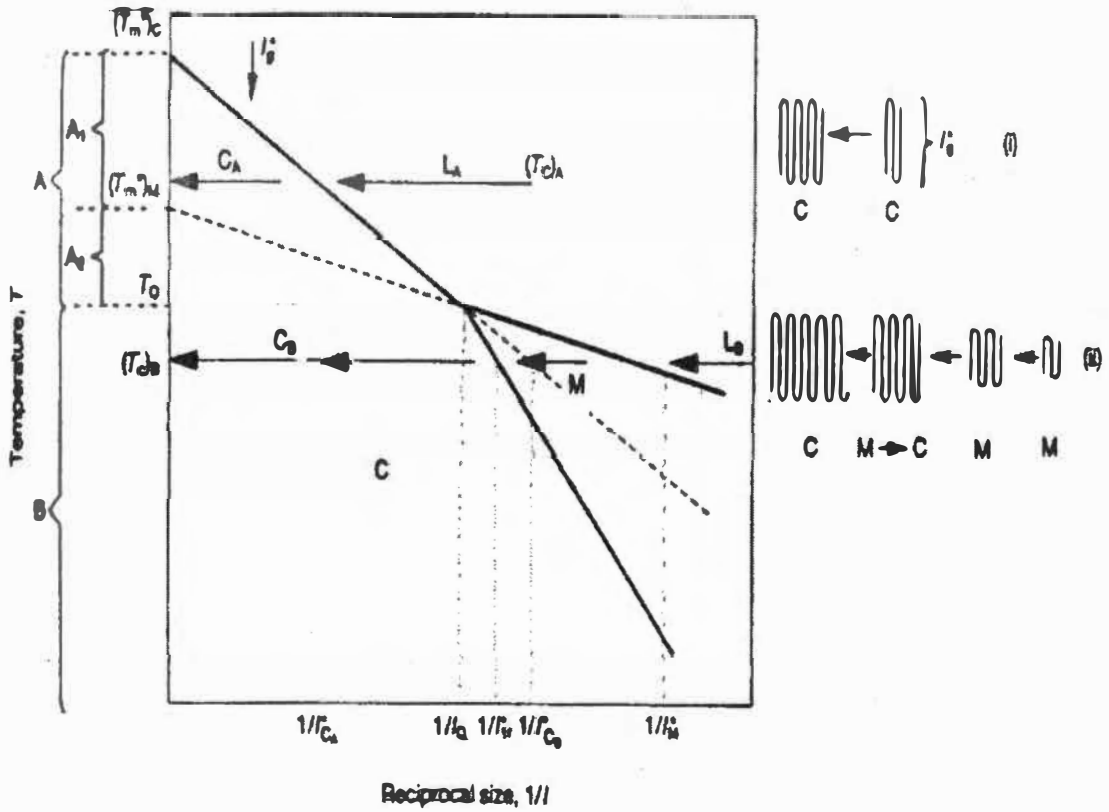


Figure (5.1.16) Phase (crystal) growth as a temperature T versus reciprocal size $1/l$, phase stability diagram [84].

pressures and temperatures. In the next paragraphs a detailed thermodynamical interpretation of the melting behavior of ethylene-octene copolymers will be implemented.

L-04 copolymer

L-04 copolymer crystallized at atmospheric pressure did not show any unusual behavior compared to orthorhombic phase crystallization. **Figure (5.1.13)** best describes its thermodynamics, where the free energy of the monoclinic phase lies beyond that of the orthorhombic phase. Raising the crystallization temperatures, on the other hand, although reducing both G_c and G_M values, is not enough to unveil the monoclinic phase. Therefore the monoclinic phase could not be observed at this pressure and only an increase in $T_{m,\,c}$ value can be noticed.

When increasing the pressure to 0.48kbar, G_L shifts to larger values where higher melting temperatures $T_{m,\,c}$ are produced. This increase is still not sufficient to unveil the intermediate phase, although it increases the G_L value enough to intersect with the other free energy lines as demonstrated by the solid lines in **figure (5.1.17)**. The intersection of the three free energies is a transition state that indicates an equivalent melting temperature for both orthorhombic and intermediate phase crystals. This accordingly might explain the single, higher than expected, melting peaks reported for this pressure (see **figure 5.1.1**). Albeit the drop in G_c and G_M values due to the increasing value of the

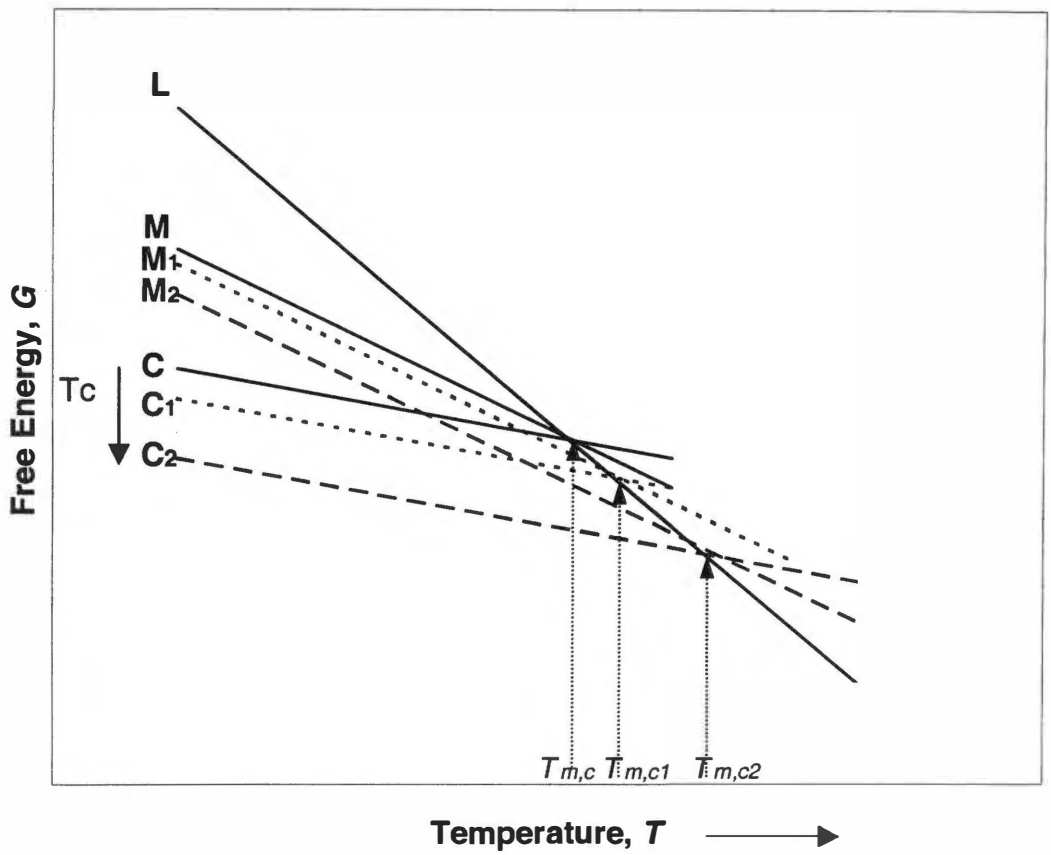


Figure (5.1.17) A schematic diagram of the expected effect of T_c on Gibbs free energy G at 0.48kabr

crystallization temperature (broken lines), the effect of temperature on the reduction of G_c value is expected to be larger at this pressure but not enough to change the $\Delta G_c > \Delta G_M$ relationship. The small difference between ΔG_c and ΔG_M helps the free energies to stay at the intersection point for wider range of temperatures before ΔG_M starts to virtually dominate.

Once pressure reaches 0.76kbar, G_L value will be raised high enough to disclose the intermediate phase, as was illustrated in **figure (5.1.14)**. In a similar fashion to the previous cases, increasing the crystallization temperature will drop the G_c and G_M values, where $\Delta G_c > \Delta G_M$. As a result, both transition and melting temperatures (T_{tr} and $T_{m,\,M}$ respectively) increases, as represented by the empty circles in **figure (5.1.18)**. However, since $\Delta G_c > \Delta G_M$, the amount of increase in $T_{m,\,M}$ is expected to be smaller than that of T_{tr}. This brings both temperatures closer to each other as T_c increases. When T_c reaches a critical value T_{cr} (solid bold lines) the free energy of the crystalline and intermediate phases become very close to each other, and theoretically intersect with G_L, similar to what was observed at 0.48kbar. The critical temperature increases with the applied pressure. Once the temperature exceeds T_{cr} the change in the free energies is believed to be comparative to each other, i.e. $\Delta G_c = \Delta G_M$. In consequence, T_{tr} remains constant with crystallization temperature, while $T_{m,\,M}$ increases more rapidly as illustrated by squares in the figure. This demeanor reflects the actual melting behavior of L-04 copolymer at 0.76kbar as described in **figure (5.1.2a)**.

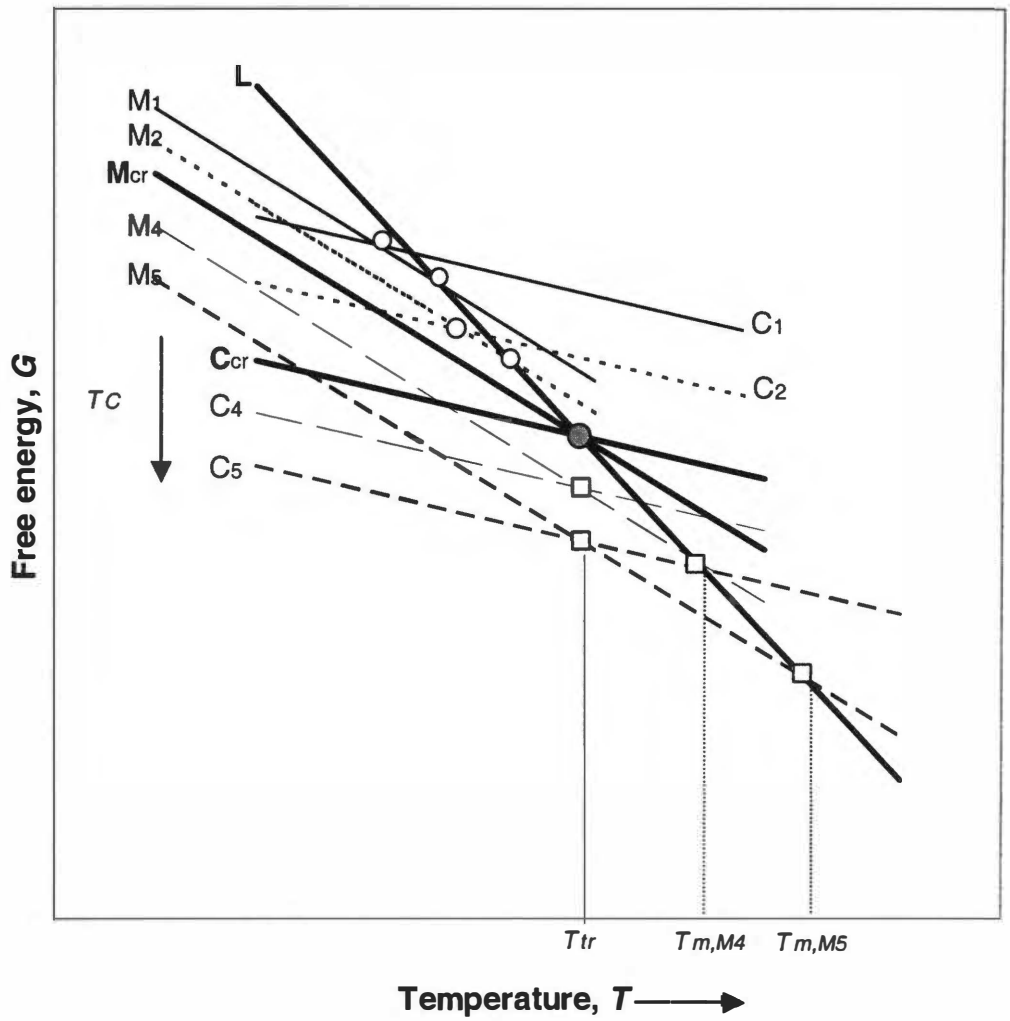


Figure (5.1.18) A schematic diagram of the expected effect of T_c on the Gibbs free energy G of L-04 at 0.76kbar. Empty circles represent the melting temperatures at $T_c < T_{cr}$, while squares are for $T_c > T_{cr}$. Shaded circle represents the melting temperature at T_{cr}. G_{ci} and G_{Mi} are the free energies obtained at the crystallization temperature T_{ci}, where $T_{c1}<T_{c2}<T_{c3}<\ldots$etc. G_L was assumed to be invariant with temperature.

Based on the $\Delta G_c = \Delta G_M$ assumption, **equation (5.1.1)** for ethylene-octene copolymers at low supercoolings can be rewritten as,

$$T = \frac{\Delta H_{f,M} - \Delta H_{f,c}}{\Delta S_M - \Delta S_c} \tag{5.1.3}$$

Sanchez and Eby [5] have derived the bulk free energy of fusion for random copolymers. They suggested that when the actual concentration of comonomer units in the crystalline phase reaches zero, i.e. exclusion model, the bulk free energy could be written as:

$$\Delta G = \Delta G^o + RT \ln(1 - X) \tag{5.1.4}$$

where ΔG^o is the bulk free energy difference of the homopolymer, and 'X' is the overall composition. On the other hand, for the uniform inclusion model the bulk free energy becomes:

$$\Delta G = \Delta G^o - \varepsilon X \tag{5.1.5}$$

where ε is the excess free energy of the defect created by the incorporation of the comonomer units into the crystalline phase.

Assuming a total exclusion of the hexyl branches in the orthorhombic phase, **equation (5.1.4)** can be substituted for the free energy difference ΔG_c. Similarly **equation (5.1.5)** can be used for the monoclinic phase, where a total inclusion of defects is expected. Accordingly, at $\Delta G_c = \Delta G_M$ condition:

$$\Delta G_c^o + RT\ln(1-X) = \Delta G_M^o - \varepsilon X \qquad (5.1.6)$$

where $\Delta G^o \cong \Delta H_f^o(1-T/T_m^o)$.

At very large temperatures and pressures (e.g. >200 °C, ≥3kbar), using the same methodology, it is expected that the drop in heat of fusion due to the increased solubility, and the increasing entropy will additionally decrease the total ΔGc value so that $\Delta G_c < \Delta G_M$. In consequence, the mobile hexagonal phase is expected to form in its most stable phase as was reported in literature [15,83,90], and the melting temperatures of both phases diverges significantly.

According to the above thermodynamics, At $T_c<T_{cr}$ both temperatures (T_{tr} and $T_{m,M}$) increase with T_c, while the difference between them decreases. This can be seen from the closing gap between the two empty circles in the figure. At $T_c>T_{cr}$, T_{tr} stabilizes while $T_{m,M}$ increases more rapidly, as can be observed from the diverging distance between the squares. Consequently, the L-04 melting behavior at pressures ≥ 0.76kbar should follow the pattern of **figure (5.1.19)**. On the other hand, at high supercoolings ($T_c < T_{cr}$) **figure**

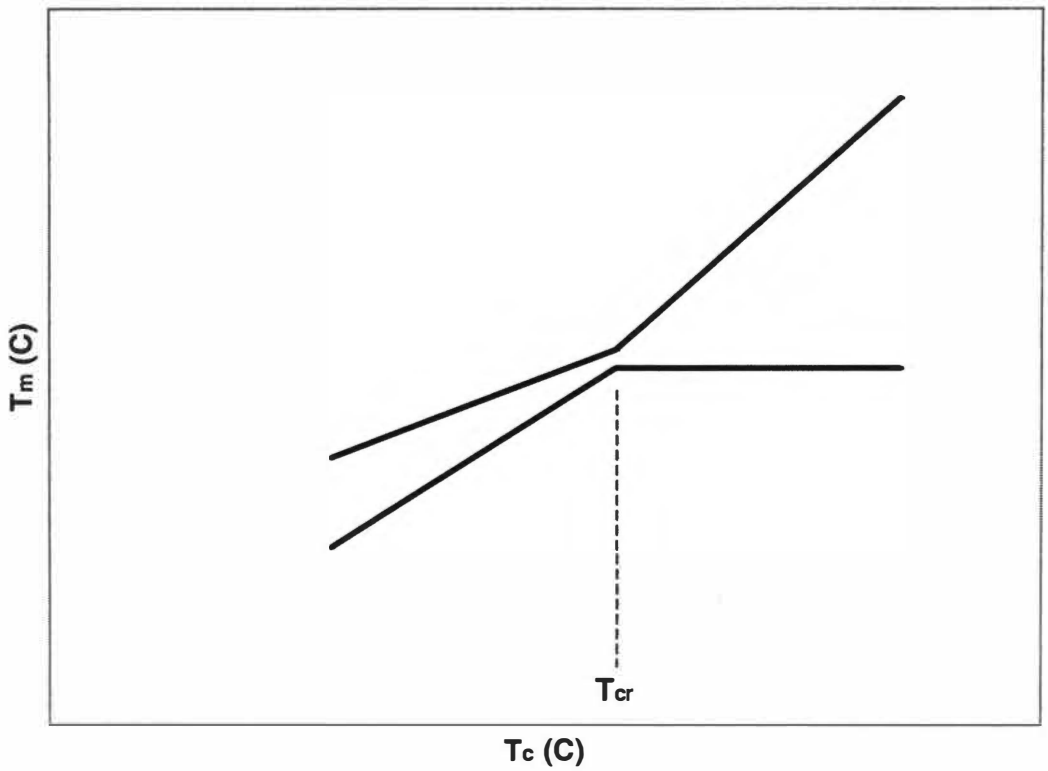


Figure (5.1.19) A schematic plot of T_m versus T_c at 0.76kbar using the thermodynamically predicted melting temperatures of figure (5.1.16).

(5.1.2a) shows a decreasing value of the higher melting temperatures as crystallization temperature increases. The discrepancy is believed to be a result of the superheating effect.

The fast growth rates of this temperature region produce more amorphousity in the material. Upon heating, the disappearance (i.e melting) or transformation of the less perfected orthorhombic crystals to monoclinic crystals provides a better environment for the latter to continue its growth, where the increased solubility of the hexyl branches with temperature tends to form thicker lamellae. The presence of pressure will expedite the thickening process due to the increasing conformational entropy of the system. The effect weakens at larger crystallization temperatures, due to the increasing melting temperatures of the orthorhombic phase.

L-11 copolymer

Thermodynamics used to describe the melting behavior of L-04 copolymer can also be used to interpret the results of L-11. The introduction of 11 hexyl branches to the system shifts the crystalline free energy G_c to larger values where the monoclinic phase can be revealed as described by **figure (5.1.15)**, even without applying pressure. Accordingly, the methodology used to describe L-04 at pressures ≥0.76 can be employed to L-11 copolymer crystallized at larger pressures. At atmospheric pressure, similar argument could be used for $T<T_{cr}$. In this temperature region the $\Delta G_c > \Delta G_M$ relation is responsible for the increase in both T_{tr} and $T_{m,\,M}$ values as T_c increases. The amount of

increase in T_{tr} is larger than that of $T_{m,\,M}$ (empty circles), which causes the converging behavior at larger temperatures. **Figure (5.1.20)** represents this behavior (broken bold lines), and agrees with the experimental data of **figure (5.1.4)**.

At $T=T_{cr}$ all free energies intersect with each other, where theoretically a single melting temperature is observed. At $T > T_{cr}$, the slow growth rates, and possibly the change in the crystallization mechanism, increase the amount of drop in G_M value or decrease the amount of drop in G_c, i.e. either ΔG_M increases or ΔG_c decreases. However, due to the absence of external pressure, the amount of increase in ΔG_M value does not correspond to the drop in ΔG_c. In other words, ΔG_c is stays slightly higher than ΔG_M. Accordingly $T_{m,\,M}$ increases more rapidly than T_{tr} as illustrated in **figure (5.1.20)** (squared symbols), and T_{tr} does not level off. The experimental results of **figure (5.1.4)** show that unlike L-04, $T_{cr} \neq T_{II\text{-}III}$ for L-11 crystallized at atmospheric pressure. The critical temperature in this case is smaller than that of the regime II-III transition. However, the extensively high melting temperature does not appear until $T_c > T_{II\text{-}III}$. The effect of superheating at high supercoolings can still be observed in L-11 at elevated pressures, but not at atmospheric pressure.

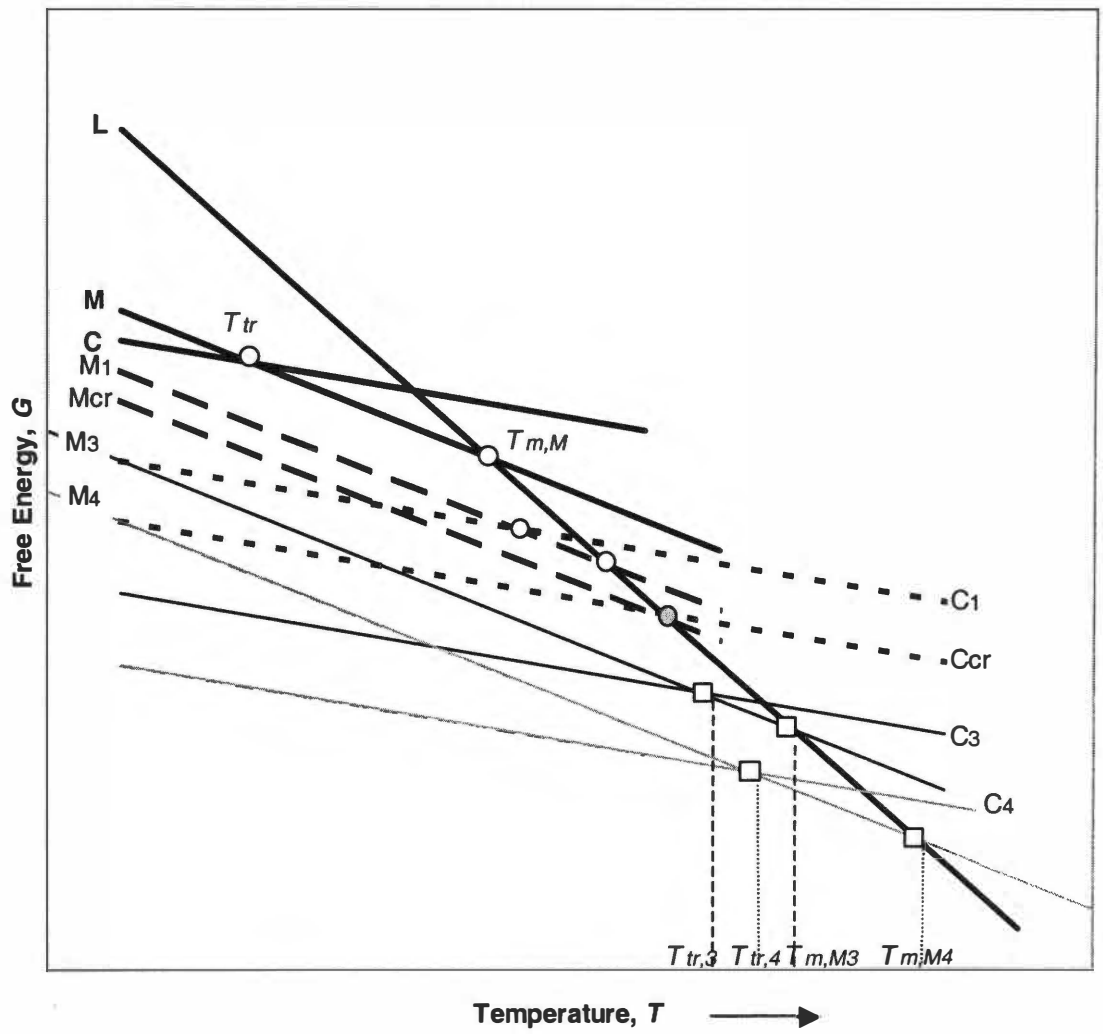


Figure (5.1.20) A schematic diagram of the expected effect of T_c on the Gibbs free energy G of L-11 at 1 atm. Empty circles represent the melting temperatures $T_c < T_{cr}$, while squares are for $T_c > T_{cr}$. Shaded circle represents the melting temperature at T_{cr}.

5.2 Morphological Studies

5.2.1 WAXD

Wide-angle x-ray diffraction patterns taken at atmospheric pressure and room temperature did not show any clear evidence of structural changes in the material, regardless of the crystallization conditions. The appearance of only the known orthorhombic diffraction peaks for L-04 and L-11 copolymers indicated that the meta-stable monoclinic phase has transformed to orthorhombic phase at room conditions, as was suggested by the eutectoid-like transformation model.

WAXD patterns taken at atmospheric pressure and as a function of temperature have not shown any significantly clear sign of the formation of another phase (hexagonal or monoclinic) beside the orthorhombic phase. The linear lattice expansion in the a-axis direction departs from its linearity at higher temperatures, and the expansion rate becomes larger as shown in **figures (4.2.7-9)**. Similar behavior was reported in literature for the lattice parameters '*a*' and '*c*' of the hexagonal intermetallic phase γ–Co_3Sn_2 [91]. The linear relationship observed for temperatures up to 800 °C was attributed to the thermal expansion of the phase. However, the deviation from linearity observed between 800 °C to 1050 °C was attributed to the change of solubility of the phase with temperature, as this phase was in a $Co_{75}Sn_{25}$ two-phase alloy. Similar attributions could be used in describing the behavior of ethylene-octene copolymers observed in **figures (4.2.7-9)**. As temperature increases the solubility of the hexyl branches into the

crystalline phase increases. The inclusion of branches lowers the latent heat of fusion and speeds up the melting process as seen at higher temperatures.

Davis *et. al.* [92] have studied the unit cell dimension of linear PE (1.4 CH_3 /1000 C atom) as a function of temperature. They reported a much smaller change in the b-axis compared to the a-axis. In addition, they found that the change in the '*a*' dimension as a function of temperature was not linear, where the expanding rate has increased at higher temperatures. Based on their results they suggested that the dominant parameter in determining the unit cell dimension for LPE at a given temperature is the length of the molecular stems between folds rather than the interaction of the molecules at the surface of the crystals or the presence of crystal defects.

Another interpretation of the above results could be the increased effect of the side-chains on the orthorhombic crystalline phase as was suggested by Androsch [93]. By studying the melting and crystallization of poly(ethylene-*co*-octene) material using modulated DSC and temperature-resolved x-ray diffraction Androsch concluded that the crystallization process starts with the formation of a crystalline phase followed by the perfection of the grown crystallites and the development of a meso-phase depending on the temperature. The two-phase model does not mirror the real structure within a semi-crystalline polymer, and that the disordered pseudo-hexagonal phase with a lateral long range order can exist.

The change in the solubility parameter at high temperatures can be explained using **figure (5.1.12)**. According to the suggested eutectoid-like transformation and SEM pictures, the stacked lamellar structure consists of thin lamellae that are packed close to each other and separated by a thin amorphous layer. On melting, the external thermal energy increases the vibrational motion of the molecular chains, and causes the lattice dimension to expand. Due to the packed lamellar structure, hexyl branches trapped in the thin amorphous layer will try to accommodate itself in the bordering crystalline phase. Once an appropriate lattice expansion is reached, hexyl branches will dissolve in the crystalline phase. However, in a high temperature environment the inclusion of branches will weaken the crystalline structure and speed up the melting.

Using the upper explanation, a general outlook to the crystallization process could be summarized as follow: orthorhombic phase has low solubility parameter that prohibits the inclusion of any defect into its crystalline phase. Elevated pressures and temperatures, however, increase the solubility parameter of the hexyl groups. To accommodate the hexyl branches into the crystalline phase, the crystallization process should occur in the meta-stable monoclinic phase where more hexyl branches can be dissolved. As a result thicker lamellar structure is formed. On removal of pressure and temperature the thick high hexyl content monoclinic crystals will transform to a thinner low hexyl content orthorhombic crystals, The transformation is akin to a eutectoid transformation as discussed earlier.

5.2.2 Interfacial Layer Thickness

Studying the existence of a third phase in the semi-crystalline polymers should not be ignored specially when the measuring of equilibrium melting temperature is of interest. SAXS intensity patterns were used for this purpose as explained in **section 4.2.3.1**. The effects of: background correction, methods used, and the crystallization temperatures and pressures on the interfacial layer thickness of quenched samples are studied in this section.

The values of the interfacial layer thickness measured using the linear-, sigmoidal-gradient model, and the 1-D correlation function methods are illustrated in **figures (5.2.1a-d)**. All numerical values demonstrated an underestimation of the interfacial layer thickness when the background effect was not corrected, except for the ones obtained by the linear model where no significant changes were observed. Unfortunately, the interference between the numerical values for all methods and conditions used does not allow us to draw a clear boarder that can characterize each behavior. For example, the atmospheric pressure there is a reasonable agreement between the interfacial layer thickness values obtained using the non-corrected linear, sigmoidal, 1-DCF, and the corrected linear model. The average value of 'Δ' calculated by the previous methods was about 26.43 Å. There is no clear dependency on the crystallization temperature. The corrected data, on the other hand, produced relatively close values with an average of 38.90 Å for both sigmoidal model and 1-DCF.

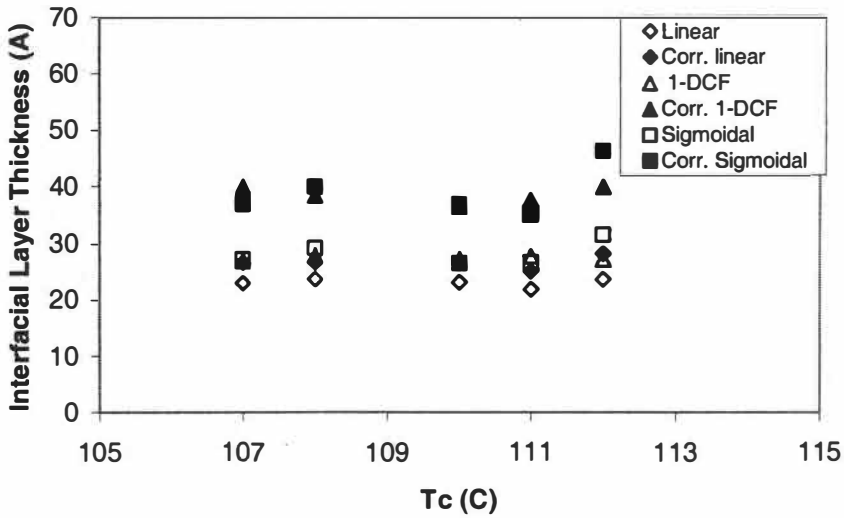


Figure (5.2.1) A plot of the interfacial layer thickness (E, Δ) versus T_c for L-04 copolymer crystallized at, a) atmospheric pressure.

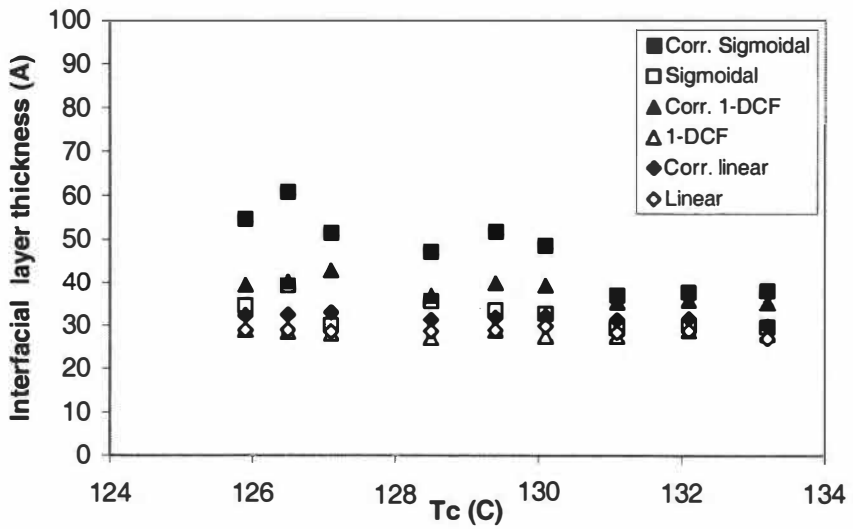


Figure (5.2.1) Continued, b) at 0.48kbar.

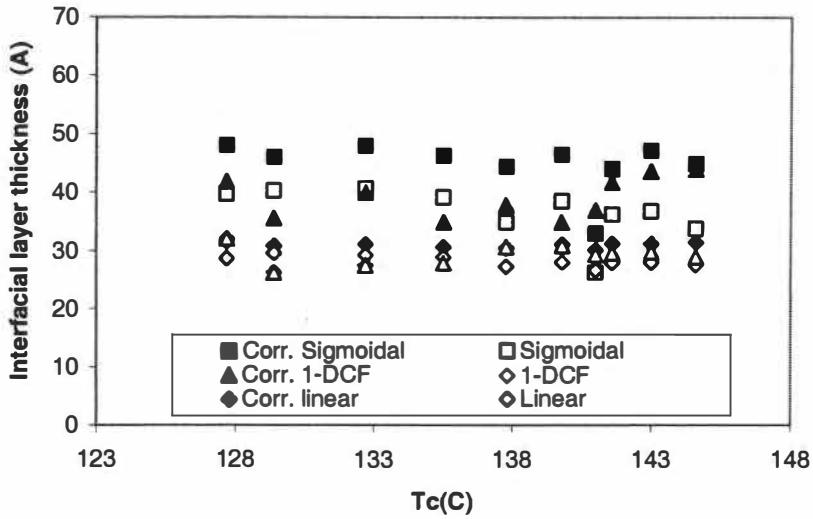


Figure (5.2.1) Continued, c) at 0.76kbar.

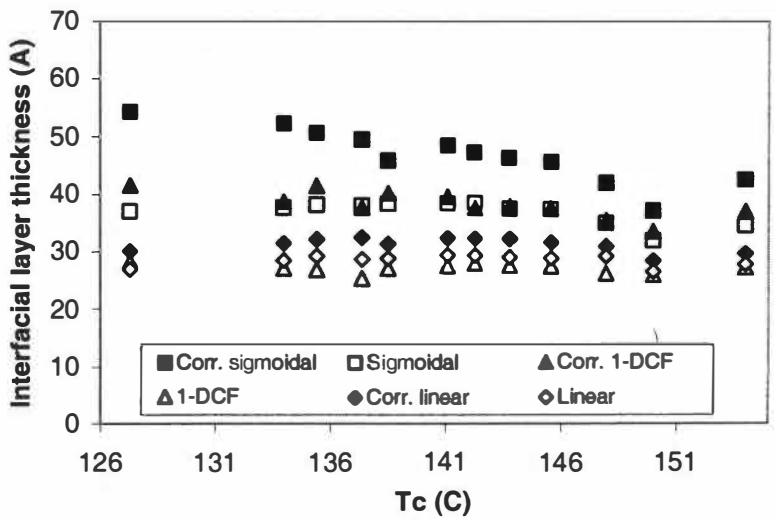


Figure (5.2.1) Continued, d) at 1.24kbar.

Another example is the P =1.24kbar set shown in **figure (5.2.1d)**. The data could be divided into three groups: the first group of data shows no temperature dependency and averages around 29 Å. Similarly, the second group of data does not depend on temperatures and averages around 37.5 Å, while the third group, resulted from the corrected data of the sigmoidal model, showed a clear dependency of the interfacial layer thickness on temperature. The decrease in the interfacial layer thickness, as a function of temperature, could be a result of the improved crystallinity of the system. In another words, the stacked lamellar structure has better packing. The increase in the lamellar thickness occurs on the expense of the trapped interfacial layer, causing its thickness to decrease. Similar behavior was observed clearly for samples crystallized at P =0.48kbar, but not for P =0.76kbar as shown in **figures (5.2.1b-c)** respectively.

To have a general view of the behavior of interfacial layer thickness, all collected data was assumed to be independent of the crystallization temperature, as is the case for most of the results. The average interfacial layer thickness is calculated and listed in **table (5.2.1)**. The values obtained by 1-D correlation function for both corrected and non-corrected interfacial layer thickness are independent of the pressure applied. The other two methods have shown a step increase in the interfacial layer thickness when pressure was raised from the atmospheric pressure to P =0.48kbar. Increasing the pressure beyond 0.48kbar did not affect the interfacial layer thickness. The independency of the interfacial layer thickness on both temperature and pressure agrees with the suggested eutectoid-like transformation theory. The expulsion of hexyl branches into the amorphous material is expected to be the same for all materials regardless of its original crystallization

Table (5.2.1) A comparison between the average interfacial layer thicknesses of L-04 obtained at different pressures. The data was assumed to be independent of the crystallization temperature.

Pressure (kbar)	Δ (Å) Sigmoidal Model		*E* (Å) Linear Model		*E* (Å) 1-DCF	
	Non-Corrected	Corrected	Non-Corrected	Corrected	Non-Corrected	Corrected
Atm	28.36±2.36	39.15±4.64	23.17±0.86	26.72±1.23	27.47±0.46	38.64±1.72
0.48	32.86±2.65	47.55±3.96	28.75±0.67	31.86±0.58	28.28±0.69	38.44±1.76
0.76	36.76±3.63	44.40±4.30	28.29±0.67	31.08±0.47	29.41±1.82	39.26±3.58
1.24	36.85±1.65	46.79±2.19	28.57±0.97	31.26±1.22	27.14±0.82	38.16±1.51

conditions. The maximum standard error obtained from averaging the data was 4.64 Å (i.e. 11.85%) and was obtained by the corrected sigmoidal model at atmospheric pressure. Because of the more credibility of the 1-D correlation function method, lamellar and interfacial layer thicknesses were obtained by this method.

5.2.3 Lamellar Thickness

Using the long period values obtained by SAXS and the degree of crystallinity determined by WAXD, the lamellar thickness was calculated and used to determine the equilibrium melting points. Four methods can be used to determine the lamellar thickness values using the original data, the Lorentz corrected data, and the 1-D correlation function. The latter method allows the calculation of the lamellar thickness in two ways: first by obtaining the long period which is represented by the position of the first peak, and second through the self-correction triangle which measures the number average lamellar thickness as illustrated in **section 2.2.3.1**.

The lamellar thickness obtained from the original and Lorentz corrected data always give larger values compared to the ones obtained by the 1-D correlation function. The reason behind this is the assumption of a sharp phase boundary between the amorphous and crystalline phases, while one dimensional correlation function considers an intermediate phase between the crystalline and amorphous phases. That latter assumption is more realistic and was used in this study.

As shown in **figures (4.2.11-14)**, the number-average lamellar thickness measured using self-correlation triangle is independent of the crystallization temperature. This is true for samples prepared at atmospheric or high pressures. The method used gives a constant lamellar thickness value of ~65Å regardless of the applied conditions. Interestingly this value is similar to what Strobl *et al* [94] have reported for poly(ethylene-*co*-octene) and poly(propene-*co*-octene) materials during both the crystallization and the subsequent heating processes. In their study the second derivative of the 1-D electron density auto correlation function $K''(z)$ described in **section 2.2.3.1** was used. The crystalline lamellar thickness (denoted d_c in **figure 2.2.3**) is equivalent to the lamellar thickness obtained by the self-correlation triangle as suggested by **figure (2.2.3)**. According to them, in the early stages of crystallization a critical thickness should be reached before a transition into higher ordered structure occurs. Once the transition occurs the formed layers solidify and thickening stops.

The constant value of the lamellar thickness obtained by Strobl, regardless of the copolymer or the branch content used, raised some doubts about the credibility of the method used. Obtaining the exact same value of the lamellar thickness in this study, and the fact that this value did not change with pressure or temperature, as shown in the previous figures, caused us to ignore this method in calculating the lamellar thickness. The results of this study do not agree with the idea that thickening process ceases beyond certain lamellar thickness during crystallization. However the occurrence of the eutectoid-like transformation and its effect on the final lamellar structure can explain some of the observations of Strobl, where the transformation of the extended-chain

crystals to stacked thin lamellae is responsible for producing constant lamellar structure, or the granular crystal layer suggested by Strobl.

When adding the value of the interfacial layer thickness (see **table 5.2.1**) to the 65Å constant value, one can obtain a total lamellar thickness of about 100Å. This value is consistent with the lamellar thickness values measured using SAXS technique. Based on the above it can be concluded that the constant lamellar thickness value obtained by the self-correction triangle represents the lamellar thickness of only the crystalline phase, while the value obtained from the first maximum of the 1-DCF includes the interfacial layer thickness.

Several objections were raised lately on Strobl's crystallization model [95,96]. Some objections dealt with the detection limits of the experimental technique [97]. Hsiao *et. al.* investigated the early stages of polymer melt crystallization using fractionated isotactic polypropylene (*i*PP) as a model system. Simultaneous synchrotron small-angle X-ray scattering (SAXS)/wide-angle X-ray diffraction (WAXD) and laser light scattering (LS) techniques were used. They conclude that WAXD technique is capable of detecting crystallinity from 0.5% to 1%. During the early stages of *i*PP isothermal crystallization, the spacing associated with SAXS peak did not increase with time, which is consistent with the formation of a finite lamellar structure. They also observed larger objects with dimensions growing from 300 nm using the more sensitive technique of polarized light scattering, prior to the detection of the lamellar period by SAXS.

Cheng *et. al.* [98] have argued that, in front of the growing crystal face there should be a thin adsorption layer instead of the independent mesomorphic phase suggested by Strobl. According to Cheng the latter failed to explain the transformation of the hexagonal mesophase, found in PE at elevated pressure, to the orthorhombic phase. The transformation according to Strobl's model will give rise to twinned symmetries, which never been reported in literature.

5.2.3.1 Gibbs-Thomson Equation

The determining of lamellar thickness using the ORNL 10m-SAXS is a very important step in this study. Normally, the knowledge of this parameter reveals a lot of information about the structural changes in the material, and most importantly allows the determination of the equilibrium melting point more accurately and with the least intervention of other variables.

The lamellar thickness determined from SAXS intensity profiles represent the average of the whole crystal thickness, including the thin lamellar thickness resulted from the quenching process. As a result, and unless a complete crystallization occurs, the average lamellar thickness measured will be less than the actual value due to the broad lamellar distribution. To avoid this problem, SAXS experiments must be run under the same crystallizing conditions. All SAXS experiments conducted by this study were run at room temperature and pressure. *In-situ* SAXS experiments at requisite pressure and

temperature are not available at any near location. This facility, as far as we know, is only available at ESRF, Grenoble on beam line ID11/BL2 in France.

The problem of underestimating the lamellar thickness persists also when very thick lamellae are produced. The melting behavior studied in **section 5.1.1** has confirmed the production of very thick lamellae. X-ray waves scattering at small angles is limited to a certain crystal size. Large lamellae, if retained on cooling, will allow x-rays to be transmitted without suffering any useful reflections. However, due to the eutectoid-like transformation the lamellar thickness measured at room conditions will always be incomparable with the melting points obtained at elevated pressures.

Two different approaches were reached in this section to understand the morphological changes of the copolymers used. In the first approach the lamellar thickness were obtained directly from the measured melting points using Gibbs-Thomson equation. The second approach used the lamellar thickness measured by SAXS and the melting points measured *in-situ* to construct the Gibbs-Thomson plots. The latter method although may not be accepted scientifically, has given a very good estimation of the equilibrium melting points of the orthorhombic structure as will be discussed later.

In the first approach, the heat of fusion and fold surface free energy obtained by Hoffman were used, and assumed to be constant at all conditions (ΔH_f=2.8X10^9 erg cm^{-3}, σ_e =90 erg cm^{-2}). Using the expected T_m^o value of the orthorhombic L-04 structure at

0.76kbar, an extensively large lamellar thickness is produced as shown in **figure (5.2.2)**. The unacceptable large lamellar thickness values are due to the underestimation of T_m^o value. Therefore, L-04 phase diagram (**figure 5.1.7**) should be used for better estimation. To include the monoclinic phase in our calculations T_m^o should be raised by an amount that is equivalent to the difference between the melting temperatures of orthorhombic and monoclinic phases. According to **figures (5.1.7-8)** the difference is about 5 °C. When adjusting for the difference (i.e. T_m^o=155.88 °C), more acceptable results are obtained as seen in **figure (5.2.3)**. The average thickness of the stacked thin lamellae measured from SEM pictures (squared symbol in the figure) is in agreement with its melting point. Values obtained by SAXS are in a reasonable agreement at lower crystallization temperatures but largely deviate at higher temperatures due to the formation of extended chain crystals. Similar argument can be used for L-04 copolymer crystallized at P=1.24kbar. **Figure (5.2.4)** shows the lamellar thickness values after correcting for T_m^o, where the difference in melting temperatures between the two phases was about 9 °C.

Based on the melting points of L-11 copolymer crystallized at atmospheric pressure, the very high melting temperatures were not observed until regime II transition was reached. However, the two melting peaks were observed even at low crystallization temperatures. In the absence of external pressure the main driving force for the

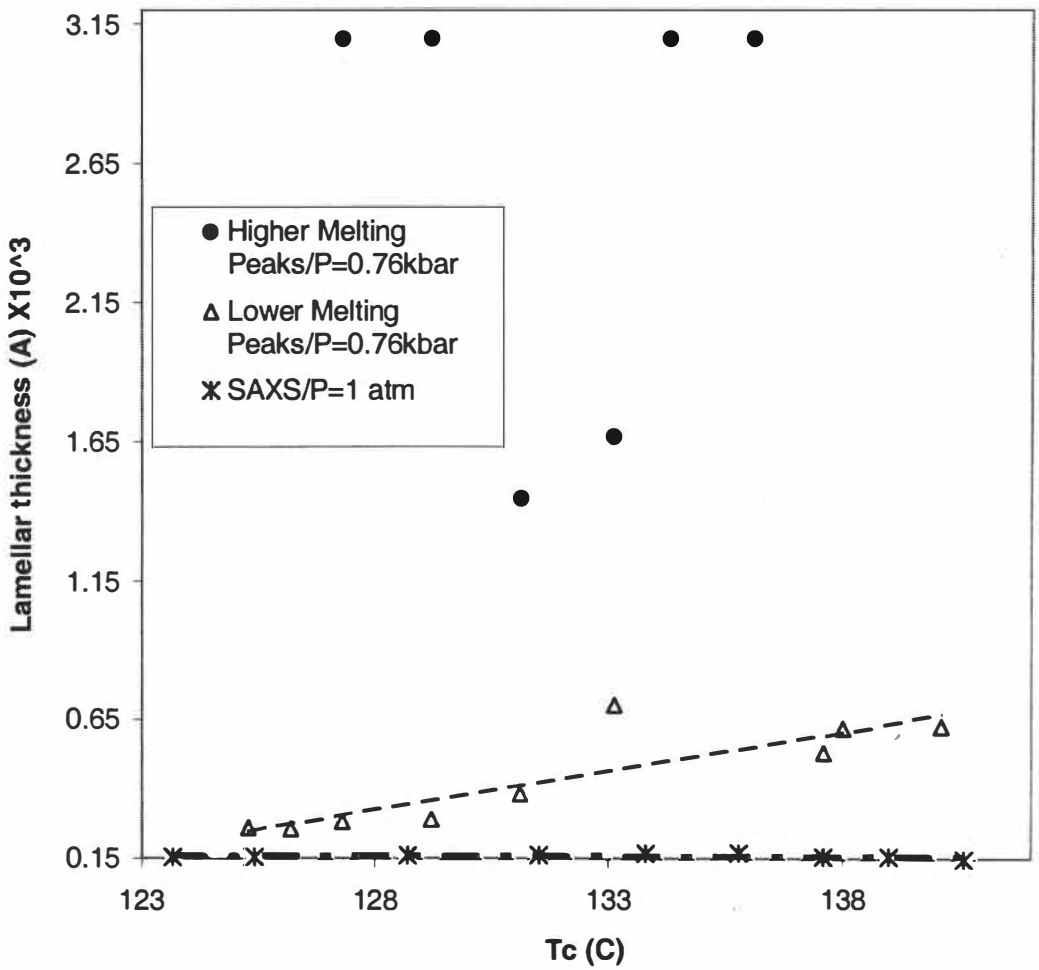


Figure (5.2.2) Comparison between the lamellar thickness of L-04 copolymer obtained at P=0.76kbar and 1 atm (T_m^o =150.88 °C).

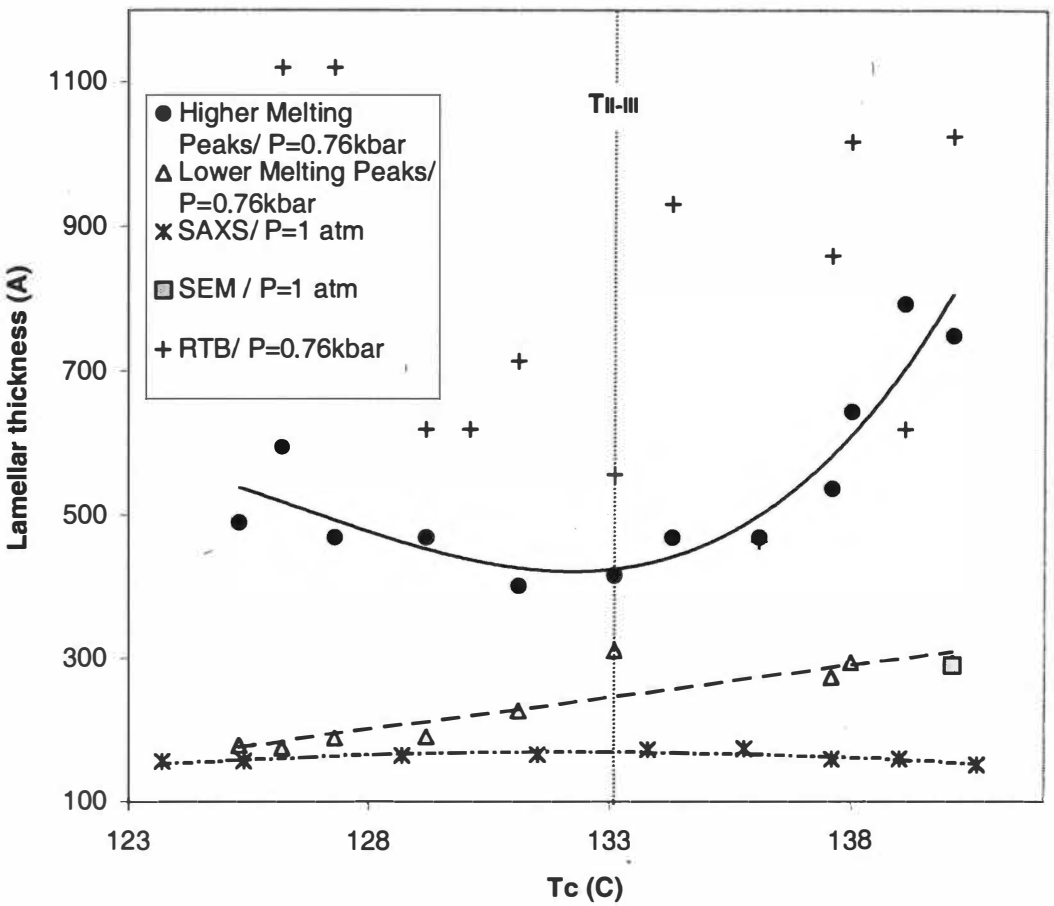


Figure (5.2.3) Comparison between the lamellar thickness of L-04 copolymer obtained at P=0.76kbar and 1 atm. (T_m^o=155.88 °C)

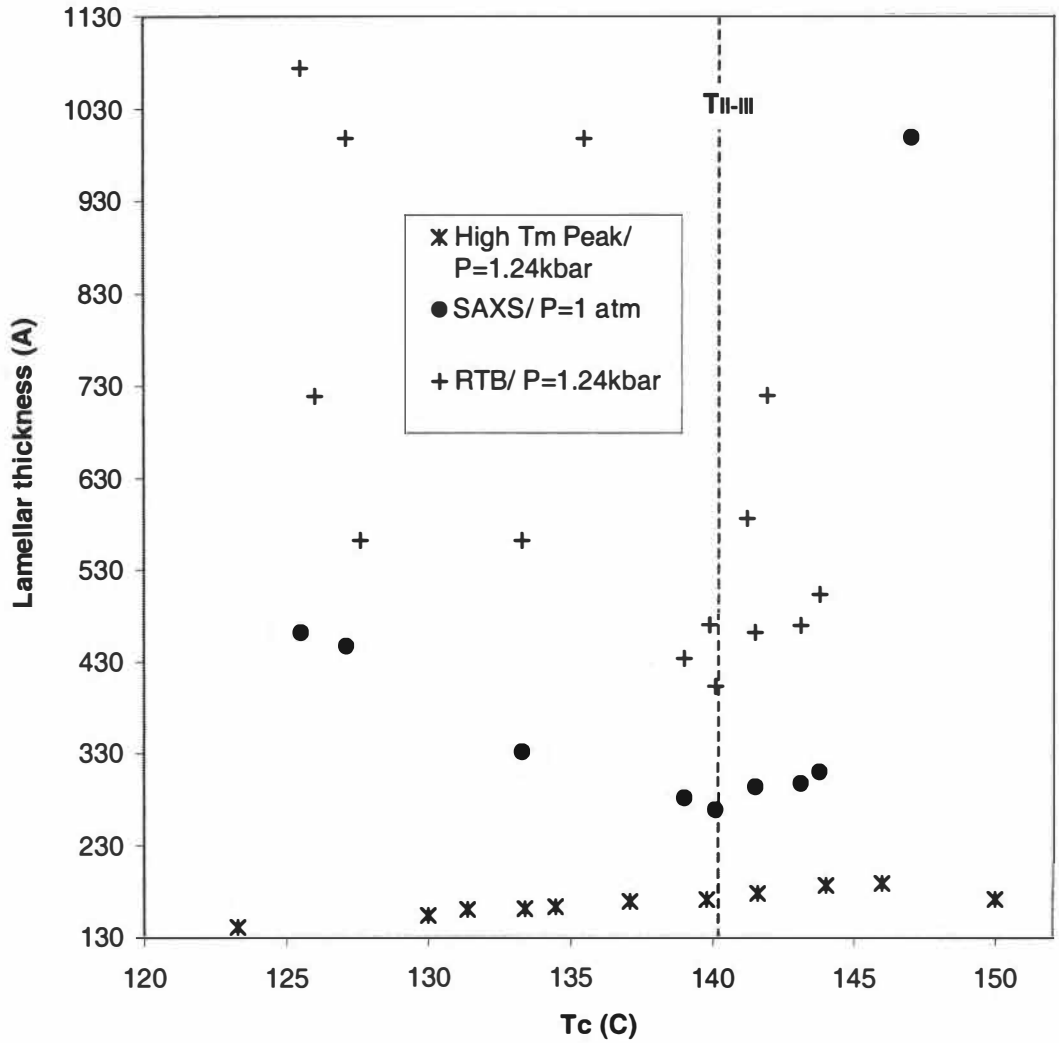


Figure (5.2.4) Comparison between the lamellar thickness of L-04 copolymer obtained at P=1.24kbar and 1 atm. (T_m^o =168.55 °C).

crystallization in the monoclinic phase is the molecular chain mobility that increases with temperature. This may justify the relatively small difference in lamellar thickness of the two phases in regime III region, i.e. $T_c \leq 114$ °C, as observed from **figure (5.2.5)**. The higher melting points represent a lamellar structure smaller than 100Å thickness. A value that is equivalent to the sequence length of L-11. The lamellar thickness of the stack and the individual lamella is in a very good agreement SAXS results. The SAXS results used in this figure were extrapolated from the actual values measured by Kim [68].

Using the second approach, Gibbs-Thomson plots of L-04 copolymer are represented in **figures (5.2.6-8)**. The lamellar thickness (l) obtained by the one-dimensional correlation function is equivalent to the summation of the crystalline lamellar thickness (l_c) and the interfacial layer thickness (l_{intf}). The melting temperatures used in these plots were measured *in-situ*, while the lamellar thickness were measured at room conditions. Crossed symbols in the figures represent the lamellar thicknesses and melting temperatures measured at room temperature.

Samples prepared at 1atm and 0.48kbar pressures followed the expected linear increase of melting temperatures as a function of lamellar thickness (**figure 5.2.6**). The T_m^o value of the atmospheric pressure data is 139.55 °C, in agreement with the 139.33 °C value obtained by Kim using the same method, and of reasonable agreement with the 137.96 °C obtained by Hoffman-Weeks plot (**figure 5.1.1**).

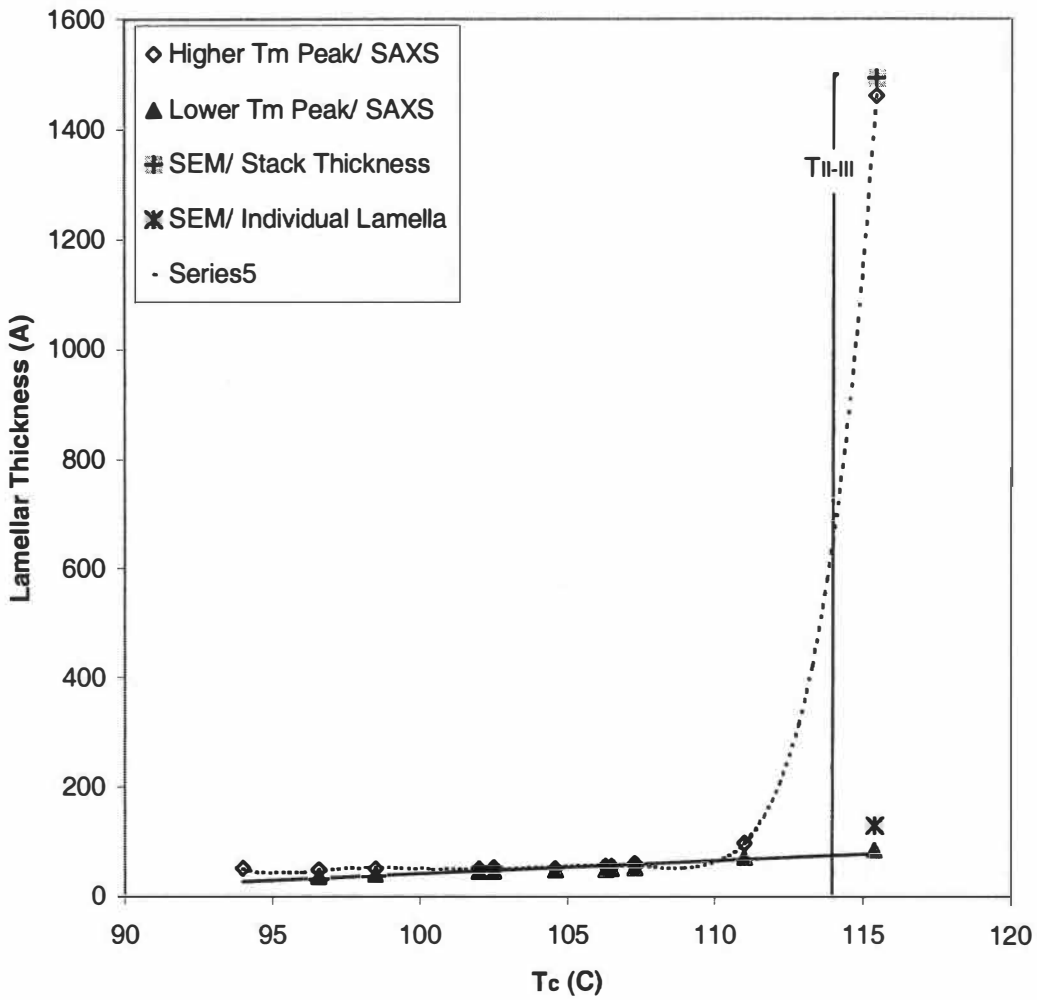


Figure (5.2.5) The lamellar thickness of L-11 copolymer crystallized at atmospheric pressure (T_m^o =134.5 °C).

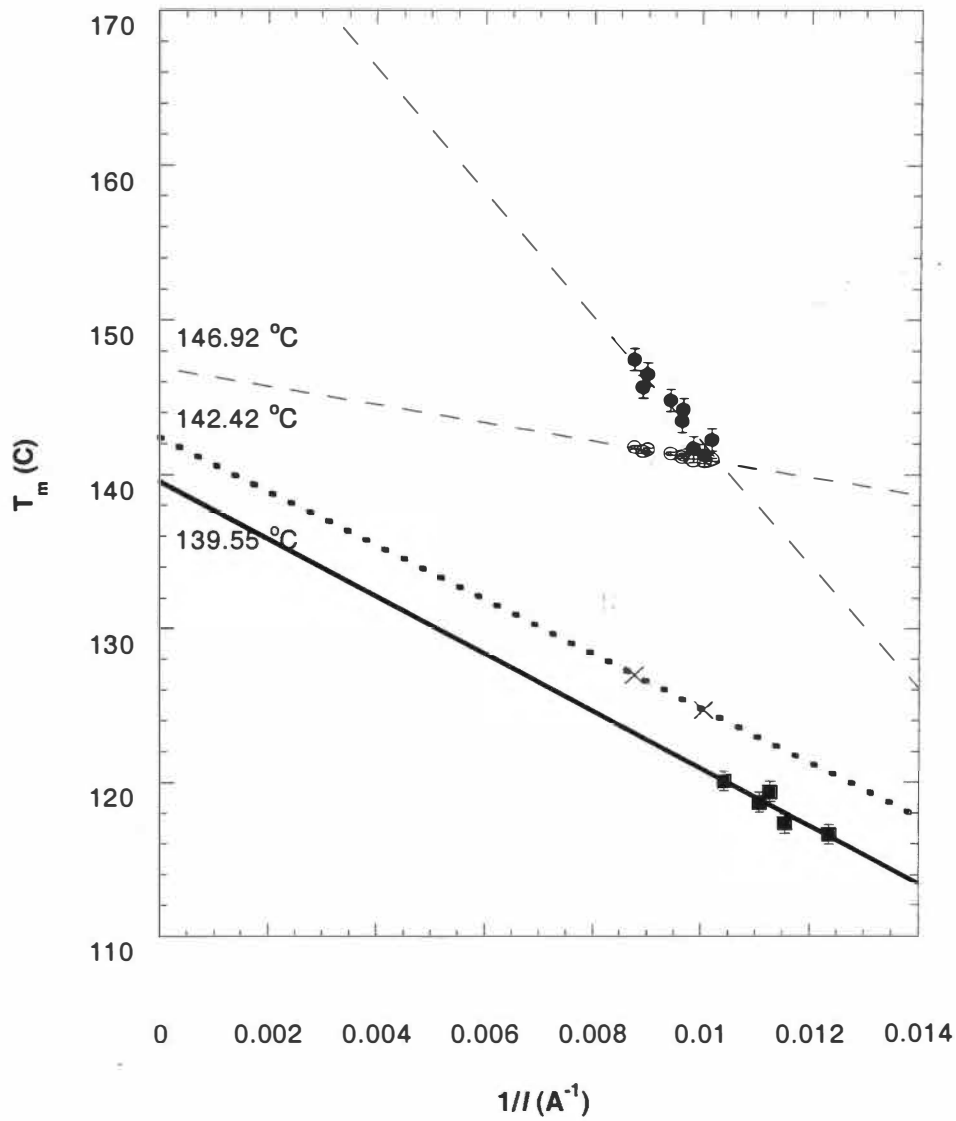


Figure (5.2.6) Gibbs-Thomson plot for L-04 copolymer crystallized at different pressures. Open and solid circles represent high and low supercoolings at 0.48kbar, respectively. (x) symbol represents the T_m values of P=0.48kbar obtained at atmospheric pressure. Squares represent the atmospheric pressure crystallization data.

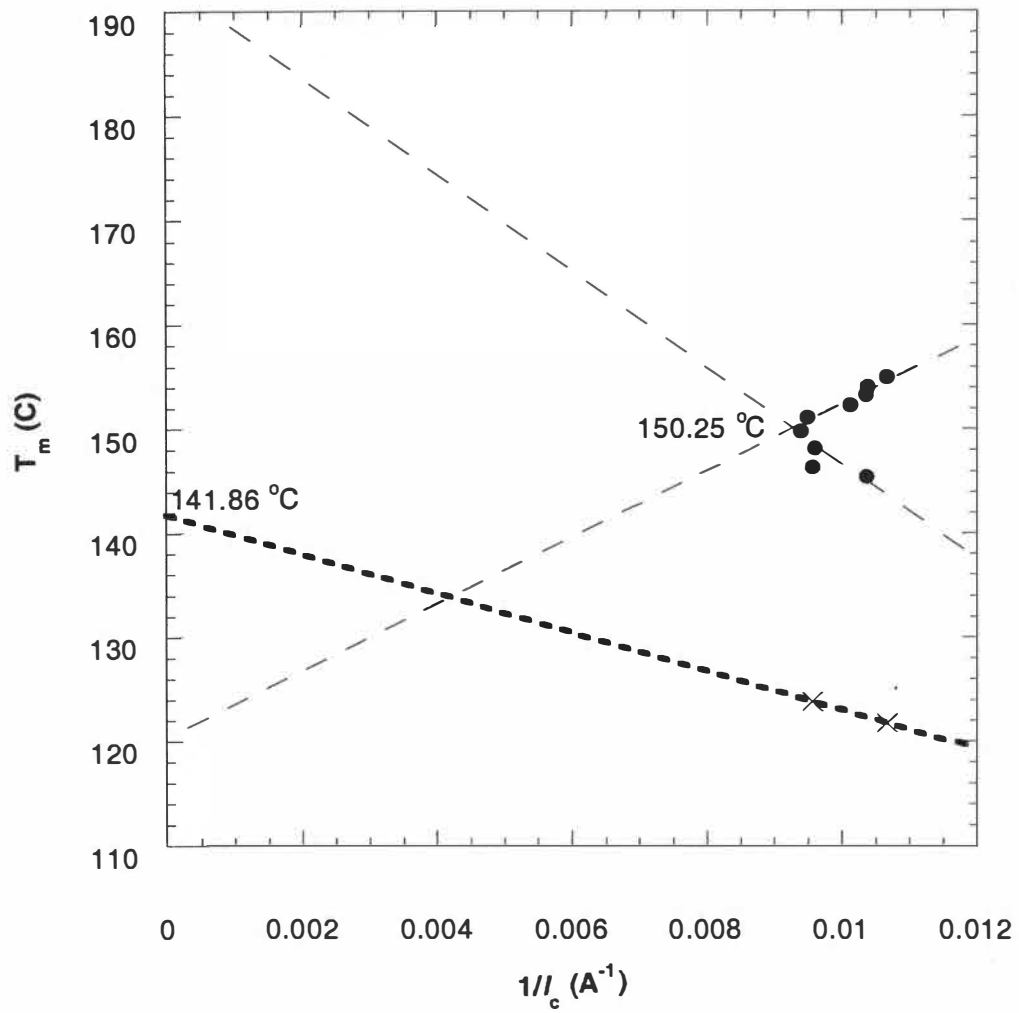


Figure (5.2.7) Gibbs-Thomson plot for L-04 copolymer crystallized at P=0.76kbar. (x) symbol represents the T_m values obtained at the atmospheric pressure.

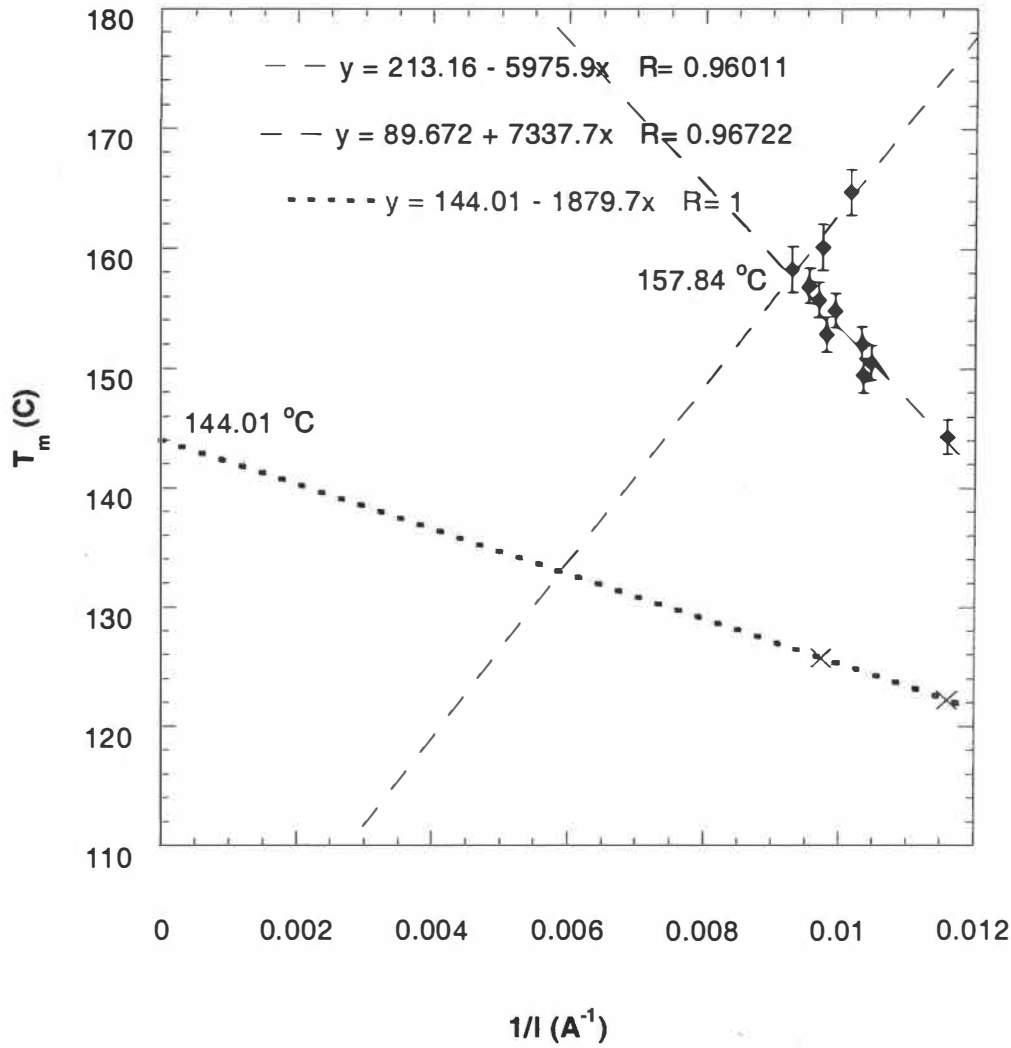


Figure (5.2.8) Gibbs-Thomson plot for L-04 copolymer crystallized at P=1.24kbar. (x) symbol represents the T_m values obtained at atmospheric pressure.

The equilibrium melting point for samples crystallized at 0.48kbar can be obtained by using either the high or low supercooling temperatures. The former gives a value of 146.92 °C, which is higher than the 143.3 °C obtained by Hoffman-Weeks method, but matches the expected T_m^o of the orthorhombic structure. The change in T_m^o value as a function of pressure dT_m/dP =15.35 °C/kbar. On the other hand, using low supercooling temperatures gives a very large value of 182.41 °C. With a careful look to **figure (5.2.6)** one can notice that the line slope of the large supercooling temperatures (dashed line), although gives the expected T_m^o value of the orthorhombic phase, is very low compared to that of the low supercoolings. The melting temperatures do not increase significantly with the lamellar thickness and are very close to the equilibrium melting temperature of the orthorhombic phase. This clearly suggests that the formed crystals have a lamellar thickness that is comparable to the infinite lamellar thickness of the orthorhombic phase. In other words the melting behavior of L-04 copolymer at 0.48kbar affirms the formation of extended-chain crystals.

At larger pressures the change in the behavior of Gibbs-Thomson plots is affected by the formation of the second phase (i.e. monoclinic) during crystallization. According to **figures (5.2.7-8)**, samples crystallized at high supercoolings followed the linear behavior, where melting temperatures increased with lamellar thickness. Once a certain lamellar thickness is reached the thickening process appears to stop and thinner lamellae start to form even when melting temperatures continue to increase. The reason behind the underestimation of the lamellar thickness obtained by SAXS was discussed earlier.

The change in slope occurred at lamellar thickness values that correspond to T_c=136.31 °C for P = 0.76kbar, and T_c =144.96 °C for P = 1.24kbar. The transition temperatures obtained from Hoffman-Weeks plot were 133.2 °C at P = 0.76kbar and 141.3 °C at P = 1.24kbar, a difference of about 3-3.5 °C from the Gibbs-Thomson results. This relatively small difference may be due to the different techniques, and the mathematical conversions used. It could also be due to the instrumental limitations of the SAXS machine to detect large lamellae. Accordingly, the temperatures obtained from Gibbs-Thomson plots reflect the domination of the extended-chain crystals.

The determination of equilibrium melting point for high-pressure samples is not a straightforward method. As shown in the figures extrapolating the points of the high supercoolings to infinite lamellar thickness gave an unacceptably high value for both pressures. In contrary, low supercooling points produced very low equilibrium melting points. However, the intersection of both extrapolated lines gave a value of 150.25 °C and 157.84 °C for 0.76 and 1.24kbar, respectively. Both values represent the expected equilibrium melting points of orthorhombic crystal at the designated pressures. **Table (5.2.2)** summarizes the T_m^o values of the orthorhombic phase determined from the above Gibbs-Thomson plots at different pressures. The values will be employed in the kinetics analyses.

According to **figures (5.2.7-8)**, the change in slopes corresponds to a lamellar thickness value of 107.19Å and 107.64Å for P = 0.76 and 1.24kbar, respectively. The sequence length of L-04, assuming uniform branch distribution, is estimated to be around

Table (5.2.2) A Summary of the different parameters determined for L-04 copolymer at different pressures.

Pressure (kbar)	T_m^o(C)	Regime	$\sigma\sigma_e$ (erg^2.cm^{-4}) [a]	σ_e (erg.cm^{-2}) [a]	$\sigma_e/\Delta H_f$ (Å) [b]	$T_{I\text{-}II}$ (°C)	$T_{II\text{-}III}$ (°C)	l_{tr} (Å)
0.001 (atm)	139.55	I	1229.08	104.16	6.67	113.5	119.5	-
		II	355.53	30.13				
		III	1565.68	132.68				
0.48	146.92	I	1376.57	116.66	11.02	126.22	128.27	-
		II	282.09	23.91				
		III	1534.89	130.08				
0.76	150.25	I	831.16	70.44	11.98	133.07	136.93	107.19
		II	93.25	7.90				
		III	812.26	68.84				
1.24	157.84	I	465.29	39.43	14.27	140.36	143.37	107.64
		II	91.40	7.75				
		III	446.51	37.84				

a) Determined using regime plot analysis (σ=11.8 erg.cm^{-2}).
b) Determined using Gibbs-Thomson equation.

320Å, and corresponds to the formation of three chain-folded stems. The calculations assumed complete exclusion of the comonomer units from the crystal. The number of stems is similar for both pressures, and resembles the number of stems in the critical nucleus found using Andrews' equation for *cis*-poly-isoprene [48], cross-linked LPE [99], and L-04 copolymer [100]. The approach assumes that the critical nucleus size does not change in a copolymer if the comonomer units were excluded from the crystal.

According to the above, the increase in melting temperatures (represented by the filled triangles in **figure 5.1.2a**) reflects the lamellar thickening of the orthorhombic folded-chain crystals. At the transition point the lamellar structure reaches its maximum thickness. Once the stem ends reach the comonomer unit (defect point), the built up energy barrier becomes very high where no more thickening is allowed before overcoming the barrier. The fixed lamellar thickness explains the leveling off of the melting points shown in the figure. The empty symbols represents the ECC that grows in the monoclinic phase, in accordance with Rastogi *et. al.*

Similar approach could be applied to **figures (5.1.4a-c)**. However, the discrepancy that appears at the higher temperatures of **figure (5.1.4a)** is believed to be a result of the absence of the external pressure.

In conclusion, Gibbs-Thomson equation cannot be used to determine the equilibrium melting point accurately in a two-phased system, since the free surface

energy and the heat of fusion of each phase are expected to be different and should not be ignored.

5.3 Crystallization Kinetics

The dependence of linear growth rate, *G*, on the crystallization temperature for L-04 copolymer at different pressures was illustrated in **figure (4.1.2)**. A plot of the growth rate logarithm against crystallization temperature and supercooling is shown in **figures (5.3.1-2)**. All curves tend to merge to a single curve at larger supercooling temperatures. Since equilibrium melting point is dependent on the applied pressure, it was necessary to plot the logarithm of the linear growth rate as a function of supercooling to ensure a fixed reference for all conditions used. The equilibrium melting points used are those of the orthorhombic phase as discussed previously.

The merging behavior of L-04 copolymer was reported earlier in literature [90]. It was found that for the lowest crystallization temperature the spherulite growth rates of all used copolymers have merged with the growth rate curve of the linear polyethylene. The effect of molecular weight and branch content, and apparently the elevated pressures, cease at higher supercoolings.

Using secondary nucleation theory (**equations 2.3.1-2**), the crystallization regime plots were established and shown in **figure (5.3.3)**. The activation energy U^* =1500 cal/mol and $T_\infty = T_g$-30 °C were used in this study. The glass transition temperature used

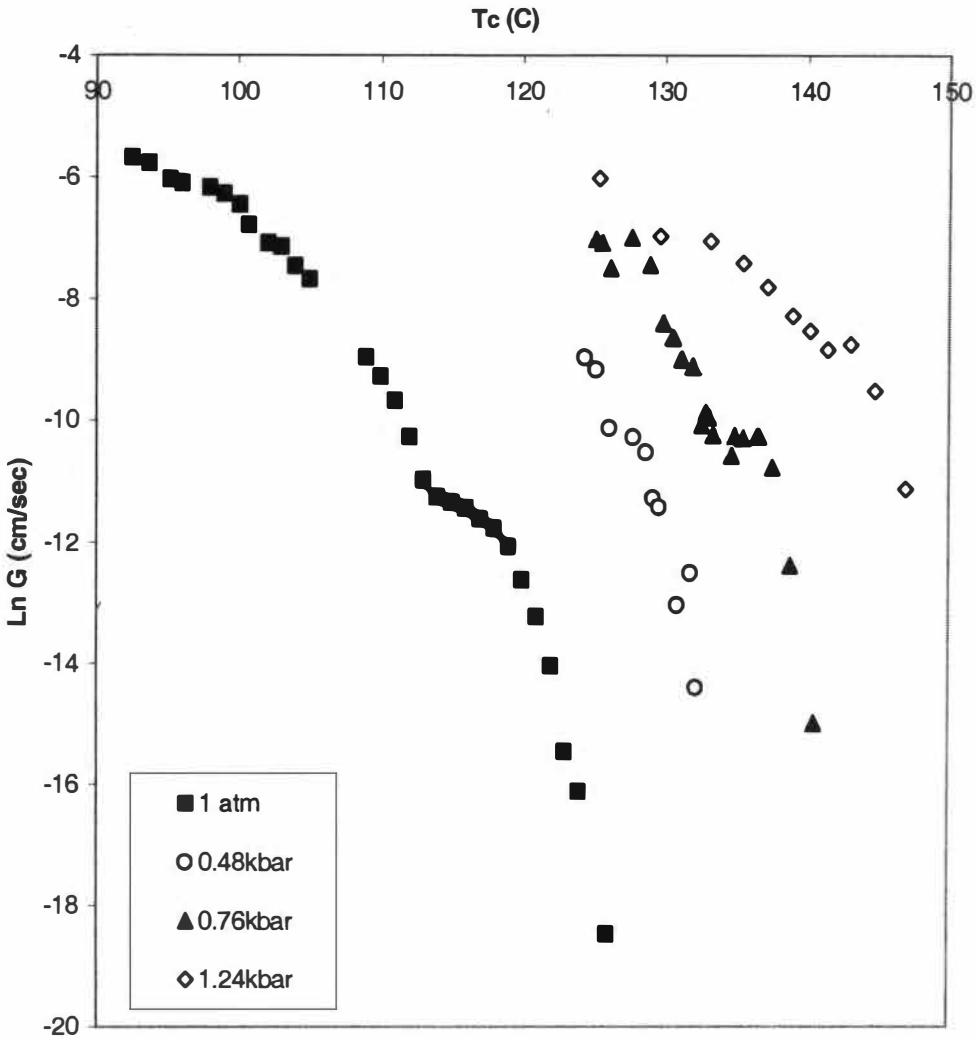


Figure (5.3.1) Logarithm of linear growth rate versus crystallization temperature for L-04 copolymer at different pressures.

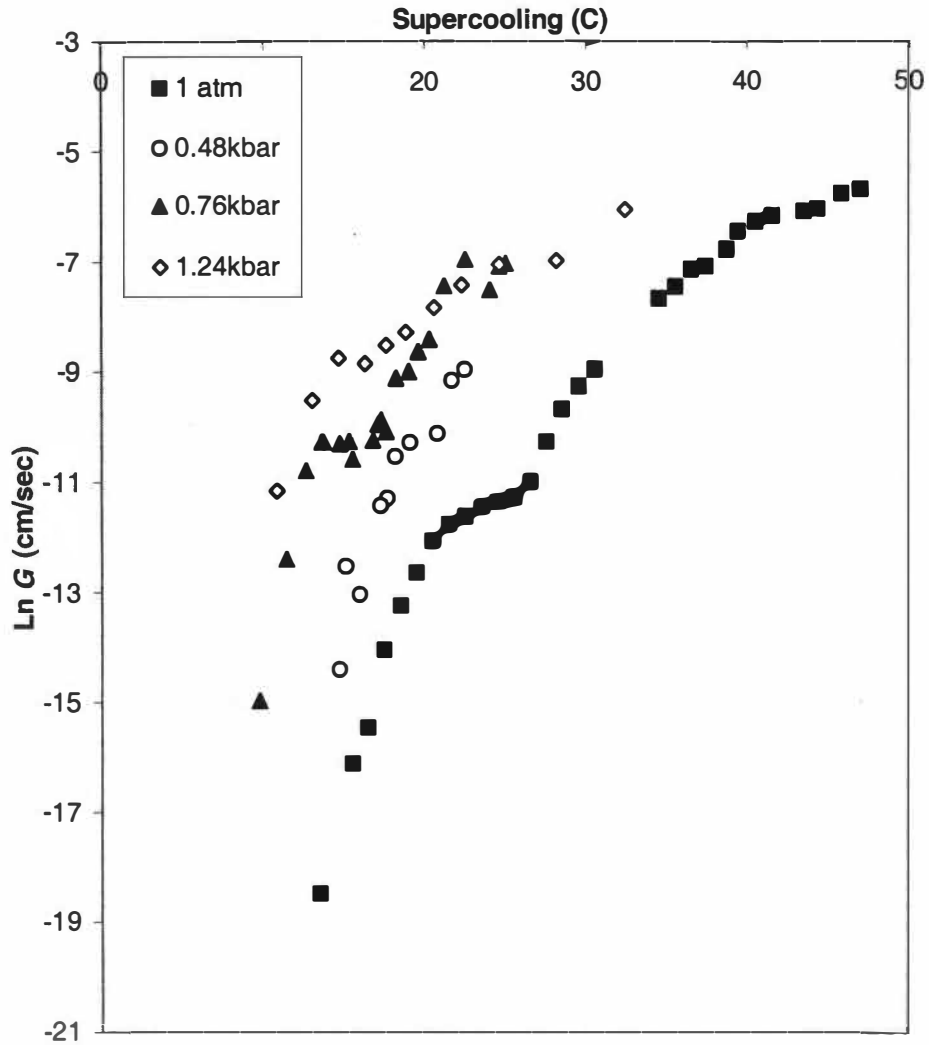


Figure (5.3.2) Logarithm of linear growth rate versus supercooling temperatures for L-04 copolymer at different pressures.

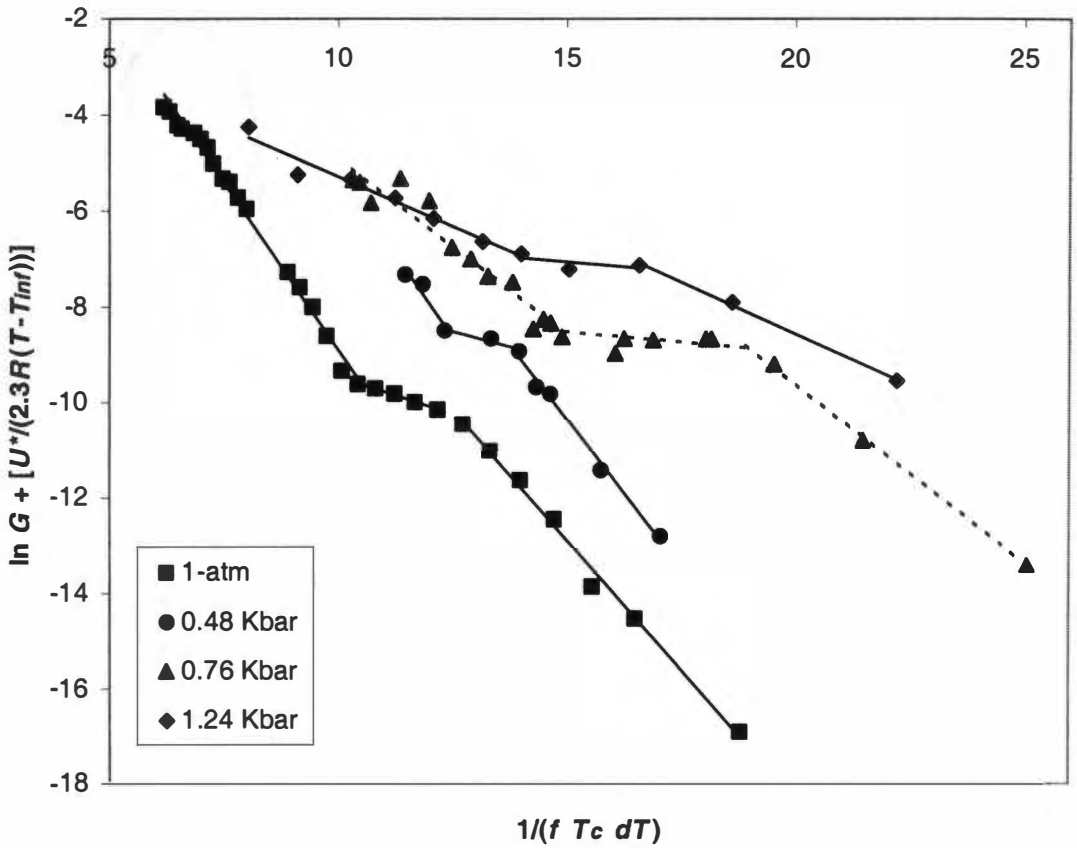


Figure (5.3.3) The regime plot of L-04 copolymer as a function of pressure.

in this work was –55 °C at atmospheric pressure. The effect of pressure on T_g value was assumed to be similar to that of the melting temperatures, where T_g is assumed to increase about 20 °C/kbar. Tseng [8] and Mezghani [70] have shown that for an ideal growth system changing T_g value largely will move the curve very slightly in the y-axis direction without any influence on the slopes, i.e. the fold surface free energy values σ_e does not change as shown in **figure (5.3.4)**. Similar effect can also be observed when using different U^* values as shown in **figure (5.3.5)**. The real effect of pressure on the T_g and U^* parameters was not considered in this report, due to the difficulties accompanying such task and their negligible effect on the regime plot.

Regime plots, on the other hand, are very sensitive to the equilibrium melting temperature and it must be determined very carefully. Any variation in T_m^o changes the slopes very significantly although it does not alter the regime transition temperature. As mentioned earlier, the formation of very thick lamellae beside the known orthorhombic crystals impedes any attempt to correctly obtain T_m^o values of the whole system. The estimated T_m^o values of the orthorhombic crystals were used in the regime plot construction since the linear growth rate was only measured for the fastest growth rate of the orthorhombic spherulitic structure.

The crystallization of L-04 copolymer occurs over a wide range of temperatures allowing for the three regimes to appear. This peculiarity persists at elevated pressures, producing very useful information about the crystallization kinetics of L-04 copolymer.

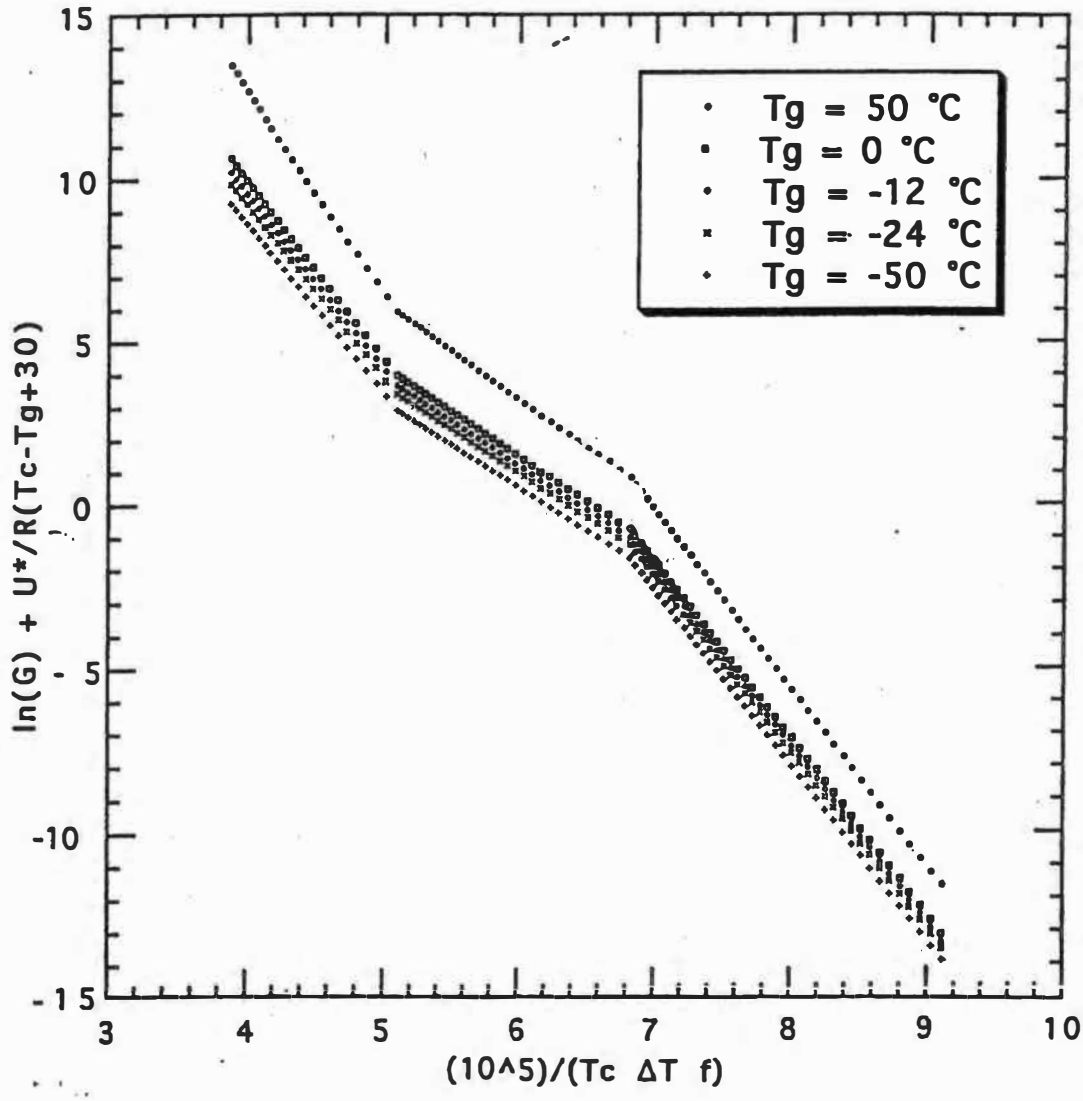


Figure (5.3.4) The effect of the glass transition T_g on the Lauritzen-Hoffman analysis.

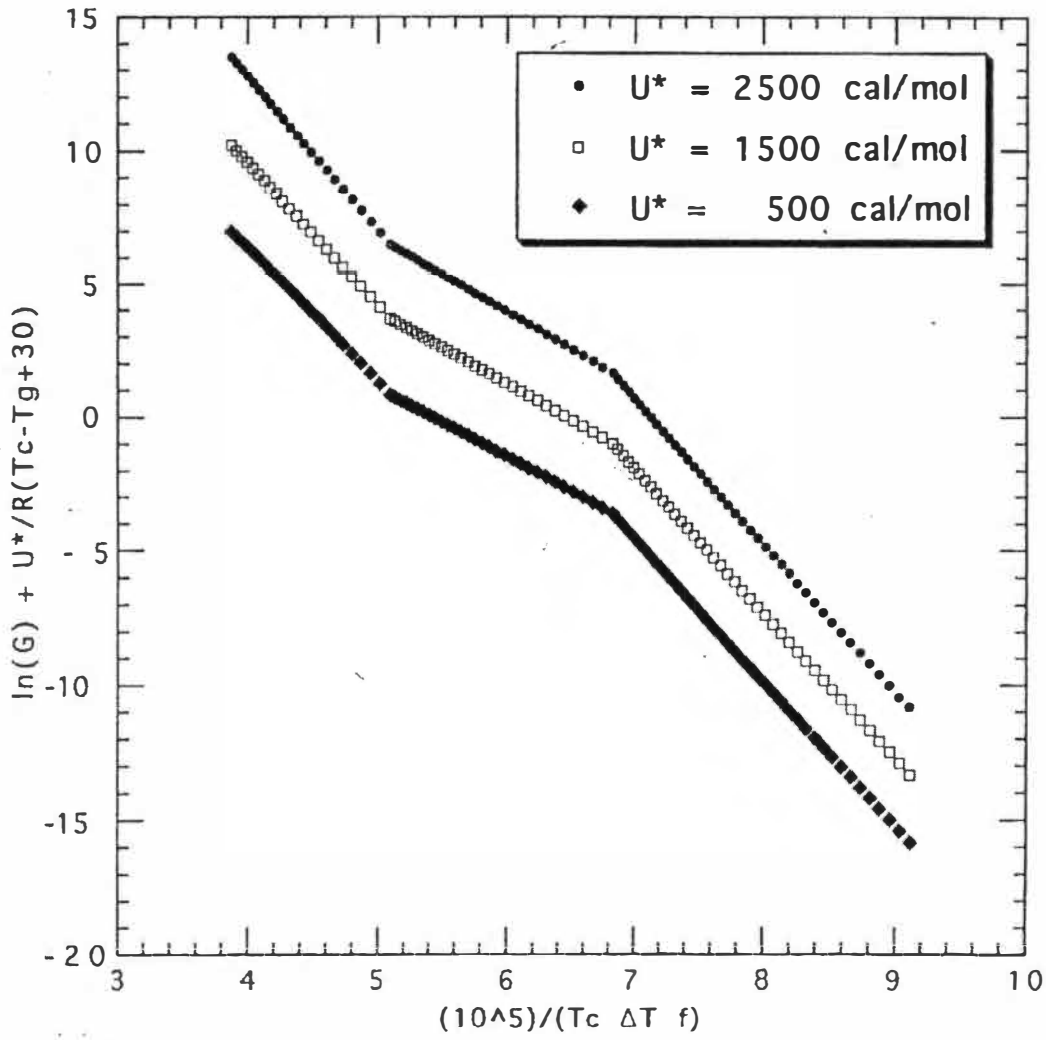


Figure (5.3.5) The effect of activation energy U^* on the Lauritzen-Hoffman analysis.

The dependency of the product of surface free energy ($\sigma\sigma_e$) on pressure was determined from the slope of the lines as discussed in **section 2.3.1.1**, and listed in **table (5.2.2)**. In contrary to the fold surface free energy (σ_e), the lateral surface free energy (σ) is expected to have small dependency on temperature and is considered constant. Hoffman [4] estimated this value for PE to be 11.8 erg.cm^{-2} at atmospheric pressure. However, due to the inaccuracy in obtaining T_m^o value and the fact that the second co-existing phase may have interfered with the crystal growth process, secondary nucleation theory cannot be relied on in measuring the surface free energies of the whole system.

Dalal and Phillips [54] have studied the pressure dependence of the fold surface free energy σ_e of *cis*-polyisoprene. They growth rate kinetics have shown a sudden increase in σ_e value at and above 1kbar to almost double its atmospheric pressure value. Similar behavior was observed from the lamellar thickness data. For samples crystallized at atmospheric pressure, σ_e value was practically independent of pressure. To explain their results Dalal and Phillips have introduced a model that assumes the possibility for two (or more) molecular conformations to form the fold. Each conformation represents a local energy minimum, where the lowest energy state at atmospheric pressure is not the lowest volume state. Consequently, another state will have the lowest total energy at some higher pressure due to the reduction in volume.

The effect of pressure on the $T_{\text{I-II}}$ and $T_{\text{II-III}}$ transition temperatures is illustrated in **figure (5.3.6)**. The linear relationship allows the estimation of the transition temperatures

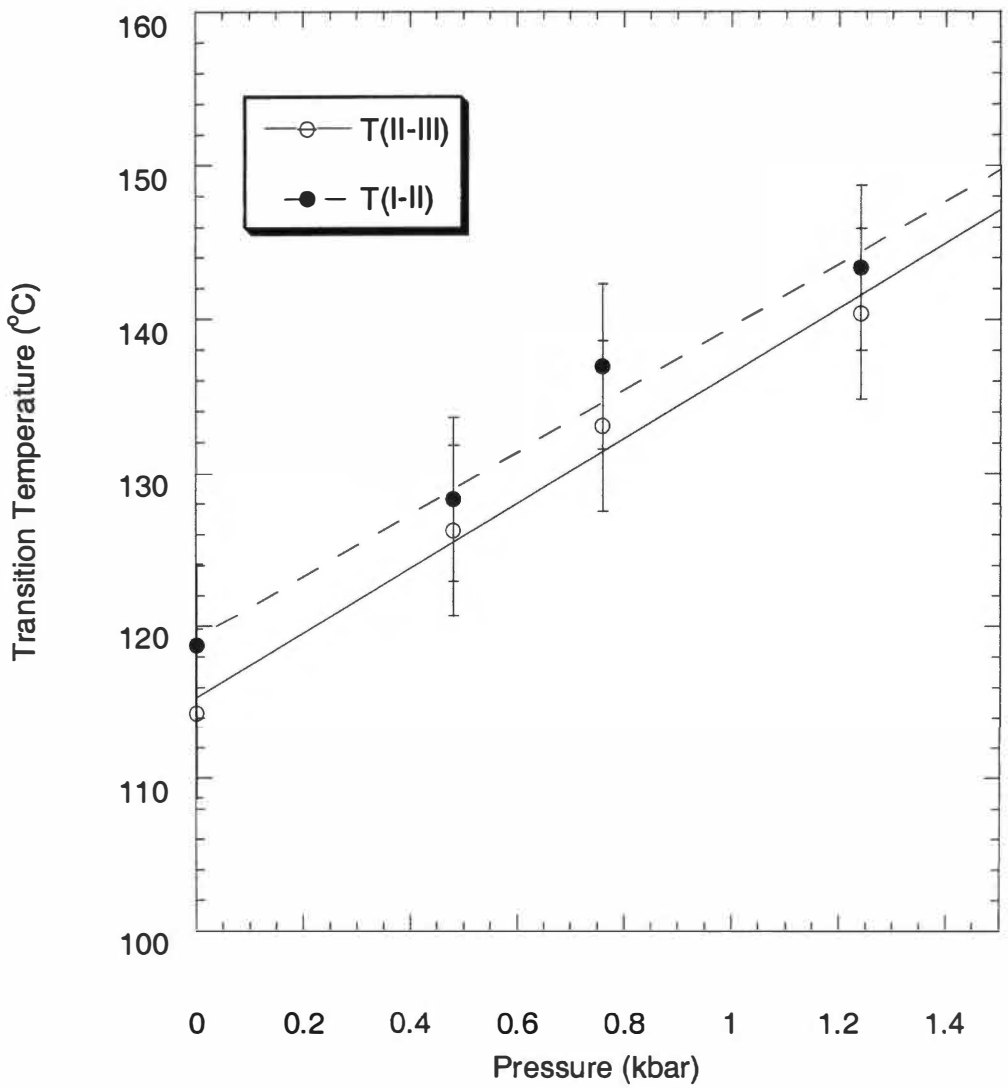


Figure (5.3.6) Regime transition temperatures as a function of pressure for L-04 copolymer.

at any pressure, assuming the validity of the relationship at higher pressures. The linear dependency of $T_{I\text{-}II}$ transition temperatures on pressure was also reported for LPE [8]. The importance of regime II-III transition temperature rise from the fact that $T_{II\text{-}III}$ coincides with the T_{cr} mentioned in **section 5.1.4.1**. It is this the temperature at which ΔG_c and ΔG_M values start to change relative to each other, and the monoclinic phase starts to dominate over the orthorhombic phase. Using this relationship, and appropriate computer software, one can plot the three-dimensional phase diagram, where all phases (orthorhombic, monoclinic, and liquid) intersect at the triple line.

5.3.1 Nucleation of ECC Under High Pressure

The correspondence between $T_{II\text{-}III}$ and T_{cr} clearly relates the kinetics with thermodynamics. For monoclinic phase to prevail, slower growth rates and possibly a change in the nucleation mechanism are needed. Hikosaka *et al* [101, 102] suggested that there is no essential difference between the mechanism of FCC and ECC formation. Primarily, lamellae crystallize from the melt to form FCC. As crystallization proceeds into the disordered hexagonal phase, an ECC grows from the FCC by lamellar thickening via chain sliding diffusion. Hikosaka derived a formula of the secondary nucleation rate j for both ECC and FCC, which can be given as,

$$j = \eta_o \left(\frac{kT}{h} \right) \left[\sum_{m=0}^{\infty} \exp \left\{ \frac{G_m}{kT} + \frac{\Delta E_m}{k(T - T_g)} \right\} \right]^{-1} \qquad (5.3.1)$$

where η_o is a constant, kT is the thermal energy at temperature T, h is Planck constant, G_m is the free energy for forming a nucleus of the mth stage, ΔE_m is the activation energy necessary for diffusion from the mth to the (m+1)th stage and T_g is the glass transition. The equation contains two competing parameters, the thermodynamic factor G_m and the kinetic factor ΔE_m. The latter consists of two kinds of diffusion activation energy, namely $\Delta E_{l,\,m}$ for diffusion of a chain within the melt, and $\Delta E_{s,\,m}$ for slide diffusion of a chain within a crystal. When PE crystallizes from the melt into the disordered hexagonal, or depending on the applied pressure, the monoclinic phase, $\Delta E_{s,\,m}$ is small because chains can easily slide within the crystal due to the high mobility of the hexagonal phase. In consequence, the thermodynamic factor G_m dominates, and ECC will develop by lamellar thickening. On the contrary, the crystallization into the orthorhombic phase produces large $\Delta E_{s,\,m}$ values due to the difficult chain-sliding diffusion within the orthorhombic crystals. As a result the kinetic factor ΔE_m dominates and FCC will form. According to this theory, polymers that crystallize from the melt into the hexagonal phase will show continuous change from the FCC to ECC as temperature increases.

Sawada [103] and Fu [104] have proposed another theory named the bundle-like nucleation theory. Both groups suggested that high-pressure crystallization starts from partially extended-chain nucleation rather than the folded-chain nucleation proposed by Hikosaka. This theory was established based on some experimental results and the fact that extended- and folded-chain crystallization are mutually independent processes,

where the former can take place prior to the folded-chain crystallization as was reported by Bassett [83,105, 106].

Based on the discussion of **section 5.2.3.1** it could be argued that the critical nucleus of L-04 copolymer is composed of multiple stem nucleus (3 in specific) instead of the single stem nucleus assumed by the secondary nucleation theory. The correlation between Gibbs-Thomson and Hoffman-Weeks plots supports this idea for the orthorhombic crystals. However, it is expected that the monoclinic phase will energetically prefer single stem nucleation to form thicker lamellae. In summary, it appears that prior to the transition (critical) temperature the fast rate of crystallization in this temperature range kinetically prefers FCC over ECC i.e. three stem nucleation is more preferable by the system. It is possible that this temperature range is not high enough to provide ECC with the required thermal energy to dominate. This might explain the sharp increasing trend of melting temperature of FCC whilst the ones that believed to belong to the ECC slightly decreases. Beyond the transition temperature the system adopts a different crystallization mechanism and converts to the single stem nucleation where the conditions of thermodynamics appear to over control that of the kinetics.

The formation of a multiple stem nucleus is completely consistent with the idea of a disordered intermediate on the growth face. In other words, the formation of a monolayer cluster of three stems partially aligned with each other and with the underlying crystal substrate is the rate-controlling event [100], particularly for regimes II

and III. Secondary nucleation theory assumes that nucleation occurs by a single stem nucleus and applies nicely for regime I.

The fold-surface free energy σ_e plays an essential rule in determining the nucleation mode. According to the theory, the faster crystallization rates at larger pressures indicate a reduction in the surface free energies of the folded-chains σ_{ef} and that of the bundle-like nucleation σ_{eb}. The extent of reduction, however, is not equal. The drop in σ_{ef} value will cease at certain pressure and reaches a constant value. Crystallization in the folded-chain mode dominates when $\sigma_{ef} < \sigma_{eb}$, while bundle-like nucleation surmounts when $\sigma_{eb} < \sigma_{ef}$.

Surface Free Energy

The surface free energies obtained by secondary nucleation theory and Gibbs-Thomson equation where plotted in **figure (5.3.7)**. Due to the lack of any useful information on how pressure affects the heat of fusion of the ethylene-octene copolymers, the surface free energy σ_e was replaced by the length unit $\sigma_e/\Delta H_f$ to include any possible changes in the heat of fusion that might take place during crystallization. According to the geometry of **figure (2.3.1)** and **equation (2.1.3)**, the ratio $\sigma_e/\Delta H_f$ represents the crystal dimension in c-axis and is measured in angstroms, as represented by **equation (5.3.2)**.

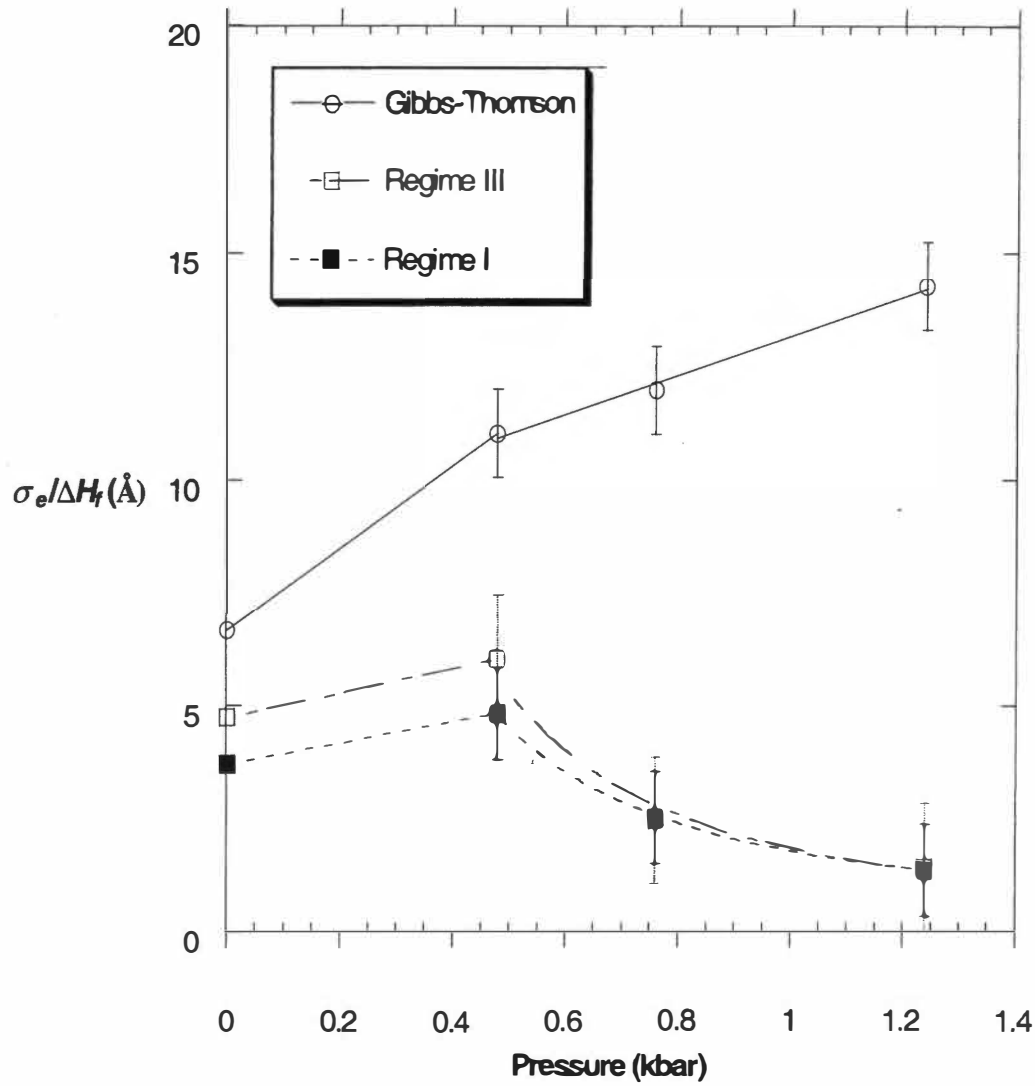


Figure (5.3.7) A comparison plot of the effect of pressure on ($\sigma_e/\Delta H_f$) ratio using secondary nucleation theory and Gibbs-Thomson equation.

$$\sigma_e / \Delta H_f = \frac{l}{2}\left(1 - \frac{T_m}{T_m^o}\right) \qquad (5.3.2)$$

Secondary nucleation analysis shows a depression in the $\sigma_e/\Delta H_f$ parameter at high pressures ($P \geq 0.48$kbar). The depression occurs in both regimes (I and III) and agrees with the expected drop in the fold-surface free energy σ_e of the extended-chain crystals, provided that the heat of fusion ΔH_f remains constant. A sign of stabilization is also observed at higher pressures. The σ_e values obtained from regime III are larger than those of regime I at lower pressures but start to converge as pressure increases. This could be attributed to the small expansion of the crystal at higher temperatures (regime I). The larger surface area, although it does not change the crystal structure, decreases the σ_e value. A change in the folding mechanism could also be a reason behind lower σ_e values. As shown in **table (5.2.2)**, the results derived from regime II were not consistent with those of regimes I and III. The small temperature range of regime II (2-4 ^{o}C), and the absence of any thermodynamical changes at regime I-II transition raises some questions about the nature of regime II region. Due to the above, σ_e values obtained from regime II will be ignored in this study. It should be reminded before preceding any further, that the regime plots were constructed by measuring the linear growth rate of the fastest spherulitic structure only. The front growth of the spherulites, however, may contain both phases (orthorhombic and monoclinic) is expected to affect the overall growth rate measurements.

When transferring from atmospheric to 0.48kbar pressure the $\sigma_e/\Delta H_f$ ratio has increased by almost one third of its value. This increase can be ascribed to either the increase of σ_e value or the reduction of ΔH_f. Since no double melting temperatures were observed at this pressure, it is believed that the monoclinic phase cannot exist at this pressure. However, this pressure could be an introductory stage to the formation of monoclinic phase. It is possible that the solubility parameter, although increases with pressure, does not reach the desired value. Consequently, the extension of the lamellar structure reaches the branch points without dissolving it into the crystalline phase bringing the surface free energy to higher values.

For data obtained by Gibbs-Thomson equation the ratio $\sigma_e/\Delta H_f$ increases with pressure. The amount of increase is larger when transferring from 1 atmosphere to 0.48kbar. Once pressure is applied the increase in ratio becomes more systematic and follows a clear linear relationship with pressure. The slope of the line is around 4 Å/kbar. To understand this behavior it has to be mentioned that the melting points used in Gibbs-Thomson equation were taken *in-situ* i.e. when pressure was applied, however the lamellar thickness was determined at atmospheric pressure. Considering this and the previous suggestion that a eutectoid-like transformation occurs upon cooling down and releasing pressure, it can be concluded that the increase in $\sigma_e/\Delta H_f$ value results from the increasing accumulation of rejected hexyl branches that accordingly raises the σ_e value. At larger pressures lamellae become thicker and more hexyl branches are dissolved in it.

As a result the more dissolved branches the more will be rejected at room conditions, thus the higher the fold surface free energy becomes.

5.3.2 Bulk Crystallization

Lauritzen and Hoffman [107] have used the reciprocal of half time $1/t_{1/2}$ (sec^{-1}) for the regime analysis instead of the linear growth rate G (cm/sec). The correspondence between reciprocal half time and linear growth rate was reported by Magil [108] and Phillips [99]. The latter have shown that $\sigma\sigma_e$ values obtained by the reciprocal half time analysis can be compatible with those from linear growth rate in their study of the kinetics of crosslinked polyethylene. Meanwhile, Lambert *et. al.* [109] have found that regime transition temperatures can be found from the bulk kinetic data, but may not be used to determine the fold surface free energy σ_e.

In accordance to Lambert, $\sigma\sigma_e$ values obtained from bulk kinetics did not correspond to those of linear growth rate for L-04 copolymer, while the regime transition temperatures are in a good agreement. **Figure (5.3.8)** shows the regime plots of L-04 copolymer obtained by using the reciprocal half time for 0.48 and 1.24kbar pressures.

The double crystallization rates observed for high-pressure samples **(figure 4.1.5)** sheds a lot of doubts on the accuracy of the parameters measured using this method. The existence of a second phase during crystallization has a definite effect on the total value

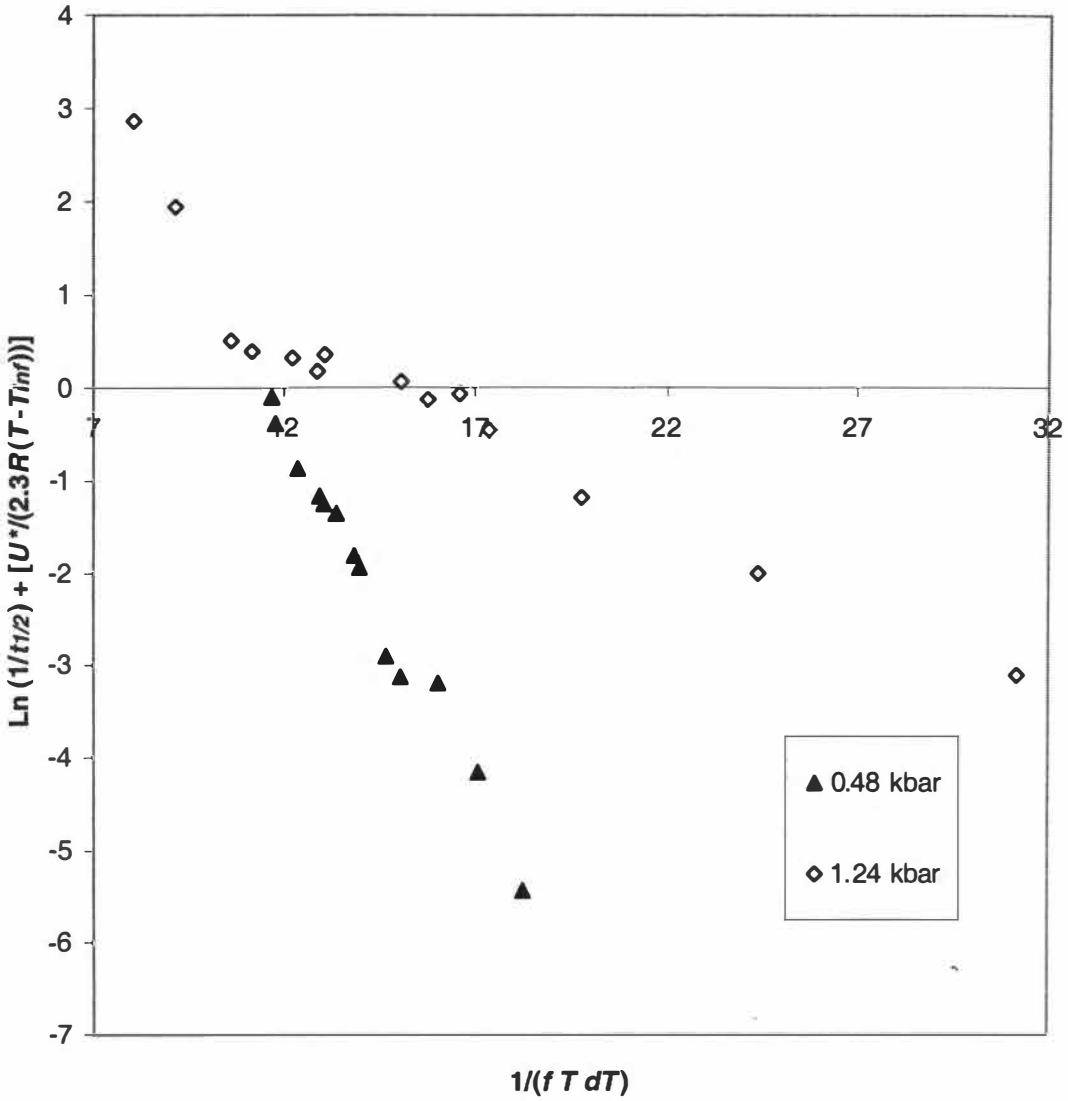


Figure (5.3.8) Regime plots of the bulk crystallization kinetics analyzed with half time ($t_{1/2}$) assuming a heterogeneous secondary nucleation (T_∞ = -155 °C, U^* =1500 cal/mole)

of the surface free energy. Crystals formed directly in the orthorhombic phase are not believed to have similar surface free energy compared to those transformed from the monoclinic to the orthorhombic phase. The high concentration of the rejected hexyl branches in the latter is believed to increase its surface free energy, and two populations with different surface free energies could co-exist. For this reason the upper method cannot be safely used to understand the kinetics of ethylene-octene copolymers, but is useful enough to explain part of the relationship between the two co-existing phases during crystallization. **Table (5.3.1)** compares the parameters measured using both methods where huge discrepancy can be observed.

The crucial information found in **figure (4.1.5)** is very helpful and corresponds with the general understanding of the behavior of ethylene-octene copolymer developed in this study. One clear example is observed at 1.24kbar where the slope of the first-crystallizing phase seems to be independent of the increasing temperature. The induction time of the second phase (i.e. orthorhombic) increases with temperature. The increase is accompanied by a slow crystallization rate, which provides a better environment for the faster monoclinic phase to prevail. The crystallization rate of the orthorhombic phase decreases with temperature as expected. In accordance, the pictures in **figure (4.4.2)** show the early fast growing entities with no clear morphology, at least under the optical microscope. It is not till certain time passes when spherulites start to form. Both phases co-exit and do not try to cancel each other. SEM pictures support this phenomenon as was discussed earlier.

Table (5.3.1) A comparison between the parameters obtained using linear growth kinetics and bulk crystallization for two pressure sets. (σ=11.8 erg/cm^2)

	Linear Growth Rate				**Bulk Crystallization**			
Pressure (kbar)	T_{I-II}(C)	T_{II-III}(C)	$(\sigma_e)_I$ erg/cm^2	$(\sigma_e)_{III}$ erg/cm^2	T_{I-II}(C)	T_{II-III}(C)	$(\sigma_e)_I$ erg/cm^2	$(\sigma_e)_{III}$ erg/cm^2
0.48	128.27	126.22	116.66	130.08	131.2	129.6	77.71	96.26
1.24	143.37	140.36	39.43	37.84	143.1	134.5	85.69	3.93

5.4 Band Spacing

Most of the past experimentations tried to understand the nature of the 'Band spacing' phenomenon qualitatively. This study, however, appeals to more quantitative considerations. The band spacing '*S*' (μm) studies were conducted only at atmospheric pressure due to the technical difficulties accompanied with elevated pressures. The wide range of crystallization temperatures was used to ensure the covering of all available regimes.

Band spacing increases with increasing crystallization temperature and/or the branch content as obviously determined by **figure (4.4.3)**. The effect of increasing branch content resembles that of adding a lower molecular weight diluent to PE as reported by Keith and Padden [71]. The linear PE used by them has almost the same molecular weight as the one used by this study. To study the effect of molecular weight they blended the linear PE with 20 *wt%* of *n*-$C_{32}H_{66}$ and of polyisobutylene of 200 000 molecular weight. Based on their experimentations they have suggested that the response of the system to the molecular mobility of the crystallizing chains is stronger than to the segregation of amorphous polymer between lamellae. The similar effect of lowering molecular weight and increasing branch content on band spacing implies that branches have no significant role in the band formation. Copolymers with larger branch content have shorter sequence lengths, where the short sequence lengths and low molecular weights appear to play the same role in affecting the banded structure, assuming that the effect of the molecular weight is real.

On the contrary, the behavior of the linear PE (denoted by M-54) contradicts that described by Keith and Padden, although the temperature ranges are comparable. Beside the horizontal displacement of the band spacing towards higher temperatures as molecular weight increases, an additional vertical displacement has occurred as seen in **figure (4.4.3)**. At low temperatures band spacing reaches a minimum limit where no extra band size reduction is observed. The equilibrium state of linear PE (M-54) occurs at larger band spacing compared to other copolymers. By comparing the behavior of ethylene-octene copolymers and M-54 it can be suggested that, if the horizontal displacement is ascribed to the addition of hexyl branches, the vertical shift of the curves would then be referred to the increase in molecular weight. This conflicts with the suggestion of Keith and Padden. It is possible that their use of different blends to study the effect of molecular weight could have possibly sent a false picture about its real influence on the band spacing. It is very likely that the blended materials have acted in a similar way to adding branches and not increasing molecular weight. This could be supported by the slight vertical shift observed for the linear PE / *n*-$C_{32}H_{66}$ blend (figure 3 in reference 71). The lower chain mobility of the high molecular weight material is expected to hinder the chain twisting process and delay the building up of stresses required for the appearance of bands. In other words increasing the molecular weight would produce a larger band spacing, which explains the M-54 behavior. Similar argument of low chain mobility could be used to interpret the behavior of the branched copolymers.

The introduction of hexyl branches has shifted the curves towards lower temperatures. The shift is relatively linear and is estimated to be 1 ^{o}C per hexyl branch per 1000 C atom (1 CH_3/1000 C atom). Applying an opposite shift by the same amount bring the curves to reasonable correspondence, as shown in **figure (5.4.1)**. More specific correction factor is required to obtain better consistency. However, the determination of this factor is beyond the goal of this study and no effort will be made to solve it.

The Influence of Regime Plots on Band Spacing

In this section an attempt to explore the relationship between band spacing and linear growth rate will be made. The importance of this relationship could improve the understanding of the mechanism of band formation. In addition, the possibility of estimating regime transition temperatures by just measuring the band spacing is a less tedious job compared to the linear growth measurements. In order to eliminate the effect of the variation of equilibrium melting temperature with comonomer content, band spacing was plotted versus the reciprocal supercooling as shown in **figure (5.4.2)**. Except for the convergence of L-04 and M-54 curves at high temperatures, the convergence in all curves was not enough to obtain an exact correspondence. This necessitates the addition of some correction factor.

The plot of reciprocal band spacing ($1/S$) versus crystallization temperature (T_c) is shown in **figure (5.4.3)** for all polymers used. As seen from the plot the reciprocal band spacing imitates the behavior of regime plots. The change in slope of ($1/S$) as

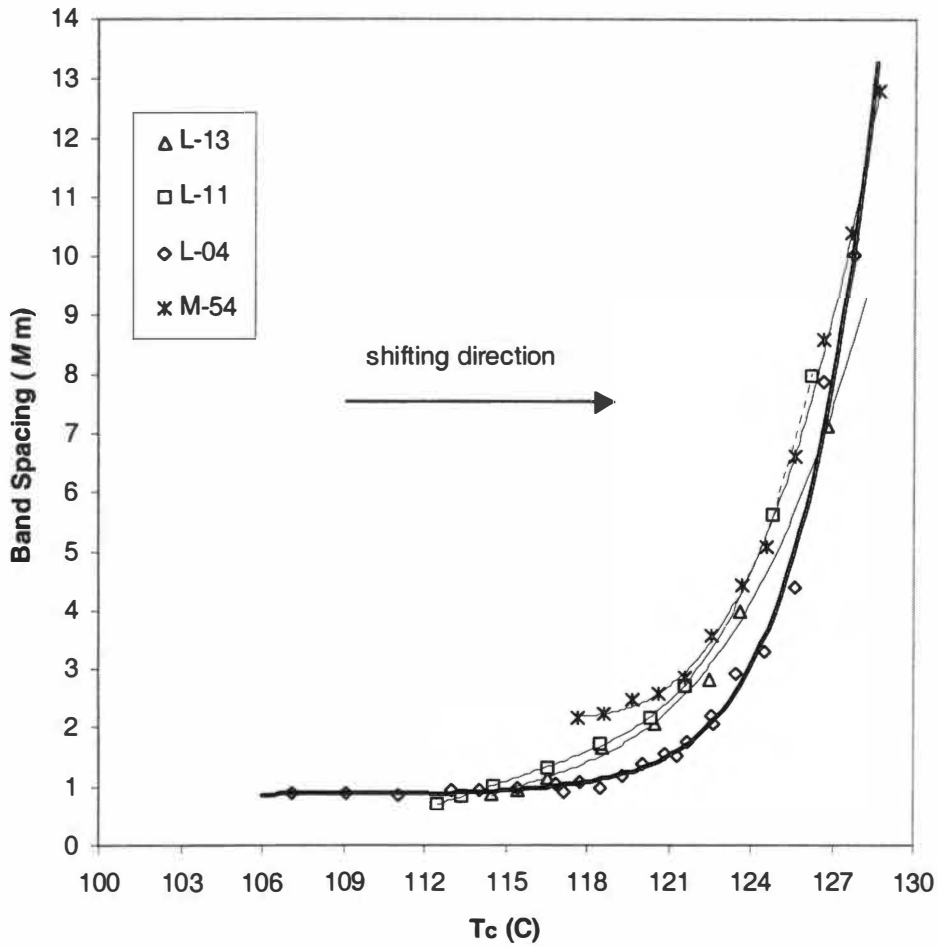


Figure (5.4.1) A plot of band spacing versus T_c shows the effect of applying an opposite shift of 1°C/hexyl/1000 C atom on the curves.

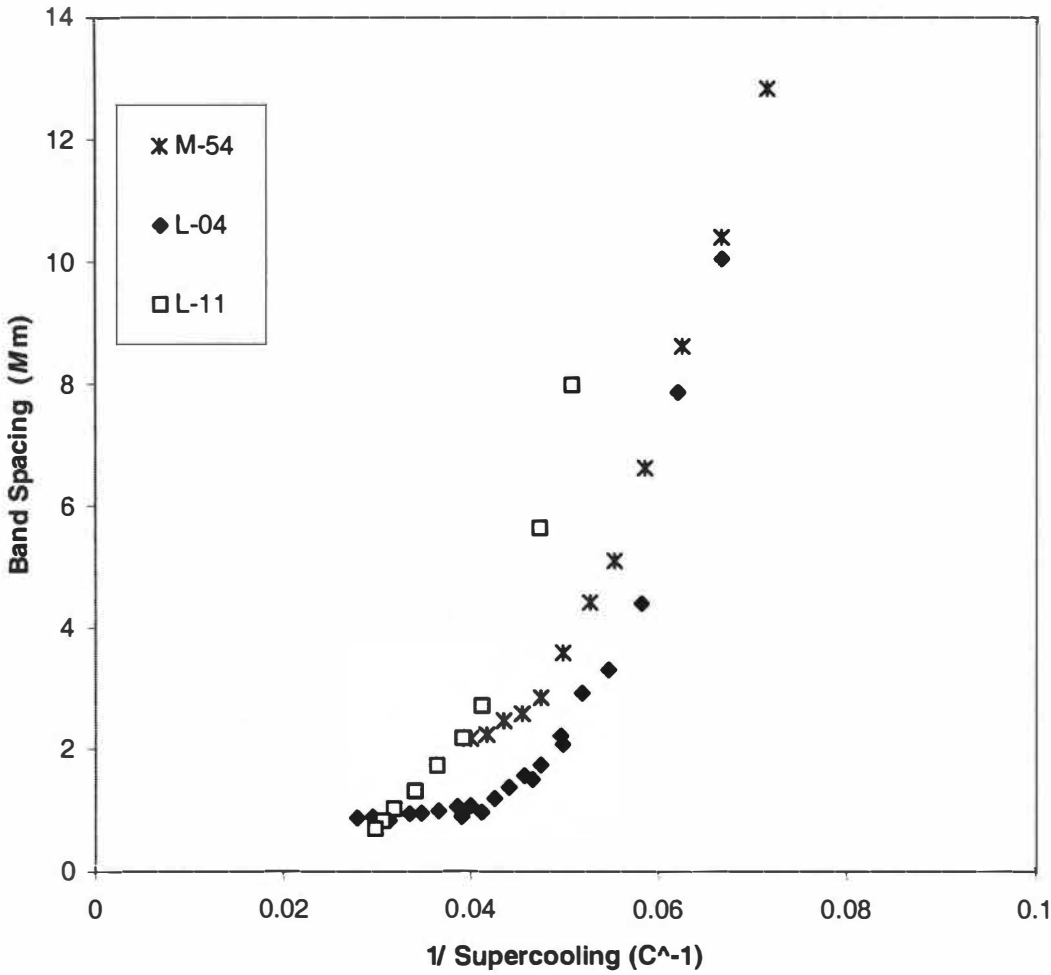


Figure (5.4.2) A plot of band spacing versus reciprocal supercooling of different materials.

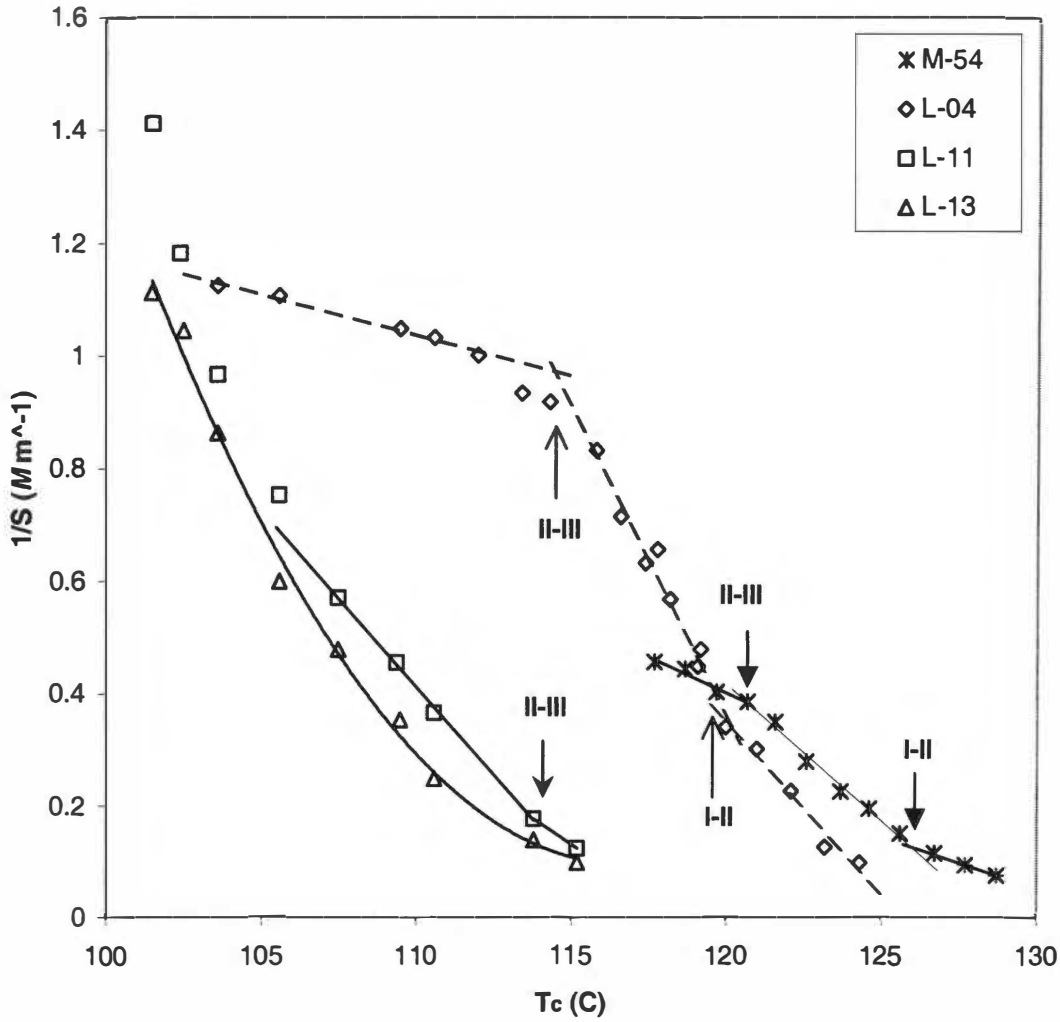


Figure (5.4.3) The effect of temperature, and branch content on the reciprocal band spacing ($1/S$).

function of temperature occurs at temperatures that coincide exactly with the regime transitions as pointed by the arrows (see also **Table 5.4.1**). As an example, L-04 copolymer crystallized at atmospheric pressure has its (II-III) and (I-II) regime transitions at 113.5 °C and 119.5 °C, respectively as listed in **table (5.3.1)**. In a very good agreement, the change in the slope of (1/*S*) for the same copolymer occurs at temperatures 114.4 °C and 119.52 °C as shown in **figure (5.4.3)**. As another example, M-54 have shown similar agreement where its (II-III) and (I-II) regime transition temperatures occurred at 120.8 °C and 125.6 °C, respectively [110], while the change in the slope of (1/*S*) occured at 120.7 °C and 126.25 °C.

The reciprocal band spacing (1/*S*) is a measure of the number of concentric circles in 1 μm distance i.e. the periodicity. From **figure (5.4.3)** the change in periodicity i.e. slope of L-04 and M-54 at low temperatures (regime III region) is smaller than that of regimes I and II. This could be referred to the reduction of molecular chain mobility at high supercoolings. The amount of reduction in periodicity tends to stabilize at very low temperatures due to the increased rigidity of the molecular chains.

The behavior of reciprocal band spacing (1/*S*) for the higher branched copolymers (L-11 and L13) differs from the others. The line curvatures for L-11 and L-13 are facing upward (exponential pattern) with no tendency to stabilize at lower temperatures. On the other hand, the line curvatures of L-04 and M-54 are generally facing downward. Consequently, the reciprocal band spacing (1/*S*) for copolymers of ≥11 hexyl branches

Table (5.4.1) A comparison between the transition temperatures obtained using linear growth kinetics and reciprocal band spacing for different materials (P =1 atm).

	Bulk Crystallization		**Reciprocal Band Spacing**	
Material	$T_{I\text{-}II}$ (°C)	$T_{II\text{-}III}$ (°C)	$T_{I\text{-}II}$ (°C)	$T_{II\text{-}III}$ (°C)
M-54	125.6	120.8	126.25	120.7
L-04	119.5	113.5	119.52	114.4
L-11	-	114.2	-	113.8

per 1000 C atom, can be represented mathematically by $1/S \sim a\, e^{-bT_c}$ where 'a' and 'b' are constants that change with branch content. The upper expression was derived from the general polynomial behavior of the curves and can be rewritten as log (S) ~ bT_c–log (a). Using supercooling temperatures the mathematical expression can be written as $1/S \sim a\, e^{b\Delta T}$ or log (S)~ log ($1/a$) $-b\Delta T$ (see **figure 5.4.4**). The correlation between secondary nucleation theory and reciprocal band spacing is represented in **figure (5.4.5)**, where clearer slope changes are observed.

The change in the line curvature of the higher branched materials (L-11 and L-13) could be attributed to the existence of the monoclinic phase at atmospheric pressure. The formation of extended chain crystals is expected to hinder the twisting mechanism, due to the reduction of its degree of free volume. As a result, the band spacing will drop faster even at low crystallization temperatures.

The minimum branch content needed for the exponential pattern to be observed was not embodied in this study, however according to the kinetics of the previous reference it is expected to be as low as 7 hexyl branches /1000 C atom. In his study Wagner has found that the linear growth rate of ethylene-octene copolymers becomes independent of the crystallization temperature beyond the 0.7% impurity content. Unlike L-04 and M-54, the banding structure of L-11 and L-13 practically disappears at regime II. The shifting of the triple point to a pressure value lower than the atmospheric pressure for L-11 and, by analogy, L-13 copolymers allows the co-existence of the monoclinic phase, as discussed earlier. The growth of thick lamellae through the monoclinic phase

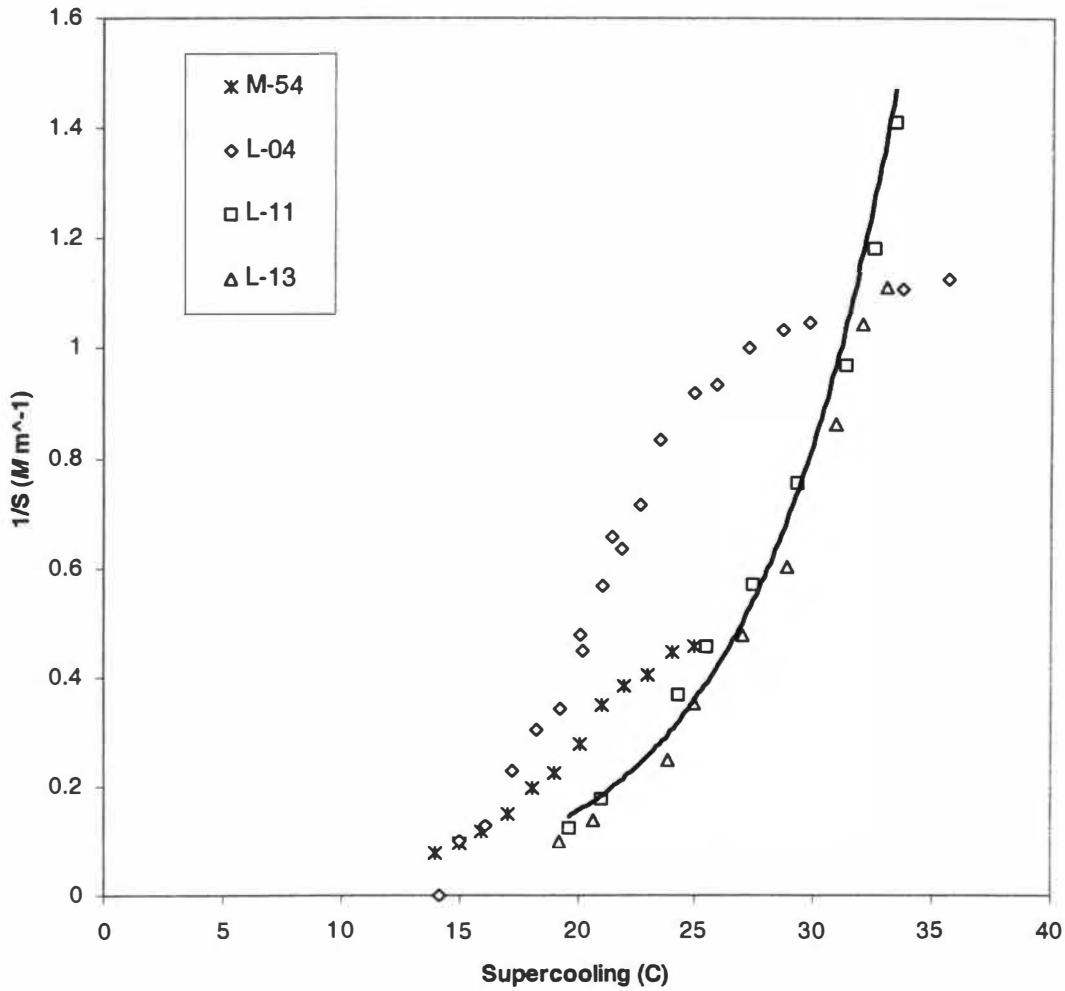


Figure (5.4.4) The effect of supercooling temperatures, and branch content on the reciprocal band spacing ($1/S$).

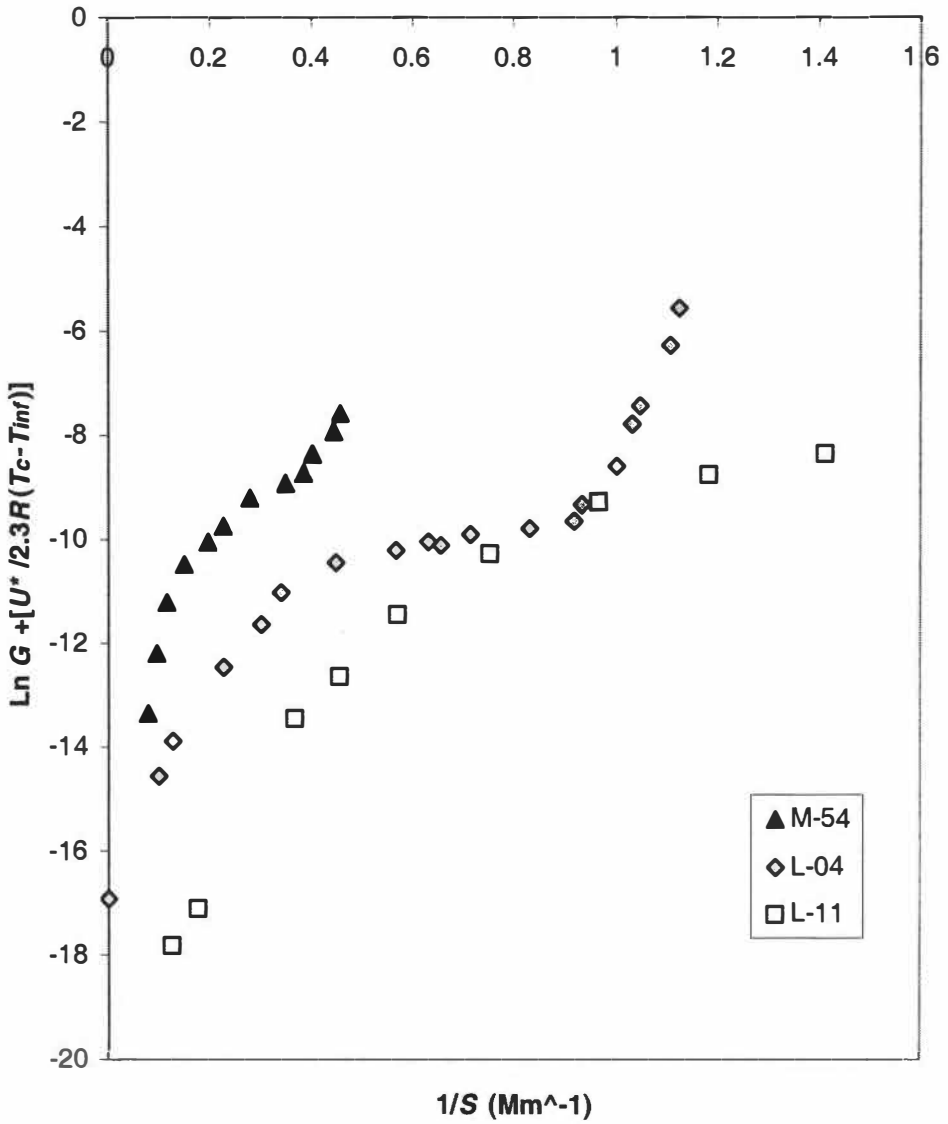


Figure (5.4.5) A plot of the secondary nucleation theory versus reciprocal band spacing for different materials.

interferes with the crystallization process and is believed to cause the observed difference in behavior between the high and low branch content materials.

In conclusion, results obtained by this study although different from those of Keith and Padden agree that the molecular mobility of the crystallizing chains have strong effect on the banding comportment. In addition, the role of isochiral dislocations, suggested by Bassett, also plays a part in banding. However, no preference can be made between the two interpretations. On the other hand, the relationship between regime plots and band spacing suggests a major role of the kinetics in the bands formation.

5.4.1 Cellulation in Polymers

Cellulation in polymers has not been studied thoroughly in literature. Only few articles exposed to this topic, possibly because of the difficulty in obtaining definitive experiments that could explain the phenomenon explicitly. Keith and Padden [111], in their study to the highly doped melts, have related this phenomenon to the diffusion coefficient where the characteristic dimension of cellulation, i.e. the radius to its onset and the average cell width, is comparable to the characteristic diffusion length $\delta=D/G$. They suggested that the existence of postulated internal 'fibers' resulted from cellulation and fibrillation of an initially planar interface of presumed close-packed lamellae that grows into the melt because of morphological instability. Bassett *et al* [66,72] have shown a little or no variation in the radial growth rate G, but a decrease in the diffusion coefficient D as

a result of increasing the branch content. Detailed discussion on the mechanism of cellulation was reported in **section 2.4.2.1**.

Cellulation was clearly observed in **figures (4.4.4-6)**, and occurred in polymers with branch content as low as 7 CH_3/1000 C atoms. Very high branch content is not necessary for cellulation to occur. However, the larger the branch content the more dominant the phenomenon becomes. This can be observed when the circular perimeters become wavier. The periodicity of the bandings, however, does not appear to be interrupted by the cellulation. The two phenomena appear to be independent of each other and are caused by separate mechanisms.

According to Bassett *et. al.*, cellulation is responsible for declining the growth rate of the spherulites. The larger the spherulite becomes the more highly branched molecules segregated at the growth front. Accumulated branched molecules will lower the equilibrium melting point in their region, and hence the isothermal supercooling at the interface, leading directly to the drop in the growth rate.

Based on the phase diagram of **figure (5.1.7)** and other evidences, the monoclinic and orthorhombic phases do co-exist at atmospheric pressure for copolymers with hexyl branches as low as 7 per 1000 C atom. The planar growth front responsible for growth rate reduction is not believed to result from the accumulation of rejected branched molecular sequences as suggested by Bassett. Instead, the growth of close-packed lamellae in the monoclinic phase is expected to produce the initial planar interface

between the molten and crystalline state, in accordance with Keith and Padden. The higher equilibrium melting point of the monoclinic phase compared to the orthorhombic phase increases the growth rate at the front. The increasing of the isothermal supercooling could possibly result in a significant growth rate increase (i.e. very rapid quenching) where only amorphous material is produced. The larger induction time of the orthorhombic fronts compared to the monoclinic will allow for almost complete crystallization of the orthorhombic fronts, hence, only fronts produced by the co-existent orthorhombic phase will be observed before any noticeable crystallization in the monoclinic front could be detected. This as a result will explain the amorphous regions within the spherulitic structure.

Another possible explanation of the cellulation effect could be the formation of extended chain crystals. It is possible that the 'fingers' appear in the cellulized structure are axialites that were grown in the monoclinic phase forming thick crystals. The fingers, however, transform to the orthorhombic phase in a eutectoid-like transformation, where bandings appear. This explanation requires a certain time interval between the formation of the crystals and the observation of the bandings, unless the transformation is abrupt.

It could also be argued that the isothermal thickening process of the lamellae in the meta-stable monoclinic crystals will, almost promptly, transform in a eutectoid-like fashion to the most stable orthorhombic crystals. Consequently, the expelled hexyl branches will segregate at the growth front. In this segregant-rich environment growth proceeds but with slower rates. The uneven distribution of segregants will then be the

reason behind the observed morphology of cellulation in spherulites. This interpretation is more consistent with the results of this research and should be adopted.

6. CONCLUSIONS

The atmospheric and elevated pressure studies of ethylene-octene copolymers have revealed several important conclusions about melting and crystallizing behaviors. The accompanied morphological changes had a great role in interpreting what seemed to be contradicting results. The analysis managed to reconcile the different models established to explain ethylene-octene copolymers.

6.1 Melting Behavior

The melting behavior of L-04 copolymer crystallized and melted at atmospheric pressure was consistent with the reported literature where the lamellar thickness increases with temperature. At elevated pressures the lamellar thickening becomes rapid and produces melting temperatures that are very close to the equilibrium melting point of the orthorhombic phase at the assigned pressure. The double melting behavior constitutes a lower melting point consistent with the orthorhombic lamellar structure, and a higher one that reflects an extended-chain crystal.

6.2 Phase Diagram

The combination of results obtained in this study, in particular the thermal behavior studies, have allowed us to construct the phase diagram of ethylene-octene copolymers. The triple point is significantly dependent on the branch content. Adding as

little as 4hexyl branches/1000 C atom has shifted the triple point to as low as 0.5kbar and 146 °C. On the other hand, the addition of 11hexyl branches/1000 C atom has shifted the triple point to below the atmospheric pressure. The triple point at pressures <3kbar can be identified to be the point where monoclinic (instead of hexagonal), orthorhombic, and molten phases co-exist. Phase diagram is also dependent on crystallization temperatures.

6.3 Eutectoid-Like Transformation

The melting of high-pressure samples at atmospheric pressure has produced inconsistently lower values of the melting points for all pressures used. The lower melting points, however, were consistent with SAXS results where no sign of large lamellar structure was detected. The large lamellar structure formed in the monoclinic phase at elevated pressures does not retain its shape and transformed into smaller orthorhombic crystals in a eutectoid-like transformation. The morphology of the final structure shows that within the large lamellar structure few thin lamellae are closely packed to each other and separated by amorphous material. The thickness of both lamellar structures was consistent with the melting points obtained for the same sample.

6.4 Crystallization Mechanism

The growth front of the crystalline phase of ethylene-octene copolymers occurs in the monoclinic phase depending on the pressure applied and branch content. The solubility parameter in the monoclinic phase is higher than that of the orthorhombic one.

As a result hexyl branches are dissolved in the crystalline phase and extended chain crystals are formed. Higher pressures stimulate the process by increasing the solubility parameter. Once cooling the material down to room temperature and releasing pressure, the monoclinic phase undergoes a eutectoid-like transformation and becomes orthorhombic. The reduction in the lattice parameter as a result to the transformation forces the hexyl branches to be expelled into amorphous phase forming a group of stacked lamellae. The eutectoid-like transformation in L-11 copolymer at atmospheric pressure occurs right behind the growth front during crystallization.

6.5 Band Spacing

Band spacing shifts, almost linearly, 1 °C towards lower temperatures at the addition of 1hexyl branch/1000 C atom. For the first time, as far as we know, band spacing was correlated to linear growth rates. The mechanism behind band formation is not simply a twisting that results from build up stresses, but is more complicated process that involves the growth mechanism of the spherulites. The pattern of the reciprocal band spacing as a function of temperature resembles that of the regime plot of LPE, L-04 and L-11 materials. Reciprocal band spacing could be used to determine the regime transition temperatures.

7. FUTURE WORK

7.1 High Pressure Studies

Although this dissertation has covered a vast range of experiments on ethylene-octene copolymers, additional high-pressure work is needed to substantiate the results of this study. Larger pressures are needed to construct better and more complete phase diagram of ethylene-octene copolymers. The experimental limitations of the lowest crystallization temperature used in this study could be overcome by using rapid-cooling instrument and high-speed camera. This, though very difficult, will increase the supercooling temperature very rapidly and could result in divulging the diffusion-controlled system of the growth rate '*G*' versus temperature '*T*' plot. In addition, the effect of molecular weight on the P-T phase diagram of ethylene-octene copolymers needs to be explored.

The theoretical developments of this study need to be expanded to generate a complete model of the crystallization behavior of ethylene copolymers. For instance, the exact correlation between regime II-III transition and the monoclinic phase is not completely understood. In addition, the actual mechanism of the eutectoid-like transformation, and the methodology of the hexyl branch rejection need to be explore also.

7.2 Diffraction Studies

SAXS and WAXD work was mainly conducted at room temperatures and pressure in this study. It is of crucial importance to conduct *in-Situ* pressure and temperature SAXS and WAXD studies for those materials. Using *in-Situ* techniques allows for detecting all the meta-stable and stable phases forming at elevated pressures. Although similar studies were reported in literature for ethylene-octene copolymers, no connection was made between the melting behavior and the diffraction results.

7.3 Mechanical Properties

Studying the mechanical properties is very significant to industry. Ethylene-octene copolymers crystallized at elevated pressures have shown a eutectoid-like transformation when pressure was released and temperature cooled down. The effect of this transformation on the mechanical properties is still unknown. Studies are needed to correlate the mechanical properties of the final product with the original applied conditions.

7.4 Electrical Studies

Studying the influence of electric field on the polymer morphology has recently gained some attention in the research area. It is of interest to investigate the effect of electrical field on the orientation of the monoclinic crystals formed at elevated pressures.

Another important aspect is to know the effect of electrical field on the eutectoid-like transformation and properties of the final product. The problem that needs to be tackled is to know how will the applied electrical field orient the expelled hexyl branches when the transformation occurs.

REFERENCES

1) Kurelec L., Rastogi S., and Lemstra P. J., *Dutch Polymer Institute*, (2000).

2) Vanden Eynde S., Rastogi S., Mathot V. B. F., and Reynaers H., *Macromolecules*, **33**, n26, 9696-9704, (2000).

3) Strobl G, *The European Physical Journal E*, **3**, 165-183, (2000).

4) Hoffman J., Miller R., *Polymer*, **38**, n13, 3151-3212, (1997).

5) Sanchez I., Eby R. K., *Macromolecules*, **8**, n5, 638-641, (1975).

6) Hauser G., Schmidtke J., Strobl G., *Macromolecules*, **31**, 6250-6258, (1998).

7) Baer E., and Kardos J. L., *J. Polym. Sci.: Part A*, **3**, 2827-2841, (1965).

8) Tseng H., Phillips P. J., *Macromolecules*, **18**, n8, 1565-1571, (1985).

9) *Handbook of Crystal Growth*, **vol. 2**, Capter 18, Ed. Hurle D. T. J., 116-1216, (1994).

10) Shahin M. M., Olley R. H., Bassett D. C., Maxwell A. S., Unwin A. P., Ward I. M., *J. materials Sci.*, **31**, 5541-5549, (1996).

11) Maxwell A. S., Unwin A. P., Ward I. M., Abo EL Maaty M. I., Shahin M. M., Olley R. H., Bassett D. C., *J. materials Sci.*, **32**, 567-574, (1997).

12) Geil P. H., Anderson F. R., Wunderlich B., and Arakawa T., *J. Polymer Sci.*, **A2**, 3707, (1964).

13) Davidson T., Wunderlich B., *J. Polym. Sci.*, **Part A-2**, 7, 2051-2059, (1969).

14) Prime R. B., Wunderlich B., *J. Polym. Sci.*, **Part A-2**, 7, 2061-2072, (1969).

15) Bassett D. C., In *Developments in Crystalline Polymers*, Part-I, 115-149, (1982).

16) Rastogi S., Hikosaka M., Kawabata H., Keller A., *Macromolecule*, **24**, 6384-6391, (1991).

17) Wright K. J., Lesser A. J., *Macromolecules*, **34**, 3626-3633, (2001).

18) *X-ray characterization of materials*, edited by Eric Lifshin, Wiley-VCH, (1999).

19) *Characterization of plastics by physical methods*, Gunther Kampf, Hanser Publishers, (1986).

20) *X-ray Characterization of Materials*, Ed. Eric Lifshin, WILEY-VCH print, (1999).

21) Ruland W., *Colloid Polym. Sci.*, **255**, 417, (1977).

22) Albrecht T., Strobl G., *Macromolecules*, **29**, 783-785, (1996).

23) Strobl G. R., Schneider M. J., *J. Polym. Sci., Poly. Phys.*, **18**, 1343, (1980).

24) Strobl G. R., Schneider M. J., *J. Polym. Sci., Poly. Phys.*, **18**, 1361, (1980).

[25]) Flory P. J., *J. Am. Chem. Soc.*, **84**, 2857, (1962).

26) Phillips P. J., *Rep. Prog. Phys.*, **53**, 549-604, (1990).

27) Mandelkern L., Quinn F. A., and Flory P. J., *J. Appl. Physics*, **25**, n7, 830-839, (1954).

28) Lauritzen J. I. Jr., and Hoffman J. D., *J. Res. Natl. Bur. Stand., Sect. A*, **64**, 73, (1961).

29) Lauritzen J. I. Jr., and Hoffman J. D., *J. Res. Natl. Bur. Stand., Sect. A*, **65**, 297, (1961).

30) Sadler D. M., Gilmer G. H., *Polymer*, **25**, n10, 1446-1452, (1983).

31) Sadler D. M., *Polymer*, **24**, n11, 1401-1409, (1983).

32) Sadler D. M., Gilmer G. H., *Physical review letters*, **56**, n25, 2708-2711, (1986).

33) Keller A., Hikosaka M., Rastogi S., Toda A., Barham P. J., Goldbeck-Wood G., In *Self-Order and Form in Polymeric Materials*, 1-15, (1995).

34) Hikosaka M., *Polymer*, **31**, 4, (1990).

35) Hikosaka M., Amano K., Rastogi S., Keller A., *Macromolecules*, **30**, 2067-2074, (1997).

36) Imai M., Kaji K., Kanaya T., *Macromolecules*, **27**, 7103-7108, (1994).

37) Imai M., Kaji K., Kanaya T., Sakai Y., *Physical Review B*, **52**, n17, 12696-12704, (1995).

38) Cahn J. W., *J. Chem. Phys.*, **42**, 93, (1965).

39) Furukawa H., *Adv. Phys.*, **34**, 703, (1985).

40) Wang Z–G., Hsiao B. S., Sirota E. B., Srinivas S., *Polymer*, **41**, 8825-8832, (2000).

41) Heck B., Hugel T., Lijima M., Sadiku E., Strobl G., *New Journal of Physics*, **1**, 17.1-17.29, (1999).

42) Phillips P. J., and Vatansever N., *Macromolecules*, **17**, 871, (1984).

43) Wagner J., Abu-Iqyas S., Monar K., Phillips P. J., *Polymer*, **40**, 4717-4721, (1999).

44) Campell R. A., *PhD Dissertation*, University of Tennessee, Knoxville, (1991).

45) Tseng Hsiung-To, *PhD Dissertation*, University of Utah, (1984).

46) Guttman C. M., DiMarzio E. A., Hoffman J. D., *Polymer*, **22**, n11, 1466-1475, (1981).

47) Mansfield M. L., *Polymer*, **29**, n10, 1755-1760, (1988).

48) Andrews E. H., Owen P. J., Singh A., *Proc. Roy. Soc. Lond.*, **A324**, 79-97, (1971).

49) Lambert W. S., Phillips P. J., Lin J. S., *Polymer*, **35**, n 9, 1809-1818, (1994).

50) Fischer E. W., *Makromol. Chem. Symp.*, **20/21**, 277, (1988).

51) Phillips P. J., Edwards B. C., *J. Polym. Sci.*, Phys., **13**, 1819, (1975).

52) Dalal E. N., Phillips P. J., *Macromolecules*, **16**, 890, (1983).

53) Dalal E. N., Phillips P. J., *Macromolecules*, **16**, 1754, (1983).

54) Dalal E. N., Phillips P. J., *Macromolecules*, **17**, 248, (1984).

55) *Polymers and their properties*, **vol. 1**, by Hearle, (1982).

56) Abo el Maaty M. I., Bassett D. C., Olley R. H., Jääskeläinen P., *Macromolecules*, **31**, 7800-7805, (1998).

57) Jenckel E., Teege E., Hinrichs W.; *Kolloidz*, **19**, 129, (1952).

58) Keller A., *Nature*, **169**, 913, (1952).

59) Bassett D. C., and Hodge A. M., *Proc. R. Soc. Lond.*, **A-377**, 61-71, (1981).

60) Toda A., and Keller A., *Colloid and Polymer Science*, **271**, 328-342, (1993).

61) Keith H. D., and Padden F. J., *Macromolecules*, **29**, n24, 7776-7786, (1996).

62) Abo el Maaty M. I., Hosier I. L., Bassett D. C., *Macromolecules*, **31**, 153-157, (1998).

63) Zhishen M., and Hongfang Z., *J. M. S. –Rev. Macromol. Chem. Phys.*, **C35**, n4, 555-580, (1995).

64) Patrick M., Bennett V., and Hill M. J., *Polymer*, **37**, n24, 5335-5341, (1996).

[65]) Wagner J. E., Abu-Iqyas S., Monar K., and Phillips P. J., *Proceedings of the ANTEC 98*, Society of Plastics Engineers, (1998).

66) Peeters M., Goderis B., Reynaers H., and Mathot V., *J. Polymer Science, Part B: Polymer Physics*, **37**, 83-100, (1999).

67) Ed. Mark J. E., *Polymer Data Handbook*, Oxford University Press, (1999).

68) Kim Man-Ho, *PhD dissertation*, University of Tennessee, Knoxville, (1996).

69) Barrall E. M., Johnson J. F., and Porter R. S., *Applied Polymer Symposia*, 8, 191, (1969).

70) Mezghani Khaled, *PhD dissertation*, University of Tennessee, Knoxville, (1996).

71) Bassett D. C., in *Developments in crystalline polymers*, **vol. 2**, (1988).

72) Lagarón J. M., López-Quintana S., Rodriguez-Cabello J. C., Merino J. C., and Pastor J. M., *Polymer*, **41**, 2999-3010, (2000).

73) Wilfong D. L., and Knight G. W., *J. Appl. Polym. Sci., Polym. Phys.*, **28**, 861, (1990).

74) Tsubakihara S., Nakamura A., and Yasuniwa M., *Polymer J.*, **23** (11), 1317-1324, (1991).

75) Tashiro K., Sasaki S., and Kobayashi M., *Macromolecules*, **29**, 7460-7469, (1996).

76) Villar M. A., Failla M. D., Quijada R., Mauler R. S., Vallés E. M., Galland G. B., and Quinzani L. M., *Polymer*, **42**, 9269-9279, (2001).

77) Schouterden P., Groeninckx G., Van Der Heijden B., and Jansen F., *Polymer*, **28**, 2099-2104, (1987).

78) Razavi-Nouri M., and Hay J. N., *Polymer*, **42**, 8621-8627, (2001).

79) Ungar G., and Keller A., *Polymer*, **28**, 1899, (1987).

80) Mandelkern L., *Crystallization of Polymers*, McGraw-Hill, New York, (1964).

81) Fang-Chyou Chiu, *PhD dissertation*, University of Akron, Akron-Ohio, (1995).

82) Hellmuth E., and Wunderlich B., *Journal of Applied Physics*, **36**, n10, 3039-3044, (1965).

83) Bassett D. C., and Turner B., *Phil. Mag.*, **29**, 925-955, (1974).

84) Keller A., Hikosaka M., Rastogi S., Toda A., Barham P. J., and Godbeck-Wood G., *J. Mater. Sci.*, **29**, 2579-2604, (1994).

85) Leonard E. Samuels, *Metals Engineering A Technical Guide*, ASM International, (1988).

86) *Heat Treating Progress*, ASM International Publication, p.p. 109, December (2001).

87) Geil P. H., Anderson F. R., Wunderlich B., and Arakawa T., *J. Polymer Sci.*, **A2**, 2043, 1964.and *J. Polymer Sci.*, **A2**, 3707, (1964).

88) Bassett D. C., Khalifa B. A., and Olley R. H., *J. Polym. Sci., Polym. Phys. Edn.*, **15**, 995, (1977).

89) M. Hikosaka, S. Rastogi, Keller A., and Kawabata H., *J. Macromol. Sci. Phys.*, **B31**, 87, (1992).

90) Hikosaka M., Tsukijima K., Rastogi S., and Keller A., *Polymer*, **33**, n12, 2502-2507, (1992).

91) Singh M., Barkei M., Inden G., and Bhan S., *Phys. Stat. Sol.*, **A87**, 165, (1985).

92) Davis G. T., Eby R. K., and Colson J. P., *Journal of Applied Physics*, **41**, n11, 4316-4326, (1970).

93) Androsch R., *Polymer*, **40**, 2805-2812, (1999).

94) Heck B., Hugel T., Iijima M., and Strobl G., *Polymer*, **41**, 8839-8848, (2000).

95) Lotz B., *The European Physical Journal*, E-**3**, 185-194, (2000).

96) Muthukumar M., *The European Physical Journal*, E-**3**, 199-202, (2000).

97) Wang Z.–G., Hsiao B. S., Sirota E. B., Agarwal P., and Srinivas S., *Macromolecules*, **33**, 978, (2000).

98) Cheng S. Z. D., Li C. Y., and Zhu L., *The European Physical Journal,* E-**3**, 195-197, (2000).

99) Phillips P. J., and Lambert, W. S. *Macromolecules*, **23**, 2075, (1990).

100) Wagner J., and Phillips P. J., *Polymer*, **42**, 8999-9013, (2001).

101) Hikosaka M., *polymer*, **28**, 1257, (1987).

102) Hikosaka M., *polymer*, **31**, 458, (1990).

103) Sawada S., Kato K., and Nose T., *Polymer J.*, **11**, 551, (1979).

104) Huang R., Zhang X., and Li G., In *Handbook of engineering polymeric materials*, **Ch. 20**, 295-316, (1997).

105) Bassett D. C., and Turner B., *Nature* (*Phys. Sci.*), **240**, 146 (1972).

106) Bassett D. C., and Turner B., *Phil. Mag.*, **29**, 285 (1974).

107) Lauritzen J. I., and Hoffman J. D., *J. Appl. Phys.*, **44**, 4340, (1973).

108) Magill J. H., *Nature* (*London*), **187**, 770, (1960).

109) Lambert W. S., and Phillips P. J., *Macromolecules*, **27**, 3537, (1994).

110) Wagner J. E., *PhD dissertation*, University of Tennessee, (2001).

111) Keith H. D., and Padden F. J., *J. Appl. Phys.*, **34**, 2409, (1963).

VITA

Samir Abu-Iqyas was born in Kuwait on October 30, 1969, where he attended his high school there. He joined the University of Jordan on January 1988, where he pursued his undergraduate studies in physics. He received his Bachelor of Science on May 1991. On the August of 1991, he was admitted to the Masters of Science program in the physics department of Al-Yarmouk University, Jordan. On September 1992, he decided to move to Aligarh Muslim University, India, where he entered the Master of Science program in the physics department. He joined the group of 'lasers and modern spectroscopy', and earned his Master of Science on September 1994.

On August 1996, he was admitted to the Ph.D. program of the physics department at the University of Tennessee. Shortly he joined the Ph.D. program of the polymer engineering in the Materials Science and Engineering at the same University. He completed all the requirements for the Doctor of Philosophy degree in Polymer Engineering in May 2002.

5179 3770 7
09/24/02 MRB